Dissertation zur Erlangung des Doktorgrades

der Fakultät für Chemie und Pharmazie

der Ludwig-Maximilians-Universität München

Targeted antitumoral siRNA delivery

Jie Luo

aus

Shandong, China

2020

Erklärung

Diese Dissertation wurde im Sinne von § 7 der Promotionsordnung vom 28. November 2011 von Herrn Prof. Dr. Ernst Wagner betreut.

Eidesstattliche Versicherung

Diese Dissertation wurde eigenständig und ohne unerlaubte Hilfe erarbeitet.

München, 21.10.2020

.....……

Jie Luo

Dissertation eingereicht am 21.10.2020

1. Gutachter: Prof. Dr. Ernst Wagner

2. Gutachter: Prof. Dr. Olivia Merkel

Mündliche Prüfung am 08.12.2020

Meiner Familie

The most important thing you can learn is fundamentals.

Robert Langer, 2009

Table of Contents

1 Introduction

*This chapter was adapted from: Jie Luo, Ernst Wagner and Yanfang Wang. Artificial peptides for antitumoral siRNA delivery. J. Mater. Chem. B, 2020, **8**, 2020-2031.*

1.1 Nucleic acid formulation as therapeutic agents

The therapy of macromolecules like proteins or nucleic acids (consisting of plasmid DNA, small interfering RNA siRNA, microRNA) is the promising way for infectious disease or cancer. As the therapeutic way, these macromolecules should be stable against degradation in the bloodstream and cleared by kidneys.

Viral vectors have been widely investigated many years for intracellular nucleic acid delivery. However, the big obstacles of this kind of vector are immunogenicity and gene recombination with host. Therefore, non-viral vector appeals many researchers.

In August 2018, FDA approved the first siRNA drug, Patisiran, a lipid nanoparticle (LNP) containing transthyretin (TTR) siRNA for treatment of hereditary transthyretin-mediated amyloidosis (ATTR). Extracellular and intracellular delivery has been critical for the success of siRNA cargo. A further refinement of delivery carriers will have a tremendous impact for efficacy of future nanomedicines. Three different directions can be considered: (i) chemical modifications of siRNA oligonucleotide backbone; (ii) covalent conjugation of siRNA with transport vehicles, such as with cholesterol for delivery to several organs, or with tri-(N-acetyl-galactosamine)-PEG for targeting the hepatocyte-specific asialoglycoprotein receptor; or (iii) supramolecular assembly into lipid-, peptide-, polymer- or inorganic-organic hybrid- based siRNA nanoparticles. siRNA LNPs have been developed for liver-specific applications and already reached drug status (see Patisiran, above). Givosiran, a completely chemically modified and tri-(N-acetyl-galactosamine)-PEG conjugated siRNA targeting aminolevulinic acid synthase, was recently approved in November 2019 as second siRNA medicine

(GIVLAARI), as subcutaneously administered drug for the treatment of acute hepatic porphyria. Clinical studies are less advanced for cancer. Nevertheless, first tumor-targeted siRNA polyplexes formed with cyclodextrin-oligocations and coated with transferrin-coated have already been tested in cancer patients and showed gene silencing of M2 subunit of ribonucleotide reductase (RRM2) in tumor tissue.

1.2 Evolution of artificial peptides as siRNA nanocarriers

Poly(amidoamines) already received a lot of attention in drug and gene delivery due to their favorable properties such as solubility, biocompatibility, low hemolysis and reduced cytotoxicity compared to other delivery carriers.[1] Hartmann and Börner applied SPS for generation of sequence-defined oligo(amidoamines) based on building blocks such as spermine and succinic acid.[2-5] Such oligomers were firstly applied in plasmid DNA (pDNA) polyplex formulations, which presented an interesting starting point of the artificial peptide based strategy developed in our own laboratory. Synthetic peptides have been previously successfully applied as siRNA carriers or targeting ligands of siRNA formulations.[6-19] Lu and collaborators designed artificial lipo-peptide carriers for siRNA delivery,[20-23] by combining one artificial building block triethylene tetramine with natural amino acids histidine, cysteine and conjugated oleic acid. Some of these carriers, such as EHCO (an ethylenediamine head group, a histidine-cysteine amino acid based linker and two oleic acid tails) and ECO (an ethylenediamine head group, a cysteine amino acid based linker and two oleic acid tails) were successfully applied in RGD-PEG siRNA formulations for tumor-targeted therapy in mice. Mixson and colleagues had designed linear and branched peptide libraries containing histidines (as endosomal buffering domain) and lysines (as nucleic acid binding domain) for pDNA and siRNA delivery.[11-16] Langel and colleagues had developed a series of cell-penetrating peptides termed PepFects, which optionally also contained a fatty acid domain, for nucleic acid delivery.[17-19]

In our laboratory, in order to utilize the well-known proton sponge activity of polyethylenimine (PEI), which is a gold standard in successful pDNA transfection,[24-26] the chemical amino ethylene motif was combined with the established methodology of SPS of peptides. Schaffert et al [27] developed a versatile approach for incorporation of fluorenyl-methoxycarbonyl (Fmoc)- and t-butyl oxycarbonyl (Boc)-protected oligoamino acids, which allowed the synthesis of orthogonally protected cationic building blocks for Fmoc-SPS. Combined with lysines as the branching sites, cysteines as crosslinking terminals and fatty acids as hydrophobic domains, the designed artificial amino acids (tetraethylenepentamine artificial peptide Stp, Gtp, triethylenetetramine artificial peptide Gtt) were applied to establish more than 300 linear, 3-arm, 4-arm, T-, i-, or U-shape sequence-defined oligomers for siRNA or pDNA delivery (Fig. 1).[28] Identification (ID) number, sequence, molecular characterization and biofunction of representative artificial peptides are displayed in Table 1. First proof-of-concept studies proved the encouraging potential of such oligoaminoamides (OAA) in siRNA delivery. Results indicated that cysteine-containing 3-arm Stp-based oligomer displayed significantly higher gene silencing efficiency than the corresponding oligomer with alanines instead of cysteines. The i-shape oligomers with two cysteines and a hydrophobic domain indicated the important contribution of cysteines and hydrophobic fatty acids to stable siRNA complex formation, thereby significantly enhancing the internalization of formed nanoparticles into cells and the subsequent gene silencing efficiency. Meanwhile, the stabilization contributed by cysteines was able to be compensated by hydrophobic stabilization contributed by fatty acids. The U-shape oligomers with diacyl groups were able to transfect in the absence of cysteines. The study not only highlighted the important role of cysteine and hydrophobic fatty acids in the design of oligomers, but also offer a convenient strategy to incorporate targeting ligands and shielding agents.[29, 30] The beneficial role of cysteine for siRNA delivery was further confirmed by Salcher et al in the evaluation of transfection efficiency by 4-arm oligomers.[31]

Based on SPS, precise sequence-defined artificial oligomers with different cationic building backbones (tetraethylenepentamine artificial peptide Stp, Gtp and Ptp, triethylenetetramine artificial peptide Gtt) and topologies (three-armed; T-shape, i-shape and U-shape) were further optimized for nucleic acid delivery.[32] Although these cationic backbones have the same 1,2-diaminoethane proton-sponge motif, siRNA binding and reporter gene silencing experiments showed that Stp-containing oligomers have the greatest potential among these artificial amino acids. The screening of fatty acids incorporated in oligomers as hydrophobic domains revealed the most effective gene silencing with oligomers containing unsaturated fatty acids compared to oligomers with saturated fatty acids. In addition, it was proven that the topology of the investigated lipo-oligomers played a minor role in siRNA transfection efficiency as compared to the effect contributed by the incorporation of different building blocks, terminal cysteines and lipid moieties. By formulating with antitumoral EG5 siRNA, two promising oligomers, T-shape ***49*** with the sequence of C-Stp_2-K[K-$(OleA)_2$]-Stp_2-C and i-shape ***229*** with the sequence of C-Stp_3-C-K-$LinA_2$, exhibited efficient gene silencing and resulted mitotic monoastral spindles formation and cell cycle arrest both *in vitro* and *in vivo*. EG5 polyplexes upon intratumoral injection showed a significant inhibition of tumor growth in subcutaneous Neuro2A-eGFPLuc-bearing mice.

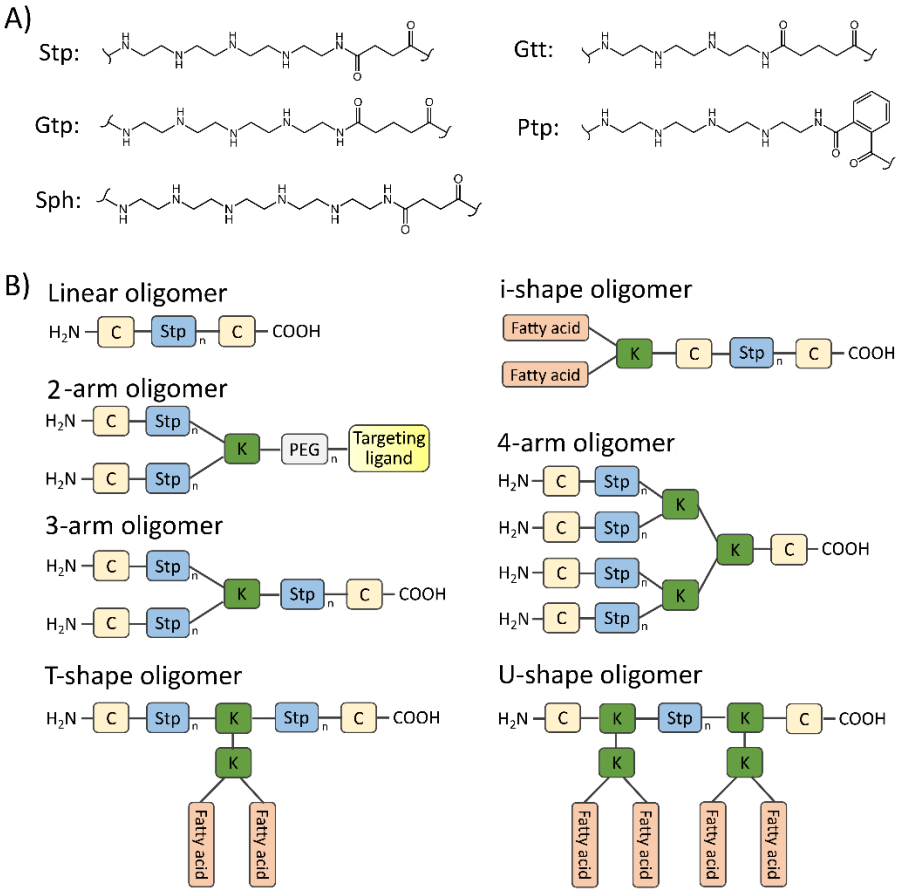

Fig.1 Schematic overview of **A)** artificial oligo-amino acids (Stp, Gtp, Gtt, Ptp and Sph) used as cationic building block, and **B)** Stp-based oligomers with different topologies: linear, 2-arm with targeting ligand, 3-arm, 4-arm, i-, T- and U- shape. K, lysine; Stp, succinoyl-tetraethylene-pentamine.

Table 1: Summary of representative artificial peptides in siRNA delivery.

Oligomer ID	Sequence (N→C)	Topology*	Biofunction	Ref.
49	C-Stp_2-K[K-$(OleA)_2$]-Stp_2-C	T-shape	Efficient gene silencing, with siEG5 both *in vitro* and *in vivo*.	32
229	C-Stp_3-C-K-$LinA_2$	i-shape		
386	C-Stp_3-K(Stp_3-C)$_2$	3-arm	Cysteine-containing oligomer exhibited significant stronger siRNA binding and higher gene knockdown as compared to the corresponding alanines-containing oligomer.	28
279	A-K[K$(LinA)_2$]-Stp_3-K[K$(LinA)_2$]-A	U-shape	Hydrophobic stabilization by four fatty acids may compensate the lack of disulfide crosslinking.	28
356	C-Stp_4-K(PEG_{24}-FolA)-Stp_4-C	2-arm	Gene silencing activity depends on use of endosomolytic INF7-conjugated siRNA.	33
640	K(Stp_4-C)$_2$-K(PEG_{24}-E_4-MTX)	2-arm	γ-glutamic acid inserted into oligomers enhanced the antitumoral effect of nanoplexes as compared with ***356***.	38
454	C-Y_3-Stp_2-K[K$(OleA)_2$]-Stp_2-Y_3-C	T-shape	Y_3-containing oligomer exhibited more stability, higher gene silencing efficiency and longer circulation time than Y_3-free oligomer ***49***.	47
1027	C-Y_3-(H-Stp)$_2$-H-K[K$(CholA)_2$]-H-(Stp-H)$_2$-Y_3-C	T-shape	Histidine-containing oligomers showed enhanced gene silencing effect than corresponding histidine-free oligomers among cysteine-containing oligomers.	50
990(CholA) ***992***(SteA) ***1082***(MyrA)	Y_3-Stp_2-K[G-ssbb-K(Fatty acid)$_2$]-Stp_2-Y_3	T-shape	ssbb-containing oligomers for GSH-triggered siRNA release exhibited higher transfection efficiency with lower cytotoxicity.	39
Series X1-MyrA-X2	Y_3-Stp_2-**X1**-K[**X2**-K$(MyrA)_2$]- **X1**-Stp_2-Y_3 *(X1 and X2=L-Arg (R, RR) or D-Arg (r, rr)*	T-shape	L-Arg dipeptides-containing oligomers for endolysosomal protease cathepsin B-triggered siRNA release displayed reduced cytotoxicity.	42
1106	K(N_3)-Y_3-Stp_2-K[G-K$(CholA)_2$]-Stp_2-Y_3	T-shape	Azido groups were introduced to provide the option for subsequent copper-free click modification of shielding and targeting ligands.	55

K, lysine; Stp, succinoyl-tetraethylene-pentamin; OleA: oleic acid; PEG, polyethylene glycol; CRC, cysteine-arginine-cysteine; ssbb, disulfide building block = succinoyl-cystamine; GSH, glutathione; MyrA, myristic acid; SteA, stearic acid; CholA, 5β-cholanic acid; Y_3, tyrosine tripeptide. *Topologies of representative artificial peptides are displayed in Fig.1.

1.3 Targeted siRNA nanoplexes

Targeted delivery to tissues different from liver remains a major barrier in the process of siRNA therapeutics. Therefore, we present a series of targeted multifunctional artificial oligomers based on SPS chemistry.

Dohmen and co-workers developed [33, 34] an oligoaminoamide core, terminated by cysteines for crosslinking, containing a monodisperse PEG chain at a defined central position and a folic acid (FolA) as cell targeting ligand. An endosomolytic influenza peptide, Inf7,[35, 36] was attached to the 5'-ends of siRNA sense strand to increase the endosomal escape ability. The multifunctional polyplexes with endosomolytic siRNA-Inf7 conjugates indicated a ligand- and Inf7- dependent reporter gene silencing. Stained slices of tumor harvested after 24 h i.t. treatment with of siEG5-Inf7 / oligomer ***356*** with the sequence FolA-PEG_{24}-K(Stp_4-C)$_2$ displayed the expected formation of mitotic asters. Although the siRNA-Inf7 ***356*** polyplexes due to their small particle size exhibited a short systemic circulation time, the strong shielding effect of PEG chain prevented the unspecific affinity to other tissues. Based on oligomer ***356*** with FolA as targeting ligand, methotrexate (MTX) was coupled to the oligo(ethanamino)amide as dual-functional ligand to induce folate-receptor (FR) targeted cellular internalization as well as cytotoxic activity directed to dihydrofolate reductase (DHFR).[37] The MTX-containing oligomers exhibited good cellular uptake and a cytotoxicity in FR-overexpressing KB cells that was enhanced by synthetic oligo-glutamylation (E_n) of the ligand. Lee et al [38] evaluated these oligomers for dual antitumoral siRNA therapy (Fig. 2A and B).

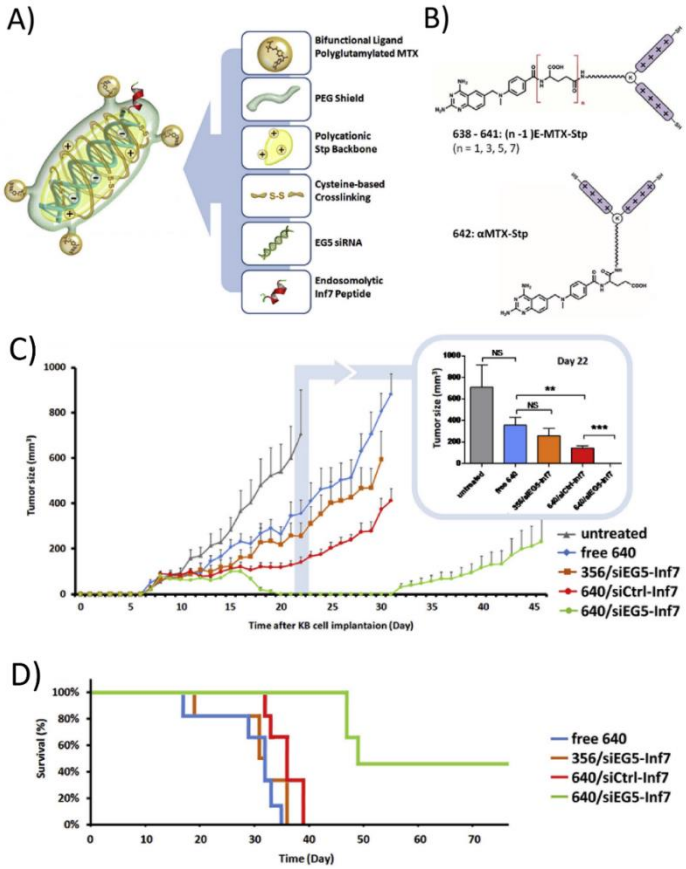

Fig. 2 Bifunctional siRNA nanoplexes. **A)** Schematic overview of the siRNA nanoplexes with MTX ligands and endosomolytic Inf7-siRNA conjugate.[38] **B)** Oligomers with MTX polyglutamates. MTX was coupled to $dPEG_{24}$ via the γ-glutamic acid (oligomers ***638-641***) or α-carboxy group (oligomer ***642***), and then linked to a 2-arm cationic backbone. E, glutamic acid. Tumor sizes **C)** and survival curves **D)** of KB tumor treated by the indicated different formulations, HBG buffer, ***640***, ***640*** containing siCtrl-Inf7 or siEG5-Inf7, or ***356***/siEG5-Inf7 polyplexes.Reproduced from Lee et al.[38] with permissions of Elsevier.

MTX-conjugated siEG5-Inf7 polyplexes exhibited efficient gene silencing *in vitro* as well as, upon intratumoral injection in KB tumors in mice, significantly extended retention of siRNA in tumors *in vivo*. Meanwhile, due to the dual antitumoral mechanism, siEG5-Inf7 polyplexes formed with oligomer ***640*** with the sequence of MTX-E_4-PEG_{24}-K(Stp_4-C)$_2$ mediated superior tumor suppression as compared to the FolA-conjugated ***356*** groups (Fig. 2C and D).

1.4 Evolution of siRNA lipopolyplexes

1.4.1 Biodegradable T-shape lipo-oligomers

For siRNA delivery, our studies indicated that extracellular stability of polyplexes is an essential requirement, yet the cytosolic release of siRNA in the intracellular space is also required. By introduction of a disulfide between the fatty acid domain and the cationic siRNA binding domain (Stp or Sph), Klein et al [39] used Fmoc-protected succinoyl-cystamine as disulfide building block (ssbb) and developed a library of bio-degradable oligomers via SPS. The new bio-degradable lipo-oligomers containing ssbb block exhibited acidic pH-triggered endosomal escape analogously to the standard lipo-oligomers. The cytosolic glutathione (GSH) levels however was expected to trigger favorable cytosolic siRNA release of siRNA polyplexes. In addition, cleavage of the disulfide bond was expected to convert a detergent-like lipo-oligomer into a neutral lipid and a nontoxic small hydrophilic oligomer. Compared with the corresponding siRNA polyplexes formed with ssbb-free oligomers, the bio-cleavable oligomers demonstrated higher transfection efficiency with lower cytotoxicity.[39]

For lipid nanoparticles, only 1-2% of siRNA is estimated to be released from endosomes into the cytosol,[40, 41] which apparently is sufficient to realize subsequent RNAi. It however also means that a large number of carriers are accumulating in the lysosomal compartment and may damage these organelles and cell functions. By precisely introducing short enzymatically cleavable *L*-arginine peptides (RR) between lipophilic di-myristic acid (MyrA) and the cationic Stp units via SPS, Reinhard et al.[42] developed a library of T-shaped oligomers for endolysosomal protease cathepsin B-triggered siRNA release. Compared with analogous non-degradable oligomers, enzymatic bio-degradable lipopolyplexes containing *L*-arginine displayed reduced lytic activity after cleavage, thereby exhibited lower cytotoxicity without affecting the transfection efficiency.

1.4.2 Targeted combination complexes TCP and TLP

Based on previous studies, FR-targeted combinatorial polyplexes (TCP) were developed by co-formulating siRNA with two different oligomers to provide efficient

alternatives for multifunctional delivery system.[43, 44] To activate the cysteine thiol groups, 5,5′-dithio-bis(2-nitrobenzoic acid) (DTNB) was reacted with one thiol-containing oligomer, resulting in a TNB modified oligomer which would undergo rapid conjugation with another thiol-containing oligomer by formation of disulfide bonds. Based on previous work, oligomers with 2, 3 or 4-arm Stp/Sph without or with PEG-FolA-conjugation were selected [28, 45, 46] or designed. The TCPs displayed significant gene silencing efficiency in FR-positive cells. Intravenous administration showed that TCP formed with a TNB-bearing PEGylated 4-arm Sph oligomer ***873*** of the sequence of K-(PEG_{24}-FolA)-K-[K-(Sph_4-C-TNB)$_2$]$_2$ with a 3-arm Stp oligomer ***386*** of the sequence of C-Stp_3-K-(Stp_3-C)$_2$ exhibited siRNA delivery into a subcutaneous L1210 leukemia site and a 46% reduction of EG5 mRNA.

Afterwards, Lee et al [47] further developed FR-targeted lipopolyplexes (TLPs) by first formulating siRNA with an optionally tyrosine-containing oligomer and then co-formulating targeted PEGylated oligomer ***356*** with the sequence of FolA-PEG_{24}-K(Stp_4-C)$_2$ by cysteine disulfide cross-linking for shielding and targeting modification. Fluorescence resonance energy transfer (FRET) showed that intracellular siRNA stability of TLP1 formed by tyrosine-containing oligomer ***454*** was superior compared with other TLPs formed by tyrosine-free oligomers. TLP1 showed folate ligand-dependent siRNA accumulation in subcutaneous L1210 leukemia with a 65% EG5 gene silencing. The results demonstrated that the incorporation of tyrosines was favorable to protect siRNA from cytosolic degradation, hence caused explicit changes to the RNAi effect.

1.4.3 Surface shielded and targeted siRNA lipopolyplexes

PEG shielding and targeting domains can be directly introduced into nanocarriers by SPS. This process however provides limitation to the nanoparticle design, formation of only very small nanoplexes in case of lipid-free formulations, or rather difficile combination formulations. An alternative approach presents the formation of stable

lipopolyplex core nanoparticles, followed by post-modification with a PEG-ligand shell. This covalent modification of siRNA core nanoparticles was performed in two different variations; either by coupling of cysteine thiols on the polyplex surface with maleimide- or OPSS- containing PEG-ligands (Fig. 3A);[48-51] or via copper-free click reaction of lipopolyplexes generated with azido-containing oligomers with dibenzocyclooctyne amine (DBCO) PEG-ligands (Fig.3B). [52-57] The oligomers as well as the shielding and targeting ligands can be synthesized by SPS, which enables precise variation of functional units, such as PEG length, or the amount of attachment sites.

Müller et al [48] used oligomers ***454*** with the sequence of C-Y_3-Stp_2-K[K-$(OleA)_2$]-Stp_2-Y_3-C and ***595*** with the sequence of CRC-Y_3-Stp_2-K[K-$(OleA)_2$]-Stp_2-Y_3-CRC to prepare core siRNA polyplexes. Then the core polyplexes were modified by coupling with maleimide-PEG reagents with or without targeting ligand folic acid (FolA) to provide FR targeting and PEG shielding, respectively (Fig. 3A). The coupling efficiency of maleimide-PEG with oligomers was monitored via an Ellman's assay. Modification with the standard FolA-PEG resulted in nanoparticle aggregation, most likely due to the low solubility of FolA. To resolve this problem, tetra-γ-glutamylated folate gE4-FolA was designed as ligand. The four negative glutamate charges improve solubility of FolA and provide the resulting nanoparticles with a negative zeta potential, which prevents nanoparticle aggregation by electrostatic repulsion interactions. The beneficial effect of such oligo-glutamylation in FR-targeted delivery was previously confirmed.[38, 58] PEGylated gE4-FolA polyplexes showed FR-mediated uptake and effective gene transfection efficacy in cervical carcinoma KB cells. Biodistribution of gE4-FolA formulations showed extended persistence in L1210 tumor bearing mice, however only a moderate *in vivo* delivery into the subcutaneous leukemia site.

The epidermal growth factor receptor (EGFR) targeting peptide ligand GE11 was also introduced onto the surface of ***454*** siRNA (or microRNA) polyplexes by coupling maleimide-PEG-GE11 with the free cysteines.[49] The resulting GE11 ***454*** siRNA (or

microRNA) lipopolyplexes showed enhanced cellular uptake in many EGFR-positive cell lines, and also functional delivery of microRNA-200c. Zhang et al [51] developed transferrin receptor (TfR) delivery on the basis of ***454*** siRNA polyplexes. Such designed Tf&Inf7 ***454*** siRNA polyplexes displayed effective receptor specific internalization and enhanced gene silencing in TfR positive tumor cell lines. *In vivo* distribution further demonstrated the enhanced tumor persistence of siRNA for Tf&Inf7 polyplexes in murine Neuro2A tumor bearing mice, as compared to the corresponding albumin or non-modified groups.

By introducing azido lysine at the N terminus, Klein et al developed oligomer ***1106*** with the sequence $K(N_3)$-Y_3-Stp_2-K[G-$K(CholA)_2$]-Stp_2-Y_3 for click functionalization of polyplexes with DBCO reagents (Fig. 3B).[55] A library of defined PEG shielding and FolA targeting reagents were precisely synthesized by SPS. This library included different PEG lengths and monovalent (DBCO-PEG or DBCO-PEG-FolA) or bivalent DBCO with biodegradable linkers ($DBCO_2$-ss_2-PEG or $DBCO_2$-ss_2-PEG-FolA) for click modification, or double-click modification, respectively. Because of the instability of DBCO under standard 95% trifluoroacetic acid (TFA) deprotection, in the 5% TFA has to be applied in the final cleavage step of SPS. ***1106*** siRNA polyplexes incorporated with bivalent DBCO reagents was superior at size distribution, cellular internalization as well as gene silencing effect *in vitro*. Intravenous injection of the resulting ***1106***/siEG5/$DBCO_2$-ss_2-PEG_{24}-FolA lipo-polyplexes displayed extended tumor retention in L1210 tumor-bearing mice, with a knockdown of ~60% of target mRNA (Fig. 3C and Fig. 3D). The click reaction between DBCO and azide is highly specific and biorthogonal to other functional domains and without by-products. [59-61] Compared to the disulfide bonding modification, click modification will not affect the main purpose of cysteines and keep the stability of core polyplexes by internal disulfide crosslinking.

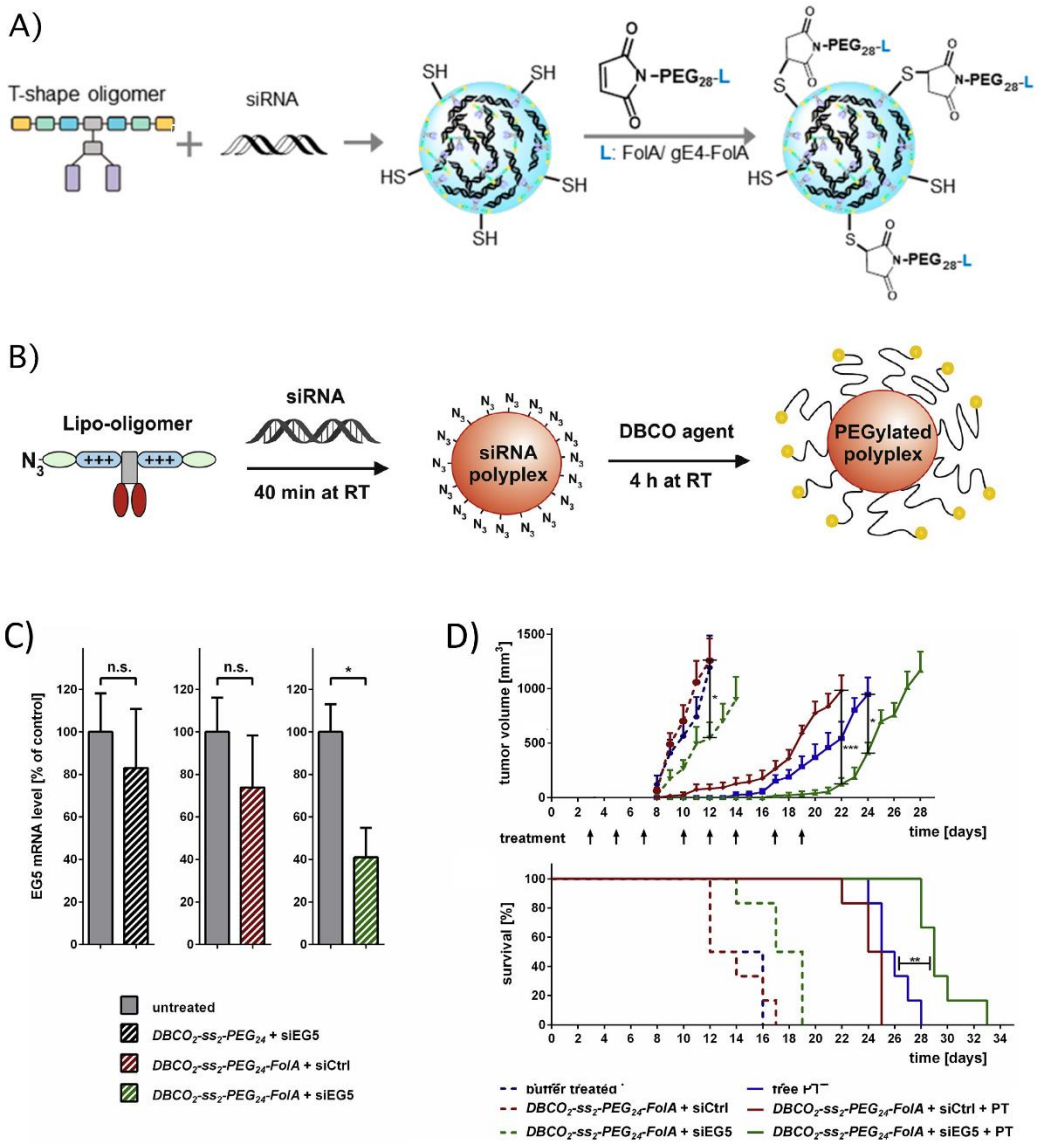

Fig. 3. Lipopolyplexes containing shielding and targeting domains. **A)** Cysteine-containing oligomers ***454*** or ***595*** were mixed with siRNA, and then the polyplexes were post-PEGylation with Mal-PEG_{24}-FolA (FolA) or Mal-PEG_{24}-gE4-FolA (gE_4-FolA) by reaction with free cysteines on the surface of polyplexes.[48] FolA: folate acid. Reproduced from Müller et al.[48] with permission of American Chemical Society. **B)** siRNA polyplexes made with azido-bearing lipo-oligomer ***1106***. Shielding or targeting reagents with monovalent or bivalent terminal DBCO were attached to the lipopolyplexes via click or double-click reaction with the exposed azides.[55] **C)** *In vivo* gene silencing efficiency of ***1106***/siRNA/$DBCO_2$-ss_2-PEG_{24}-FolA lipopolyplexes. EG5 mRNA expression level in L1210 tumor mice was measured by qPCR.[55] **D)** Tumor sizes and survival curves of mice treated by HBG, PT, ***1106***/siRNA/$DBCO_2$-ss_2-PEG_{24}-FolA lipopolyplexes with siCtrl or siEG5, without or in combination with pretubulysin (PT). The arrows indicate the days of treatment.[55] B) to D) reproduced from Klein et al. [55] with permission of Elsevier.

Conventionally, siRNA polyplexes were prepared by rapid manual pipetting up and down. Loy et al developed a microfluidic platform by designing two successive Y junctions for controlled and sequential formulation of functionalized polyplexes.[62] The core siRNA polyplexes were first assembled through single-meander channel (SMC). Then the polyplexes were click-modified with DBCO-PEG-FolA of different PEG lengths by a double-meander channel (DMC). The results demonstrated a clear influence of the PEG linker on gene silencing efficacy, which was consistent with previous findings. [55]

1.5 Aim of thesis

siRNA therapeutics has shown great potential, yet the downregulation of targeted gene expression may only partially inhibit tumor progression. Therefore, combined siRNA together with chemotherapeutic drugs or miRNA into one delivery system has to be developed to increase the therapeutic efficiency. Compared with monotherapy of cancer treatment, combination therapy enables different therapeutic entities simultaneously arrive the respective target site, results increased therapeutic efficiency due to the synergistic effect as well as lower side effects due to reduced dosage of chemotherapeutic drugs.[56, 63, 64] With regard to future optimization of this class of siRNA cancer therapeutics, emphasis has to be directed to (i) siRNA functionalized by chemical modification to combine with some antitumoral peptides/drug, and (ii) optimization of cationic oligo-formulation to fast attach to the tumor endothelial cells and achieve siRNA function *in vivo*.

The first aim of the thesis was to present a monodisperse carrier synthesized by solid phase supported chemistry. The sequence-defined assembly contains two oleic acids attached to a cationizable oligoaminoamide backbone in T-shape configuration, and a terminal azide functionality for coupling to the atherosclerotic plaque-specific peptide-1 (AP-1) as cell targeting ligand for interleukin-4 receptor (IL-4R) which is overexpressed in a variety of solid cancers. For combined cytosolic delivery with siRNA,

different apoptotic peptides (KLK, BAK and BAD) were covalently conjugated via bioreversible disulfide linkage to the 5'end of the siRNA sense strand. The optimized targeted carrier was complexed with dual antitumoral siEG5-KLK conjugates. The functionality of each subdomain was individually confirmed. The lipo-oligomer conferred stable assembly of siRNA conjugates and was click-shielded with dibenzocyclootyne-PEG-AP-1 (DBCO-PEG-AP-1). Structure-activity relationships of these oligomers were investigated, and the further mechanism of apoptotic peptide and siRNA *in vitro* function were also evaluated and discussed.

The second aim of the thesis was that a cationizable sequence-defined lipo-oligoaminoamide (lipo-OAA) modified with an N-terminal azide and HA modified with DBCO groups were used as clickable modules, respectively. By variation of the ratio of DBCO-HA to OAA azide of the siRNA nanoparticle, colloidal stable cationic and anionic HA-based siRNA polyplexes were established. Evaluation of these nanoparticles should explore any relations of surface charge with *in vivo* tumor accumulation, tumor penetration and subsequent gene silencing efficacy *in vivo*. The effect of the different coatings on the cellular uptake, endocytic pathways, endosomal escape *in vitro*, and tumor accumulation, tumor penetration, and gene silencing of siRNA carriers *in vivo* should also be evaluated.

2. Materials and Methods

2.1 Materials

Materials: 2-Chlorotrityl Chloride resin, protected Fmoc-α-amino acids, N, N-dimethylformamide (DMF), N,N-diisopropylethylamine (DIPEA), N-methyl-2-pyrrolidone (NMP) and trifluoroacetic acid (TFA) were obtained from Iris Biotech (Marktredewitz, Germany). 1-hydroxybenzotriazole (HOBt), triisopropylsilane (TIS), dibenzocyclooctyne-PEG_4-maleimide, dimethyl sulfoxide (DMSO) and oleic acid were purchased from Sigma-Aldrich (Munich, Germany). Syringe microreactors for peptide synthesis and (benzotriazol-1-yloxy) tripyrrolidino phosphonium hexafluorophosphate (PyBOP) were obtained from MultiSynTech (Witten, Germany). Fmoc-N-amido-dPEG24-acid from Quanta Biodesign (Powell, Ohio, USA). siRNA duplexes were obtained from Axolabs GmbH (Kulmbach, Germany): eGFP-targeting siRNA (siGFP) (sense: 5'-AuAucAuGGccGAcAAGcAdTsdT-3'; antisense: 5'-UGCUUGUCGGCcAUGAuAUdTsdT-3') for silencing of eGFPLuc; EG5-targeting siRNA (siEG5) (sense: 5'-ucGAGAAucuAAAcuAAcudTsdT-3'; antisense: 5'-AGUuAGUUuAGAUUCUCGAdTsdT-3') for silencing EG5 motor protein; control siRNA (siCtrl) (sense: 5'-AuGuAuuGGccuGuAuuAGdTsdT-3'; antisense: 5'-CuAAuAcAGGCcAAuAcAUdTsdT-3'); Cy5-labeled siRNA (Cy5-siAHA1) (sense: 5'-(Cy5)(NHC6)GGAuGAAGuGGAGAuuAGudTsdT-3'; antisense: 5'-ACuAAUCUCcACUUcAUCCdTsdT-3'); Apoptotic peptides modified siRNA, disulfide-siEG5 (sense: 5'-(C6SSC6)ucGAGAAucuAAAcuAAcudTsdT-3'; antisense: 5'-AGUuAGUUuAGAUUCUCGAdTsdT-3') and disulfide-siCtrl (sense: 5'-(C6SSC6)AuGuAuuGGccuGuAuuAGdTsdT-3'; antisense: 5'-CuAAuAcAGGCcAAuAcAUdTsdT-3'); small letters: 2'-methoxy-RNA; s: phosphorothioate. Cell culture media, antibiotics and fetal calf serum (FCS) were purchased from Invitrogen (Karlsruhe, Germany), HEPES from Biomol GmbH (Hamburg, Germany), glucose from Merck (Darmstadt, Germany), agarose (NEEO

Ultraquality) and ammonia solution 25% from Carl Roth GmbH (Karlsruhe, Germany), and GelRed™ from VWR (Darmstadt, Germany). Cell culture lysis buffer and D-luciferin sodium salt were obtained from Promega (Mannheim, Germany).

2.2 Methods

2.2.1 Loading of 2-chlorotrityl chloride resin with Fmoc-protected amino acids

2-chlorotrityl chloride resin (500 mg, chloride loading 1.55 mmol/g) was swelled in dry DCM for 10 min for two times. Subsequently, 0.4 eq mmol Fmoc-L-Cys(Trt)-OH (or Fmoc-L-Tyr(tBu)-OH) and 0.9 eq mmol DIPEA were added to the resin and incubated at RT for 1 h. After removing the reaction solvents, the resin was incubated with a mixture of DCM/MeOH/DIPEA (80/15/5 v/v/v) for 10 min for two times at RT. After removal of the reaction mixture, the resin was washed 5 times with DCM and about 30 mg of the resin was separated for the loading determination. Therefore, an exact amount of resin was treated with 1 mL deprotection solution (20% piperidine in DMF) for 1 h. Afterwards, the solution was diluted, and absorption was measured at 301 nm. The loading was then calculated according to the equation: resin load [mmol/g] = (A*1000)/(m [mg]*7800*d_f) with d_f as dilution factor. The rest resin was washed 3 times with DMF, and then was treated 5 times for 10 minutes with 20 % piperidine in DMF. Reaction progress was monitored by Kaiser test. Finally, the resin was washed 3 times with DMF, 3 times with DCM, 3 times with n-hexane and dried under vacuum.

2.2.2 Synthesis of oligomers

Oligoaminoamides were synthesized analogously as previously reported [28, 65-68] by standard Fmoc-based solid phase supported peptide synthesis in syringe reactors. 2-Chlorotrityl chloride resin was used as solid support. The synthesis of oligomers contained three main process: loading, coupling and cleaving off the resin. The protocol of TFA cleavage condition was used as previously described, with pre-cooling to avoid hydroxylation of the oleic acid double bonds.[67] For the PEG-AP-1 targeting

domain, the 3-mercaptopropionic acid-PEG-AP1 sequence was synthesized manually by Fmoc solid-phase peptide synthesis using a syringe microreactor. After standard deprotection and cleavage condition (TFA/TIS/H_2O 95:2.5:2.5), the peptide conjugate was specifically coupled *via* its N-terminal 3-mercaptopropionic acid with maleimide-PEG_4-DBCO at neutral pH in solution. For the apoptotic peptide syntheses, the sequences were synthesized by Fmoc solid-phase peptide synthesis using a syringe microreactor. An N-terminal cysteine was incorporated onto these apoptotic peptides for subsequent coupling with the free thiol of siRNA sense strand.

2.2.3 Synthesis of different siRNA-Apoptotic peptide conjugates

The sense strand of the applied siRNA contained a 5'-end modification with C6-ss-C6 spacer. The modified siRNA was incubated with tris(2-chlorethyl) phosphate (TCEP, 10 equiv.) for 30 min at 25 °C, resulting in a free thiol on the 5'-end. Purification was performed by ethanol precipitation and dissolved in water to a concentration of 1 mM. The apoptotic peptides were incubated with 5,5'-dithiobis (2-nitrobenzoic acid) (DTNB, 10 equiv.) for 1h at RT to activate the thiol. The activation product was purified by HPLC (VWR Hitachi Chromaster consisting of 5430 Diode array detector and 5160 gradient pump, Darmstadt, Deutschland). The products were separated with a XTerra C8 column (5 µm, 4.6 x 150 mm, Waters, Eschborn, Germany) and eluted with an ACN/0.1M triethylammonium acetate gradient (95:5 to 35:65 in 45 min, pH 8). Product containing fractions were lyophilized. The resulting activated apoptotic peptides (1.5 equiv.) was incubated with free thiol of siRNA. The resulting siRNA-apoptotic peptide conjugates were purified by HPLC using the same conditions as described above. Fractions were collected and lyophilized and dissolved in 20mM HEPES buffered 5% glucose pH 7.4 (HBG) at a concentration of 500 ng/mL. The siRNA conjugates were analyzed in a 3.5% agarose gel (100 mV for 100 min) and MALDI-TOF-MS analysis. The dimer siRNA and pure siRNA were regarded as controls to determine the purity of siRNA conjugate.

2.2.4 Synthesis of modified Hyaluronic acid-DBCO

HA (20 kDa sodium salt, 5 mg, 0.012 mmol monomers), NHS (N-hydroxysuccinimide, 5eq. 0.06 mmol, 6.9 mg), EDC (3-(ethyliminomethyleneamino)-N,N-dimethylpropan-1-amine; 5eq. 0.06 mmol, 11.5 mg) were dissolved in 100 mL activation buffer (0.1M, TES, 2-[[1,3-dihydroxy-2-(hydroxymethyl)propan-2-yl]amino]ethanesulfonic acid). The pH was adjusted to 7. Afterwards, DBCO-amine (2eq. 0.024 mmol, 6.6 mg) in DMF was added into above solutions. After overnight, the product was purified by dialysis with a 3500 Da cut-off membrane against deionized water. The yield of DBCO-HA was 75 % by calculation of weight after lyophilization. The substitution degree for HA carboxylic groups was 8% according to the ^{1}H-NMR spectrum, which was also confirmed by the increase in absorbance at 309 nm using an extinction coefficient of 12,000 $M^{-1} \cdot cm^{-1}$.

2.2.5 Kaiser Test

Free amines of deprotected amino acids on the resin were determined qualitatively by the Kaiser test [67]. A small sample of DCM washed resin was transferred into an Eppendorf reaction tube. One drop of each 80 % phenol in EtOH (w/v), 5 % ninhydrin in EtOH (w/v) and 20 µM potassium cyanide (KCN) in pyridine (mixture of 1 mL aqueous 0.001 M KCN solution and 49 mL pyridine) were added. The tube was incubated at 99 °C for 4 min under shaking. The presence of free amines was indicated by a deep blue color.

2.2.6 General Cleavage conditions

All oligomers were cleaved off the resin by incubation with TFA–TIS–H_2O (95 : 2.5 : 2.5) (10 mL g−1 resin) for 90 min. The cleavage solution was concentrated by flushing nitrogen and oligomers were precipitated in 50 mL of pre-cooled MTBE – n-hexane (1 : 1). All oligomers were purified by size exclusion chromatography using a Äkta purifier system (GE Healthcare Bio-Sciences AB, Uppsala, Sweden), a Sephadex G-10

column and 10 mM hydrochloric acid solution–acetonitrile (7 : 3) as solvent. All oligomers were lyophilized.

2.2.7 Cleavage of oligomers containing oleic acid

The cleavage of the structures off the resin was performed according to an optimized protocol by incubation with TFA–TIS–H2O 95 : 2.5 : 2.5 (10 mL/g resin cooled to 4 °C prior to addition) for 30 min followed by immediate precipitation in 40 mL of pre-cooled MTBE – n-hexane (1 : 1). The oleic acid containing oligomers were then purified by size exclusion chromatography using a Äkta purifier system (GE Healthcare Bio-Sciences AB, Uppsala, Sweden), a Sephadex G-10 column and 10 mM hydrochloric acid solution–acetonitrile (7 : 3) as solvent. The oligomers were lyophilized.

2.2.8 siRNA formulation

500 ng of siRNA and the calculated amount of oligomers at the indicated nitrogen/phosphate (N/P) ratios were separately diluted in 10 µL of HBG. Only protonatable nitrogens were considered into N/P calculation. The oligomers solution was added in the nucleic acid solution and mixed by pipetting up and down (3 times) to obtain a homogeneous state. The polyplexes were incubated for 45 min at RT. For modification of siRNA polyplexes with DBCO agents, the ratio of volume of DBCO solutions and polyplexes was 1/4. Equivalents refer to the molar ratios of shielding or targeting agents to oligomers in the final solution. The incubation time between azide and DBCO click chemistry was 4 h.

2.2.9 High-performance liquid chromatography (HPLC)

The siRNA-Apoptotic peptides conjugates were purified by HPLC (VWR Hitachi Chromaster consisting of 5430 Diode array detector and 5160 gradient pump, Darmstadt, Deutschland). The products were separated with a XTerra C8 column (5 µm, 4.6 x 150 mm, Waters, Eschborn, Germany) and eluted with an ACN/0.1M

triethylammonium acetate gradient (95:5 to 35:65 in 45 min, pH 8). Product containing fractions were lyophilized.

2.2.10 ^{1}H-NMR spectroscopy

^{1}H NMR spectra was performed using a Jeol JNMR-GX 400 (400 MHz) or JNMR-GX 500 (500 MHz) without TMS as internal standard. Deuterium oxide (D_2O) was used as solvent. All chemical shifts were calibrated to the residual proton signal of the solvent and are reported in ppm. Data are presented as s = singlet, d = doublet, t = triplet, m = multiplet. The spectra were analyzed with MestReNova (MestReLab Research).

2.2.11 MALDI mass spectrometry

One µL matrix droplet consisting of a saturated solution of Super-DHB (sum of 2,5-dihydroxybenzoic acid and 2-hydroxy-5-methoxybenzoic acid) in acetonitrile / water (1 : 1) containing 0.1 % (v/v) TFA was spotted on an MTP AnchorChip (Bruker Daltonics, Bremen, Germany). After the Super-DHB matrix had crystallized, one µL of the sample solution (10 mg/mL in water) was added to the matrix spot. Samples were analyzed using an Autoflex II mass spectrometer (Bruker Daltonics, Bremen, Germany). All spectra were recorded in positive mode.

2.2.12 siRNA binding assay

A 2.5% agarose gel containing GelRed® was prepared. Formulations were prepared with 500 ng of siRNA and diluted to a final volume of 20 µL. Samples were mixed with loading buffer (6 mL of glycerol, 1.2 mL of 0.5 M EDTA, 2.8 mL of H_2O, 0.02 g of bromophenol blue). Electrophoresis was performed at 100 V for 40 min.

2.2.13 siRNA polyplexes stability in 90% serum

Polyplexes were formed using 2.5 µg siRNA mixed with the oligomer at N/P 12 resulting in a total volume of 10 µL. Afterwards, the incubation 90 µl fetal bovine serum

(FBS) was added to the samples. All samples had a final concentration of 90 % FBS. The samples were incubated at 37 °C for 2 h. 20 µL of the samples and 4 µL loading buffer were carefully mixed and a binding assay (see 2.2.12) was performed.

2.2.14 Particle size and zeta potential

Polyplexes were formed using 4 µg siRNA and diluted with HBG to a total volume of 20 µL. After 45 min incubation time, polyplexes were diluted with HEPES solution to 800 µL volume. The polyplex solution was measured in a folded capillary cell (DTS 1070) using a Zetasizer Nano ZS (Malvern, Worcestershire, UK) with a flexible attenuator at an angle of 173 °. The refractive index of the solvent was 1.330 and the viscosity was 0.8872 mPa·s. Samples where measured three times with six sub runs each. Afterwards, zeta potential was measured with a flexible attenuator at a 90 ° angle. Samples were measured three times (10000 total counts, usually 12-15 sub runs). The temperature was set at 25 °C.

2.2.15 Cell culture

Human cervix carcinoma cells HeLa, KB (subclone of HeLa) and human liver carcinoma cells Huh 7 were cultured in Dulbecco's modified Eagle's medium (DMEM), supplemented with 1 g/L glucose, 10% FBS, 4 mM stable glutamine, 100U/mL penicillin and 100 µg/mL streptomycin. Human breast adenocarcinoma cells MDA-MB-231 stably transfected with the eGFPLuc gene (MDA-MB-231/eGFPLuc) and KB cells stably transfected with the eGFPLuc gene (KB/eGFPLuc) were cultured in RPMI 1640 medium (Invitrogen, Karlsruhe, Germany), supplemented with 10% FBS, 4 mM stable glutamine, 100U/mL penicillin and 100 µg/mL streptomycin. Huh 7 cells stably transfected with the eGFPLuc gene (Huh 7/eGFPLuc) were cultured in Dulbecco's modified Eagle's medium (DMEM)/Nutrient Mixture F-12 Ham, supplemented with 10% FBS, 4 mM stable glutamine, 100U/mL penicillin and 100 µg/mL streptomycin. Human lung carcinoma cells A549 was cultured in Dulbecco's modified Eagle's medium

(DMEM), supplemented with 4.5 g/L glucose, 10% FBS, 4 mM stable glutamine, 100U/mL penicillin and 100 µg/mL streptomycin. The cells were maintained in ventilated flasks in the incubators at 37 °C with 5% CO_2 in a humidified atmosphere. Cell lines were grown to 80-90% confluency and harvested.

2.2.16 Cell internalization

Cells were seeded in 24-well plates at a density (90000 cells/well for Huh 7) for 24h before the experiment. Polyplexes containing 1.35 µg of siRNA, including 20% Cy5-labeled siRNA, were added into each well incubated 45 min at 37 °C in 5% CO2. Afterwards, cells were treated with PBS to remove non-bound polyplexes. Then cells were incubated with 500 I.U. heparin to remove the polyplexes associated to the cells surface. Finally, the cells were collected and resuspended in PBS buffer with 10% FBS. The samples were mixed with DAPI at a final concentration of 1 ng/µL before flow cytometry measurement. Dead cells were differentiated by DAPI fluorescence and removed by gating in order to analyze the cellular uptake of polyplexes into living cells. The amount of Cy5-labeled living cells was counted through excitation at 635 nm and detection of emission at 665 nm. The results were evaluated by the FlowJo 7.6.5 software. All experiments were performed in triplicates.

2.2.17 Endocytosis pathway

For the endocytosis pathway, KB and Huh 7 cell lines were seeded into 24-well-plates at a density of 16000 cells/well. To determine the endocytosis pathway, the cells were pre-incubated with different inhibitors diluted in Millipore water at different concentrations (nystatin 15 µg/mL, sucrose 154 mg/mL, amiloride 133 µg/mL, sodium azide 1 mg/mL, HA 10 mg/mL) for 1 h at 37°C. The medium was changed and incubated at 37°C for 2h after adding polyplexes containing 1.35 µg of siRNA (containing 20% of Cy5-labeled siRNA). The samples were prepared for flow cytometric measurements with LSR Fortessa (BD biosciences, Singapore) as

described above. All experiments were performed in triplicates and evaluated by the FlowJo 7.6.5 software.

2.2.18 Transmission electron microscopy (TEM)

Carbon coated copper grids (Ted Pella, Redding, CA, USA, 300 mesh, 3.0 mm O. D.) were hydrophilized with a plasma cleaner under argon atmosphere. Afterwards, the grids were placed activated face down on 10 µL of the siRNA polyplex solution at N/P 12 (diluted in water). Incubation time was 3 min. The liquid was removed using a filter paper. Subsequently, the copper grid was washed with 5 µL staining solution (1% uranyl format in purified water, Sigma-Aldrich, Munich, Germany), which was immediately removed. Staining was achieved with 5 µL of the same solution that was left on the grid for 5 s. Afterwards, all liquid was removed with a filter paper. Grids were stored at room temperature and they were analyzed using JEM 1011 transmission electron microscope (JEOL, Tokyo, Japan) at 80 kV acceleration voltage.

2.2.19 Lysotracker assay

For subcellular distribution, Huh 7 cell lines were seeded into 8-well chamber at a density (15000 cells/well) for 24h prior to the experiment. Polyplexes were formed as described using 20% Cy5-labeled siRNA at N/P 12 and diluted to a final siRNA concentration of 370 nM in HBG. After 2 h of incubation at 37°C, the medium was changed before 0.1 µL of LysoTrackerGreen solution (Fisher Scientific) was added into each well. The cells were washed twice with 100 µL PBS and incubated for 1h in 37°C incubators. After adding the Hoechst 33342, the cells were directly measured by confocal laser scanning microscopy.

2.2.20 Gene silencing with siRNA

Gene silencing experiments were performed with IL4 receptor-positive KB/eGFPLuc cells and Huh 7/eGFPLuc cells. Applied siRNAs were siGFP for silencing the eGFPLuc

fusion protein and the control siCtrl. Cells were seeded in 100 µL of medium using 96-well plates at a density (8000 cells/well for Huh 7/eGFPLuc cells and KB/eGFPLuc cells) for 24h prior to the experiment. After the medium was replaced with 80 µL of fresh medium, cells were transfected with 20 µL of polyplexes containing 500 ng of siRNA at certain N/P ratio at 37 °C for 4 h. Afterwards, the medium was replaced with fresh one and cells were incubated 48h. Before measuring the luciferase activity, 100 µL of cell lysis regent (Promega, Mannheim, Germany) was added to cells per well. The luciferase assay kit (Promega, Mannheim, Germany) and a Centro LB 96 plate reader luminometer (Berthold, Bad Wildbad, Germany) were used. The relative light units (RLU) were related to HBG buffer-treated control cells.

2.2.21 Cell viability

To measure cytotoxicity mediated by EG5 knockdown and/or apoptotic peptide conjugates, the apoptotic peptide modified siRNAs siEG5-apoptotic peptide (siEG5-KLK, siEG5-BAK, siEG5-BAD) and their control siCtrl-apoptotic peptide conjugates (siCtrl-KLK, siCtrl-BAK, siCtrl-BAD) were used. Cells were seeded on 96-well plate in 100 µL of medium 24h before the experiment. Medium was replaced by 80 µL of fresh medium. Formulation were formed using 20 µL of polyplexes containing 500 ng either siRNA or siRNA-apoptotic peptide conjugates at N/P ratio of 12. After incubation at 4h, the medium was replaced with 100 µL of fresh medium and cells were cultured for 48 h. MTT assay (Life Technology, Darmstadt, Germany) was performed to evaluate the cell viability. The experiments were performed in triplicates using SpectraFluor Plus microplate reader (Tecan, Austria).

2.2.22 Fluorescence microscopy of aster formation

Huh 7 cells and KB cells (20 000 cell/well) were seeded in 300 µL of medium using 8-well Lab-Tek chamber slides for 24 h. After seeding medium was replaced with 250 µL of fresh medium, 50 µL of polyplexes containing 1.5 µg of either siRNA or siRNA-

apoptotic peptide conjugate was added. Medium was replaced by fresh medium 4 h after transfection. After 48 h medium was removed, PBS was added to wash the cells. The cells were fixed with 4 % PFA and then cell nuclei were stained by DAPI. The data was obtained from Axiovert 200 fluorescence microscope (Carl Zeiss, Oberkochen, Germany).

2.2.23 JC-1 assay

Huh 7 cells (140 000 cells per well) were seeded into 12-well plates for 24 h. The cells were incubated with 1) the ***1208*** + siCtrl + AP-1; 2) ***1208*** + siCtrl-KLK + AP-1; 3) ***1208*** + siEG5 + AP-1; 4) ***1208*** + siEG5-KLK + AP-1, loaded with siRNA at a dose of 2.7 µg for 4 hours. The medium was replaced with fresh medium and cells were cultured for 48 hours. Afterwards, the cells were collected and suspended in 1 mL of warm PBS buffer. For positive control, 1 µL of 50 mM CCCP was added and cells were incubated for 5 min. Afterwards, 10 µL of 200 µM JC-1 was added each sample and incubated for 20 min. Cells were collected and analyzed by a flow cytometry using 488 nm excitation.

2.2.24 Annexin V-FITC / PI apoptosis assay

Huh 7 cells (140 000 cells per well) were seeded into 12-well plates for 24 h. The cells were incubated with 1) the ***1208*** + siCtrl + AP-1; 2) ***1208*** + siCtrl-KLK + AP-1; 3) ***1208*** + siEG5 + AP-1; 4) ***1208*** + siEG5-KLK + AP-1, loaded with siRNA at a dose of 2.7 µg for 4 h. The medium was replaced with fresh medium and cells were cultured for 24 h and 48 h. Afterwards, the cells were collected and suspended in 0.5 mL of 1 × binding buffer, followed by washes twice with ice-cold PBS. Annexin V-FITC (2 µL, 0.15 mg/mL, BioVision, USA) was added into the cell suspension with an incubation for 15 min and the cells were immediately analyzed by a flow cytometry after adding 2 µL of propidium iodide PI (1 mg/mL, BioVision, USA).

2.2.25 Animal tumor model

Female 8-week-old nude mice, Rj: NMRI-nu (nu/nu) (Janvier, Le Genest-Saint-Isle, France), were housed in isolated ventilated cages and acclimated for at least 7 days prior to experiments. Animals were injected with 5×10^6 Huh 7 hepatocellular carcinoma cells subcutaneously for biodistribution study and EG5 silencing assay in vivo. The body weight was recorded, and the tumor volume was measured by caliper and calculated as [0.5 × (longest diameter) × (shortest diameter)^2]. All animal experiments were performed according to guidelines of the German law for the protection of animal life and were approved by the local animal ethics committee.

2.2.26 Biodistribution

For near infrared (NIR) in vivo imaging, unlabeled control siRNA (siCtrl) was spiked with 50% of Cy7-labeled siRNA (Cy7-siAHA1). When tumors reached the size of 500 mm^3, the mice (n = 3/per group) were anesthetized with 3% isoflurane in oxygen. siRNA polyplexes (N/P 12) in 250 µL of HBG were injected intravenously (i.v.), and fluorescence was measured with a CCD camera at different time points. For evaluation of images, efficiency of fluorescence signals was analyzed after color bar scales were equalized using IVIS Lumina system with Living Image software 3.2 (Caliper Life Sciences, Hopkinton, MA, USA).

2.2.27 Gene silencing of EG5 *in vivo*

When tumors reached 500 mm^3, mice (n = 5/per group) were injected i.v. with siRNA polyplexes containing 50 µg of siEG5 or siCtrl (N/P 12) 48 h and 24 h before euthanasia. As a part of terminal procedure, blood samples were obtained by cardiac puncture for blood biochemistry examinations. After tumors were harvested and homogenized, total RNA was extracted using Trifast (Peqlab, Erlangen, Germany) according to the manufacturer's protocol, and then the reverse transcription and qRT-PCR were performed. Total RNA was isolated followed by reverse transcription using qScriptTM

cDNA Synthesis Kit (Quantabio, Beverly, USA) according to the manufacturers' protocols. Quantitative RT-PCR was performed in triplicates on a LightCycler 480 system (Roche, Mannheim, Germany) using UPL Probes (Roche, Mannheim, Germany) and Probes Master (Roche, Mannheim, Germany) with GAPDH as housekeeping gene. The following probes and primer sequences were used: human GAPDH (ready-to-use in UPL, UPL Probe #45), human EG5 (UPL Probe #53) (forward: CATCCAGGTGGTGGTGAGAT, reverse: TATTGAATGGGCGCTAGCTT). Results were analyzed by the ΔCT method. CT values of GAPDH were subtracted from CT values of EG5. ΔCT values of cationic and anionic siRNA polyplexes groups were calculated as percentage relative to untreated HBG control groups.

2.2.28 Blood biochemistry examinations

To isolate plasma, blood samples were collected in EDTA-coated tubes (Multivette 600, Sarstedt, Nümbrecht, Germany) and centrifuged at 3000 rpm for 7 minutes. The supernatant was analyzed for clinical biochemistry parameters: alanine aminotransferase (ALT), aspartate aminotransferase (AST), blood urea nitrogen (BUN) and creatinine in the Clinic of Small Animal Medicine, Faculty of Veterinary Medicine, Ludwig-Maximilians-Universität München.

2.2.29 Staining, imaging and 3D reconstruction

Mice (n = 3/per group) with tumor xenograft over 500 mm^3 were injected intravenously with cationic or anionic polyplexes containing 50 µg of siCtrl spiked with 50% of Cy3-labeled siRNA (Cy3-siAHA1) (N/P 12), and anesthetized with Ketamine/Xylaxin at 0.1 mL/10g bodyweight at 5 min and 45 min after injection. Upon sacrification, mice were perfused transcardially using PBS at 10mL/min for 1min, followed by 1% paraformaldehyde PFA in PBS at the above same speed for 3min. Subsequently, mice were blocked with 1% BSA (97061-420; VWR, PA, USA) in PBS at 10mL/min for 1min and stained by 50mL DyLight 488 labeled lycopersicon esculentum tomato lectin (20

µg/mL in PBS, DL-1174-1; Vector Laboratories, Burlingame, CA, USA) at 10mL/min. Finally, mice were washed using 1% BSA in PBS for 1 min. Tumor xenograft and organs (kidneys) were harvested for 50 µm thick sections using a Vibratome (VT1000S; Leica, Wetzlar, Germany). Free-floating sections were then collected and mounted with antifade mounting medium (H-1400, Vector Laboratories, Burlingame, CA, USA) and scanned in a Z-stack manner with 1 µm interval using a confocal microscope system (LSM780, Zeiss, Oberkochen, Germany) within 12h due to the easily degradable character of tomato lectin. Corresponding 3D reconstruction was performed using Imaris 9.0.1(Bitplane, Belfast, UK).

3. Results and Discussion

3.1 IL4-receptor-targeted antitumoral apoptotic peptide - siRNA conjugate lipoplexes

Section 3.1 has been adapted from: Jie Luo, Miriam Höhn, Sören Reinhard, Dominik M. Loy, Philipp Michael Klein and Ernst Wagner, Adv. Funct. Mater. 2019, 29, 1900697.

siRNA has the potential to downregulate disease-related gene expression in a selective and sequence-dependent manner, and thereby provides a promising therapeutic approach for severe diseases including genetic diseases or cancer.[69] The first siRNA drug, Patisiran, a liposomal formulation of transthyretin (TTR) siRNA for treatment of hereditary transthyretin-mediated (ATTR) amyloidosis by gene silencing in the liver, has obtained market approval by the US FDA in August 2018.[70] Although the biological process of gene silencing is well understood, the main challenge of siRNA therapeutics remains the efficient delivery to target sites different from liver tissue.[71-73] Steps such as specific recognition of the target cells, stability and protection in the cellular environment, and entrance into the cytosol remain challenging bottlenecks in the delivery process. Naked siRNA molecules have limited stability in biological environments, subjected to fast elimination by the kidneys, and their crossing of cell membranes is restricted by the hydrophilicity, negative charge and large molecular weight. Thus chemical modification, conjugation or formulation of siRNA with carriers, such as liposomal or polymers-based complexes, can improve the intracellular delivery.[74-76]

Sequence-defined oligoaminoamides present a class of nucleic acid carriers with multifunctionality and high chemical precision.[17, 77, 78] In our previous work, we developed a series of sequence-defined oligoaminoamide carriers with targeting and shielding domains for nucleic acid transfections.[28, 33, 79-81] Libraries of lipo-oligomers were precisely assembled *via* solid phase-supported synthesis (SPSS)

using artificial oligoamino acids and fatty acids.[32, 65, 82, 83] These different structures of oligomers with functional moieties mediated enhanced cellular uptake, protection of siRNA against degradation, endosomal escape into the cytosol, and thus improved gene silencing efficiency. Introduction of shielding and ligand domains was found to be essential for specific siRNA delivery into cancer cells.[28, 84, 85] Polyethylene glycol (PEG) is known to improve stability of polyplexes and to shield their surface, thus reducing binding and aggregation with negative-charged serum proteins within the blood circulation.[86-88] Targeting ligands for binding to overexpressed cell surface receptors have been also taken into consideration for preferential transfection of the intended tissue.[65, 89]

Based on our understanding of the relationship between structure and activity of previous oligoaminoamide libraries and nanoparticle shields, the present study aims at a more effective design of a dual-antitumoral siRNA conjugate formulated with a new precise multifunctional carrier.

Previous studies applied siRNA targeting Eglin 5 (EG5), a member of the kinesin-5 family, which is involved in the assembly of the mitotic spindle apparatus and required for centrosome separation.[90] EG5 silencing results in mitotic arrest and tumor cell death.[38, 91, 92] In our previous studies potent antitumoral activity required combination with other drug agents (methotrexate or pretubulysin).[38, 65] Pro-apoptotic peptides present another class of potent anti-cancer agents, provided that they can be effectively delivered into cells, such as by covalent attachment to polymeric carriers.[93] Our current study explores the novel strategy to conjugate an apoptotic peptide with siRNA for efficient intracellular co-delivery. After screening siRNA conjugates with various apoptotic peptides (KLK, BAK, BAD), EG5 siRNA conjugated with KLK provided enhanced tumor cell killing by the combined mechanism of EG5 silencing and destabilization of mitochondrial membranes.

Furthermore, the current study capitalizes on targeting the siRNA-apoptotic peptide containing nanoparticles to the interleukin-4 receptor (IL-4R), which is overexpressed on a variety of solid cancers.[94-96] AP1, a peptide designed as a ligand from atherosclerotic plaque-specific peptide-1, was utilized for binding to the IL-4R; this peptide has been previously used for tumor targeted liposome and nanoparticle delivery.

3.1.1 Design and synthesis of azide-bearing T-shaped oligoaminoamides

Based on the cationizable building block succinoyl-tetraethylene-pentamine (Stp) and related analogs,[28, 97] which enable electrostatic interaction with nucleic acids (polyplex formation) and endosomal escape of delivered cargo into the cytosol due to further endosomal protonation, we have synthesized by solid phase-supported synthesis (SPSS) a library of more than 1200 cationizable structures as carriers for drug,[98] protein,[99] and nucleic acid delivery.[80, 100] T-shapes present a topological subclass of such carriers especially suitable for the delivery of siRNA.[32, 82, 101] siRNA is far smaller than plasmid DNA and therefore requires additional polyplex stabilization beyond electrostatic interaction.[30, 102] The T-shape structured oligomer ***454*** (**Tab. 2**), which was one starting point for this work, contains a cationic backbone of four repeats of Stp, as well as N- and C-terminal units of three tyrosines and a cysteine, as well as a central branch containing two oleic acids (OleA) for hydrophobic siRNA polyplex stabilization.[103, 104] An analog, oligomer ***992*** (**Tab. 2**), containing the bioreducible building block ssbb[66] incorporated into the oligoaminoamide backbone, was previously found to be more effective and biocompatible than the ssbb-free stable analog. N-terminal incorporation of an azido lysine into T-shape oligomers resulted in the design of oligomers like ***1106*** (**Tab. 2**) which enabled subsequent shielding and targeting of formed polyplexes by copper-free click chemistry.[65, 105]

Designing new multifunctional oligoaminoamides (**Fig. 4)** for the IL-R4 targeted delivery of apoptotic peptide-siRNA conjugates, we considered the following five points. 1) an azido function was to be incorporated into all oligomers for subsequent functionalization with AP1 targeting peptides; 2) as the cargo (siRNA-SS-apoptotic peptide) presents a bioreducible conjugate, the carrier had to be free of terminal cysteines as contained in ***454***; 3) optionally the bioreducible building block ssbb was incorporated into the oligomer backbone, in order to see whether a reducible lipopolyplex would perform better; 4) incorporation of histidines[79] and especially alternating histidine – Stp units might improve the endosomal escape capability;[79, 98] and 5) extension of the cationic backbone by duplication of the Stp (or Stp-His) domains for enhanced polyplex stability.[81] Based on these considerations, we synthesized four oligomers (***1208***, ***1209***, ***1210*** and ***1211***) derived from oligomers ***454*** and four bio-reducible oligomers (***1217***, ***1218***, ***1219*** and ***1220***) derived from the ssbb building block containing oligomers ***992*** (**Fig. 4**, **Tab. S1**, **Fig. S1** and **Fig. S2**).

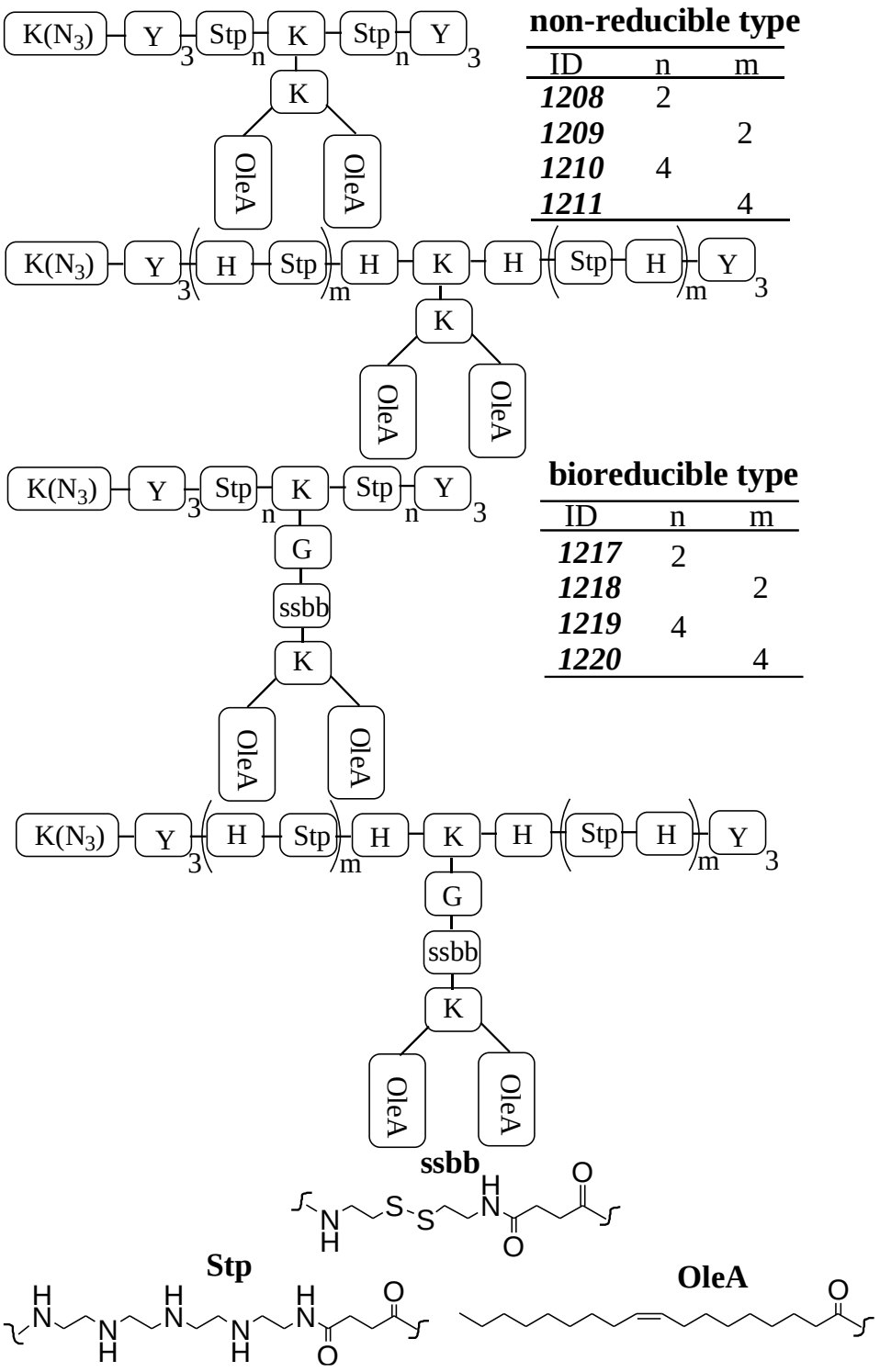

Fig. 4. Overview of chemical compounds. Schematic illustration of new sequence-defined oligomers, non-reducible (***1208***, ***1209***, ***1210*** and ***1211***) and bioreducible type (***1217***, ***1218***, ***1219*** and ***1220***). Units of the oligomers: Y: tyrosine, K: lysine, H: histidine, Stp: succinoyl-tetraethylene-pentamine, OleA: Oleic acid, G: glycine, ssbb: succinoyl-cystamine, ss building block. The ID are the internal database identification number.

Tab. 2 Sequences of plain lipo-oligomers. CholA: cholanic acid. Sequences (left to right) from N- to C-terminus.

ID	Oligomer sequences
454	C-Y_3-Stp_2-K(K(OleA)$_2$)-Stp_2-Y_3-C
992	Y_3-Stp_2-K(G-ssbb-K(CholA)$_2$)-Stp_2-Y_3
1106	K(N_3)-Y_3-Stp_2-K(G-K(CholA)$_2$)-Stp_2-Y_3

Tab. 3 Sequences of different apoptotic peptides, which were provided with N-terminal cysteines for conjugation with siRNA by disulfide bond formation, and AP-1 targeting and PEG shielding domains. Sequences (left to right) from N- to C-terminus.

Peptide name	Peptide sequences	Molecular weight
Apoptotic peptide KLK	CGGKLAKLAKKLAKLAK	1741
Apoptotic peptide BAK	CGGQVGRQLAIIGDDINR	1883
Apoptotic peptide BAD	CGNLWAAQRYGRELRRMSDEFVD	2773
AP-1 targeting domain	DBCO-(3-mercaptopropionic acid)--PEG_{24}-NRDLRKR	2846
PEG shielding domain	DBCO-(3-mercaptopropionic acid)-PEG_{24}	1907

3.1.2 Design and synthesis of the AP-1 targeting domain

For shielding and targeting siRNA core nanoparticles formed with the azido-lipo-oligomers, DBCO–PEG-AP-1 conjugates were synthesized. In our previous work, DBCO-PEG-folate conjugates were synthesized completely by SPSS.[65] As DBCO was found unstable under standard (95% TFA) peptide deprotection and cleavage conditions,[65] a cleavage protocol using 5% TFA was developed. In the current work, a different strategy had to be applied. The IL-4 receptor binding peptide AP-1[94] (sequence listed in **Tab. 3**) was first synthesized by standard SPSS, with a precise monodisperse PEG_{24} (24 ethylene oxide units) and an N-terminal 3-mercaptopropionic acid also incorporated into the sequence. After cleavage of this PEG-AP-1 sequence from solid phase, the terminal thiol group was specifically reacted in solution with maleimide-DBCO at neutral pH.

3.1.3 Design and synthesis of dual antitumoral siRNA-apoptotic peptide conjugates

The targeted siRNA polyplex delivery system is designed to include multifunctional substructures for siRNA intracellular delivery, but the overall siRNA antitumoral effect remains a critical decisive aspect. Short peptides containing pro-apoptotic subgroups that antagonize anti-apoptotic biological factors have been developed as means of restoring normal apoptotic signaling.[93] Some reported concept used lytic or apoptotic peptide covalently attached to polymeric carriers. Sarangthem et al. showed that elastin-like polypeptide (ELP) as basic delivery carrier could enhance the cytotoxic effect of peptide KLAK. Albarran et al. published that the incorporation of pH-responsive, membrane-destabilizing poly (propylacrylic acid) (PPAA) markedly enhanced the killing effect of BAK BH3 peptides, which induces apoptosis *via* antagonization of suppressor targets such as Bcl-2. In our study, three apoptotic peptides (KLK, BAK, BAD), which are the antibacterial and mitochondrial membrane disruptive artificial peptide KLK, or peptides derived from the BH3 domain of BAK and BAD proteins (**Tab. 3**), for the first time were directly coupled to the siRNA's backbone to ensure cytosolic co-delivery and thereby achieving a dual antitumoral effect. Cysteine was chemically integrated at the N-terminus of these peptides sequences, and the peptides were covalently conjugated to the 5'-end of the siRNA's sense strand, to avoid any negative steric effect of the modification on the silencing efficiency. Importantly, the conjugate linkage by disulfide bond allows cytosolic separation of the two different antitumoral agents after delivery. When conjugates reach the cytosol of tumor cells, the strongly increased concentration of glutathione (GSH, ~ 1-11 mM) is supposed to cleave the disulfide linkage, and the two active substructures could thereby separately achieve their apoptotic functions in different pathways. As shown in **Fig. 5A**, the conjugates were prepared by activation of the apoptotic peptide's C-terminal cysteine and subsequent reaction with the siRNA's thiol group. After purification of conjugates by high-performance liquid chromatography (HPLC), the purity of conjugates was analyzed by agarose gel electrophoresis; the apoptotic

peptide-siRNA conjugates were also analyzed by MALDI-TOF-MS (**Fig. 5 B-D**, **Fig. 6 and Fig. 7**)

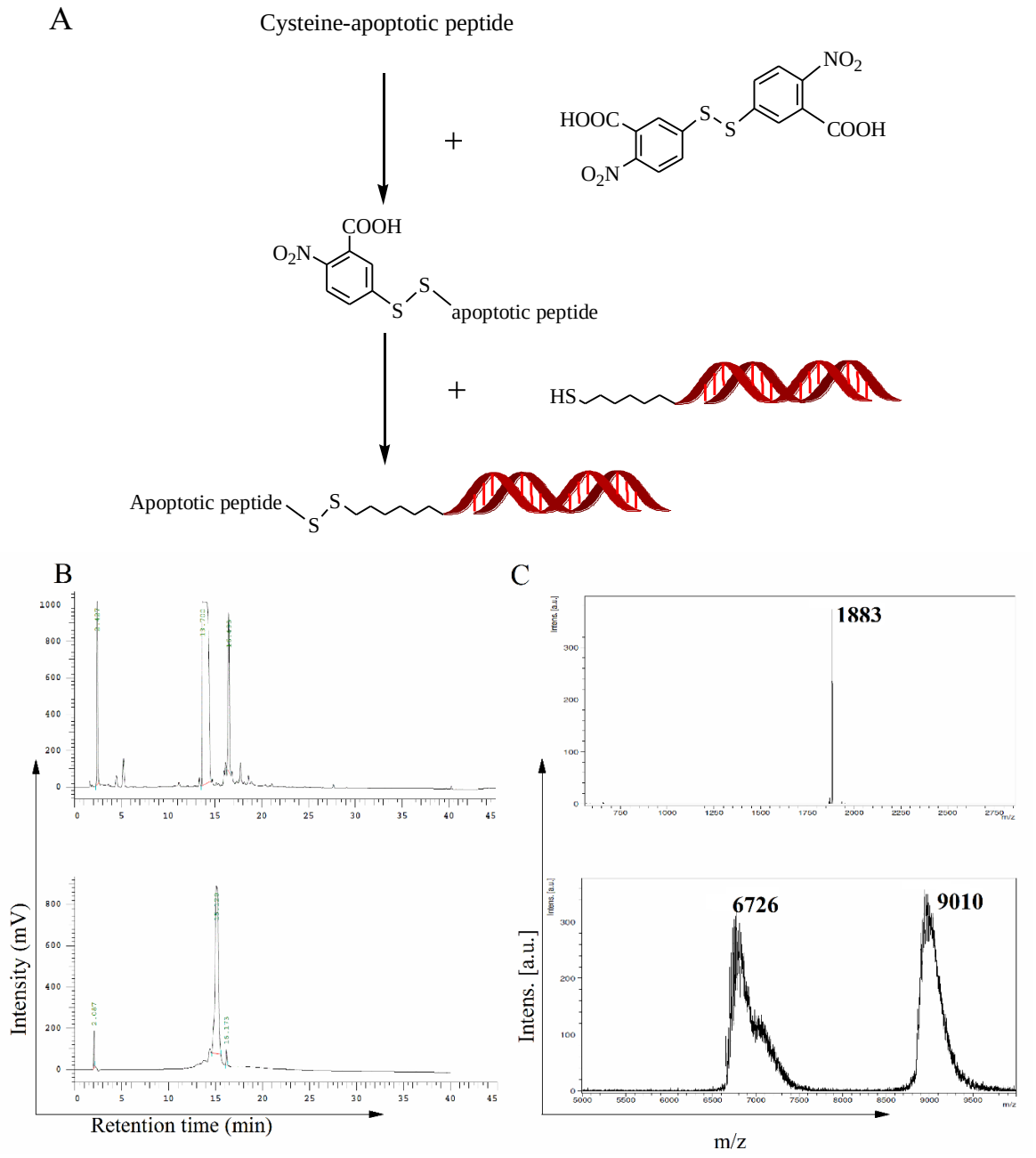

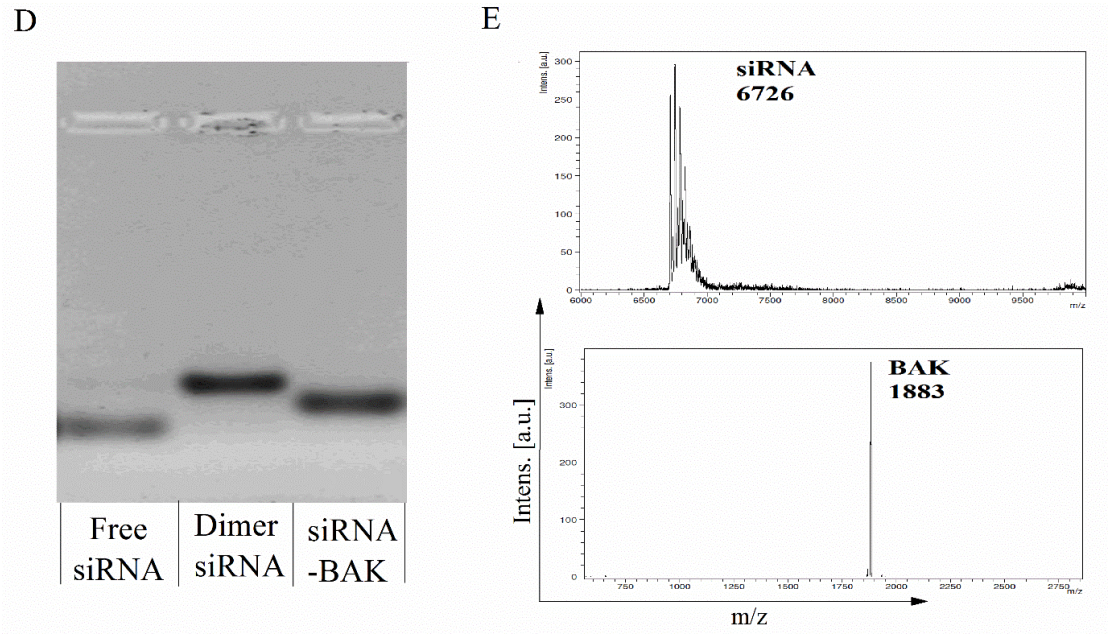

Fig. 5. A) Overall scheme of synthesized siRNA-apoptotic peptide by disulfide bond. B-D) Characterization of siRNA-apoptotic peptide, displayed for the siRNA-BAK conjugate; characterization of the other two siRNA-KLK and siRNA-BAD conjugates is shown in the Supplementary Information. B) Top: DTNB modified TNB-BAK peptide. Bottom: siRNA-BAK conjugate. C) MS data of BAK and siRNA-BAK conjugate. For the siRNA-BAK conjugate, the MS data show the molecular weight of two peaks from unconjugated antisense and conjugated sense strand. D) Gel electrophoresis to demonstrate the purity of siRNA-based conjugate. Free siRNA and disulfide dimer siRNA as control. E) Tris (2-carboxyethyl) phosphine (TCEP) was used to cleave the siRNA-BAK conjugate and the fragments were purified by HPLC and then characterized by MS, respectively.

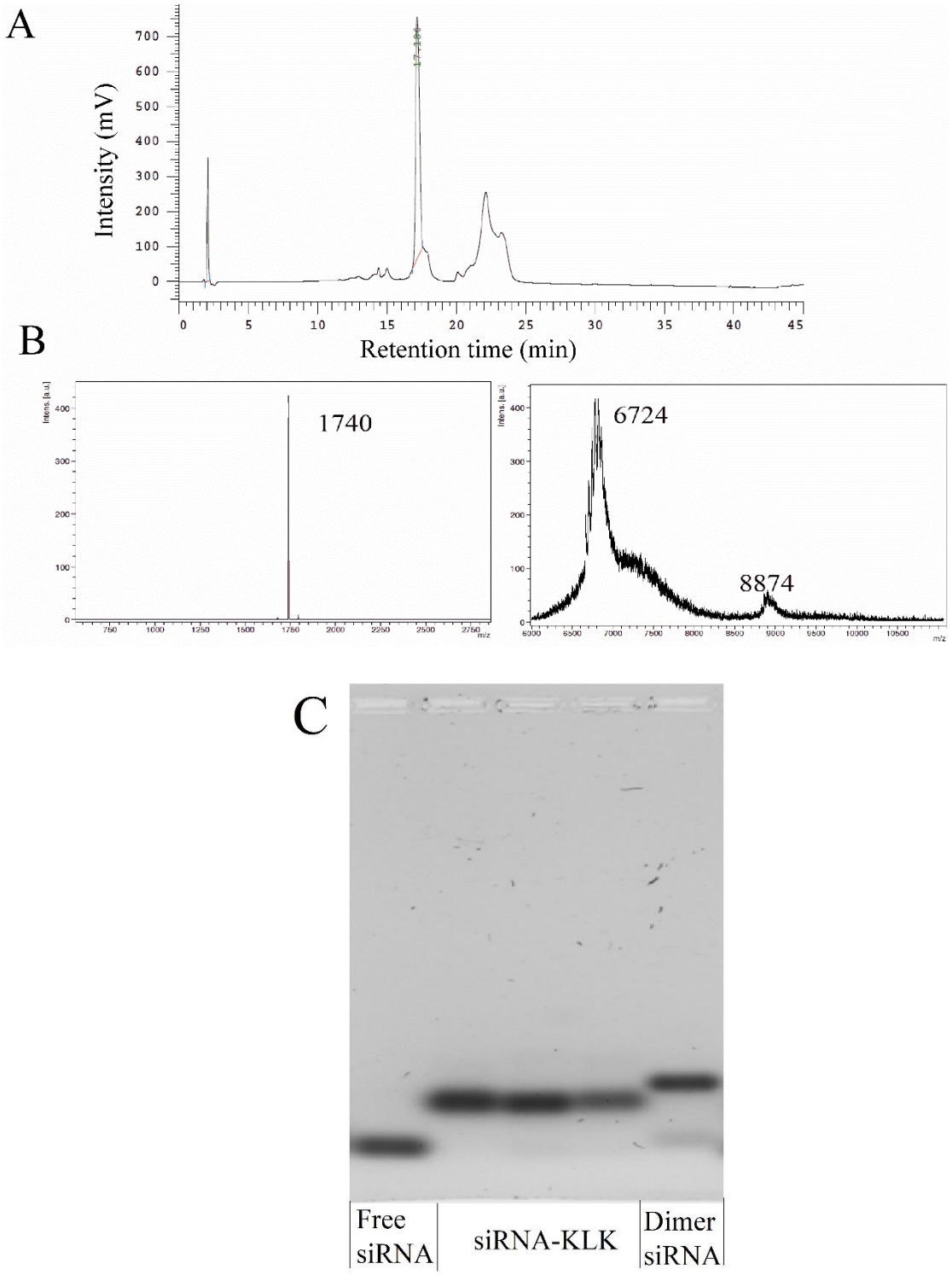

Fig. 6 (A) HPLC data of siRNA-KLK conjugate. B) MS data of KLK (left) and siRNA-KLK conjugate (right). For the siRNA-KLK conjugate, the MS data show the molecular weight of two peaks from unconjugated antisense and conjugated sense strand. C) Gel electrophoresis to demonstrate the purity of siRNA-based conjugate. Free siRNA and disulfide dimer siRNA as control.

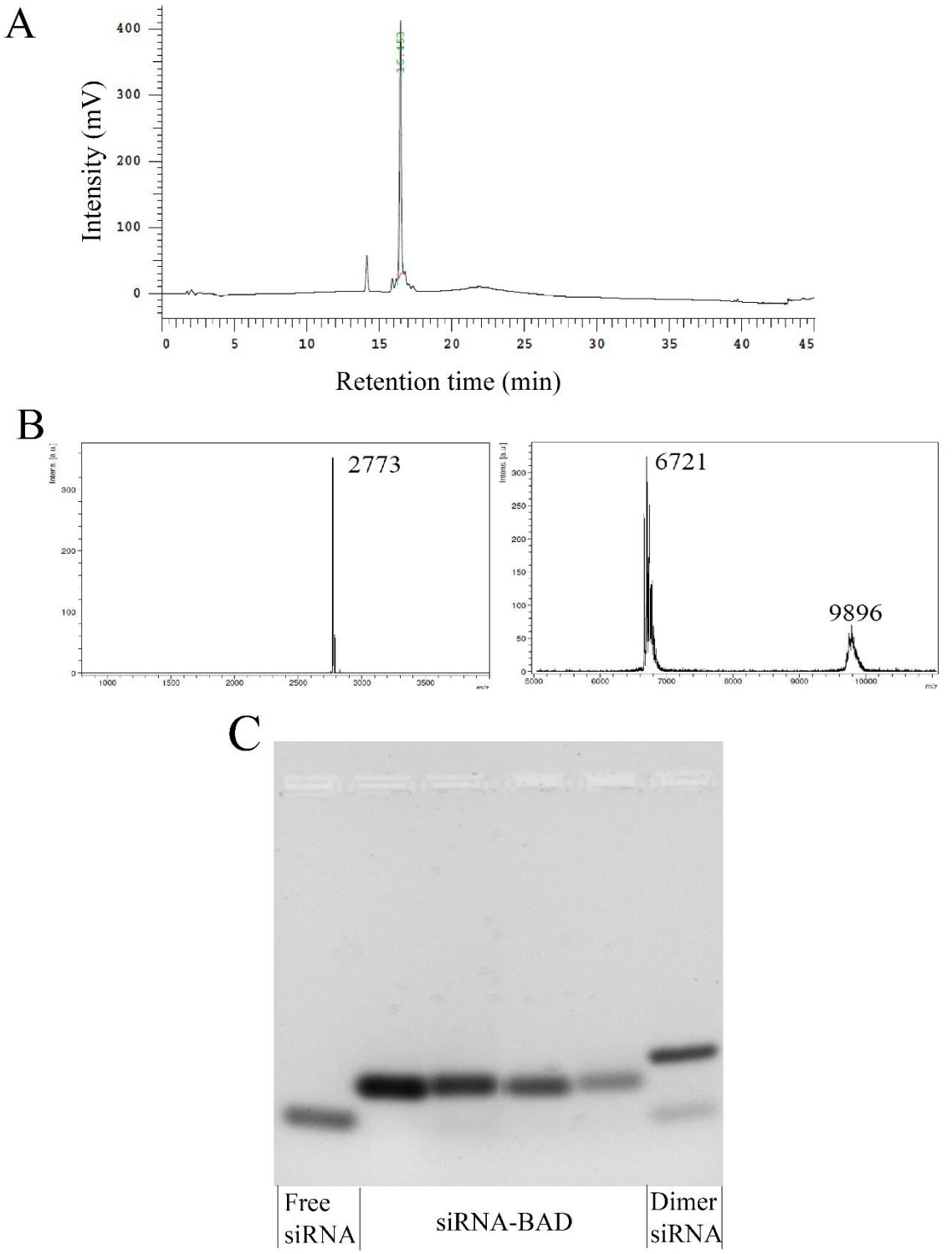

Fig. 7 (A) HPLC data of siRNA-BAD conjugate. B) MS data of BAD and siRNA-BAD conjugate. For the siRNA-BAD conjugate, the MS data show the molecular weight of two peaks from unconjugated antisense and conjugated sense strand. C) Gel electrophoresis to demonstrate the purity of siRNA-based conjugate. Free siRNA and disulfide dimer siRNA as control.

3.1.4 Screening of lipo-oligomers for siRNA delivery

In aqueous solution, lipo-oligomers and siRNA spontaneously assemble into lipo-polyplexes. The siRNA binding ability of lipo-oligomers was determined by measuring the electrophoretic mobility of siRNA in a 2.5% agarose gel (**Fig. 8A**). Different N/P ratios represent the ratio of protonatable amines (N) of the oligomers to phosphates (P) of the siRNA. To simulate *in vivo* stability, polyplexes were incubated with 90% fetal bovine serum for 2h and 24 h followed by the agarose gel electrophoresis assay. For the non-reducible oligomers (***1208***, ***1209***, ***1210*** and ***1211***), at 2 h incubation time, some siRNA was released from the polyplex at N/P of 6. At the N/P ratio of 12 and higher, the oligomers showed complete gel retardation of siRNA. At 24 h incubation time with serum, the qualitative analysis of released siRNA amount was ***1210***>***1211***>***1209***≥***1208*** at N/P ratio of 12. The oligomers ***1208*** and ***1209*** with smallest hydrophilic backbones (4 Stp without or with histidines) showed best serum stability, with complete retention of siRNA at N/P ratios of 12 and higher. An N/P ratio of 12 was used for all formulations in the subsequent experiments.

Polyplexes with the reducible oligomers ***1217***, ***1218***, ***1219*** released some siRNA at N/P ratio of 12 already after 2 h incubation with serum, whereas ***1220*** mediated higher stability. After 24 h incubation time, all reducible oligomer polyplexes showed significant siRNA release even at the highest N/P ratio of 20.

The size and shape of siRNA polyplex was evaluated by dynamic light scattering (DLS) and transmission electron microscopy (TEM). Polyplexes had a hydrodynamic diameter of 150-300 nm by DLS (**Tab. 4**). Oligomers containing histidines and oligomers containing 8 Stp groups showed a trend of increased size compared to the histidine-free analogs and oligomers containing only 4 Stp groups, respectively.

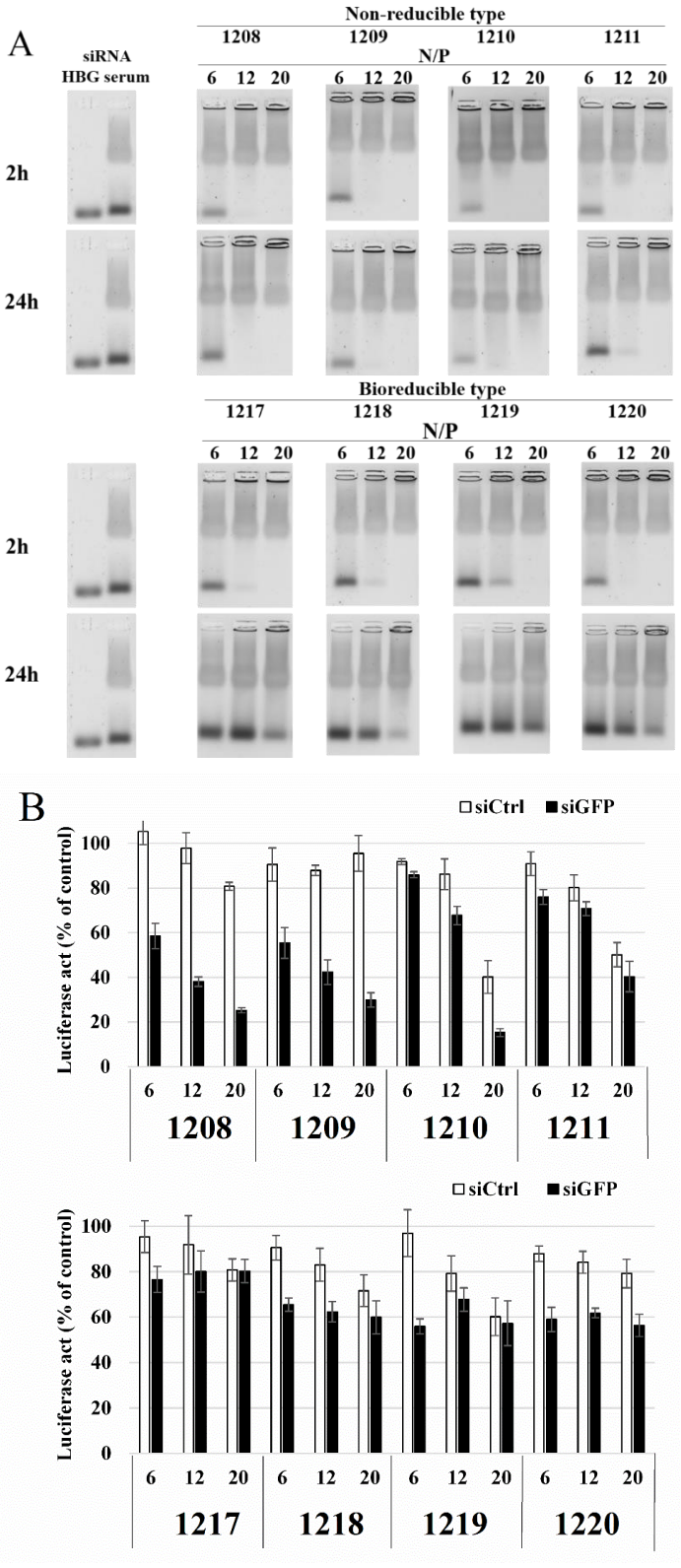

Fig. 8. A) Gel electrophoresis of eight oligomers with siCtrl at different N/P ratios incubated 2h and 24h in 90% serum. B) Luciferase activity of siRNA formulations at different N/P ratios in KB/eGFPLuc cells.

Tab. 4 Particle size (z-average) and zeta potential of siCtrl formulations determined with a DLS zetasizer. The siRNA polyplex were prepared at N/P 12.

Oligomers ID	Z-average[nm]	Mean PDI	Mean Zeta Potential[mV]
1208	191.8 ± 1.9	0.22 ± 0.02	28.5 ± 0.5
1209	218.1 ± 1.8	0.17 ± 0.01	30.6 ± 0.6
1210	221.2 ± 2.0	0.24 ± 0.01	22.8 ± 0.3
1211	283.4 ± 2.6	0.32 ± 0.04	25.1 ± 0.7
1217	179.6 ± 1.5	0.20 ± 0.04	28.7 ± 0.6
1218	199.0 ± 2.6	0.21 ± 0.02	28.7 ± 0.8
1219	192.0 ± 1.2	0.18 ± 0.01	26.8 ± 0.4
1220	223.2 ± 3,6	0.35 ± 0.04	29.7 ± 0.9

To evaluate the transfection efficiency of untargeted oligomer polyplexes, gene silencing experiments (**Fig. 8B**) were performed in KB cells stably expressing an eGFPLuc fusion protein gene (enhanced green fluorescent protein/luciferase). Silencing of the eGFPLuc fusion protein by siRNA against was quantified by a standard luciferase assay. Oligomers ***1208*** and ***1209*** (containing 4 Stp units without or with alternating histidines, respectively) showed better transfection efficiency than the other oligomers. Interestingly, both oligomers with the longer hydrophilic backbones containing 8 Stp units (***1210*** and ***1211***) displayed far lower gene silencing activity. This was not predictable from previous results of DNA and siRNA delivery[12, 13, 98] and might reflect small differences such as in stabilizing domains (e.g. lipids) as well as in the nucleic acid cargo.[13, 30, 102]

The reducible oligomers containing the ssbb building block showed lack of gene silencing efficiency. The reason is most probably based in the selected KB tumor cell system; while the ssbb building block was found to be most favorable in siRNA delivery to Neuro2A cells or DU145 cells,[79] it was observed to hamper siRNA delivery in KB /HeLa cells, most likely due to immature disulfide bond cleavage before or during

cellular internalization into these cells which contain a highly reductive potential.[106] Considering the above mentioned results, oligomers ***1208*** and ***1209*** were the most suitable candidates for the next steps, developing an AP-1 targeted siRNA delivery system and subsequent application for siRNA-apoptotic peptide conjugate delivery.

3.1.5 Evaluation of AP-1 as targeting ligand for receptor-mediated siRNA delivery

The azido function on the surface of ***1208*** and ***1209*** siRNA polyplex serves as anchors for modification of shielding and targeting domains. The amount of added DBCO surface modified-agents is indicated as molar equivalents (equiv.) related to the cationic oligomers (mol/mol). Obviously, as considerable extent of oligomers will be located within the interior of the core lipopolyplexes, only a fraction of azides will be available for nanoparticle surface modification.

The unmodified ***1208*** and ***1209*** core lipopolyplexes had a hydrodynamic diameter of 190-220 nm (**Fig. 9**). Modification with up to 1 equiv. of PEG-AP-1 did not show any considerable change in size of formulations, whereas modification with 0.75 and 0.1 equiv. of PEG showed a decrease in size. The zeta potential of the two ***1208*** and ***1209*** siRNA lipopolyplexes showed similar trends in PEG-AP-1 targeted and PEG shielded groups. For the ***1208*** oligomer, the PEG-AP-1 modification resulted in slightly decreased zeta potentials from 28.3 to 22.8 mV (**Fig. 9C**). In contrast, modification with ligand-free PEG represented a sharp decrease in zeta potential. Highest amount of PEG at ratio of 1 reduced zeta potential to 10 mV, indicating efficient shielding effect for the polyplex. The ***1208*** formulation with PEG-AP-1 targeting domain visualized by TEM (**Fig. 9D**) has a spherical shape and size around 100 nm, which is similar to unshielded ***1208*** polyplexes. Agarose gel electrophoresis (**Fig. 9E**) demonstrated a complete siRNA binding at N/P 12 for all formulations using different ratios of targeting and shielding modification.

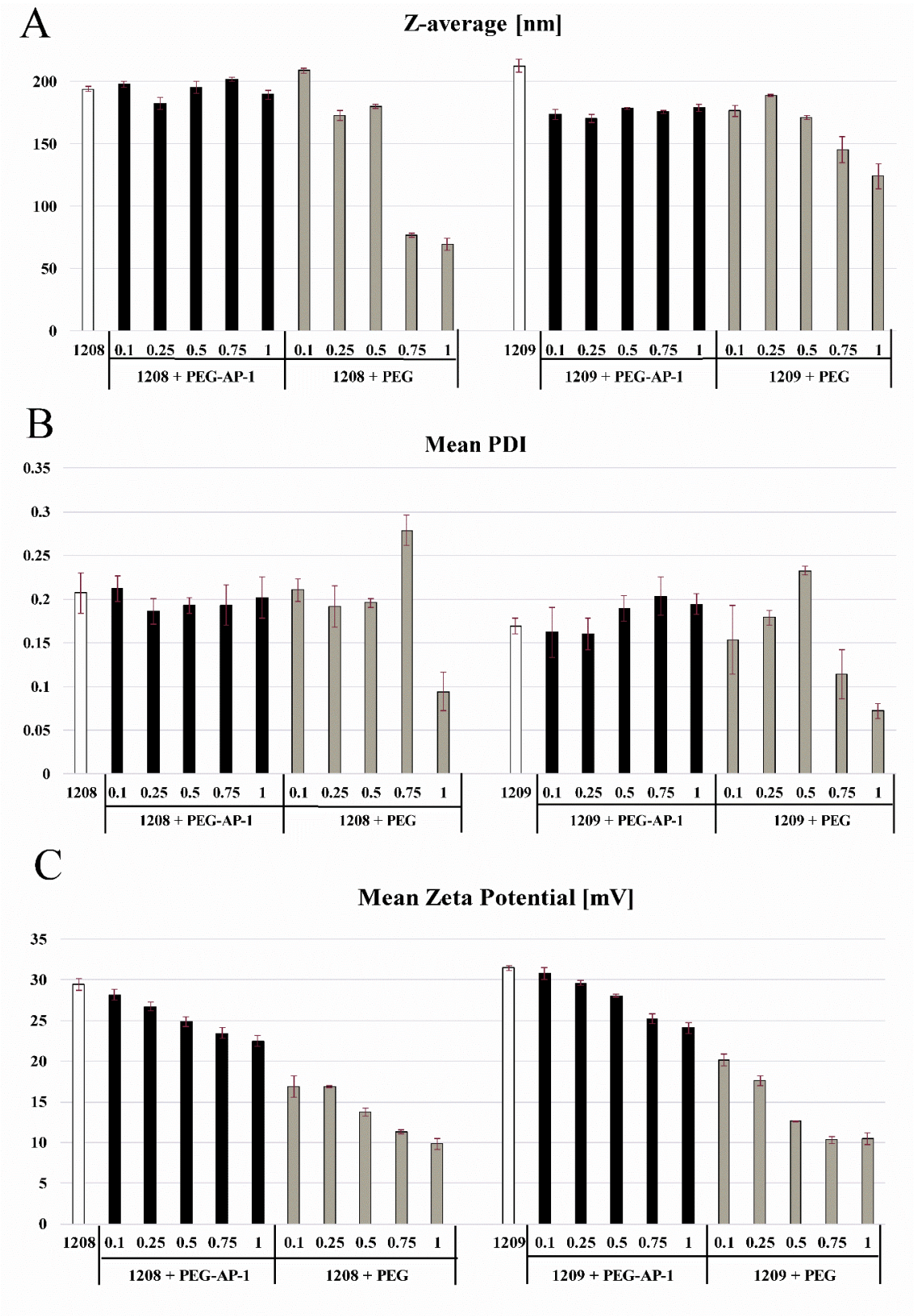
A
Z-average [nm]
200
150
100
50
0
1208
0.1 0.25 0.5 0.75 1
0.1 0.25 0.5 0.75 1
1208 + PEG-AP-1
1208 + PEG
1209
0.1 0.25 0.5 0.75 1
0.1 0.25 0.5 0.75 1
1209 + PEG-AP-1
1209 + PEG
B
Mean PDI
0.35
0.3
0.25
0.2
0.15
0.1
0.05
0
1208
0.1 0.25 0.5 0.75 1
0.1 0.25 0.5 0.75 1
1208 + PEG-AP-1
1208 + PEG
1209
0.1 0.25 0.5 0.75 1
0.1 0.25 0.5 0.75 1
1209 + PEG-AP-1
1209 + PEG
C
Mean Zeta Potential [mV]
35
30
25
20
15
10
5
0
1208
0.1 0.25 0.5 0.75 1
0.1 0.25 0.5 0.75 1
1208 + PEG-AP-1
1208 + PEG
1209
0.1 0.25 0.5 0.75 1
0.1 0.25 0.5 0.75 1
1209 + PEG-AP-1
1209 + PEG

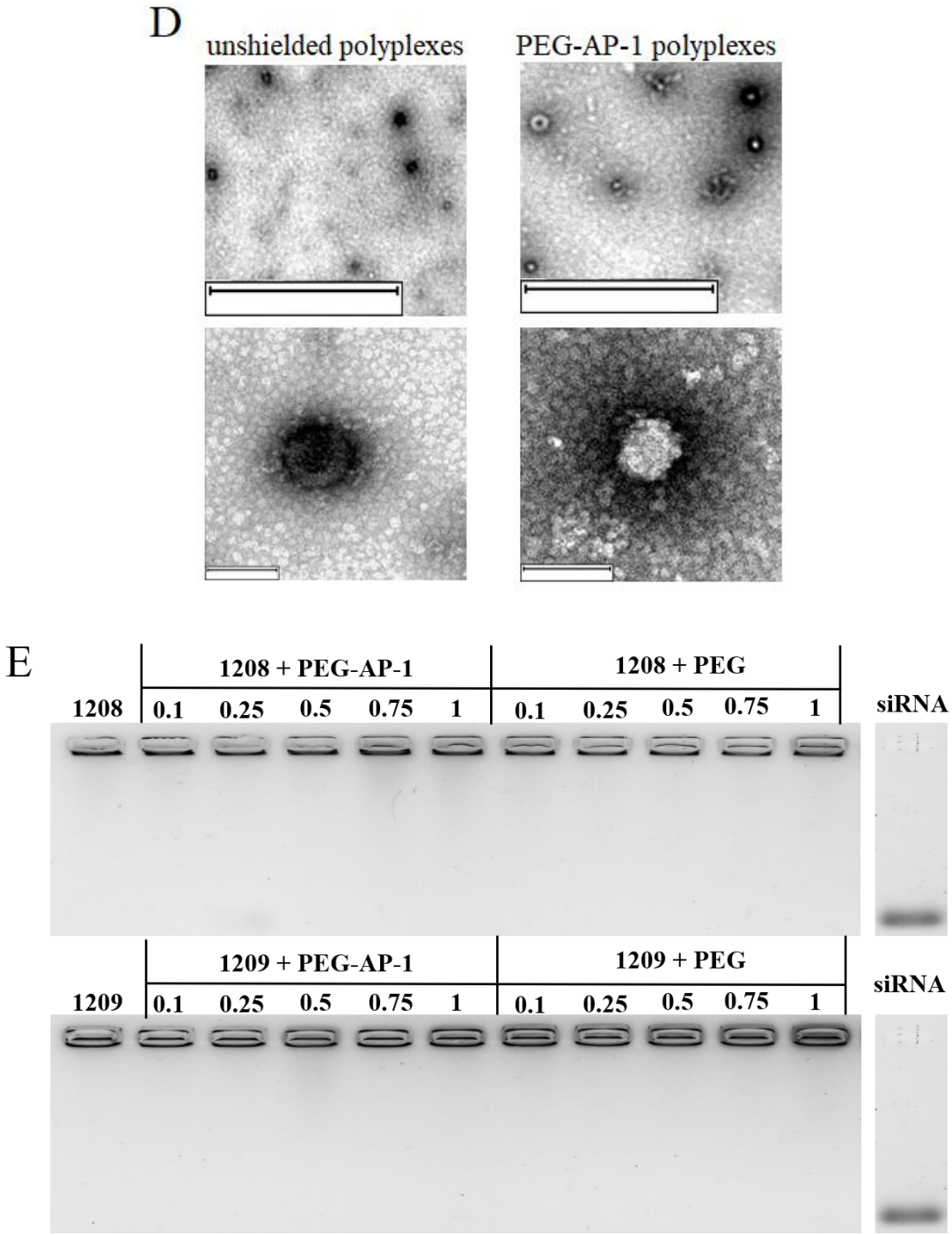

Fig. 9. Particle size (z-average) (A), PDI (B) and zeta potential (C) of ***1208*** and ***1209*** formulations with siCtrl, as determined by DLS zetasizer. Lipopolyplexes were prepared at N/P 12 and modified with indicated different molar equiv. of shielding and targeting domains PEG or PEG-AP-1. D) TEM pictures of ***1208*** polyplex before (unshielded) and after functionalization with PEG-AP-1. Scale bars: upper graph 2 µm, lower graph 60 nm. TEM experiment performed by Dominik Loy (Department of Pharmacy, LMU Munich). E) Gel electrophoresis of ***1208*** and ***1209*** formulations with PEG-AP-1 targeting domain or PEG shielding domain.

To verify AP-1 mediated receptor targeting, the IL-4R overexpressing human carcinoma cell lines KB (cervix), MDA-MB-231 (breast) and Huh 7 (liver) were selected and treated with PEG-AP-1 targeted or PEG shielded Cy5-labeled siRNA polyplexes as well as non-targeted, non-shielded control Cy5-labeled siRNA polyplex at N/P 12. Cells were incubated with all formulations for 45 min at 37 °C, to enable the cells to actively internalize polyplexes for a limited short period. Subsequently cells were washed by PBS and heparin before quantifying the Cy5 intensity by flow cytometry. The negatively charged heparin can largely dissociate extracellularly associated polyplexes from cell surface membranes. **Fig. 10A** displays cellular uptake of polyplexes by Huh 7 cells, which reaches highest cellular uptake at nanoparticle surface modification with 0.5 equiv. PEG-AP-1 targeted agent. Data indicate that AP-1 can effectively target nanoparticles to Huh 7 cells. In contrast, modification of nanoparticles with more than 0.1 equiv. PEG agent decreased uptake of polyplex in a PEG-dependent fashion, indicating an efficient polyplex shielding by PEG. In CLSM images (**Fig. 10B** and **Fig. 11**), generated by an analogous protocol without the heparin washing step), the PEG-AP-1 targeting group showed higher degree of polyplex internalization into cells compared to the control and PEG shielded groups. To demonstrate that the binding of polyplexes to the Huh 7 cells is ligand-dependent, we performed an AP-1 peptide competition assay. As shown in **Fig. 10A** and **Fig. 12**, the cellular uptake of AP-1 targeted polyplexes was almost completely blocked when cells were pre-treated with high concentration of AP-1.

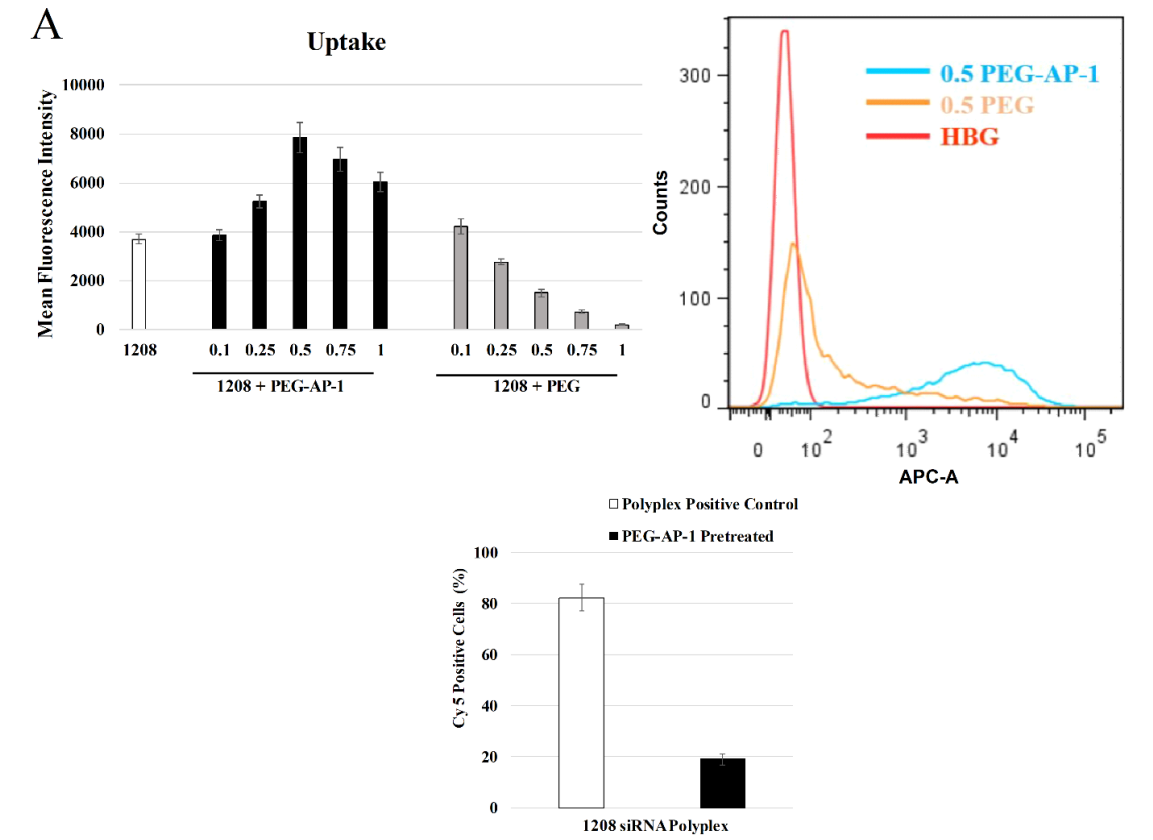
A
Uptake
Mean Fluorescence Intensity
10000
8000
6000
4000
2000
0
1208
0.1 0.25 0.5 0.75 1
0.1 0.25 0.5 0.75 1
1208 + PEG-AP-1
1208 + PEG
Counts
300
200
100
0
0.5 PEG-AP-1
0.5 PEG
HBG
0 10^2 10^3 10^4 10^5
APC-A
Polyplex Positive Control
PEG-AP-1 Pretreated
Cy5 Positive Cells (%)
100
80
60
40
20
0
1208 siRNA Polyplex

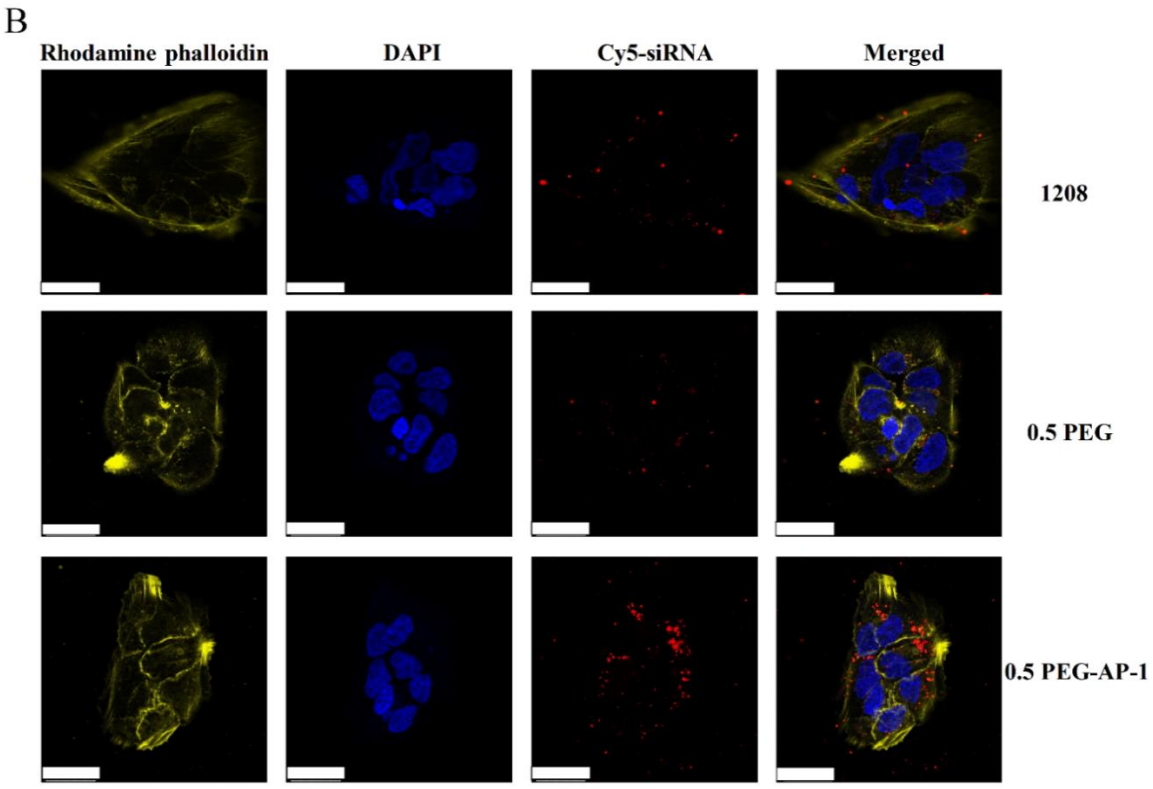
B
Rhodamine phalloidin
DAPI
Cy5-siRNA
Merged
1208
0.5 PEG
0.5 PEG-AP-1

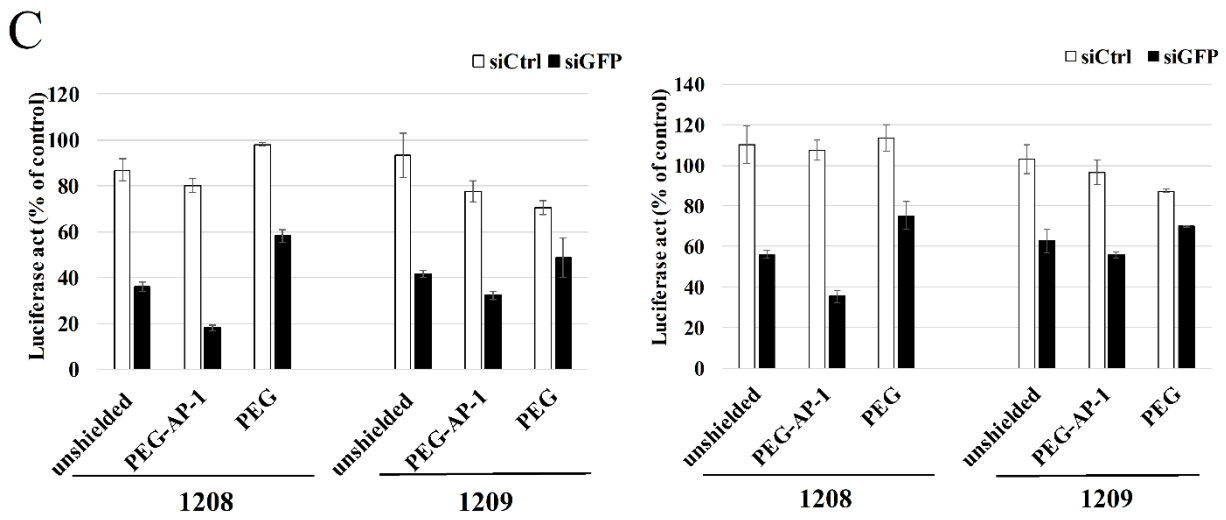

Fig. 10. A) Uptake (upper graph) of targeted formulations into Huh 7 cells determined by flow cytometry after 45 min incubation at 37° Cand heparin wash. ***1208*** siRNA polyplexes were prepared containing 20% Cy5-labeled siRNA and modified with different ratios of PEG-AP-1 targeting or PEG-shielding agents. The ligand competition study (lower graph) was performed in the presence of excess free PEG-AP-1. Huh 7 cells were pre-incubated with 100 µM of PEG-AP-1 for 45 min before incubation with ***1208*** siRNA polyplexes for 4h. PEG-AP-1 targeted siRNA polyplexes were formed at N/P 12 using Cy5-labeled siRNA. The number of Cy5-positive cells was analyzed by flow cytometry. Polyplex positive control: without ligand competition. B) Cellular association of ***1208*** siRNA formulations in Huh 7 cells acquired by confocal laser scanning microscopy (CLSM). Cells were incubated with the formulations for 45 min at 37 ° Cand washed with PBS buffer. Actin cytoskeleton was stained with rhodamine phalloidin, nuclei were stained with DAPI and siRNA was Cy5-labeled. White scale bars indicate 25 µm. Experiment performed by Miriam Höhn (Department of Pharmacy, LMU Munich). C) Gene silencing of targeted formulations in Huh 7/eGFPLuc cells (left) and KB/eGFPLuc cells (right). Polyplex formulations with 500 ng eGFP-targeted siRNA (siGFP) or control siRNA (siCtrl) and ***1208*** or ***1209*** were tested at N/P 12 with 0.5 molar equiv. of PEG-AP-1 targeting or PEG shielding domains. Cells were incubated with the formulations for 45 min at 37° Cbefore cell culture medium was replaced. The luciferase activity of the eGFPLuc fusion protein was measured at 48 h. The results are presented as percentage of the luciferase gene expression obtained with untreated control cells.

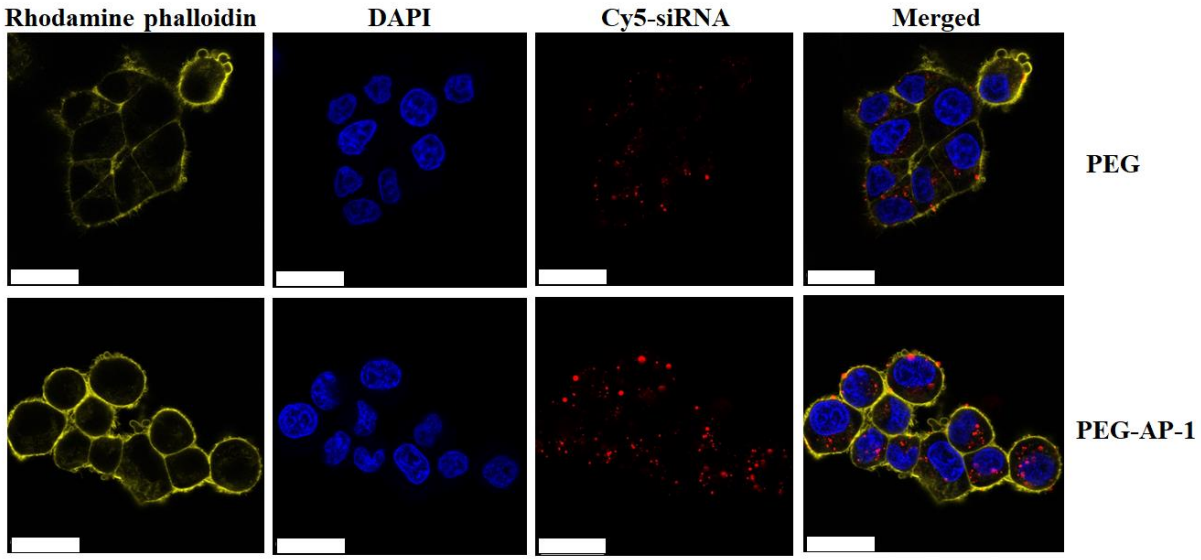

Fig. 11 Cellular association of siRNA formulations in KB cells acquired by confocal laser scanning microscopy (CLSM). Cells were incubated with the formulations for 45 min at 37 ℃ and washed with PBS buffer. Actin cytoskeleton was stained with rhodamine phalloidin, nuclei were stained with DAPI and siRNA was Cy5-labeled. White scale bars indicate 25 µm. Experiment performed by Miriam Höhn (Department of Pharmacy, LMU Munich).

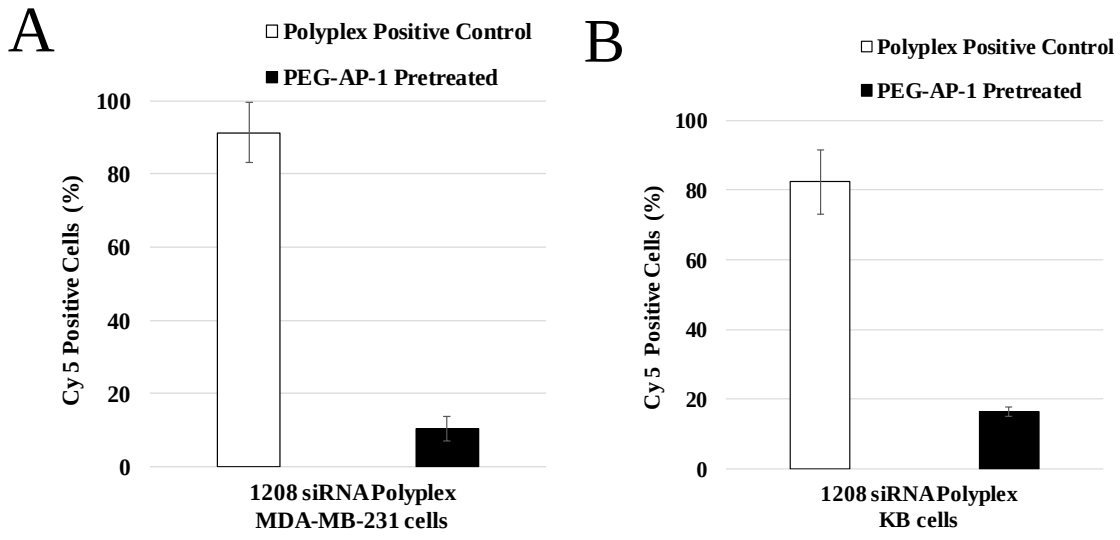

Fig. 12 Ligand competition studies were performed with polyplexes in the absence or presence of excess free PEG-AP-1. In the competition experiments, MDA-MB-231 (A) and KB (B) cells were pre-incubated with 100 µM of PEG-AP-1 for 45 min before incubation with ***1208*** siRNA PEG-AP-1 polyplexes for 4h. siRNA polyplexes were formed at N/P 12 using Cy5-labeled siRNA. The number of Cy5-positive cells was analyzed by flow cytometry.

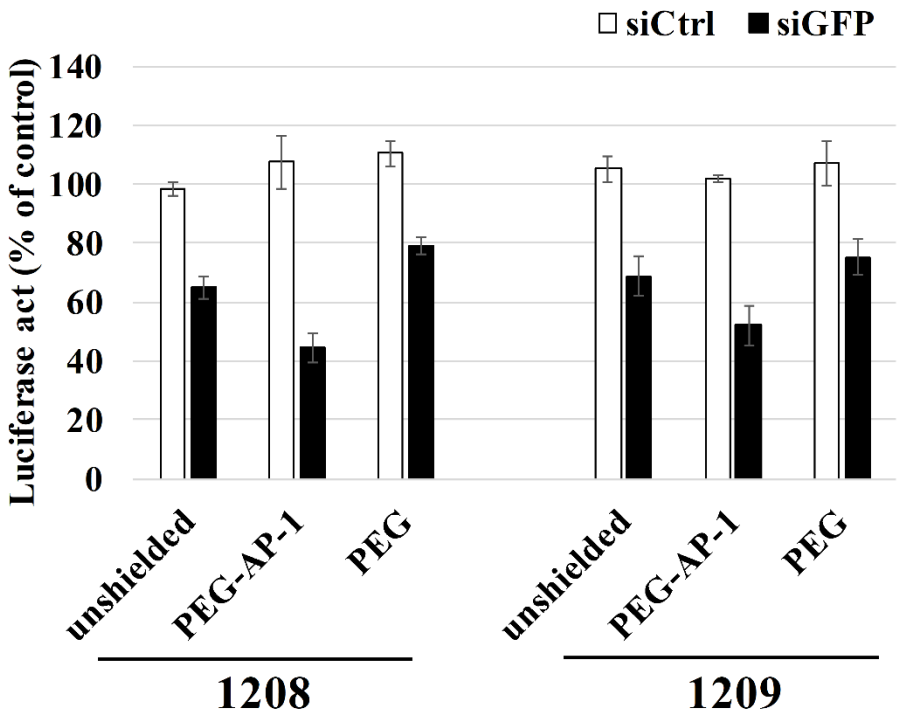

Fig. 13 Gene silencing of targeted formulations in MDA-MB-231/eGFPLuc cells. Polyplex formulations with eGFP-targeted siRNA (siGFP) or control siRNA (siCtrl) and ***1208*** or ***1209*** were tested at N/P 12. Cells were incubated with the formulations for 45 min at 37°C before cell culture medium was replaced. The luciferase activity of the eGFPLuc fusion protein was measured at 48 h. The results are presented as percentage of the luciferase gene expression obtained with untreated control cells.

To evaluate the targeted transfection efficiency of formulations, gene silencing experiments were performed in Huh 7/eGFPLuc (**Figure 10C**, left), KB/eGFPLuc cells (**Figure 10C**, right), and MDA-MB-231/eGFPLuc (**Fig. 13**). The silencing of the eGFPLuc fusion gene product was evaluated by a luminometric luciferase assay. For non-modified ***1208*** and ***1209*** siRNA lipo-polyplexes, the knockdown of luciferase activity was almost 60% in Huh 7/eGFPLuc and 40% in KB/eGFPLuc, respectively. PEG-AP-1 targeting increased the gene silencing efficiency and PEG_{24} shielded domains decreased the silencing efficiency in both cell lines (**Fig. 10C**). The targeted ***1208*** polyplexes provided the highest efficiency and were notably more effective than analogous ***1209*** polyplexes. The luciferase expression levels of cells treated with siCtrl polyplexes was not significantly altered, indicating that formulations had no intrinsic

unspecific cytotoxicity. Also in MDA-MB-231/eGFPLuc cells, PEG-AP-1 targeted ***1208*** polyplexes resulted in the highest silencing efficiency (**Fig. 13**). In sum, in all three cell lines the targeted ***1208*** polyplexes (containing 4 Stp units without histidines in the oligomer backbone, analogously as in ***454*** and ***1106***) were most effective and more potent than targeted ***1209*** polyplexes (containing 4 Stp-histidine units per oligomer).

3.1.6 Cell killing by siRNA-apoptotic peptide conjugates without or with IL4R-targeted delivery

We sought to investigate whether we could enhance the antitumoral cytotoxicity of siRNA lipopolyplexes by using siRNA conjugated with apoptotic peptides. An initial comparison of cell-killing by polyplexes with standard siRNA or the siRNA-apoptotic peptide conjugates was performed using the previously established lipo-oligomer ***1106*** (**Tab. 2**) without shielding and targeting. ***1106*** had comparable transfection efficiency as ***1208*** in Huh 7/eGFPLuc cells and KB/eGFPLuc cells (**Fig. 14**). Standard siEG5 or siEG5 conjugated with one of the three apoptotic peptides (siEG5-KLK, siEG5-BAK, siEG5-BAD) or the analogous control siCtrl apoptotic peptide conjugates (siCtrl-KLK, siCtrl-BAK, siCtrl-BAD) were transfected into HeLa cells (Figure 6A, left) or A549 cells (Figure 6A, right). Cell killing effects were very consistent in both cancer cell types. As expected, siEG5 conjugates always mediated superior cell killing over the analogous siCtrl conjugates, clearly demonstrating RNA interference contributing to the antitumoral effect. Notably, siCtrl-peptide conjugates contributed an up to 40% reduction in cell viability, demonstrating a RNA interference-independent cell killing. Comparing the apoptotic peptide conjugate, cytotoxicities were in the order of siEG5-KLK ~ siEG5-BAD > siEG5-BAK > siEG5 in HeLa cells, and siEG5-KLK > siEG5-BAD > siEG5-BAK ~ siEG5 in A549 cells (**Fig. 15A**). Biophysical analysis (binding, DLS and cellular uptake) did not show any significant difference between standard siRNA and siRNA-KLK conjugates (**Tab. 5, Fig. 16 and Fig. 17**).

Next we examined the cytotoxic effect of the three siEG5-apoptotic peptide conjugates or unmodified siEG5 ***1208*** lipoplex formulation on Huh 7 cells (**Fig. 15B**) without or with PEG-AP-1 targeting or PEG-shielding. For the untargeted formulations, KLK-siEG5 and BAD-siEG5 again enhanced cytotoxicity compared with siEG5 polyplexes, whereas the BAK-siEG5 did not present enhanced killing. Consistent with the other delivery results of the current report, in general PEG shielding of lipopolyplexes reduced and modification with the PEG-AP-1 targeted domain recovered or even enhanced tumor cell killing. In particular, PEG-AP-1 targeted ***1208*** polyplexes of KLK-siEG5 conjugates showed significantly superior cytotoxicity in Huh7 cells. In sum, reviewing all data, out of the three investigated apoptotic peptide conjugates, only siEG5-KLK conjugates mediated a robust superior cell killing over siEG5 polyplexes, resulting in 2.15-fold, 2.04-fold and 1.77-fold reduced cell viability in HeLa cells, A549 or Huh7 cells, respectively. To further explore the value of siRNA-KLK conjugates versus siRNA, dose-response relationships were performed in Huh 7 cells (**Fig. 15C and Fig. 18**). **Fig. 15C** shows cell-killing potency of untargeted (left) and AP-1 targeted (right) siEG5-KLK versus siEG5 polyplexes, formed either at the standard siRNA concentration of 370 nM and ***1208*** at N/P 12 (14.36 µM), or at different lower concentrations of siEG5-KLK conjugates or siEG5. The dose of ***1208*** was kept constant (at the fixed amount of 14.36 µM), in order to avoid delivery problems (such as hampered endosomal release) by carrier dilution. The dilution study demonstrated superior cell killing by siEG5-KLK even at <20 nM. Dilution studies performed with untargeted ***1208*** polyplexes at N/P 12 (**Fig. 18**), also demonstrated superior cytotoxicity of siEG5-KLK conjugates compared to siEG5. We inferred that the augmented tumor cell killing effect was mediated by a dual mechanism from both EG5 gene silencing and KLK apoptotic peptide action.

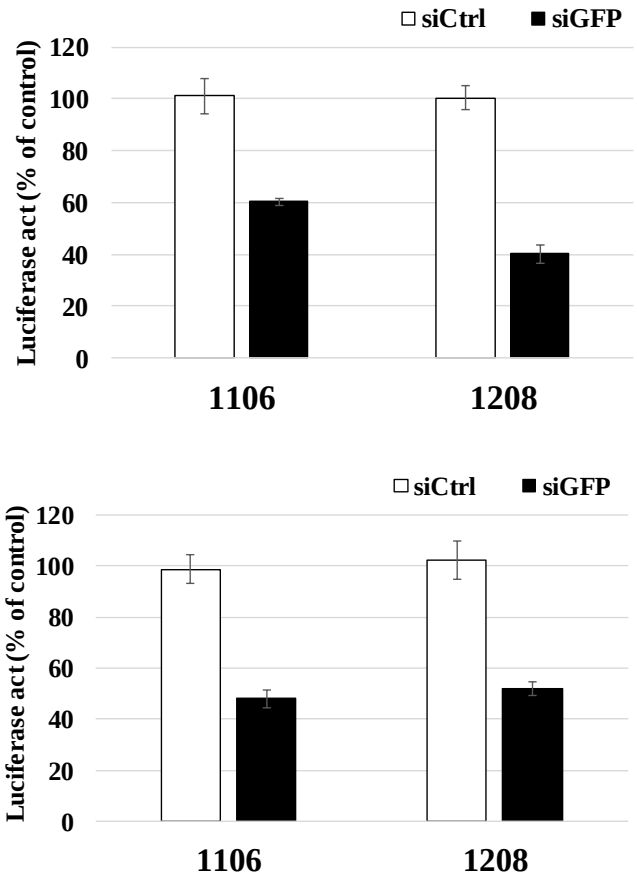

Fig. 14 Comparison of oligomers *1106* and *1208*. Gene silencing of untargeted formulations in Huh 7/eGFPLuc cells (upper) and KB/eGFPLuc cells (lower). Polyplex formulations with eGFP siRNA (siGFP) or control siRNA (siCtrl) and ***1106*** or ***1208*** were tested at N/P 12. The luciferase activity of the eGFPLuc fusion protein was measured at 48 h. The results are presented as percentage of the luciferase gene expression obtained with untreated control cells. ***1106*** as positive control for testing the gene silencing efficiency of ***1208***.

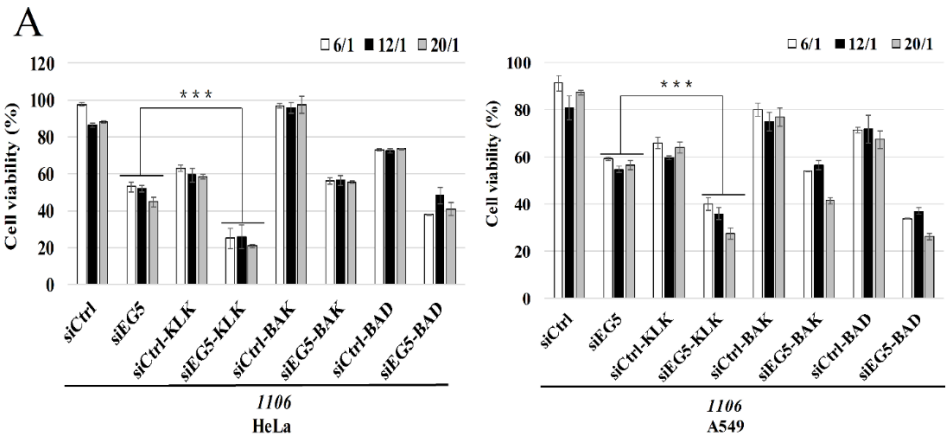

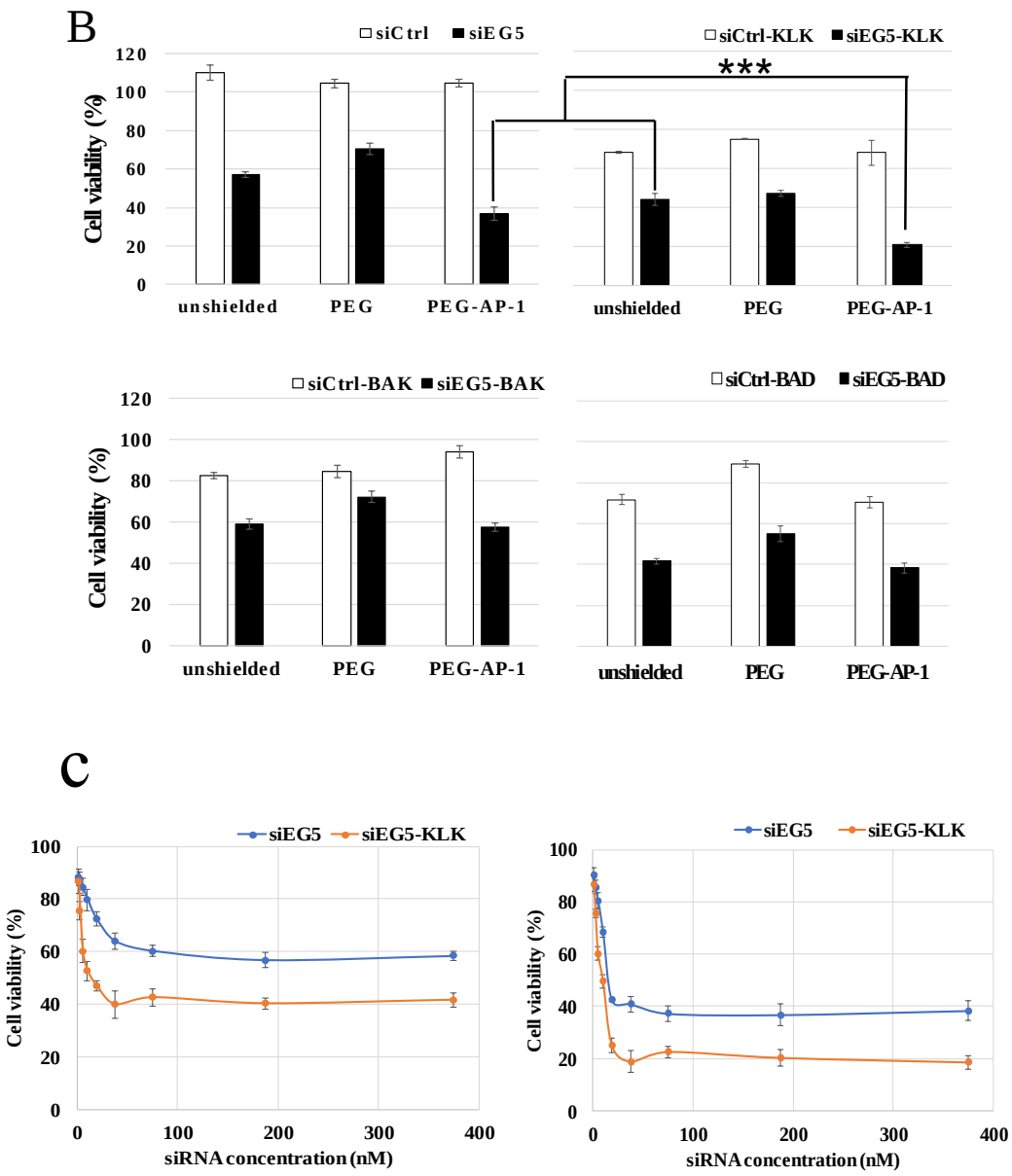

Fig. 15. Transfection with siEG5-apoptotic peptide or control siCtrl-apoptotic peptide conjugates as lipopolyplex formulations in three different cell lines. A) Viabilities of HeLa cells (left) and A549 cells (right) after 48 h transfection with siRNA-apoptotic peptides conjugates formulated with ***1106*** at indicated N/P ratios without targeting and shielding domain. B) Cell viability of Huh 7 cells after 48 h transfection with siRNA-apoptotic peptides conjugate formulations with ***1208*** at N/P = 12 with 0.5 molar equiv. of PEG-AP-1 targeting or PEG shielding domains. *** $p < 0.001$. C) Dose-response relationship of siRNA versus siRNA-KLK conjugates in Huh 7 cells. Untargeted (left) and AP-1 targeted ***1208*** polyplexes (right) formed with a fixed amount of ***1208*** (14.36 µM) and different concentrations of siEG5 or siEG5-KLK conjugates. Standard siRNA concentration was 370 nM (500 ng/well).

Tab. 5 Particle size (z-average) and zeta potential of polyplex formulations with siCtrl or siCtrl-KLK conjugate and ***1208*** determined with a DLS zetasizer. The polyplexes were prepared at N/P 12.

Polyplex	Z-average [nm]	Mean PDI	Mean Zeta Potential [mV]
siCtrl	190,3 ± 2,5	0,18 ± 0,01	28.1 ± 0.5
siCtrl-KLK	185,6 ± 2,1	0.21 ± 0.02	29,5 ± 0.4

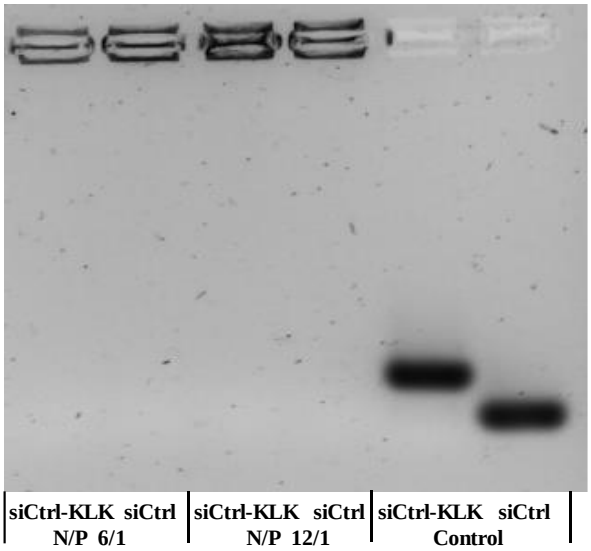

Fig. 16 Gel electrophoresis of ***1208*** formulations with siCtrl or siCtrl-KLK conjugate at different N/P ratios of 6 and 12.

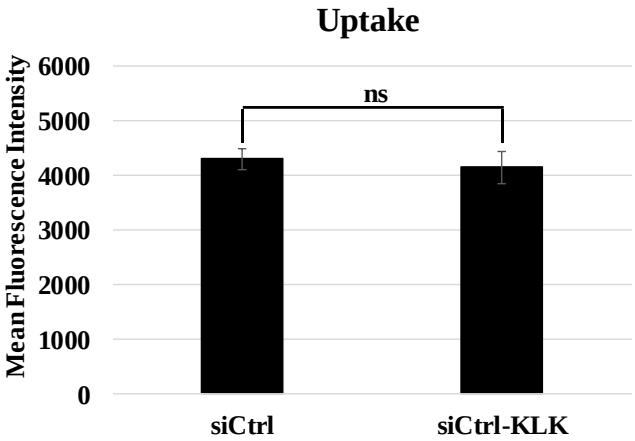

Fig. 17 Uptake of untargeted formulations into Huh 7 cells determined by flow cytometry after 45 min incubation at 37°C and heparin wash. ***1208*** siRNA polyplexes were prepared containing 20% Cy5-labeled siRNA (Cy5-siCtrl and Cy5-siCtrl-KLK). ns: no significant difference.

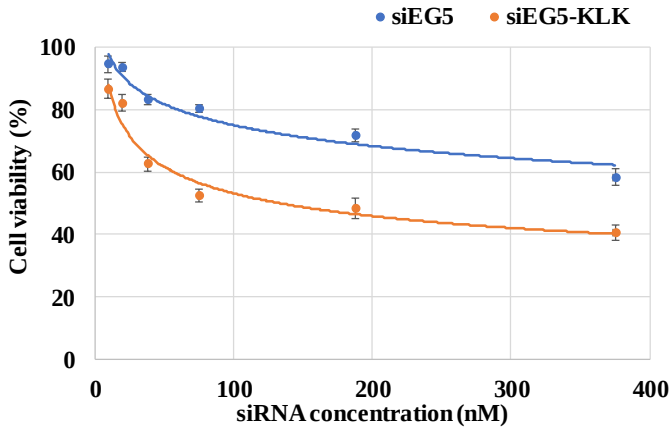

Fig. 18 Dose-response relationship of siRNA-KLK conjugates versus siRNA in Huh 7 cells. Untargeted ***1208*** polyplexes at N/P 12 with different concentrations of siEG5 or siEG5-KLK conjugates were tested. Standard siRNA concentration (highest concentration) was 370 nM (500ng/well).

3.1.7 Mechanism of augmented cytotoxicity of AP-1 targeted siRNA-KLK conjugates

All subsequent experiments were performed with 0.5 equiv. PEG-AP-1 targeted ***1208*** lipopolyplexes (N/P 12) identified above as the most potent delivery system. As mentioned above, EG5 is involved in the assembly of the mitotic spindle apparatus and responsible for centrosome separation in cell division. Thus, siRNA against EG5 would block the formation of bipolar mitotic spindles, causing cell-cycle arrest and subsequent apoptosis of tumor cells. Functional EG5 gene silencing was confirmed *via* aster formation of nuclear DNA (**Fig. 19A and Fig. 20**), where downregulation of EG5 induced a mitotic arrest in all siEG5 groups (siEG5-KLK and siEG5). Aster formation could not be observed after application of control siRNA groups (siCtrl-KLK and siCtrl). We further examined EG5-specific gene silencing at mRNA level in Huh 7 cells by quantitative real-time polymerase chain reaction (qRT-PCR) (**Fig. 19B**). All the siEG5 groups triggered efficient downregulation of EG5 mRNA expression levels. In the siCtrl groups, the mRNA expression levels were similar to untreated cells.

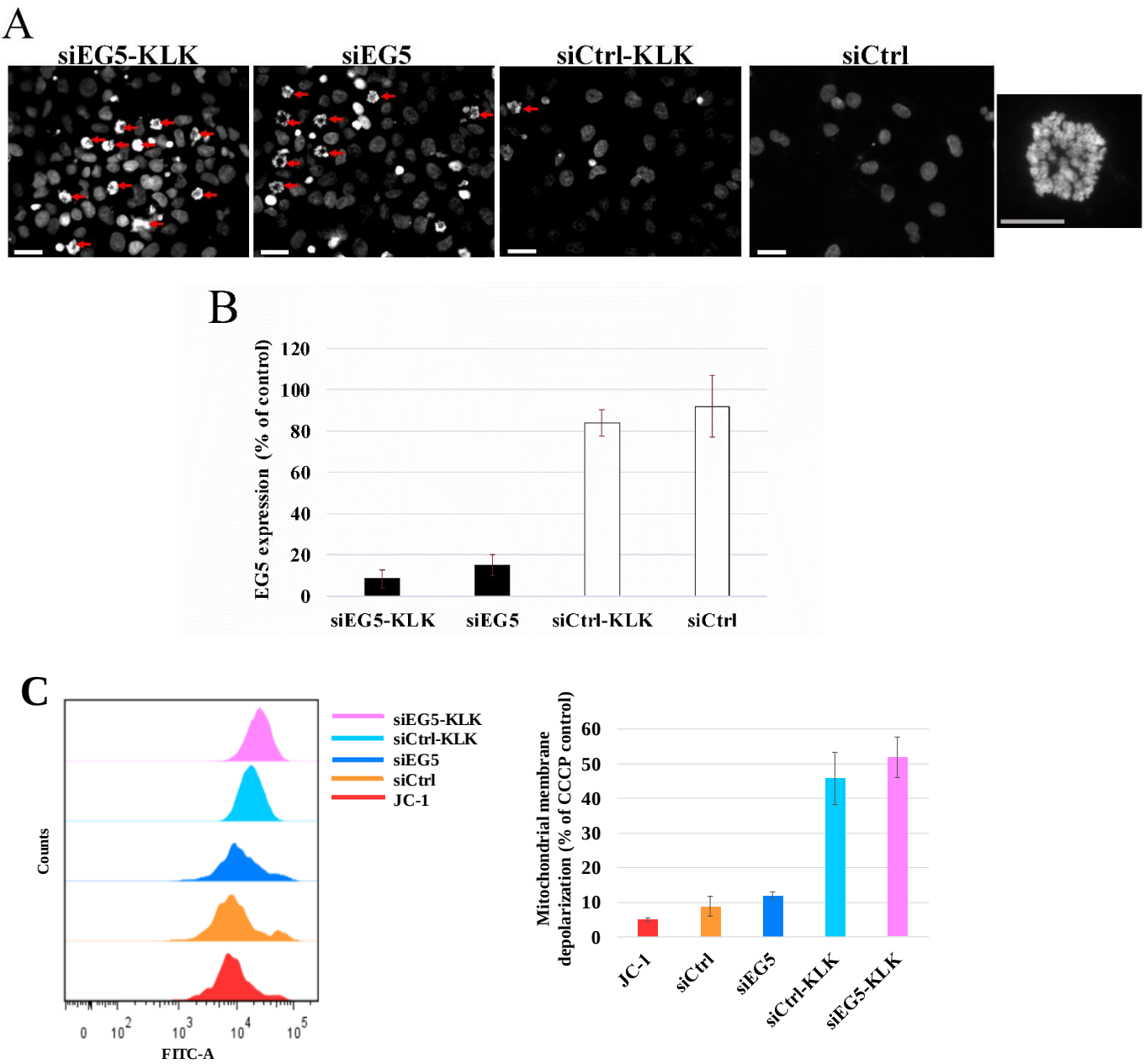
A
siEG5-KLK
siEG5
siCtrl-KLK
siCtrl
B
EG5 expression (% of control)
120
100
80
60
40
20
0
siEG5-KLK
siEG5
siCtrl-KLK
siCtrl
C
Counts
FITC-A
0
10^2
10^3
10^4
10^5
siEG5-KLK
siCtrl-KLK
siEG5
siCtrl
JC-1
Mitochondrial membrane depolarization (% of CCCP control)
60
50
40
30
20
10
0
JC-1
siCtrl
siEG5
siCtrl-KLK
siEG5-KLK

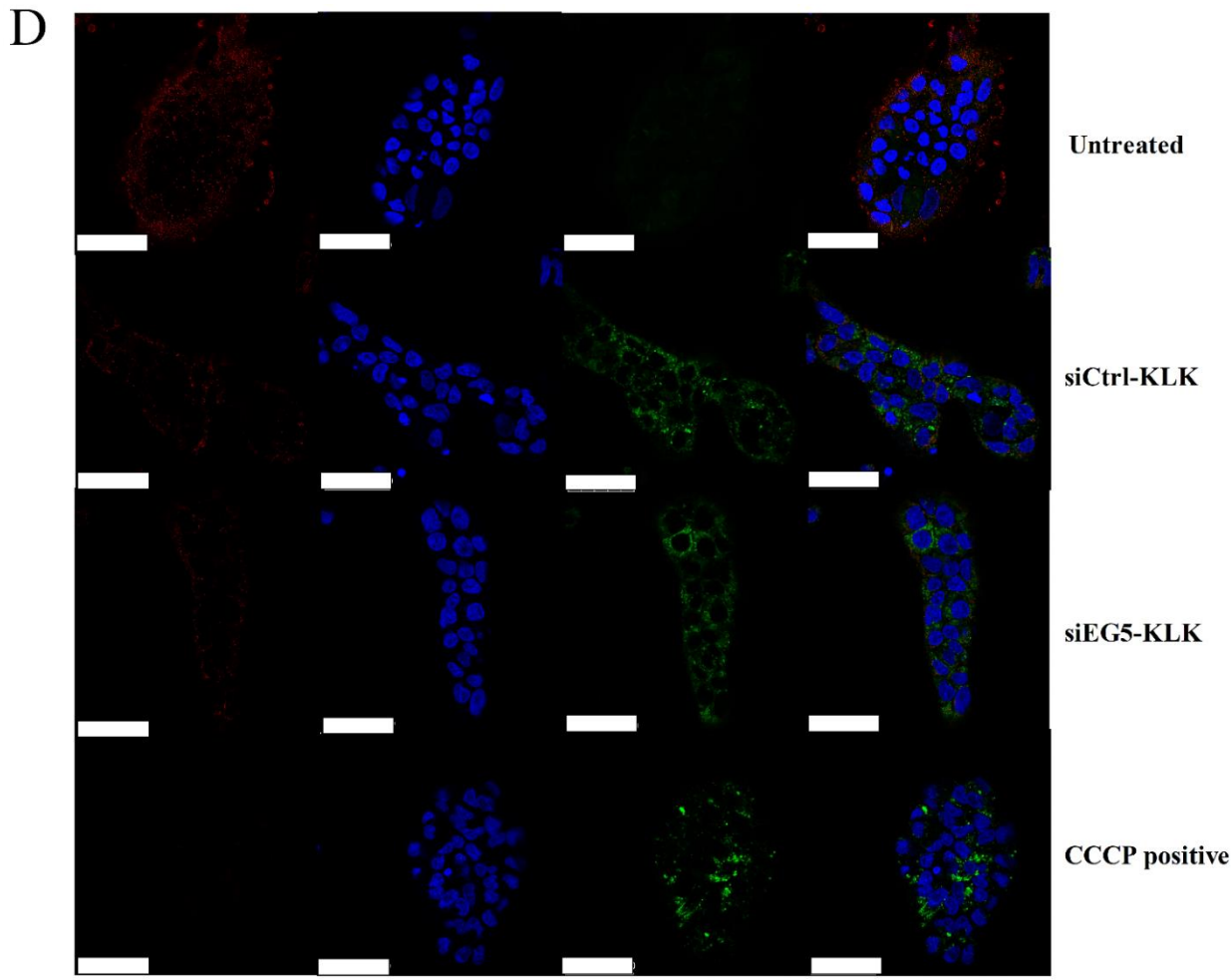

Fig. 19 Mechanism of AP-1 targeted ***1208*** mediated delivery of siEG5-KLK conjugates. A) Mitotic aster formation induced by siEG5 in Huh 7 cells after 48 hours. Scale bars: 20 µm, and 10 µm (magnification in right). B) EG5 mRNA expression levels of different formulations after 48 hours. C) Mitochondrial membrane disruption induced by siRNA-KLK conjugates determined by using a JC-1 dye assay; flow cytometry data presenting the shift of green fluorescence by various polyplex treatments for 48 h (*left*), expressed as % mitochondrial membrane depolarization compared to the CCCP (carbonyl cyanide 3-chlorophenylhydrazone) positive control (*right*). D) CLSM images of treated cells (scale bars: 50 µm) displaying high intensity of green JC-1 fluorescence (mitochondrial membrane depolarization) from the KLK conjugated groups (siEG5-KLK and siCtrl-KLK polyplex treatment for 48 h) and 50 µM of the mitochondrial membrane potential disrupter CCCP as positive control. From *left* to *right*: Red fluorescence of J-aggregates; blue stain of nuclei by Hoechst 33342; green fluorescence of monomeric form of JC-1; overlay of all images. All experiments were performed with ***1208*** polyplexes formed at N/P 12 and modified with 0.5 equiv. PEG-AP-1 targeting agent.
Experiment performed by Miriam Höhn (Department of Pharmacy, LMU Munich).

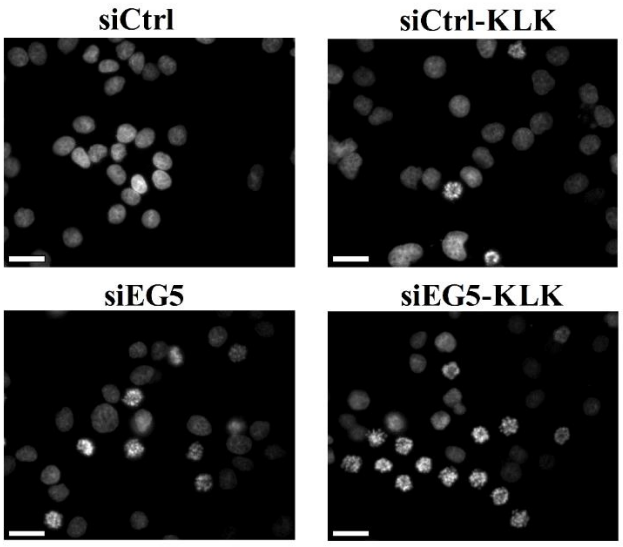

Fig. 20 AP-1 targeted ***1208*** mediated delivery of siEG5-KLK conjugates. Mitotic aster formation induced by siEG5 in KB cells after 48 hours. Scale bars: 20 μm.

Therefore, these results clearly supported that AP-1 targeted polyplexes enable efficient silencing of EG5 expression at mRNA level, followed by mitotic blockade and finally cell death in AP-1 receptor-positive cells. Meanwhile, comparing siRNA-KLK with peptide free siRNA, we found that the KLK apoptotic peptide did not influence the gene silencing of EG5, indicating that siEG5 and KLK independently contributed their function in the process of cell death.

We next investigated the hypothesized function of KLK as inducer of intrinsic mitochondrial apoptosis pathway by using a JC-1 assay (**Fig. 19C and 19D**). The mitochondrial membrane potential $\Delta\psi_M$ is an important parameter of mitochondrial function and has been used as an indicator of cell death. JC-1 can enter the mitochondrion and change its fluorescent properties to red wavelength based on the aggregation of the probe. In healthy cells with high potential $\Delta\psi_M$, JC-1 forms complexes known as J-aggregates with intense red fluorescence. However, in apoptotic cells with low potential $\Delta\psi_M$, JC-1 remains in the monomeric form, which exhibits green fluorescence. The higher the ratios of green to red fluorescence, the lower is the polarization of the mitochondrial membrane. As shown in **Fig. 19C**, both KLK groups (siEG5-KLK and siCtrl-KLK) showed an enhanced shift of green

fluorescence, compared to the groups without KLK and negative JC-1 control groups, which indicated the higher ratio of cells were in the state of mitochondrial membrane depolarization. Comparing the flow cytometry histogram data of the siEG5-KLK and siCtrl-KLK groups, we conclude that the siEG5 had a very little influence on the KLK function of disruption of mitochondrial membrane. Confocal laser scanning microscopy (CLSM, **Fig. 19D**) confirmed the KLK induced mitochondrial membrane depolarization. The green staining is observed siCtrl-KLK and siEG5-KLK as well as the mitochondrial membrane potential disrupter CCCP, but not in healthy cells.

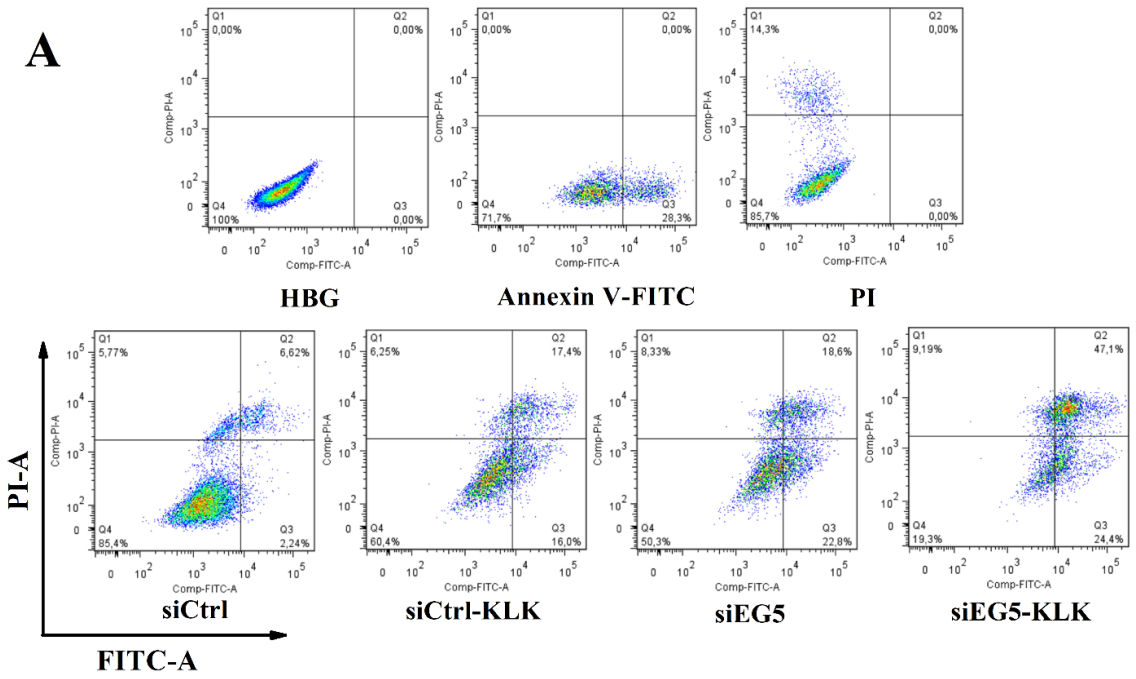

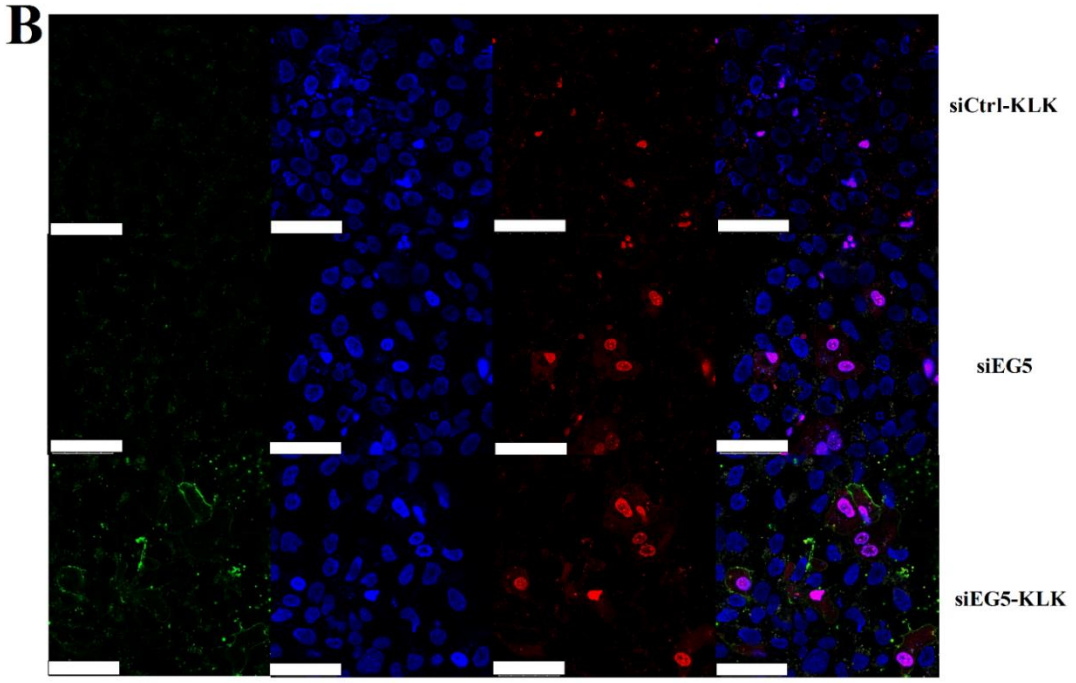

Fig. 21. Apoptosis of Huh 7 cells at 48 h (A) after transfection with different formulations determined by the annexin V-FITC/PI assay. The viable, early apoptosis, and late apoptosis cell populations (%) were shown in the lower left, lower right, and upper right quadrants, respectively. B) Confocal laser scanning microscopy of cells treated for 24 h. Green fluorescence, annexin V-FITC; blue fluorescence, nuclei stained by Hoechst 33342; red fluorescence, PI staining of nuclei. Scale bars, upper graph (white) 25 µm, lower graph (gray) 50µm. Experiment performed by Miriam Höhn (Department of Pharmacy, LMU Munich).

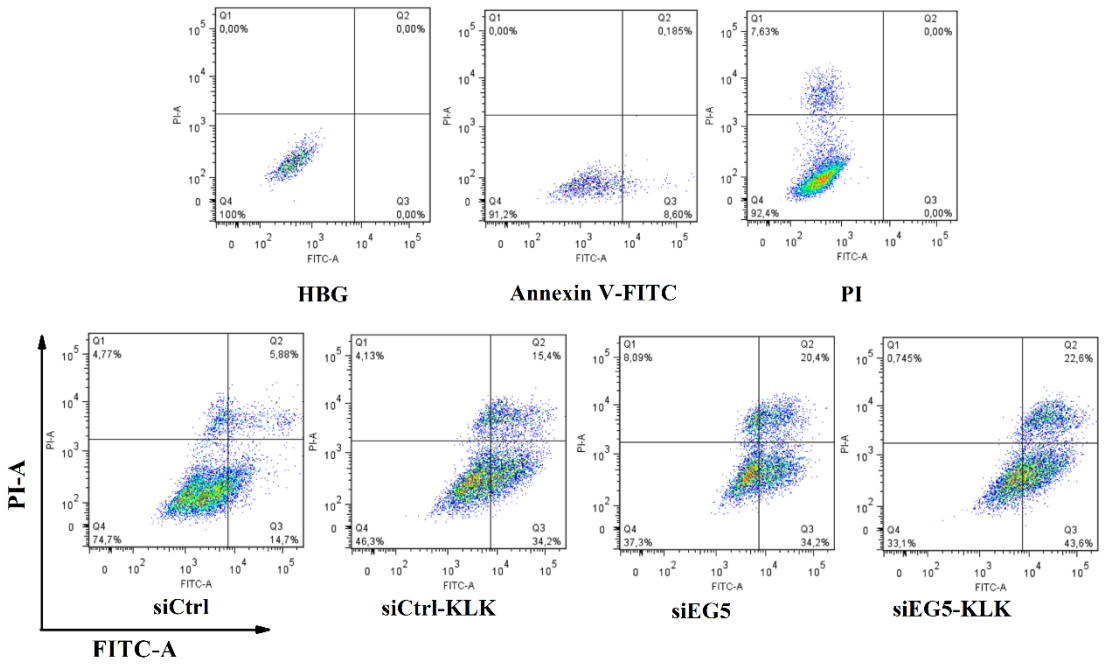

Fig. 22 Apoptosis of Huh 7 cells at 24 h after transfection with different formulations determined by the annexin V-FITC/PI assay. The viable, early apoptosis, and late apoptosis cell populations (%) were shown in the lower left, lower right, and upper right quadrants, respectively.

We further characterized apoptosis of tumor cells induced from these two components (apoptotic peptide conjugated with siRNA) using an annexin V-FITC/propidium iodide (PI) assay, as depicted in **Fig. 21**. Annexin V staining of cells was used to indicate cell membrane changes (phosphatidylserine flips from the cytosol to the outer surface of the membrane lipid bilayer) that occur in the early stage of apoptosis. Annexin V specifically binds to phosphatidylserine in the presence of calcium. By using fluorescent-labeled annexin V, the apoptotic cells can be identified by flow cytometry or fluorescence microscopy. PI is a membrane impermeant DNA intercalating dye that is excluded from viable cells but can stain DNA of dying cells such as the late stage of apoptosis. Apoptosis of Huh 7 tumor cells treated with the different formulations for 24 or 48 h (**Fig. 21**) was most pronounced for siEG5-KLK, followed by siEG5 > siCtrl-KLK >> siCtrl formulations. It has to be noted that the flow cytometric assay provides qualitative and not quantitative information, because viability of siEG5-KLK treated cells is low (only 20% at 48 h), and dead cells are largely not covered by the cytometric assay. Analysis at an earlier time point of 24 h confirms the results (**Fig. 22**), with siEG5-KLK treatment triggering the highest number of apoptotic stage (about 65% of cells). The early and late stage of apoptosis cells were also measured by confocal laser scanning microscopy (**Fig. 21B**) confirming that siEG5-KLK exhibits the best apoptosis inducing capacity.

3.2 Hyaluronate siRNA nanoparticles with positive charge display rapid attachment to tumor endothelium and penetration into tumors

Section 3.2 has been partly adapted from: Jie Luo, Johannes Schmaus, Mochen Cui, Elisa Hörterer, Ulrich Wilk, Miriam Höhn, Maike Däther, Simone Berger, Teoman Benli-Hoppe, Lun Peng and Ernst Wagner, Hyaluronate siRNA nanoparticles with positive charge display rapid attachment to tumor endothelium and penetration into tumors, Journal of Controlled Release, 2020. DOI:

Small interfering RNA (siRNA) has emerged as a promising therapeutic approach for genetic diseases or cancer due to its potent gene-silencing activity.[69, 107-109] Within the last two years the first two siRNA drugs were approved, Patisiran (ONPATTRO) for treatment of hereditary transthyretin-mediated amyloidosis[110] and Givosiran (GIVLAARI) for treatment of hereditary acute hepatic porphyria,[111] and further siRNA drugs are in advanced clinical development.[112] Although arduous and impressive efforts have been made, a remaining challenge for siRNA therapeutics is the efficient delivery to target sites different from liver tissue and for non-inheritable common diseases including cancer.

Cationic carrier-based siRNA delivery systems are highly dependent on a suitable control of relationship among physiochemical properties, stability of siRNA binding and toxicity.[29, 113, 114] Among other examples, [14, 23, 115] cationic PEI polyplexes facilitate delivery of siRNA and microRNA into tumors, resulting in therapeutic RNAi efficacy.[116] However, complexes with high positive surface charge often are subjected to interaction and aggregation with blood components, inflammatory and innate immune responses after intravenous administration, thus yielding toxicities in vivo.[26, 117-120] To solve this issue, numerous hydrophilic natural or synthetic polymers such as polyethylene glycol (PEG) have been incorporated into polyplexes for surface shielding.[73] One encouraging strategy has been the introduction of a polyanionic coating with hyaluronic acid (HA) in order to shield the positive charge of

the nanoparticle.[121-124] In addition to surface shielding, HA can be also used for active targeting of CD44. CD44 is a cell surface adhesion molecule, which is expressed in most cell types, such as leukocytes, epithelial cells, endothelial cells and tumor cells; it was also found to be overexpressed in solid tumor vasculature. [125, 126]

We previously prepared a series of sequence-defined oligoaminoamide (OAA) carriers [28] for intracellular transfer of siRNA or other nucleic acids with shielding (PEG, poly(N-(2-hydroxypropyl)methacrylamide) pHMPA, polysarcosine) and targeting (folate, epidermal growth factor EGF receptor or c-Met binding peptides, interleukin-4 IL-4 or interleukin-6 IL-6 receptor binding peptides) domains.[33, 52, 80, 100, 127-130] These OAAs mediated ligand-enhanced cellular uptake, endosomal escape into the cytosol, protection of siRNA against degradation, and thus improved gene transfer or gene silencing efficiency. Results included successful systemic tumor targeting in vivo in mouse models resulting in therapeutic effects.[80, 128, 130] Based on our understanding of the structure and activity relationships of previous OAA libraries and post-modification strategies of polyplexes, the present study refined OAAs for stable siRNA lipopolyplex formation, suitable for subsequent surface modification with an anionic polymer for in vivo administration. For this purpose, hyaluronic acid (HA) was selected as the polyanion with good biocompatibility, biodegradability, cell targeting potential, and an excellent record of previous application for nanoparticle surface modification.[121-124] Commonly, electrostatic polyplex coating with HA has been performed. To avoid the risk of competitive displacement under in vivo conditions, our work aimed at covalent attachment of HA to siRNA nanoparticles via copper-free, strain-promoted alkyne-azide cycloaddition (SPAAC). Based on this intention, OAAs modified with an N-terminal azide and HA modified with DBCO groups were used as clickable modules, respectively. By variation of the ratio of DBCO-HA to OAA azide of the siRNA nanoparticle, colloidal stable cationic and anionic HA-based siRNA polyplexes were established. Evaluation of these nanoparticles should explore any relations of surface charge with in vivo tumor accumulation, tumor penetration and

subsequent gene silencing efficacy *in vivo*. We investigated the effect of the different coatings on the cellular uptake, endocytic pathways, endosomal escape in vitro, followed by study of tumor accumulation, tumor penetration in 3D sight, and gene silencing of siRNA carriers *in vivo*.

3.2.1 Design of novel T-shaped lipo-oligoaminoamides

A library of more than 1400 cationizable OAA structures had been developed by solid phase-supported synthesis (SPSS), based on the building block succinoyl-tetraethylene-pentamine (Stp) and related analogs,[28, 97] for use as drug,[98] protein,[99] and nucleic acid delivery carriers[80, 100]. T-shaped lipo-OAAs belong to a topological subclass of such carriers that is well suitable for siRNA delivery. Oligomer ***1208*** (see **Fig. 23**, middle left; non-reducible, no histidines, R = oleic acid) as an previously reported efficient representative[52] contains a cationic backbone of four repeats of Stp, terminated at both ends by three tyrosines and an N-terminal azido group. It is branched in T-shape configuration by a central lysine which carries a lipidic branch containing two oleic acids (OleA). The integration of tyrosine tripeptides and additional disulfide-forming terminal cysteines into the OAA design enhanced stability of polyplexes and subsequent transfection efficacy;[103, 131] the azido function enables subsequent covalent click-coupling.[65] From this starting point, in the current work we designed a new library (**Fig. 23**) consisting of three main classes of lipo-OAA backbones; a cysteine-containing disulfide stabilizing type, a non-reducible type, and a bio-reducible type containing a cystamine linkage between the lipid domain and cationizable Stp backbone; all classes were tested with different incorporated saturated and unsaturated fatty acids, and optional also endosomal buffering histidines[13, 132, 133] that were integrated into the Stp backbone in alternative fashion. Sequences of lipo-OAAs, library identification (ID) numbers, mass spectra and proton NMR spectra confirming these structures are presented in **Tab. S2, S3** and **Fig. S3, S4**.

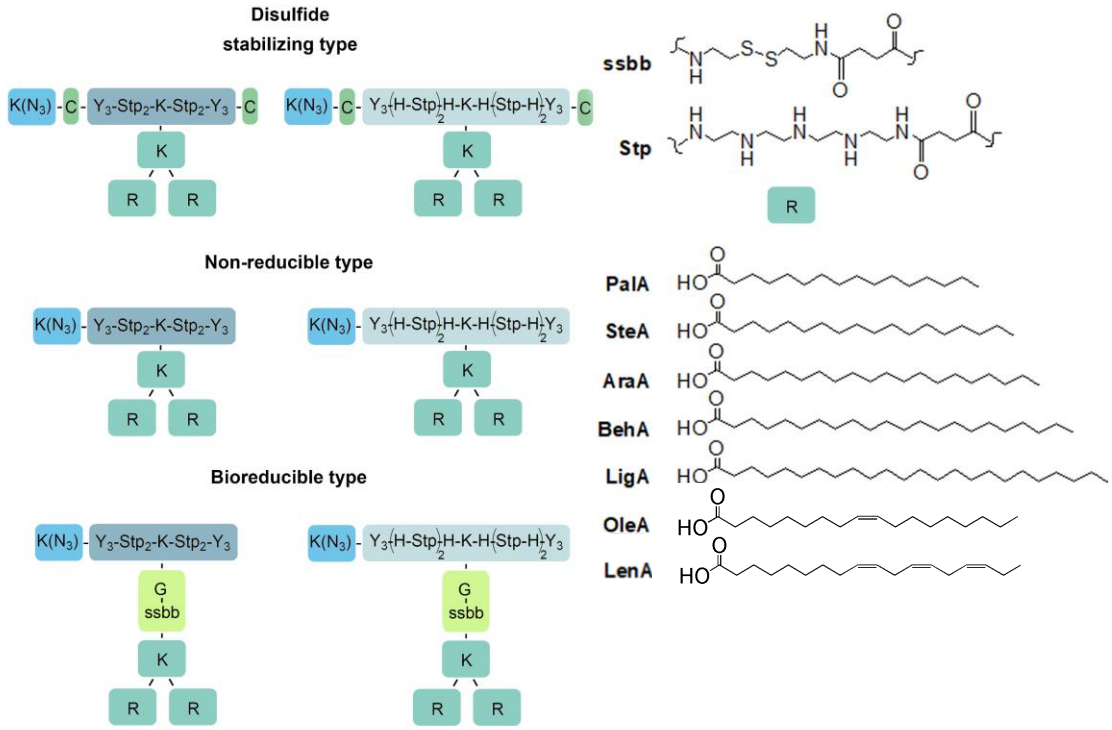

Fig. 23. Overview of chemical compounds. Schematic illustration of new sequence-defined oligomers, disulfide stabilizing, non-reducible and bioreducible types. Units of the oligomers: Y: tyrosine, K: lysine, H: histidine, Stp: succinoyl-tetraethylene-pentamine, G: glycine, saturated fatty acids (PalA: palmitic acid, SteA: stearic acid, Ara: arachidic acid, BehA: behenic acid, LigA: lignoceric acid), unsaturated fatty acids (OleA: oleic acid, LenA: linolenic acid), ssbb: succinoyl-cystamine, ss building block.

3.2.2 Lipo-oligoaminoamides screening for siRNA delivery

Screening the novel lipo-OAA library identified oligomer ***1214*** (**Fig. 24A)** (containing cysteines and histidines in the backbone as well as oleic acids in the lipidic domain) as the most suitable siRNA carrier for subsequent surface modification. siRNA polyplexes were formed by mixing at a defined azido-oligomer /siRNA N/P ratio and incubated for 45 min. Based on previous titrations, the N/P ratio, representing the ratio of protonatable amines (N) of the oligomers to phosphates (P) of the siRNA (**Tab. S2**), was set to 12. The sizes, PDIs, and zeta potentials of siRNA polyplexes was determined by dynamic light scattering (DLS) (**Fig. 24B** and **Fig. 25**). Most polyplexes had a hydrodynamic diameter of 150-300 nm by DLS; the superior ***1214*** polyplexes

had a stable ~200 nm nanoparticle size, which was also confirmed by a low PDI of 0.20. The average zeta potentials of siRNA polyplexes were around 20-30 mV; ***1214*** had a relatively high zeta potential of +28.5 mV.

Stability of siRNA / lipo-oligomer complexes was analyzed after incubation in 90% fetal bovine serum (FBS) followed by the electrophoresis in a 2.5% agarose gel (**Fig. 26**). For the first two classes of cysteine-containing disulfide stabilizing and non-reducible types, the oligomers without or with histidine modified backbone containing stearic acid (steA) or OleA fatty acids showed complete gel retardation of siRNA and no release of free siRNA. For the bioreducible type, all types of polyplexes showed significant siRNA release in serum. Incorporation of histidines had no significant influence on stabilization of non-reducible type of polyplexes. For disulfide-stabilizing oligomers containing PalA side chains, the alternative histidine-Stp backbone improved stability of siRNA polyplexes compared to the non-histidine backbone. Among the disulfide stabilization and non-reducible types, SteA and OleA both showed stronger binding with siRNA compared to other saturated and unsaturated fatty acid. In summary, the disulfide stabilizing oligomers containing cysteine, histidine and SteA or OleA hydrophobic fatty acid domains mediated suitable stabilization of siRNA polyplexes.

Gene silencing experiments (**Fig. 24C** and **Fig. 27**) were performed using Huh 7 hepatocellular carcinoma cells stably expressing an eGFPLuc (enhanced green fluorescent protein/luciferase fusion protein) marker gene. Specific silencing of the eGFPLuc fusion gene by siGFP was measured by a luminometric luciferase assay. Unspecific reduction of reporter activity was determined using the analogous siCtrl formulations. For all three types of oligomers (disulfide-stabilizing, non-reducible, and bioreducible types), oligomer ***1214*** mediated highest gene silencing efficiency, as indicated by the lowest eGFP-luciferase marker activity. In general, the stabilizing cysteine-containing class (including oligomer ***1214***) showed highest functional siRNA transfer, followed by non-reducible oligomers with moderate gene silencing, and the

bioreducible lipo-OAAs (containing the ssbb building block) lacking gene silencing efficiency in the screened reporter cells. In regard to the carbon numbers of fatty acids (from C16 to C24), C18 mediated higher silencing efficiency, and the unsaturated fatty acid OleA higher efficiency then the saturated fatty acid stearic acid, consistent with a previous lipo-OAA screen.[32] In sum, the screening for stabilizing and transfection-active polyplexes revealed 1) terminal cysteines and 2) alternative Stp and histidine on the backbones, as well as 3) oleic acids as unsaturated fatty acids in the lipidic domain as most favorable elements.

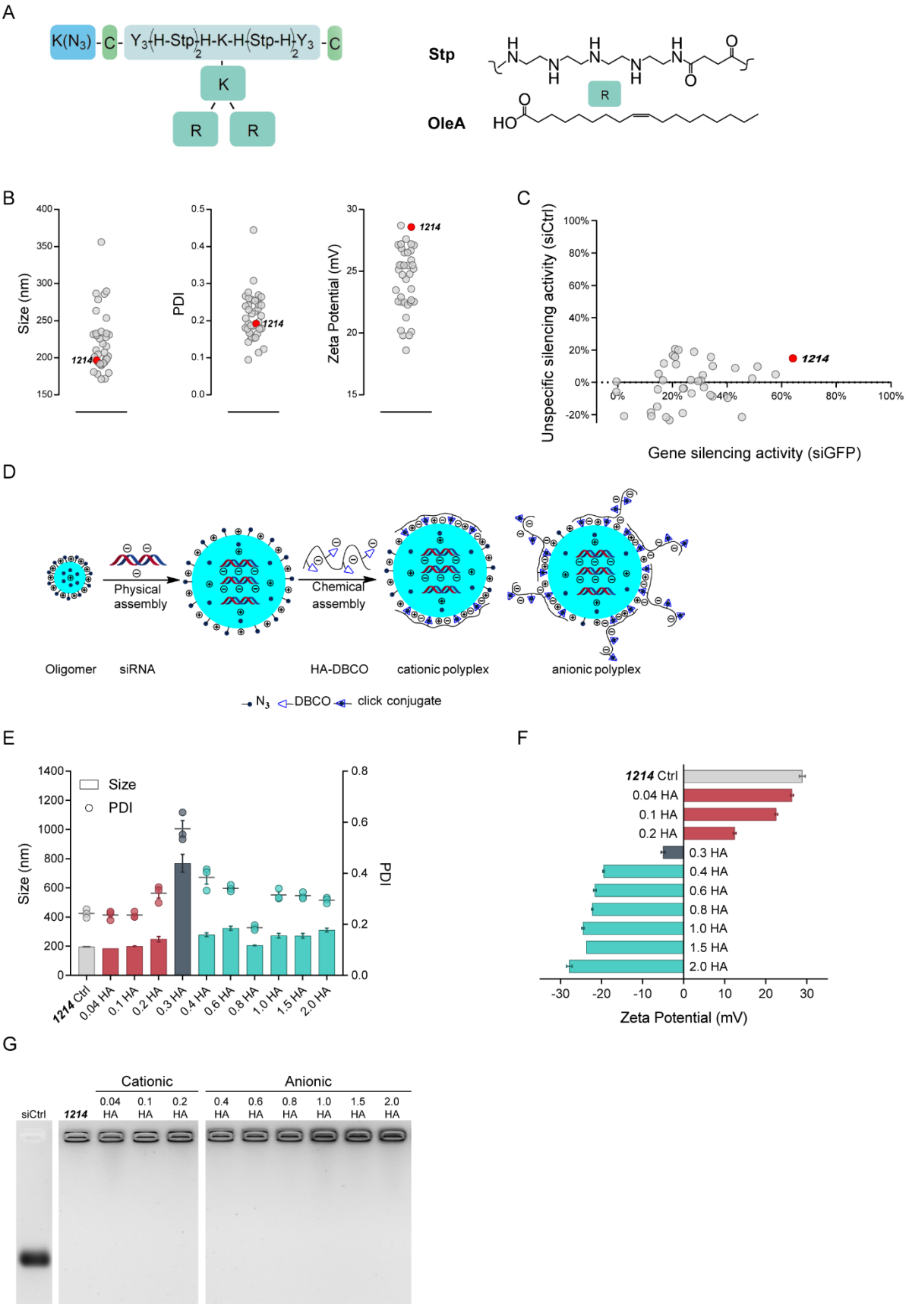

Fig. 24. A) Chemical structure of oligomer ***1214***. Y: tyrosine, K: lysine, H: histidine, Stp: succinoyl-tetraethylene-pentamine, G: glycine, OleA: oleic acid. B) Particle size (z-average)

and zeta potential of siCtrl formulations determined with a DLS zetasizer. The ***1214*** siRNA polyplex were prepared at N/P 12. C) Gene silencing activity of siRNA formulations at N/P ratio 12 tested by luciferase assays in Huh 7/eGFPLuc reporter cells. Specific gene silencing (using siGFP) is compared with unspecific reporter silencing (by siCtrl formulations). D) Click modification of siRNA polyplexes with HA-DBCO. Particle size (z-average) (E), PDI (E) and zeta potential (F) of ***1214*** formulations with siCtrl, as determined by DLS zetasizer. Lipopolyplexes were prepared at N/P 12 and modified with indicated different molar equiv. of HA-DBCO. G) Gel electrophoresis of ***1214*** formulations with different equiv. of HA-DBCO. The molar equivalents (equiv. HA) relate to the molar ratio of HA-linked DBCO to the azide of the cationic oligomers (DBCO/azide, mol/mol).

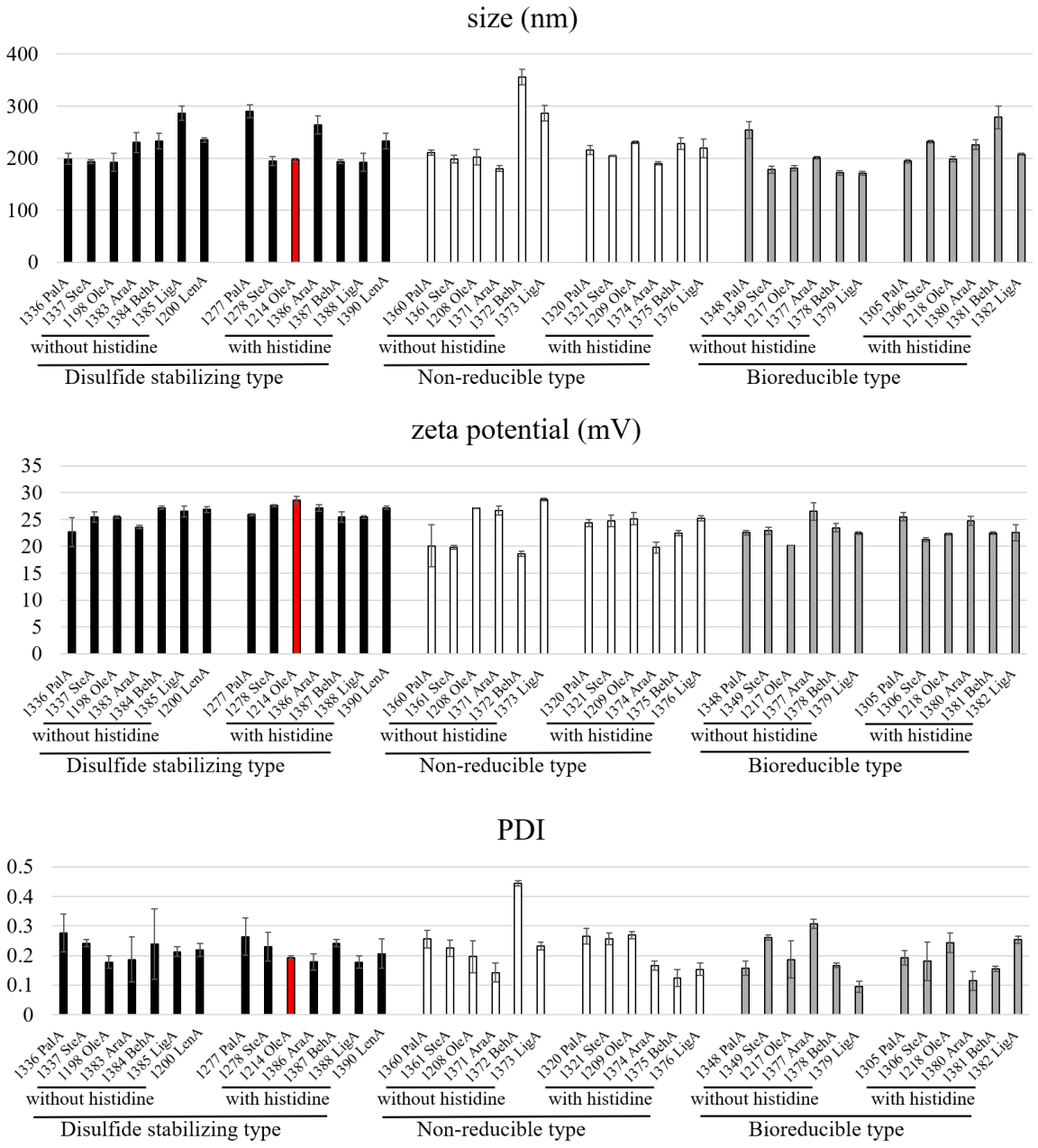

Fig. 25. **Detailed presentation of zetasizer data as presented in main Fig.1B.** Particle size (z-average diameter in nm), PDI, and zeta potential of siCtrl formulations as determined with a DLS zetasizer. The siRNA polyplexes were prepared at N/P 12.

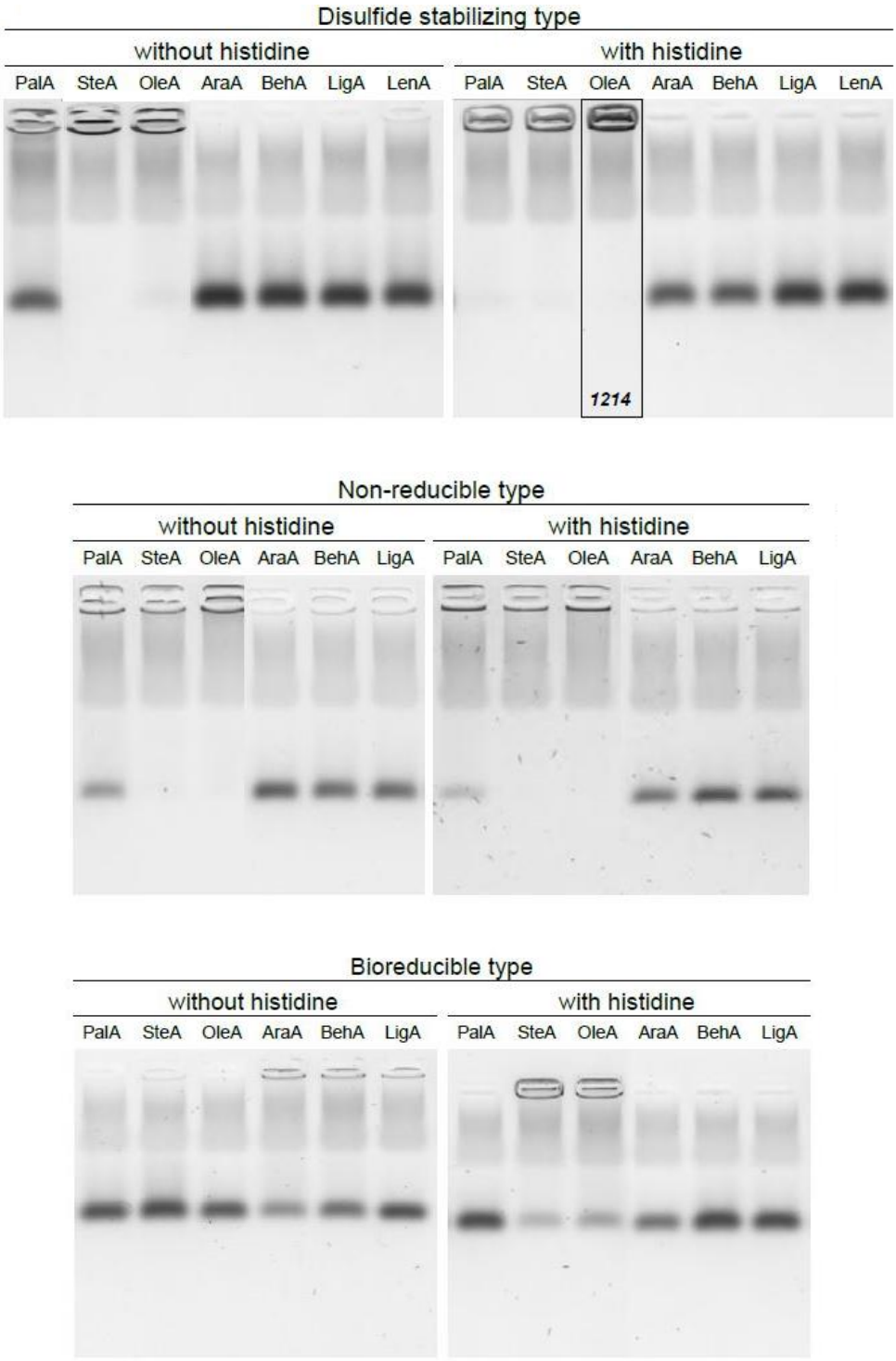

Fig. 26. **Gel electrophoresis of oligomers** (disulfide stabilizing, non-reducible and bioreducible types) with siCtrl at N/P ratio 12 incubated for 4h in 90% serum.

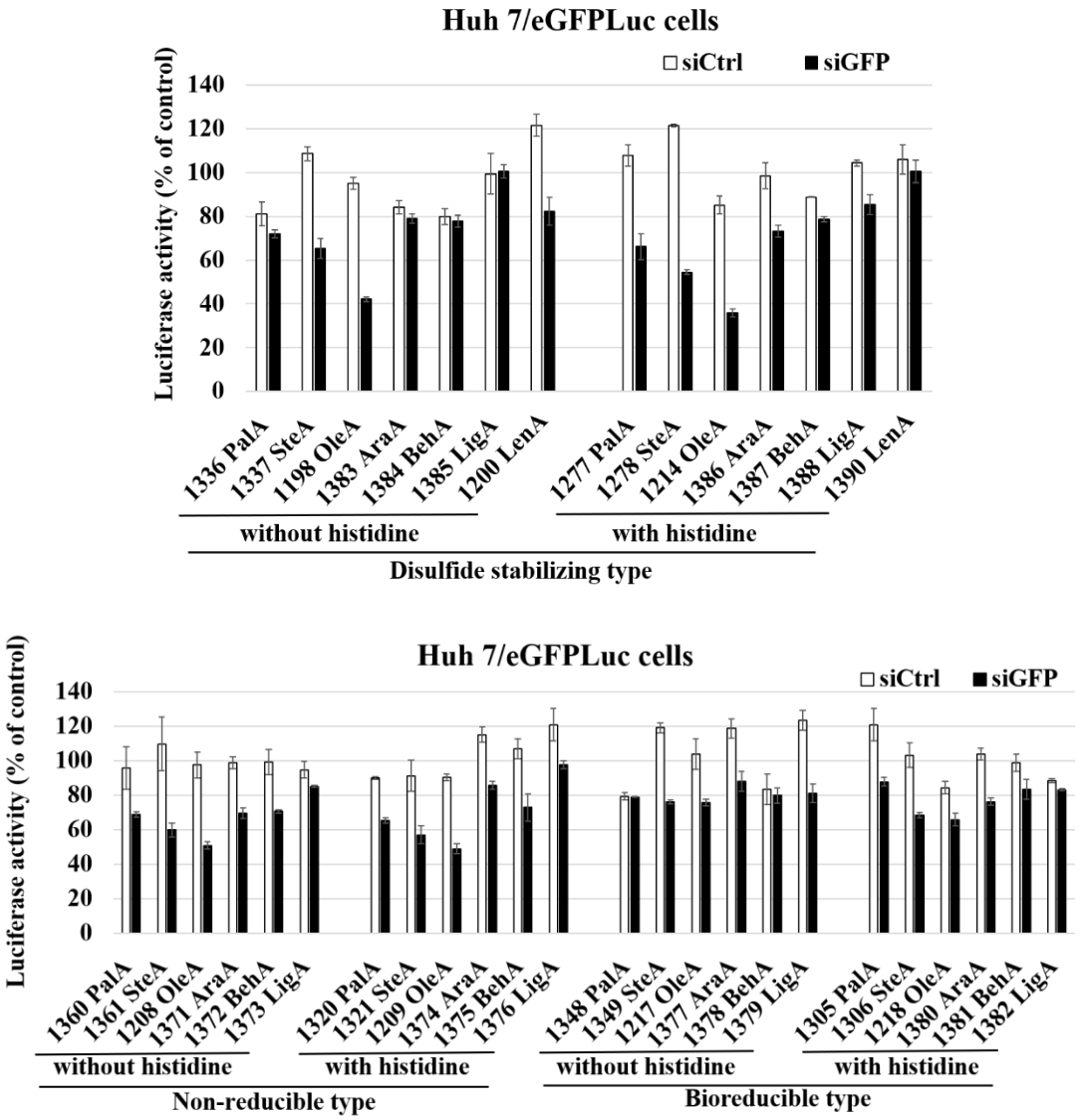

Fig. 27. **Detailed presentation of data as presented in main Fig.1 C.** Luciferase activity of siRNA formulations (500ng siRNA/well) at N/P ratio 12 in Huh 7/eGFPLuc cells after 48 h incubation.

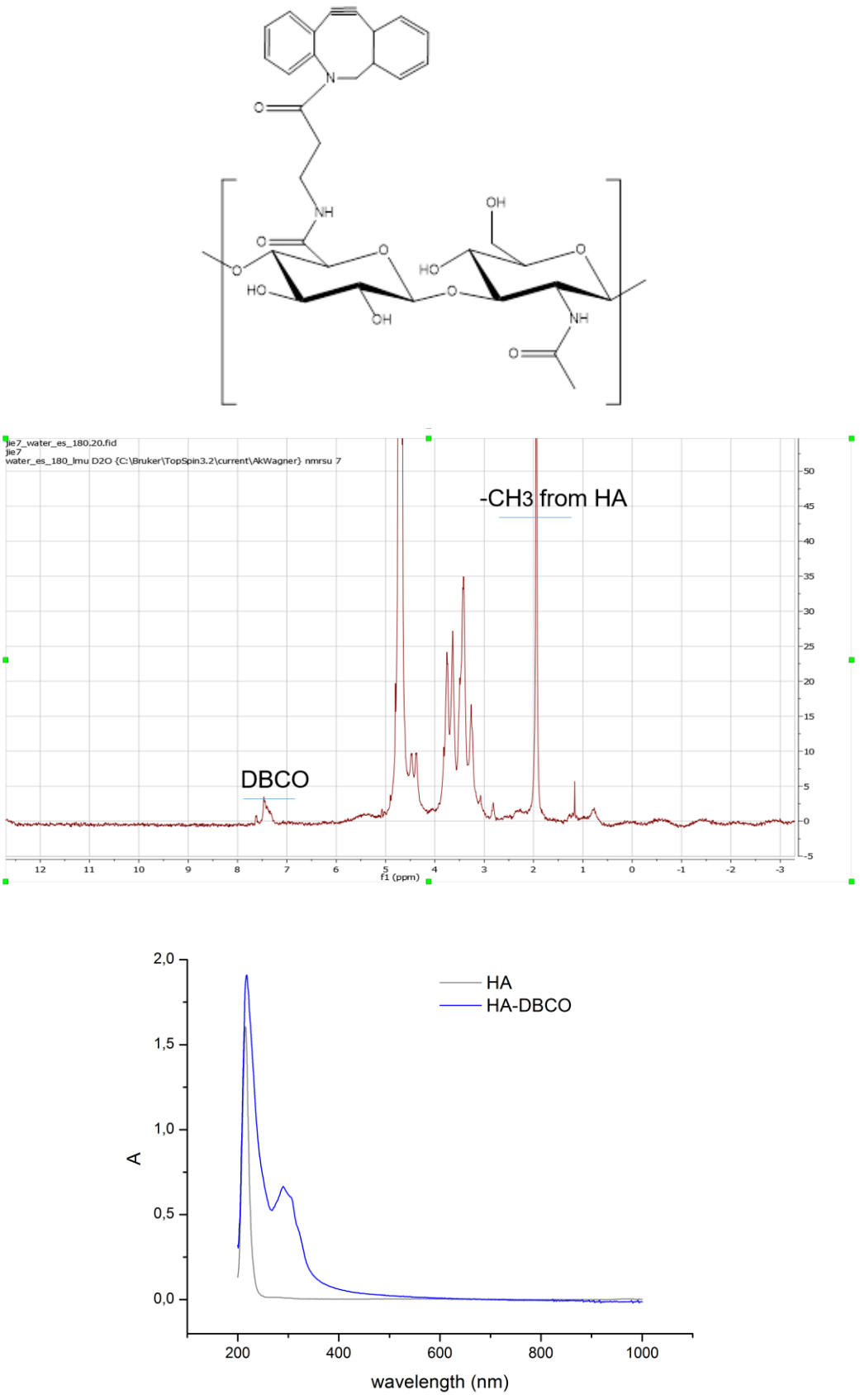

Fig. 28 Structure, NMR and UV-VIS of DBCO modified hyaluronic acid (HA).

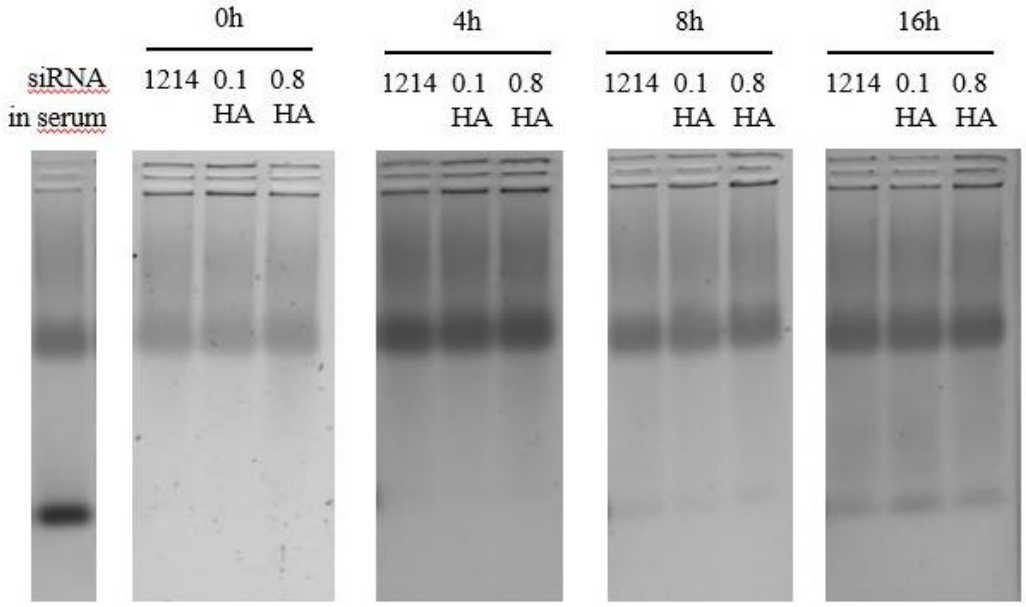

Fig. 29 Gel electrophoresis of ***1214*** formulations with different equiv. of HA-DBCO. The molar equivalents (equiv. HA) relate to the molar ratio of HA-linked DBCO to the azide of the cationic oligomers (DBCO/azide, mol/mol). Polyplexes containing 500ng siRNA were incubated in 90% serum and analyzed at different time points.

3.2.3 Hyaluronic acid (HA) for covalent modification of siRNA polyplexes

For covalent decoration of lipo-OAA / siRNA polyplexes with polyanionic HA (**Fig. 24D**), we had designed lipo-oligomers such as ***1214*** with an N-terminal azido-lysine, and HA was modified with DBCO units as linkage modules. The modification degree of HA's carboxylic groups with DBCO-amine was 8%, as confirmed by UV-VIS and NMR data (**Fig. 28**). This represents approximately 4 DBCO molecules per 20 kDa HA polymer chain.

3.2.4 Formation and stability of cationic and anionic HA-modified siRNA polyplexes

After screening of lipo-OAAs, oligomer ***1214*** was selected for all subsequent investigations. The azido function of ***1214*** exposed on the surface of siRNA polyplexes serves as anchor for polyplex modification with hyaluronic acid (HA). Each 20 kDa HA molecule was modified with approximately 4 DBCO linkers (see above) to enable

covalent copper-free, strain-promoted alkyne-azide cycloaddition (SPAAC) to the siRNA polyplexes. The amount of HA-DBCO is presented as molar equivalents (equiv.) of DBCO related to the cationic ***1214*** oligomer azides (mol/mol). Obviously, as considerable extent of oligomers will be located within the interior of the core lipopolyplexes, only a fraction of azides is available at the siRNA nanoparticle surface for click modification.

Unmodified ***1214*** polyplexes had a hydrodynamic diameter of 200 nm (**Fig. 24E**). Modification with up to 0.2 equiv. of HA-DBCO or between 0.4 to 2.0 equiv. HA-DBCO did not show any considerable change in nanoparticle size, whereas modification with 0.3 equiv. of HA-DBCO showed a sharp increase in size (around 810 nm), indicating the presence of aggregates. This was confirmed by the high PDI of 0.58 (**Fig. 24E**) and can explained by an almost neutral zeta potential (**Fig. 24F**). With the increase of HA-DBCO modification from 0.04 to 2.0 HA-DBCO, the zeta potential of the ***1214*** siRNA lipopolyplexes decreased shifting from positive charge to negative charge (**Fig. 24F**). The stability of positively and negatively charged polyplexes was also confirmed by agarose gel electrophoresis. Both the positively and negatively charged polyplexes displayed colloidial stability. In 20 mM HEPES buffered 5% glucose (HBG, pH 7.4) buffer (**Fig. 24G**), a complete siRNA binding at N/P ratio of 12 for all cationic and anionic formulations was observed. Also, in 90% serum, all formulations were stable up to 8h (**Fig. 29**).

3.2.5 Gene silencing activity and cellular uptake of cationic and anionic HA / siRNA polyplexes

Unless indicated differently, cationic and anionic polyplexes modified with 0.1 equiv. HA-DBCO or 0.8 equiv. HA-DBCO, respectively, were selected for subsequent experiments. Though the two nanoparticle formulations were similar in sizes (200.3± 3.9 nm and 205.8 nm± 4,7 in diameter), the difference in zeta potential between low 0.1HA (+22.7 mV) and high 0.8HA (-21.8 mV) is very large. These two formulations

(0.1HA and 0.8HA) also showed the highest cellular uptake in their cationic and anionic groups, respectively. Reporter gene silencing experiments with the two HA formulations were performed again in Huh 7/eGFPLuc (**Fig. 30A**). For unmodified ***1214*** siRNA lipo-polyplexes, the knockdown of reporter activity was around 60%. Compared to this unmodified control, cationic HA modification polyplexes increased the gene silencing efficiency by further 5%. The anionic HA polyplexes mediated a higher silencing activity of 72% knockdown. eGFP-luciferase marker expression levels of cells treated with siCtrl polyplexes did not significantly change compared to untreated cells, indicating that the formulations did not have any intrinsic RNAi-independent cytotoxicity.

Cellular uptake of cationic and anionic HA polyplexes was evaluated by flow cytometry. Cells were incubated with Cy5 siRNA formulations for 2 h at 37 °C, and washed with PBS and heparin for dissociation of extracellularly associated polyplexes from cell surface membranes before analysis. **Fig. 30B** displays the cellular uptake of siRNA polyplexes into Huh 7 cells. Both cationic and anionic polyplexes modified with 0.1 equiv. HA-DBCO or 0.8 equiv. HA-DBCO, respectively, showed high uptake, which was superior over non-coated cationic ***1214*** siRNA polyplexes. The same formulations showed also the highest cellular uptake in KB cells (**Fig. 31**).

Further on, endocytotic pathways of cationic and anionic HA siRNA nanoparticles into Huh 7 cells were characterized by monitoring the change of Cy5-siRNA internalization after pretreatment with different inhibitors for specific pathways,[121, 134] such as nystatin (15 µg/mL) for inhibiting caveolin-mediated endocytosis,[135] sucrose (154 mg/mL) for inhibiting clathrin-mediated endocytosis,[136] amiloride (133 µg/mL) for inhibiting macropinocytosis,[137] sodium azide (1 mg/mL) for inhibiting energy-dependent endocytosis[138] and excessive amount of free HA (10 mg/mL, 20 KDa) for competition of HA-mediated endocytosis (**Fig. 30C-30D, Fig. 32 and Fig. 33**). The cytotoxicity of inhibitors at indicated concentrations used in following experiments was evaluated and not significantly different from the HBG treated control cell group (**Fig.**

32). The pretreatment of sucrose inhibited the cellular uptake of cationic HA ***1214*** polyplexes, suggesting clathrin-medicated endocytosis as main uptake mechanism, whereas both amiloride and sucrose inhibited anionic HA ***1214*** polyplex internalization, indicating both clathrin- and macropinocytosis-mediated uptake pathway (**Fig. 30C**). Negatively charged HA has been previously characterized to enter cells by macropinocytosis.[139] Entry of anionic 0.8HA polyplexes by macropinocytosis is consistent with the fact that the polyplex surface is completely covered with HA. Cationic medium-sized (~50-200 nm) nanoparticles such as PEI polyplexes were previously found to enter via clathrin- and/or caveolae-mediated endocytosis and not macropinocytosis.[140] In HA competition studies (**Fig. 30D**), excess amount of HA decreased cellular uptake of cationic and anionic HA polyplexes into Huh 7 cells by >76% or 46%, respectively.

According to confocal laser scanning microscopy (CLSM) images (**Fig. 30E** and **Fig. 34**), the anionic polyplexes with 0.8 equiv. HA-DBCO showed a higher degree of polyplex internalization in two cell lines (Huh7 and KB cells) compared to the non-coated control and cationic 0.1 equiv. HA-DBCO polyplexes. For all following experiments, ***1214*** polyplexes with either 0.1 HA-DBCO or 0.8 HA-DBCO were selected as representative cationic or anionic HA siRNA nanoparticles, respectively. The subcellular distribution of cationic and anionic HA polyplexes in Huh 7 cells was examined using CLSM (**Fig. 30F**). After cells were incubated with the different polyplexes for 2h, siRNA was mainly colocalizing with Lysotracker, a late endosome and lysosome marker, indicating that both types of HA polyplexes were effectively taken up by Huh 7 cells into the endosomal compartment. 3D colocalization of cationic and anionic polyplexes with CD44 as cellular receptor of HA was demonstrated (**Fig. 35**).

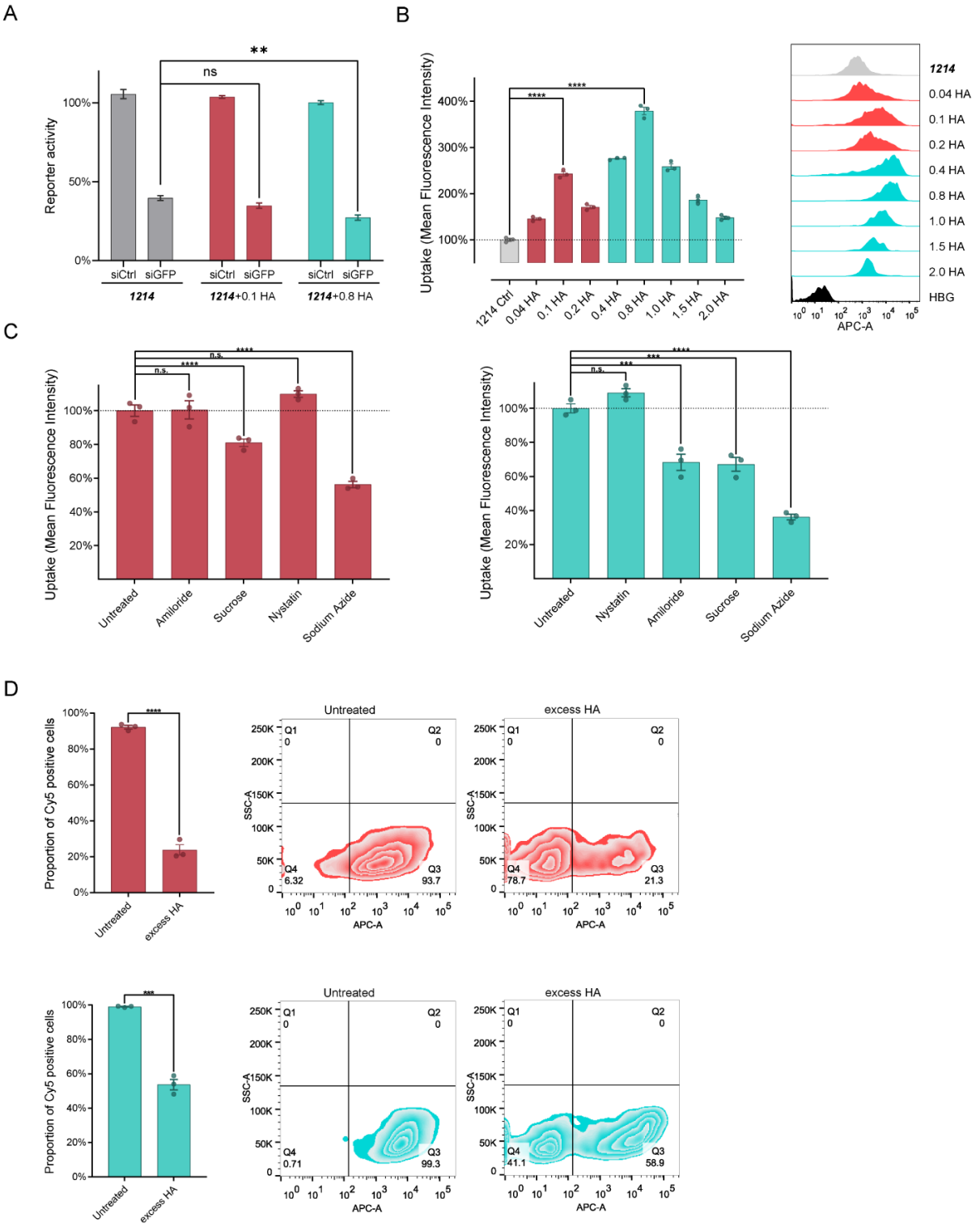
A
B
C
D
Reporter activity
siCtrl
siGFP
1214
1214+0.1 HA
1214+0.8 HA
Uptake (Mean Fluorescence Intensity)
1214 Ctrl
0.04 HA
0.1 HA
0.2 HA
0.4 HA
0.8 HA
1.0 HA
1.5 HA
2.0 HA
HBG
APC-A
Untreated
Amiloride
Sucrose
Nystatin
Sodium Azide
Proportion of Cy5 positive cells
excess HA
SSC-A
Q1
Q2
Q3
Q4
6.32
93.7
78.7
21.3
0.71
99.3
41.1
58.9

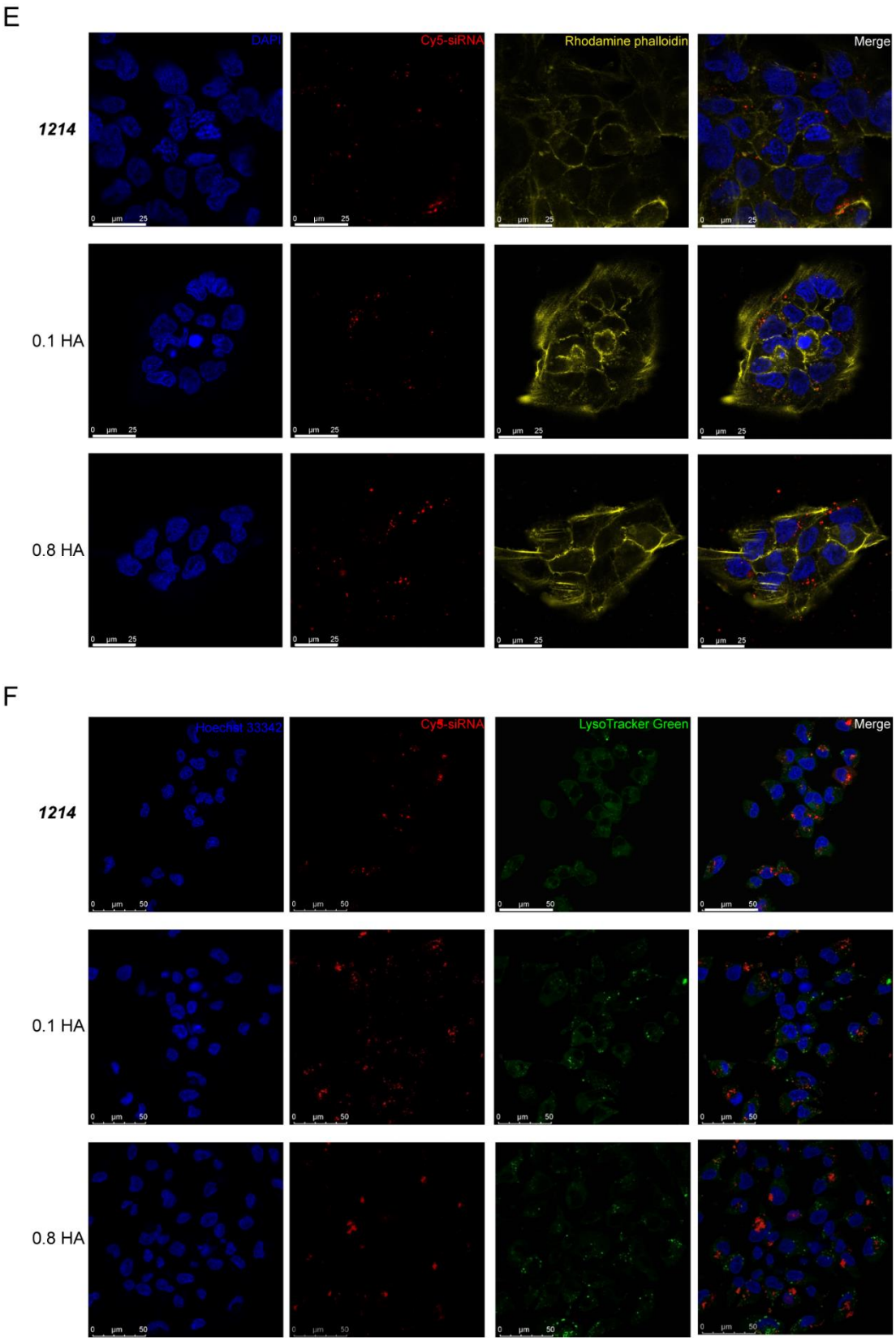

Fig. 30. Intracellular siRNA delivery mediated by cationic and anionic ***1214*** polyplexes. A) Luciferase activity of cationic and anionic formulations at N/P ratio 12 in Huh 7/eGFPLuc reporter cells. The luciferase activity of the eGFPLuc fusion protein was measured at 48 h. The results are presented as percentage of the luciferase gene expression obtained with untreated

control cells. (B) Uptake of ***1214*** formulations into Huh 7 cells was determined by flow cytometry after 2h incubation at 37°C. ***1214*** siRNA polyplexes were prepared containing 20% Cy5-labeled siRNA and modified with indicated different equiv. of HA-DBCO. C) Endocytosis pathways of cationic (left) and anionic (right) ***1214*** formulations characterized by different pretreatments with endocytosis inhibitors in Huh 7 cells determined using the flow cytometry. D) To test whether the HA-polyplexes uptake was mediated by receptor, the ligand competition study was performed in presence of excess of HA (10 mg/mL, 20 kDa) in Huh 7 cells for 1 hour before adding various cationic (upper) and anionic (lower) ***1214*** HA-polyplexes for additional 2 hours. siRNA polyplexes were formed at N/P 12 using Cy5-labeled siRNA. The number of Cy5-positive cells was analyzed by flow cytometry. Polyplex positive control: without HA modification competition. E) Cellular association of ***1214*** siRNA formulations in Huh 7 cells acquired by confocal laser scanning microscopy (CLSM). Cells were incubated with the formulations for 2h at 37℃ and washed with PBS buffer and heparin. Actin cytoskeleton was stained with rhodamine phalloidin, nuclei were stained with DAPI and siRNA was Cy5-labeled. Scale bars: 25 µm. F) Subcellular distribution of cationic and anionic ***1214*** HA formulations complexed with Cy5-siRNA in Huh 7 cells. The late endosomes and lysosomes were stained with LysoTracker Green. Scale bars: 50 µm. The statistical significance was determined by one way ANOVA (A, B, C); unpaired t test (D). *P < 0.05, **P < 0.01, ***P < 0.001, ****P < 0.0001, n.s., not significant. Confocal microscopy was performed by Miriam Höhn (Department of Pharmacy, LMU Munich).

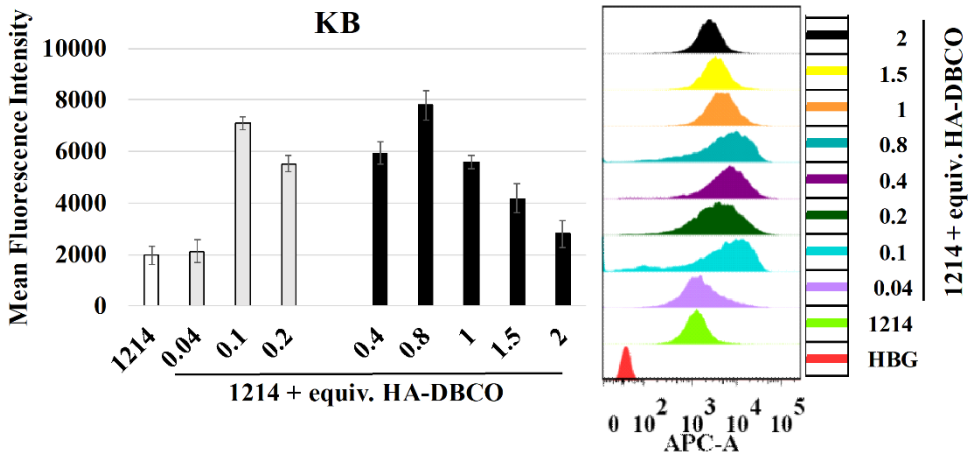

Fig. 31 Uptake of ***1214*** formulations into KB cells (A) was determined by flow cytometry after 2h incubation at 37°C. ***1214*** siRNA polyplexes (1.25 µg siRNA/well) were prepared containing 20% Cy5-labeled siRNA and modified with different equiv. of HA-DBCO.

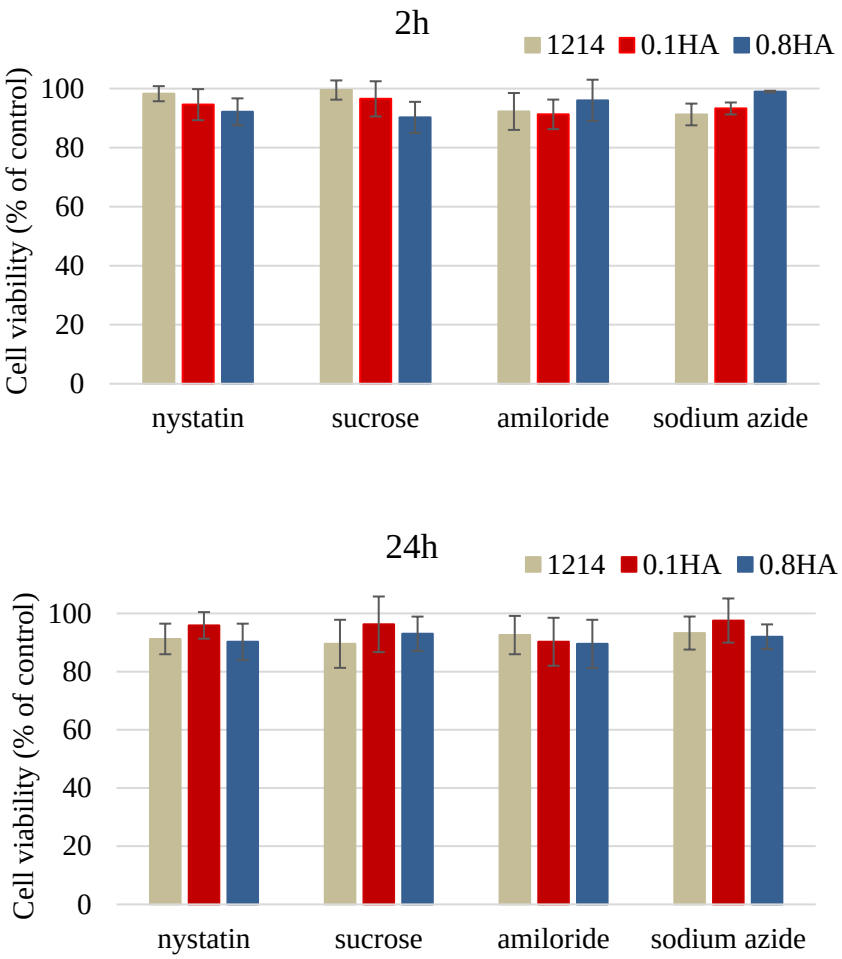

Fig. 32 Viability of Huh7 cells pre-treated with different inhibitors for 1h and subsequent incubation for 2h (upper) and 24h (lower) with unmodified (***1214***) and targeted cationic (0.1HA) or anionic (0.8HA) ***1214*** siRNA polyplexes.

Huh7 cells were seeded on 96-well plates at a density (8000 cells/well) in 100 µL of medium 24 h before the experiment. Medium was replaced by 80 µL of fresh medium. The cells were pre-incubated with 20µL of inhibitor solution (final concentration: nystatin 15 µg/mL, sucrose 154 mg/mL, amiloride 133 µg/mL, sodium azide 1 mg/mL) for 1 h at 37°C. Afterwards, the medium changed and incubated at 37°C for 2h after adding different cationic and anionic formulations containing 0.5 µg of siRNA (N/P ratio of 12). The medium was then replaced with 100 µL of fresh medium and cells were cultured for 2h and 24h time points. MTT assays (Life Technology, Darmstadt, Germany) were performed to evaluate the cell viability. The experiments were performed in triplicates using SpectraFluor Plus microplate reader (Tecan, Austria). The relative percentage were related to HBG buffer-treated control cells.

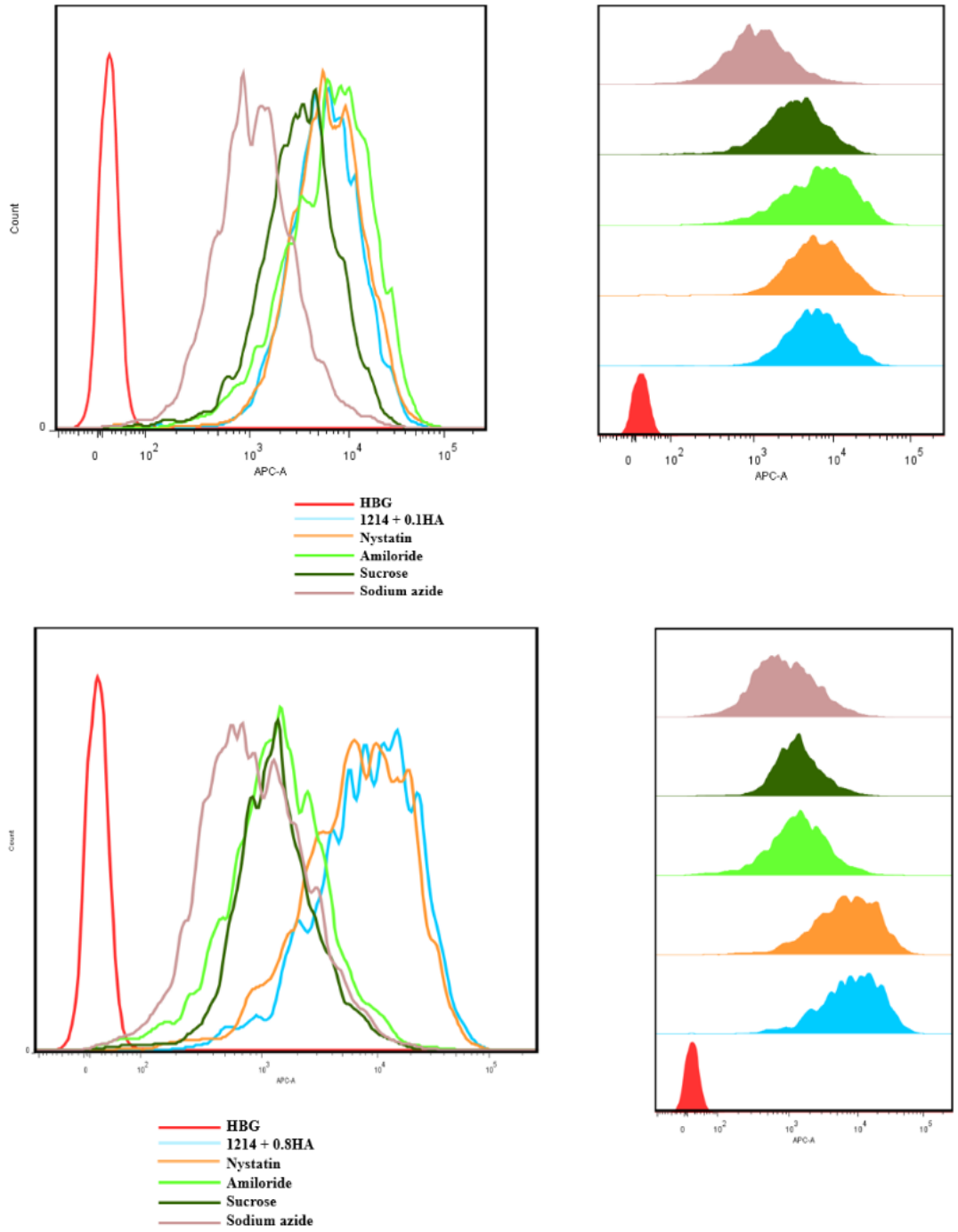

Fig. 33 Cellular uptake of cationic (upper) and anionic (lower) targeted ***1214*** siRNA polyplexes into KB cells determined by flow cytometry. Polyplexes (1.25µg siRNA/well) were formed at N/P 12 using 20% Cy5-labeled siRNA. Cells were pre-treated with different inhibitors for 1h.

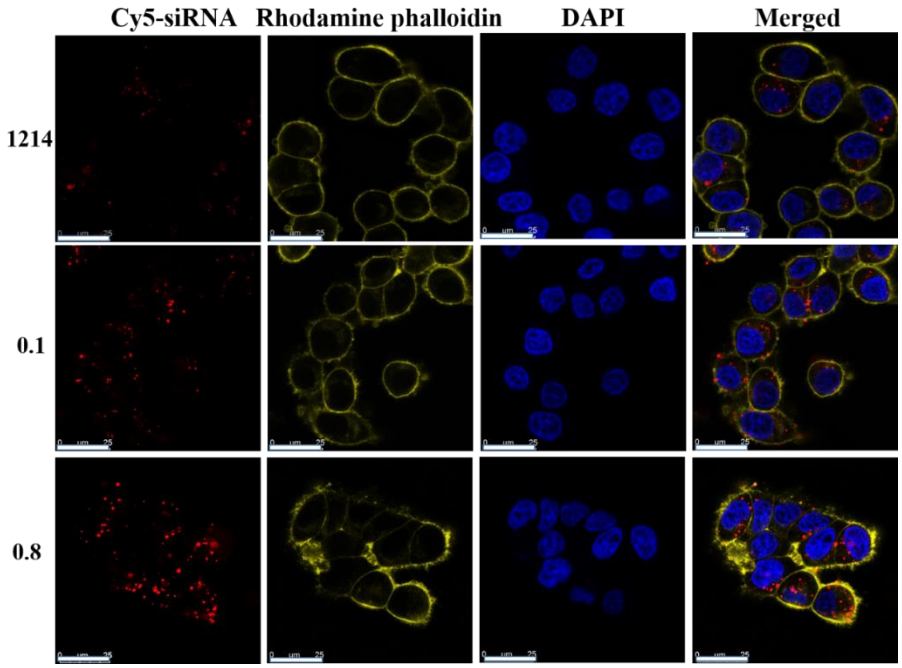

Fig. 34 Cellular association of siRNA formulations in KB cells determined by confocal laser scanning microscopy (CLSM). Actin cytoskeleton was stained with rhodamine phalloidin, nuclei were stained with DAPI and Cy5-labeled siRNA was used. White scale bars indicate 25 µm. Experiment performed by Miriam Höhn (Department of Pharmacy, LMU Munich).

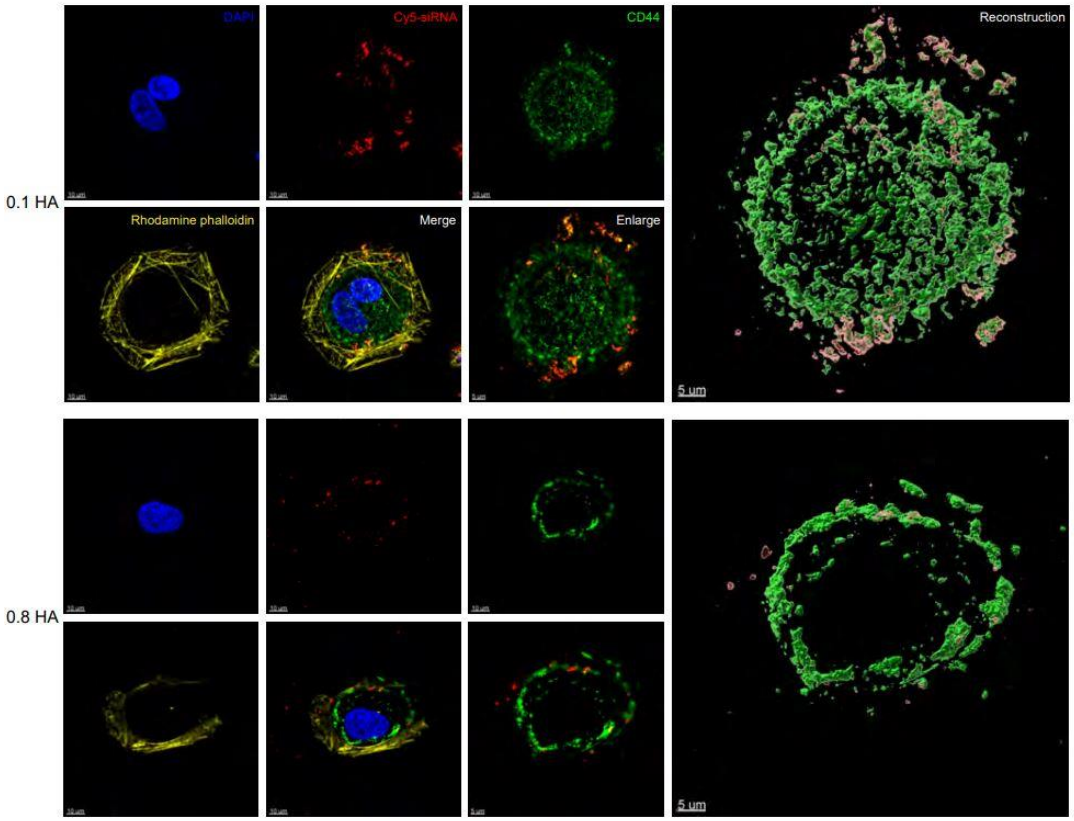

Fig. 35 Colocalization of cationic (upper) and anionic (lower) nanoparticles target CD44 receptor using Imaris analysis. Scale bar: 10 µm. For enlarged figure, scale bar: 5 µm. Together with Mochen Cui (Faculty of Medicine, LMU Munich).

3.2.6 Delivery of cationic and anionic HA-modified siRNA polyplexes *in vivo*

After the screening and evaluation of polyplexes for intracellular delivery, these formulations should undergo evaluation in tumor models *in vivo* by biodistribution and gene silencing assays. ***1214*** polyplexes and ***1214*** polyplexes with 0.1 equiv. or 0.8 equiv. of HA-DBCO modification were analyzed for systemic biodistribution in mice bearing subcutaneous Huh7 tumors (**Fig. 36A**). Mice were injected with polyplexes formulating Cy7-conjugated siRNA *via* tail vein, and the biodistribution of the dye was monitored at various time points with a NIR bioimaging system. Compared to the unmodified ***1214*** siRNA polyplexes, it was interesting to note that the ***1214*** polyplexes with 0.1 equiv. of HA-DBCO modification rapidly appeared with a strong fluorescence signal in the tumor remaining high for up to 1 h, whereas anionic ***1214*** siRNA polyplexes with 0.8 equiv. of HA-DBCO modification did not accumulate in the Huh 7 tumor as evidenced by the lack of pronounced fluorescence. In previous experiments with this tumor model, we had observed that analogous PEG shielded polyplexes did not accumulate in Huh 7 tumors (**Fig. 37**). The well-understood ‘passive’ enhanced permeability and retention (EPR) mechanism for PEGylated nanoparticles would require long-term circulation times. Consistent with our previous reports,[130] our class of siRNA polyplexes circulates only short-term (**Fig. 38**). Obviously, transient accumulation in tumors must proceed by a different “active” mechanism. Huh 7 tumor cells are known to express CD44. Therefore we also applied these formulations in another tumor mouse model bearing poorly differentiated CD44 deficient Neuro2a neuroblastoma cells known to be non-responsive for HA binding [141] (**Fig. 39**). Nevertheless, we observed also in this model that the cationic 0.1 equiv. HA-DBCO containing nanoparticles (0.1HA) display a higher tumor accumulation, compared to the cationic unmodified and the anionic 0.8 equiv. HA-DBCO containing (0.8HA) formulations. Apparently, 0.1HA polyplexes demonstrated favorable accumulation in both (CD44 positive Huh 7 and CD44 negative Neuro2A) tumor cell models. CD44 is known to be overexpressed in solid tumor vasculature.[125, 126] Therefore, we

hypothesize that in both cases a CD44/HA interaction with tumor vasculature might play an active role in the observed tumor accumulation. This hypothesis remains to be experimentally proven, for example by replacing HA for other anionic polymers, or by in vivo (HA/CD44) competition experiments.

HA polyplexes were then analyzed for gene silencing in Huh 7 tumors (**Fig. 36B**). Polyplexes were prepared with siEG5 against the kinesin-related motor protein EG5 or siCtrl (50 µg of siRNA). Five mice per group were subcutaneously injected with Huh 7 tumor cells and the weight of the animals was monitored. When tumors reached a size of 500mm^3, the formulations were administered *via* tail vein twice at daily interval. At 24 h after the second injection of formulations, the tumors were harvested, RNA was extracted and the EG5 mRNA levels were quantified by quantitative real-time polymerase chain reaction (qRT-PCR). The ***1214*** siEG5 group with 0.1 equiv. of HA-DBCO modification induced a strong and significant downregulation of EG5 mRNA expression by ~78% in tumor treated animals as normalized to untreated HBG group. The unmodified ***1214*** siEG5 group mediated a moderate gene silencing (~30%) of EG5 mRNA. Interestingly, the formulation of ***1214*** siEG5 with 0.8 equiv. of HA-DBCO, which was most effective in cell culture, revealed negligible gene silencing (~10% on EG5 mRNA level). None of the control groups with siCtrl formulation showed significant reduction of EG5 mRNA as compared to animals treated with HBG control buffer. In summary, the ***1214*** formulation with 0.1 equiv. of HA-DBCO coating targeted Huh 7 tumors and achieved a strong 78% knockdown of EG5 *in vivo*.

Systemic circulation of siRNA polyplexes might also cause potential side effect and inflammatory response when they reach non-targeted tissues. Therefore, blood biochemistry examinations were carried out in order to realize the biocompatibility of the polyplexes (**Fig. 36C-36F**). Blood samples were collected 24 h after two injections of siRNA formulations in healthy mice and four relevant clinical parameters were

determined. There is no increase of liver enzymes (ALT and AST) or renal parameters (BUN and CREA) were found compared to the untreated HBG group.

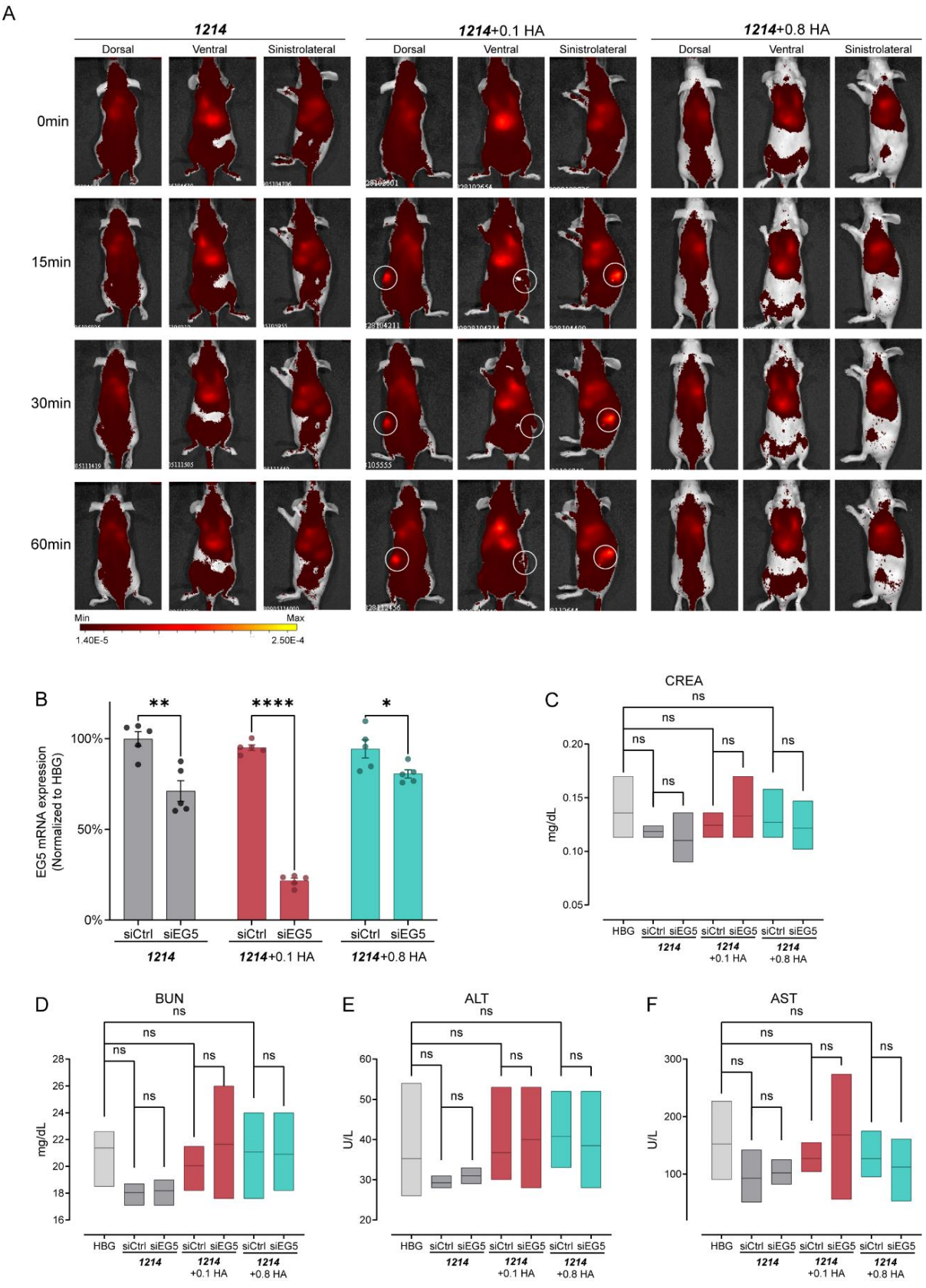

Fig. 36. *In vivo* performance of siRNA polyplexes. (A) Biodistribution of siRNA formulations (50 µg siRNA, 50% Cy7-labeled, with ***1214*** at N/P 12) after i. v. administration in Huh 7 tumor-bearing NMRI nude mice. Biodistribution was determined by NIR fluorescence bioimaging comparing unmodified ***1214*** siRNA polyplexes with polyplexes modified with different equiv. of HA-DBCO. The tumor sites containing accumulated siRNA nanoparticles are highlighted by white circles. Experiment performed by Johannes Schmaus (veterinary MD student, LMU Munich). (B) Tumor-targeted gene silencing efficiency of cationic and anionic ***1214*** siRNA formulation with 0.1 and 0.8 equiv. of HA-DBCO with 50 µg of siEG5 or siCtrl (mean ± SEM; n=5). (C-F) Clinical biochemistry parameters creatinine (CREA), blood urea nitrogen (BUN), alanine aminotransferase (ALT) and aspartate aminotransferase (AST) after the treatment (5 animals per group) were performed in the Clinic of Small Animal Medicine, Faculty of Veterinary Medicine, LMU Munich. Statistical analysis was performed by unpaired t test (B); one way ANOVA (C-F). *P < 0.05, **P < 0.01, ***P < 0.001, ****P < 0.0001, n.s., not significant.

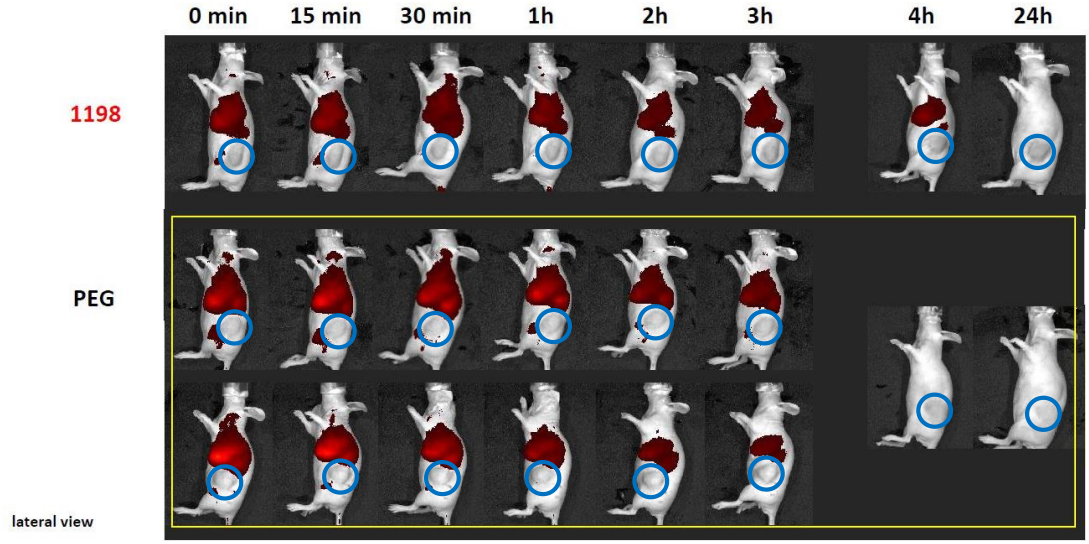

Fig. 37 Biodistribution of siRNA formulations (50 µg siRNA, 50% Cy7 labeled, with 1198 at N/P 12) after i. v. administration in Huh7 tumor-bearing mice. The fluorescence scale between 1.80e-5 and 1.70e-4. The tumor sites are highlighted by blue circles in lateral view. For structure of ***1198*** (His-free analog of ***1214***) see Table S2. Experiment performed by Sarah Kern (veterinary MD student, LMU Munich).

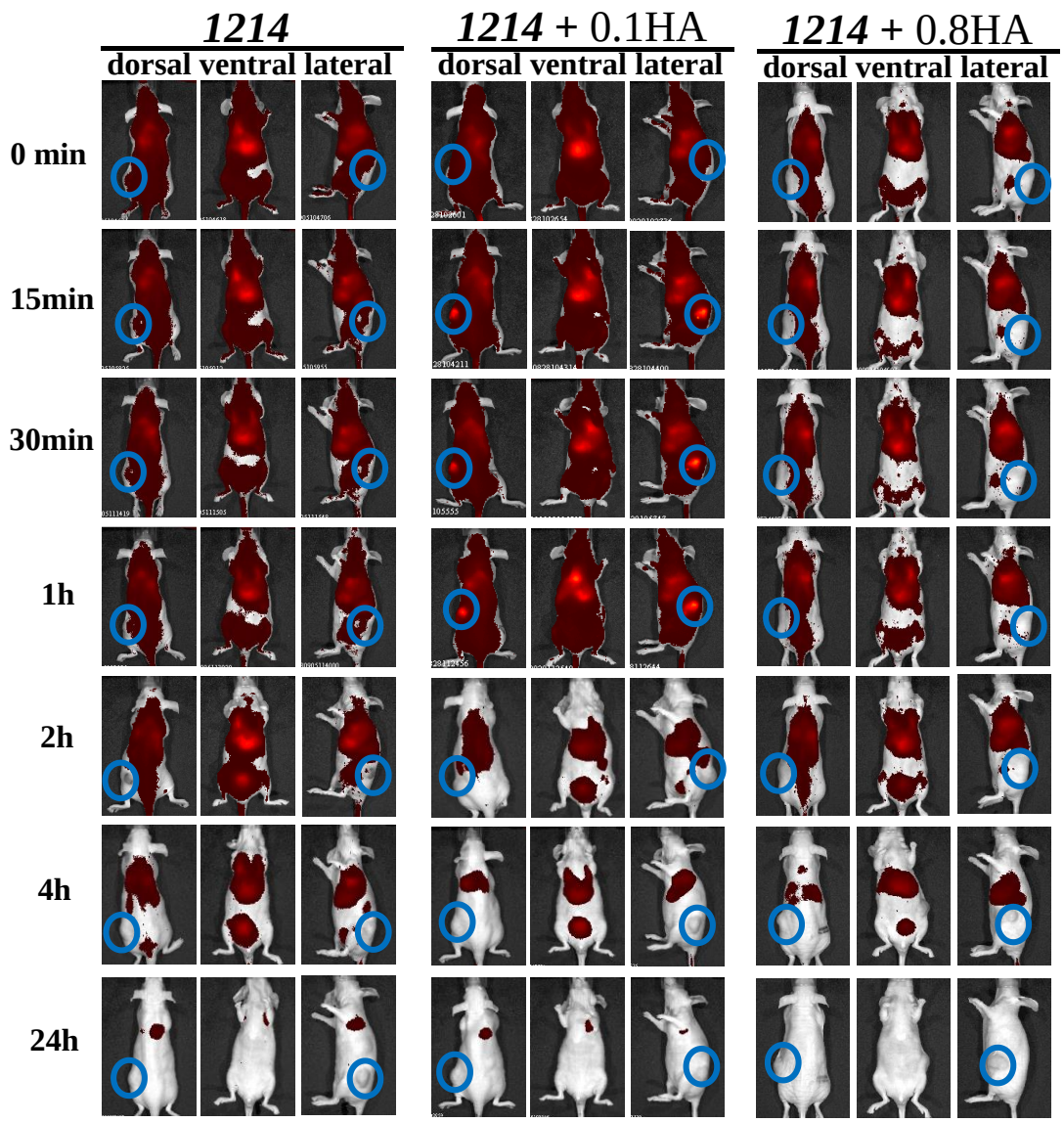

Fig. 38 Biodistribution of siRNA formulations (50 µg siRNA, 50% Cy7 labeled, with ***1214*** at N/P 12) after i. v. administration in Huh7 tumor-bearing mice. Biodistribution was determined by NIR fluorescence bioimaging comparing unmodified ***1214*** siRNA polyplexes with polyplexes modified with different equiv. of HA-DBCO. The fluorescence scale between 1.40e-5 and 2.5e-4. The tumor sites are highlighted by blue circles. Experiment performed by Johannes Schmaus (veterinary MD student, LMU Munich).

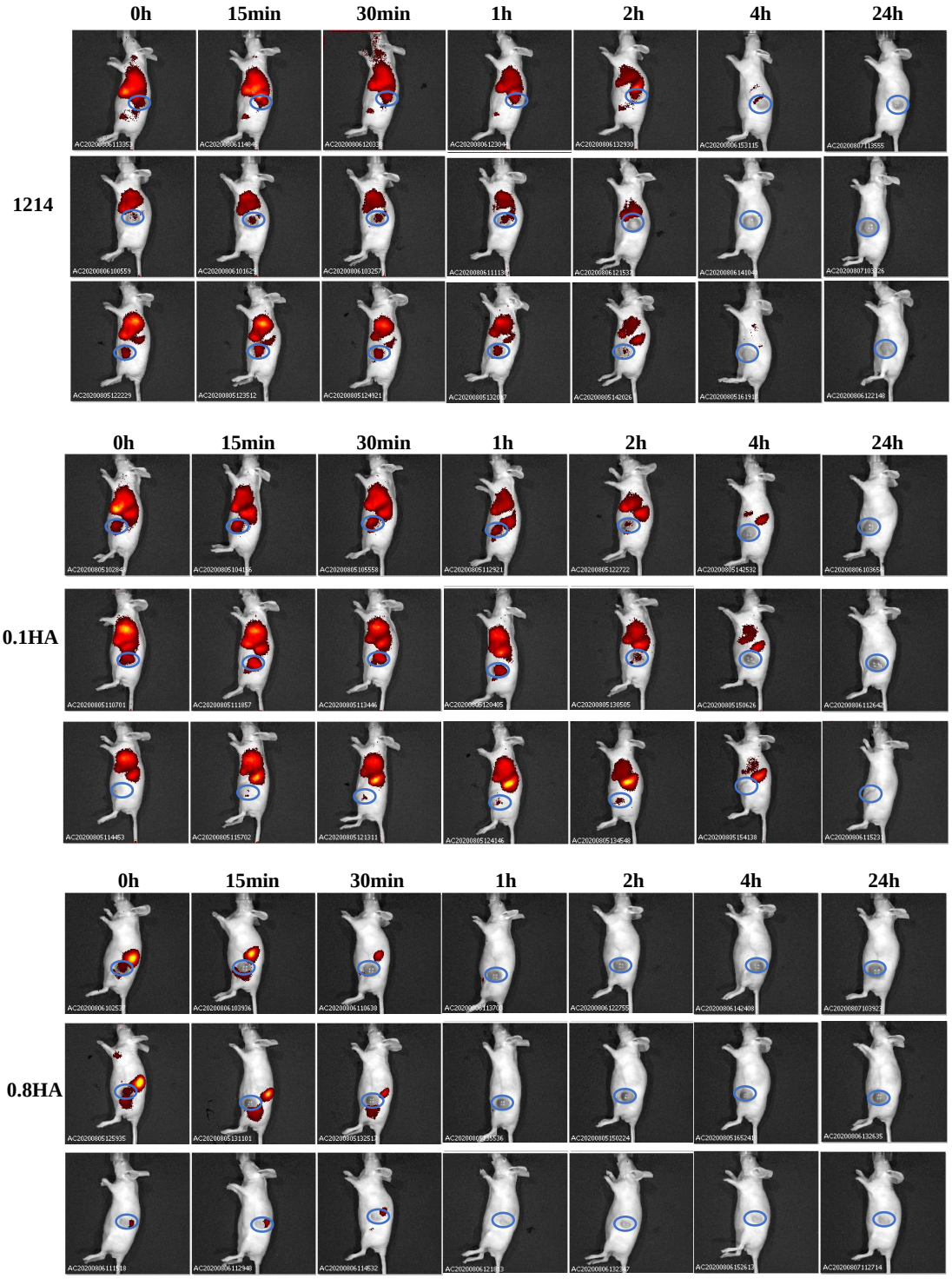

Fig. 39 Biodistribution of siRNA formulations (50 µg siRNA, 50% Cy7 labeled, with 1214 at N/P 12) after i. v. administration in Neuro2a neuroblastoma-bearing mice. Biodistribution was determined by NIR fluorescence bioimaging comparing unmodified 1214 siRNA polyplexes with polyplexes modified with 0.1 or 0.8 equiv. of HA-DBCO. The fluorescence scale of upper and middle figures between 2.20e-5 and 7.00e-5. The fluorescence scale of lower figures between 5.50e-5 and 1.50e-4. The tumor sites are highlighted by blue circles. Experiment performed by Elisa Hörterer and Ulrich Wilk (veterinary MD students, LMU Munich).

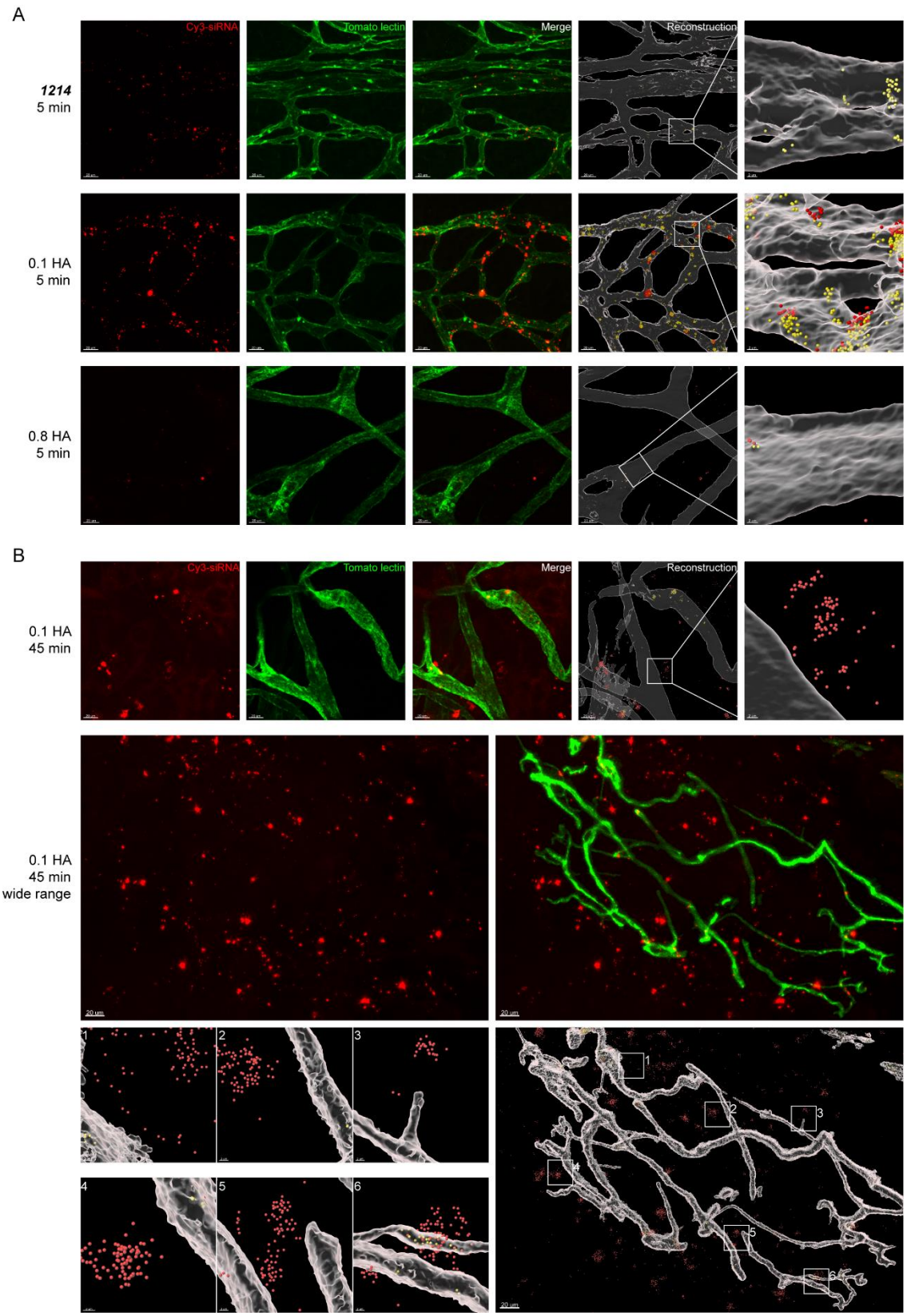
A
Cy3-siRNA
Tomato lectin
Merge
Reconstruction
1214
5 min
0.1 HA
5 min
0.8 HA
5 min
B
Cy3-siRNA
Tomato lectin
Merge
Reconstruction
0.1 HA
45 min
0.1 HA
45 min
wide range
20 µm
20 µm
1
2
3
4
5
6
1
2
3
4
5
6
20 µm

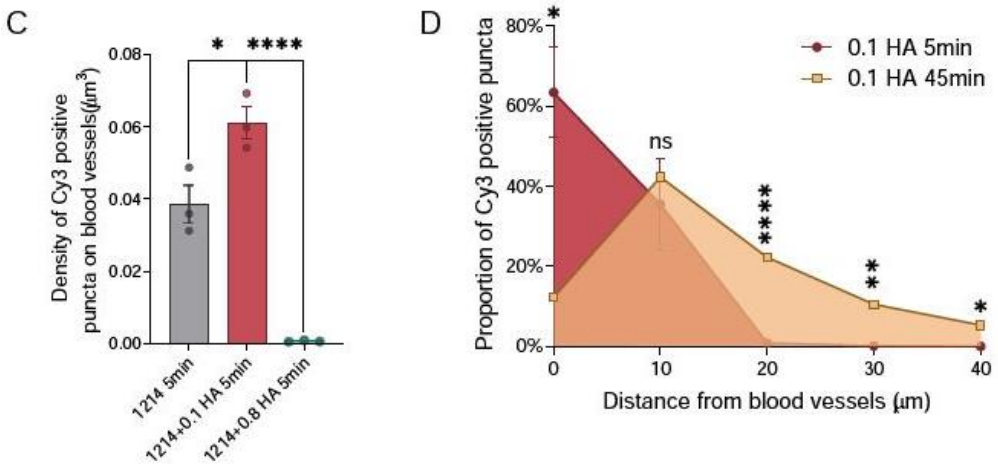

Fig. 40 Colocalization and microenvironmental distribution of cationic and anionic siRNA polyplexes in Huh 7 tumors. (A) Observation of three formulations (unmodified ***1214***, 0.1HA cationic and 0.8HA anionic polyplexes) after 5 min i.v. injection adhesion to endothelial cells of tumor blood vessels by confocal laser scanning microscopy. Scale bar = 20 μm. Enlarged sites from blood vessels to tumor tissue in the selected region. Scale bar = 2 μm. siRNA polyplexes were labeled with cy3, endothelial cells of blood vessels were stained with DyLight 488 labeled lycopersicon esculentum (tomato) lectin. Yellow was meant to colocalization of nanopolyplexes (Red) in endothelial cells (Green). (B) Distribution of 0.1HA cationic siRNA polyplex in tumor tissues after 45 min i.v. injection. Scale bar = 20 μm. Enlarged sites, scale bar = 2 μm. (C) Quantitative data of cationic and anionic siRNA polyplexes colocalizing or having passed across tumor endothelium after 5 min i.v. injection. (D) Comparison of distance of ***1214*** 0.1HA nanoparticles from endothelium after 5 min and 45 min i.v. injection. Statistical analysis was performed by unpaired t test (C, D). *P < 0.05, **P < 0.01, ***P < 0.001, ****P < 0.0001, n.s., not significant. Confocal microscopy was operated by Mochen Cui (Faculty of Medicine, LMU Munich)

3.2.7 Tumor penetration of HA coated siRNA polyplexes *in vivo*

We further investigated the micro-environmental distribution of HA coated siRNA polyplexes in Huh 7 tumor mice by 3D analysis of 50 μm thick tumor/organ sections using CLSM microscopy (**Fig. 40**). This method is far more sensitive and space-resolved than NIR fluorescence bioimaging and also more quantitative in micro-environmental distribution of nanoparticles. We used Imaris software in 3-dimensional sight to demonstrate the accurate distribution of nanoparticles inside/outside the endothelium of tumor (**Fig. 41-43**) and in different organs (**Fig. 44-45**). As indicated in **Fig. 40A**, at the very early time point of 5 min post injection, the red fluorescence was

mainly retained within the endothelial cells of blood vessels. In the magnification figure of each formulation, the yellow dots indicate the colocalization of Cy3-nanoparticles within lectin-labeled endothelial cells, and the red dots show the nanoparticle released from endothelial cells. The ***1214*** polyplexes with 0.1 equiv. of HA-DBCO modification indicated much higher colocalization with endothelial cells, compared to the unmodified ***1214*** polyplexes and anionic ***1214*** polyplexes with 0.8 equiv. of HA-DBCO (**Fig. 40A, Fig. 41** and **Fig. 42**). Afterwards, at 45 min post-injection (**Fig. 40B** and **Fig. 43**), the fluorescence signals of 0.1 equiv. of HA-DBCO modified ***1214*** polyplexes diffused from blood vessels to further distribute in the extravascular regions.

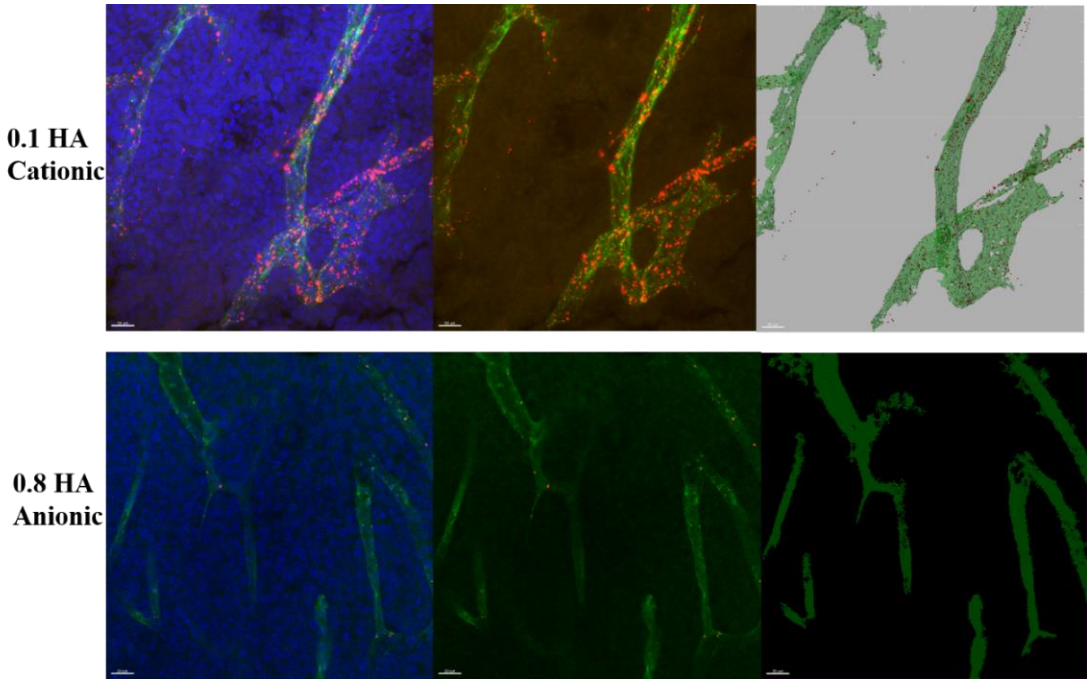

Fig. 41 Testing for colocalization for two formulations (0.1HA cationic and 0.8HA anionic polyplexes) after 5 min i.v. injection adhesion to endothelial cells of tumor blood vessels by confocal laser scanning microscopy. Scale bar = 20 µm. siRNA polyplexes were labeled with Cy3, endothelial cells of blood vessels were stained with DyLight 488 labeled lycopersicon esculentum (tomato) lectin. Yellow was meant to colocalization of nanopolyplexes (Red) in endothelial cells (Green). Confocal microscopy was operated by Mochen Cui (Faculty of Medicine, LMU Munich)

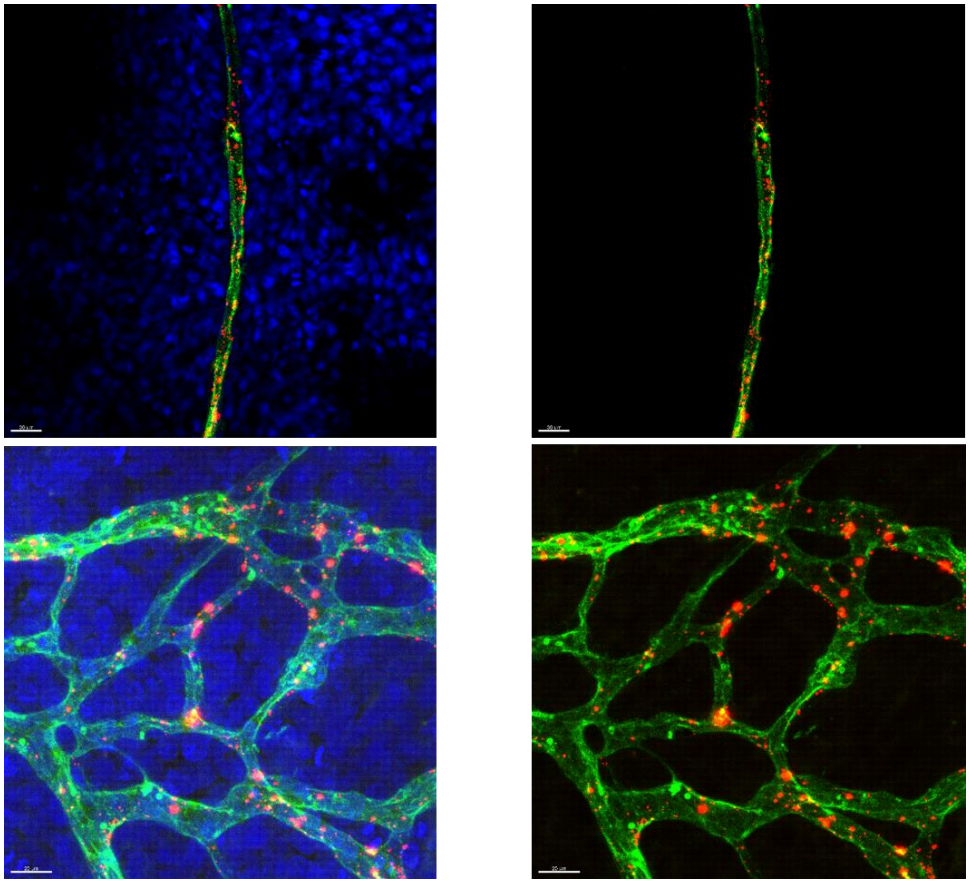

Fig. 42 Colocalization of 0.1HA cationic after 5 min i.v. injection adhesion to endothelial cells of tumor blood vessels as evaluated by confocal laser scanning microscopy. Scale bar = 20 µm. siRNA polyplexes were labeled with Cy3, endothelial cells of blood vessels were stained with DyLight 488 labeled lycopersicon esculentum (tomato) lectin. Yellow was meant to colocalization of nanopolyplexes (Red) in endothelial cells (Green). Confocal microscopy was operated by Mochen Cui (Faculty of Medicine, LMU Munich)

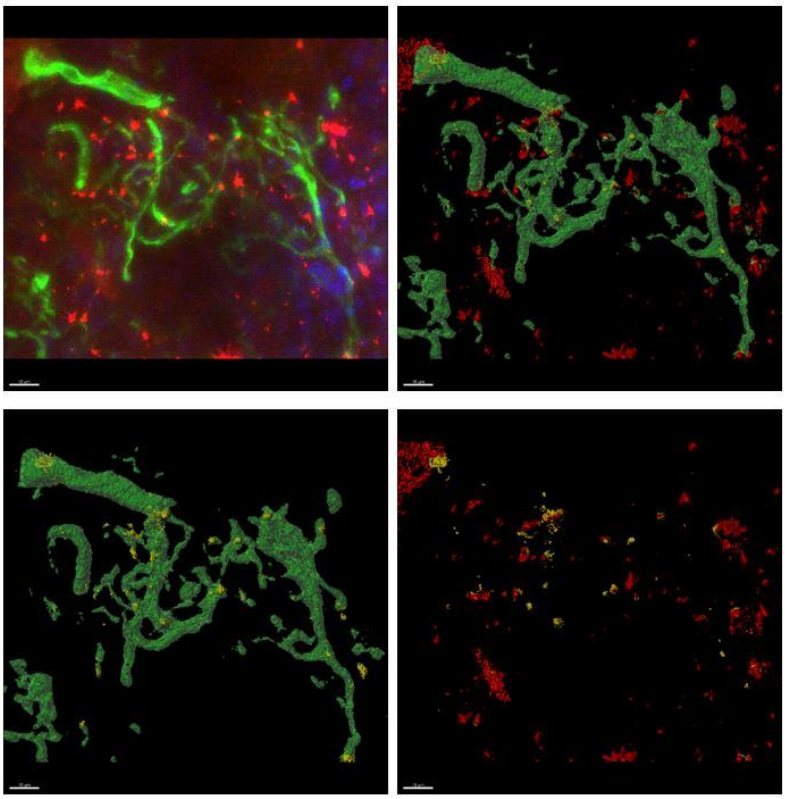

Fig. 43 Imaris reconstruction of 0.1HA cationic siRNA polyplexes in different site of Huh 7 tumors. Observation of polyplex after 45 min i.v. injection from endothelial cells by confocal laser scanning microscopy. Scale bar = 15 µm. siRNA polyplexes were labeled with Cy3, endothelial cells of blood vessels were stained with DyLight 488 labeled lycopersicon esculentum (tomato) lectin. Yellow refers to colocalization of nanopolyplexes (red) with endothelial cells (green). Confocal microscopy was operated by Mochen Cui (Faculty of Medicine, LMU Munich)

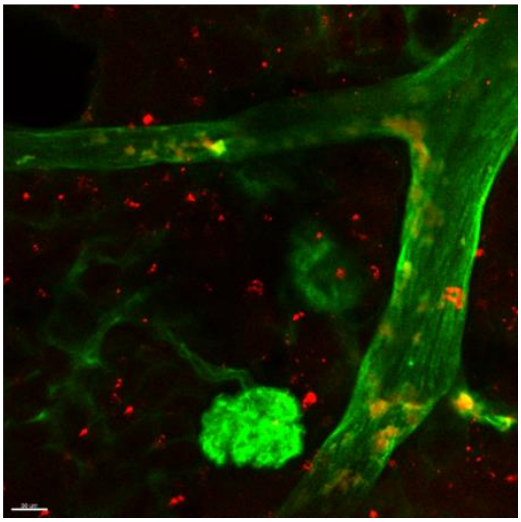

Fig. 44 Distribution of 0.1HA cationic polyplexes in kidneys after 5min i.v. injection. Scale bar = 30 µm. siRNA polyplexes were labeled with Cy3, endothelial cells of blood vessels were stained with DyLight 488 labeled lycopersicon esculentum (tomato) lectin. Experiment performed by Mochen Cui (Faculty of Medicine, LMU Munich)

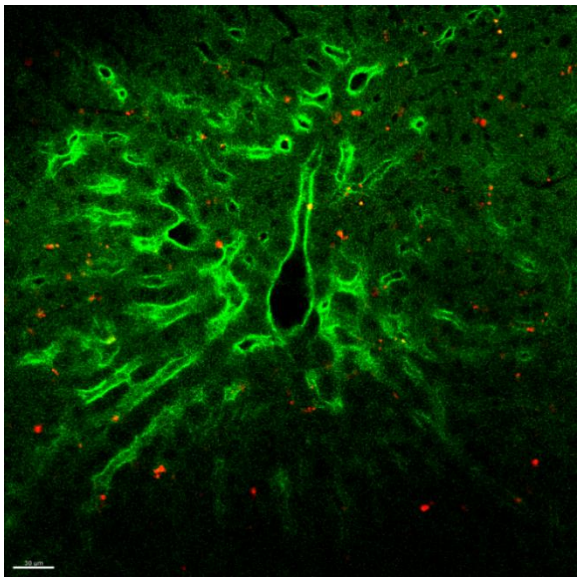

Fig. 45 Distribution of 0.1HA cationic polyplexes in liver after 5min i.v. injection by confocal laser scanning microscopy. Scale bar = 30 µm. siRNA polyplexes were labeled with Cy3, endothelial cells were stained with DyLight 488 labeled lycopersicon esculentum (tomato) lectin. Experiment performed by Mochen Cui (Faculty of Medicine, LMU Munich)

The quantitative data of cationic and anionic siRNA polyplexes associated with endothelial cells are shown in **Fig. 40C.** Both cationic siRNA polyplex types (non-coated and 0.1HA coated) show far higher association with endothelial cells after 5 min i.v. than the negatively charged polyplexes (0.1HA > ***1214*** >> 0.8HA). In tumor sections, accumulation of ***1214*** unmodified HA nanoparticles was significant lower (~60%) than 0.1HA and far lower (~2%) for 0.8HA. Evaluation of the distribution of ***1214*** 0.1 HA polyplexes in tumor tissue with time (**Fig. 40D**) demonstrated that this formulation can penetrate from endothelial cells into the tumor core up to 40 µm within the short period of only 45 min.

The other organs (kidneys, liver and brain) of tumor-bearing mice were also analyzed by confocal laser scanning microscopy (**Fig. 44-45**). We observed 0.1HA ***1214*** polyplexes also distributed in kidneys and liver.

3.2.8 Tumor-targeting mechanisms of HA siRNA polyplexes in perspective of state-of-the-art mechanistic models.

Our results obtained with cationic 200 nm nanosized 1214 0.1HA nanoparticles that are short-term circulating, attach to tumor endothelium within 5 min and subsequently penetrate into tumors in short time need to be placed in perspective with the common mechanistic models for tumor targeting.

After investigations over several decades, the mechanisms of delivery of nanoparticle drugs into solid tumors (‘tumor targeting’) are still not fully understood. However, a series of reliable mechanistic models (**Fig. 46**) have been developed and are under continuous review and refinement. [142-156] Nanoparticles sized up to 400 nm in diameter and well surface–shielded to enable a stable long-term systemic circulation may passively accumulate in solid experimental tumors, as can be explained by the mechanism of enhanced permeability and retention (EPR) effect of tumor tissues containing leaky blood vessels.[142-144] This EPR principle was first observed by Maeda and colleagues in 1986. [142] The passive tumor accumulation takes time (several hours to days), the enhanced permeability is attributed to the fenestration in leaky tumor blood vessels, and the retention of macromolecules or nanoparticles arises from the poor lymphatic drainage in tumors. Jain and colleagues independently confirmed this principle; they injected differently sized liposomes into blood and investigated molecular size dependence of microvascular permeability in tumors.[143] In the pharmacological and clinical reality, tumor targeting of nanoparticles is often suboptimum and far lower than an EPR effect might promise.[144, 145] Such low accumulation values can be partly attributed to suboptimum nanoparticle properties, such as lack of extended blood circulation times due to insufficient stability and surface shielding. Obviously, the demonstrated positive tumor targeting observed with our 0.1HA siRNA nanoparticles cannot be explained by an EPR-dominated mechanism. Apart from nanoparticle issues, the EPR-effect can be strong in some solid tumor types, but between tumors a high heterogeneity in degree of accumulation was observed. [146]

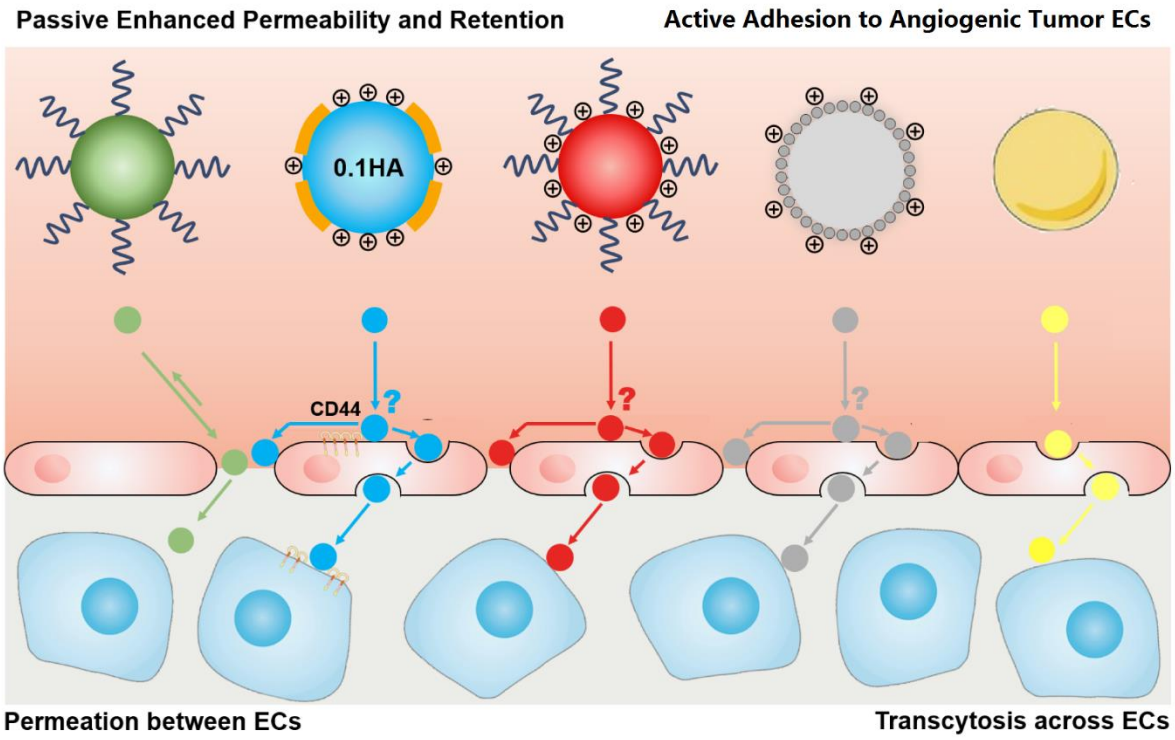

Fig. 46 Possible mechanisms of nanoparticle accumulation in tumors. For details see section 3.2.8. Mechanistic models include passive enhanced permeability and retention (EPR) and active adhesion to tumoral vasculature. Transfer across tumor endothelial cell (EC) barrier can be by transfer between ECs (permeation or paracellular transport) or transcytosis. Examples of nanoparticles (NPs) from left to right: long circulated PEGylated NPs accumulating by the EPR effect, 0.1HA ***1214*** polyplexes, cationic PEGylated NPs, cationic liposomes, or NPs using transcytosis, respectively.

As known from literature,[157, 158] nanoparticles with neutral and negative charges display a reduced absorption of serum proteins, resulting in longer circulation times in vivo. The extension of circulation time of nanoparticles would favor tumor accumulation by the mentioned EPR effect, but may not be the only and sufficient factor for achieving systemic delivery into tumors. In our study, the negatively charged, well coated 0.8HA siRNA nanoparticles neither accumulated nor mediated gene silencing in tumors.

Another mechanistic solid tumor targeting model comprises effective adhesion to angiogenic tumor endothelial cells. Early work by Donald McDonald and coworkers[147] demonstrated that cationic liposomes or cationic DNA lipoplexes display high binding to tumor endothelial cells and internalization into tumors. Dellian et al. demonstrated[148] that modified cationized bovine serum albumin and IgG

extravasate faster from tumor endothelial cells into tumors compared to similar proteins with neutral or negative charges. More recent work by Kam Leong and Jun Wang demonstrated that a cationic surface charge on PEGylated stable nanoparticles was required for enhanced tumor penetration and therapeutic efficacy of anti-cancer nanomedicines.[149] Consistently, also in our study only the cationic 0.1HA-containing nanoparticles displayed very fast and effective attachment to tumor endothelium. However, in our study cationic charge was necessary but not sufficient for the observed fast tumor attachment of nanoparticles; coating with 0.1HA, a known ligand for cell surface CD44, was another requirement for nanoparticle attachment. CD44 is known to be overexpressed in several tumor types and also tumor vasculature. [125, 126] As 0.1HA polyplexes demonstrated favorable accumulation in both CD44 positive Huh 7 and CD44 negative Neuro2A tumor cells in vivo models, we hypothesize that in both cases a HA interaction with CD44 on tumor vasculature might play an active role in the observed tumor accumulation.

The further process of 0.1HA nanoparticle penetration from tumor vasculature into the tumor was also a fast process as detectable by 3D confocal microscopy already at 45 min after nanoparticle administration. The involved mechanism, transcellular transfer across endothelial cells, or paracellular transfer between endothelial cells of leaky vasculature, and a possible active participation of HA/CD44, remains to be clarified. Early pioneering work by Schnitzer in 1992 [150] reported that albumin is actively transported through the vascular endothelium by transcytosis. Schnitzer and co-workers also found[151] that the active transendothelial portal to infiltrate tumors can be explained by caveolae pumping system. Recently, Chan and co-workers[152] reported that nanoparticles penetrate into tumors mainly through an active transcytosis process (up to 97%) across endothelial cells, rather than via the endothelial gaps or fenestrae. Recent evidence on penetration into tumor lesions via an active transcytosis process was provided by Tao and colleagues [153].

4. Summary

In the first part, a systematic approach was applied to rationally design a more effective and multifunctional carrier with dual-antitumoral siRNA conjugate based on the thorough understanding of the relationship between structure and activity of previously designed oligoaminoamides. We designed new siRNA carriers based on sequence-defined cationizable oligoaminoamides containing an N-terminal azido domain and a hydrophobic bis (oleic acid) domain attached with T-shaped topology in either a reducible or non-reducible form. Following a screening discovering the histidine-free lipo-oligomer ***1208*** formulation as most favorable for siRNA delivery, DBCO-functionalized PEG-AP-1 targeting and PEG shielding agents were designed for copper-free click chemistry surface functionalization by ***1208*** siRNA polyplexes via their integrated azido groups. Independently, three siRNA-apoptotic peptide conjugates were designed, and siEG5-KLK was identified as the most antitumoral entity. Incorporation of siEG5-KLK into the optimized PEG-AP-1 ***1208*** nanoparticles which target IL-4 receptor-positive tumor cells induced a strong antitumoral effect, based on EG5 gene silencing and KLK mediated mitochondrial destabilization as two separate mechanisms. In sum, dual antitumoral siRNA-KLK conjugates and their targeted formulations present an encouraging strategy; future *in vivo* tumor targeting experiments will be critical for understanding their *in vivo* biosafety and potency.

The ‘passive tumor targeting’ mechanism (EPR effect) requires a prolonged circulation of nanoparticles in blood for accumulation in tumors. This process cannot be utilized by the siRNA nanoparticles of the current study which are short-term circulating. Direct comparison of tumor penetration of three very similar siRNA nanoparticle formulations, containing the same optimized cationic lipooligoaminoamide core, but differing in the surface by charge and covalently coupled hyaluronic acid (HA) content (two cationic formulations: 0HA, 0.1HA, and one anionic: 0.8HA), demonstrated upon intravenous administration a very fast

accumulation of one formulation (0.1HA). This fast, apparently more active tumor targeting process differs from the well-established EPR mechanism. As evidenced by 3D nanoparticle distribution within the tumor, 0.1HA-coated cationic siRNA nanoparticles attach to the tumor endothelium within 5 minutes and deeply penetrate into the tumor within 45 minutes. The finding that only one (0.1HA) of the two cationic systems and not the better shielded negatively charged (0.8HA) system is superior, goes beyond common knowledge. Common assumption would predict that better shielded NPs would result in improved blood circulation and subsequent improved tumor accumulation. The intravenous treatment with 0.1HA cationic nanoparticles also resulted in potent gene silencing in the distant tumor. Notably, neither the non-coated cationic siRNA nanoparticles nor the analogous HA-coated anionic siRNA nanoparticles mediated such a strong tumor accumulation and gene silencing. The cationic formulation without HA displayed some reduced attachment to tumor vasculature and subsequent moderate gene silencing. Against our initial expectations based on in vitro results, the anionic siRNA nanoparticles with the high degree of HA coating and highest gene silencing activity in cell culture were neither accumulating nor gene silencing in the tumor in vivo. This was surprising because a complete coating with the natural carbohydrate biopolymer was predicted to provide a better surface shielding in the blood stream.

5 Supporting Information

Tab. S1 Definition of protonable amines in the newly synthesized lipo-oligomers in N/P calculations. The new sequence-defined oligomers, non-reducible (***1208***, ***1209***, ***1210*** and ***1211***) and bioreducible type (***1217***, ***1218***, ***1219*** and ***1220***) differ in number of protonable N. For historic reasons and compatibility with our previous publications, only protonable nitrogens of the Stp backbone units were included in these calculations, but not protonable histidine nitrogens. Units of the oligomers: Y: tyrosine, K: lysine, H: histidine, Stp: succinoyl-tetraethylene-pentamine, OleA: Oleic acid, G: glycine, ssbb: succinoyl-cystamine, ss building block. For siRNAs, the number of phoshates (P) of siRNA was always used as fixed value (i.e. 42). Note that the few charges (if any) of conjugated apoptotic peptides were not included in the calculations.

Oligomer	MW free base	MW (with HCl)	amines in total	protonable amines (N)	structures:
1208	3022	3496.5	13	13	K(N_3)-Y_3-Stp_2-K(K($OleA)_2$)-Stp_2-Y_3
1209	3844	4537.5	19	13	K(N_3)-Y_3-(H-$Stp)_2$-H-K(K($OleA)_2$)-H-(Stp-$H)_2$-Y_3
1210	4107	5019.5	25	25	K(N_3)-Y_3-Stp_4-K(K($OleA)_2$)-Stp_4-Y_3
1211	5478	6755.5	35	25	K(N_3)-Y_3-(H-$Stp)_4$-H-K(K($OleA)_2$)-H-(Stp-$H)_4$-Y_3
1217	3313	3787.5	13	13	K(N_3)-Y_3-Stp_2-K(G-ssbb-K($OleA)_2$)-Stp_2-Y_3
1218	4135	4828.5	19	13	K(N_3)-Y_3-(H-$Stp)_2$-H-K(G-ssbb-K($OleA)_2$)-H-(Stp-$H)_2$-Y_3
1219	4399	5311.5	25	25	K(N_3)-Y_3-Stp_4-K(G-ssbb-K($OleA)_2$)-Stp_4-Y_3
1220	5769	7046.5	35	25	K(N_3)-Y_3-(H-$Stp)_4$-H-K(G-ssbb-K($OleA)_2$)-H-(Stp-$H)_4$-Y_3

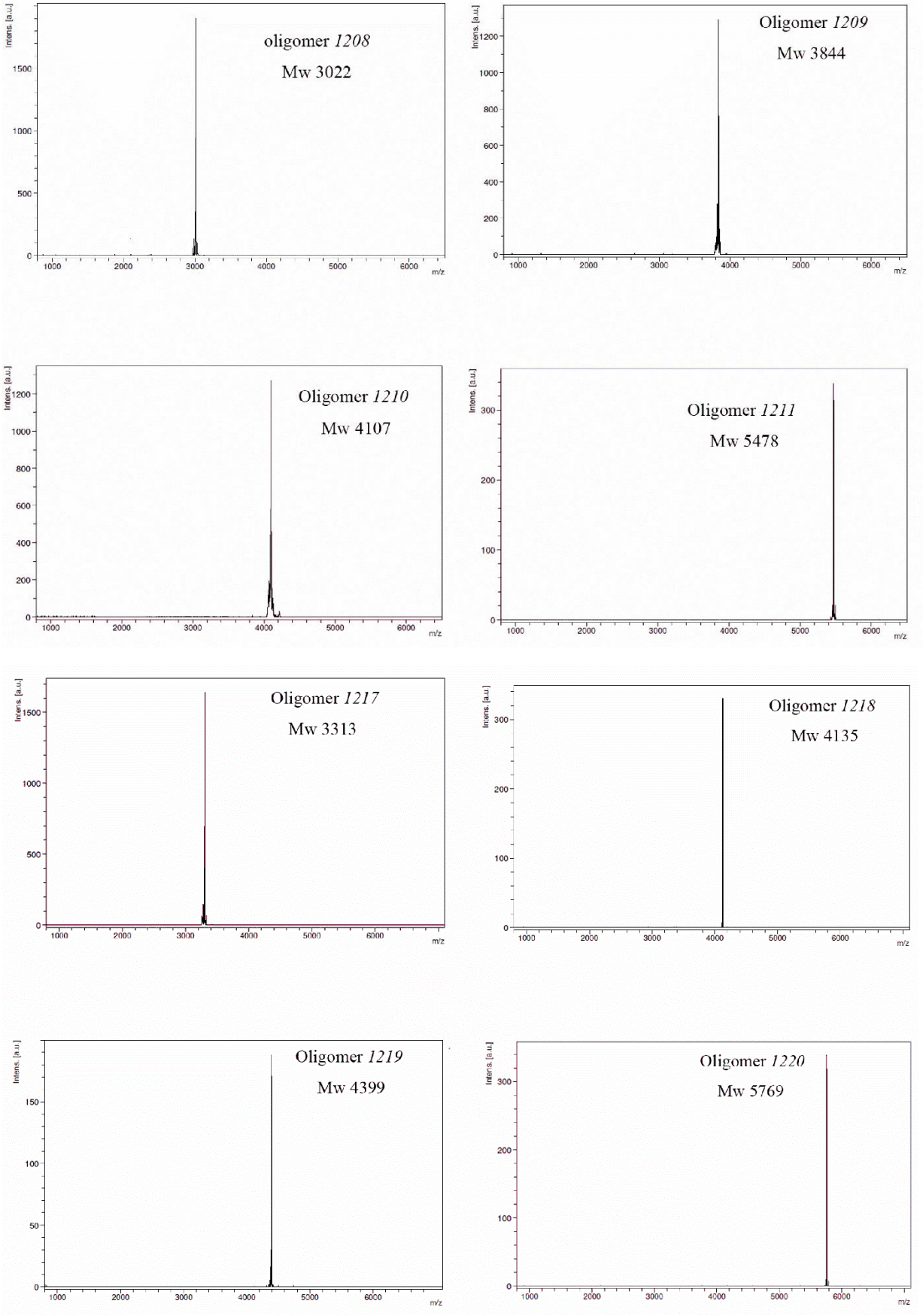

Fig. S1 MS data of the eight oligomers.

1208: Sequence (C→N) Y_3-Stp_2-[$(OleA)_2$-K]K-Stp_2-Y_3-K(N_3)

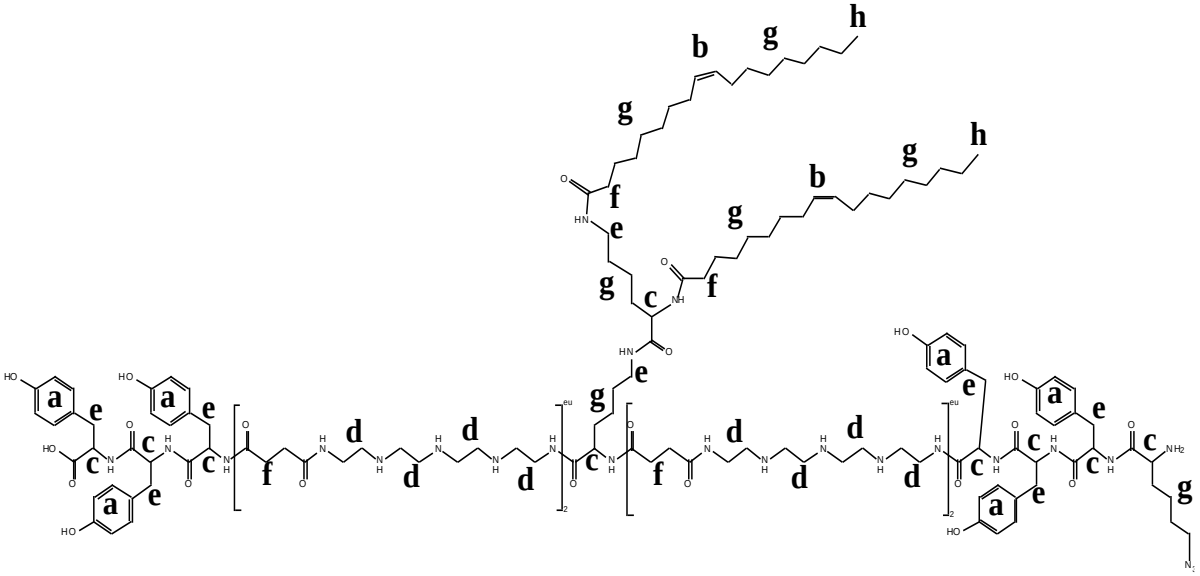

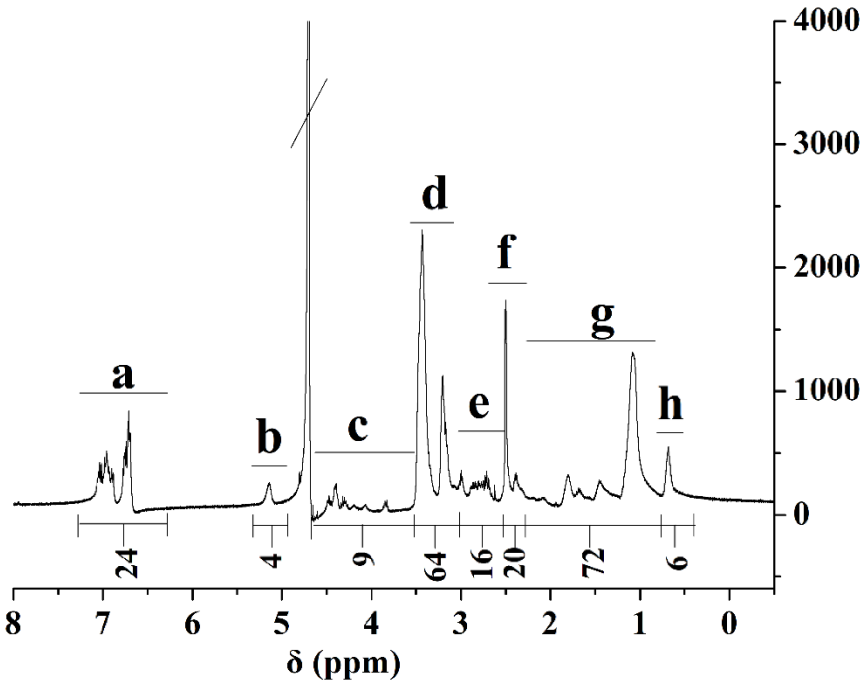

^{1}H NMR (500 MHz, Deuterium oxide) δ (ppm) = 0.60-0.85 (s, 6 H, -CH_3 oleic acid), 0.85-2.25 (m, 72 H, βγδH lysine, βγδεH azidolysine ,-CH_2- oleic acid), 2.25-2.60 (m, 20 H, -CO-CH_2-CH_2-CO- Stp, -CO-CH_2- oleic acid), 2.65-3.1 (m, 16 H, εH lysine and tyrosine), 3.1-3.65 (m, 64 H, -CH_2- Stp), 3.70-4.55 (m, 9 H, αH amino acids), 5.05 – 5.25 (s, 4 H, -CH=CH- oleic acid), 6.60 -7.15 (m, 24 H, -CH- tyrosine).

Fig. S2 NMR data of the eight oligomers.

1209: Sequence (C→N) Y_3-(H-Stp)$_2$-H-[(OleA)$_2$-K]K-(H-Stp)$_2$-H-Y_3-K(N_3)

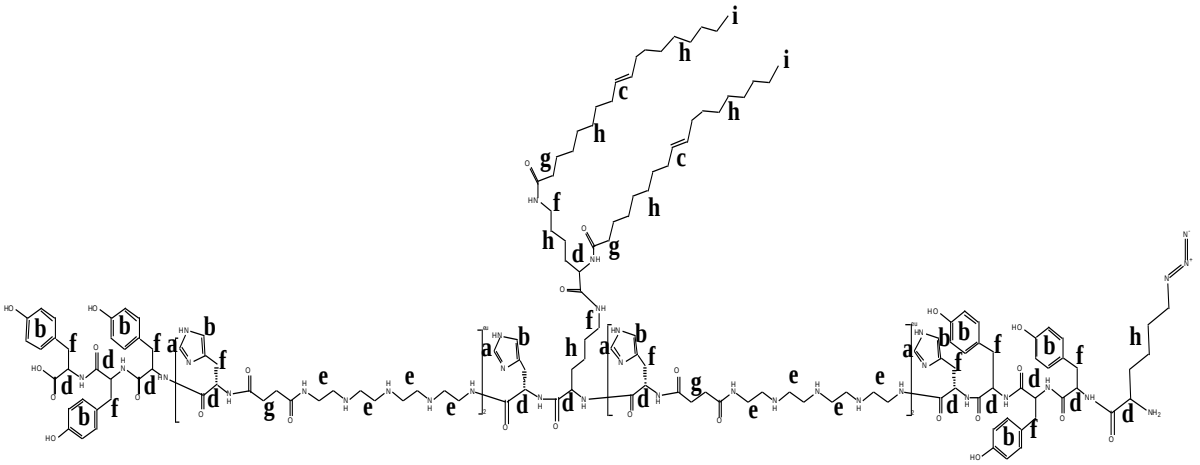

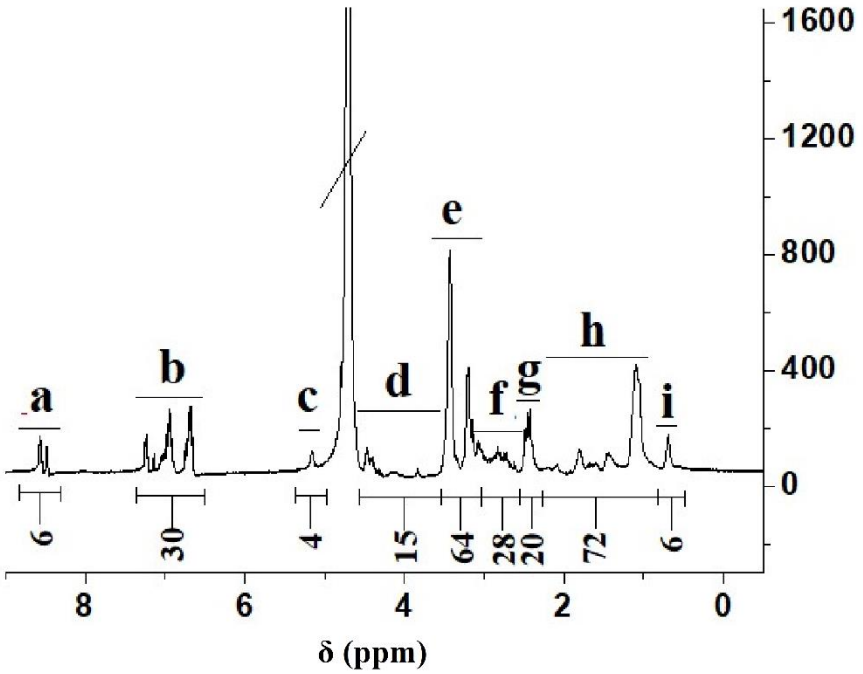

^{1}H NMR (500 MHz, Deuterium oxide) δ (ppm) = 0.60-0.85 (s, 6 H, -CH_3 oleic acid), 0.85-2.25 (m, 72 H, βγδH lysine, βγδεH azidolysine ,-CH_2- oleic acid), 2.25-2.60 (m, 20 H, -CO-CH_2-CH_2-CO- Stp, -CO-CH_2- oleic acid), 2.65-3.1 (m, 28 H, εH lysine, tyrosine and histidine), 3.1-3.65 (m, 64 H, -CH_2- Stp), 3.70-4.55 (m, 15 H, αH amino acids), 5.05 – 5.25 (s, 4 H, -CH=CH- oleic acid), 6.60 -7.15 (m, 30 H, -CH- tyrosine, aromatic H histidine), 8.45-8.60 (m, 6 H, aromatic H histidine).

Fig. S2 (continued).

1210: Sequence (C→N) Y_3-Stp_4-[$(OleA)_2$-K]K-Stp_4-Y_3-K(N_3)

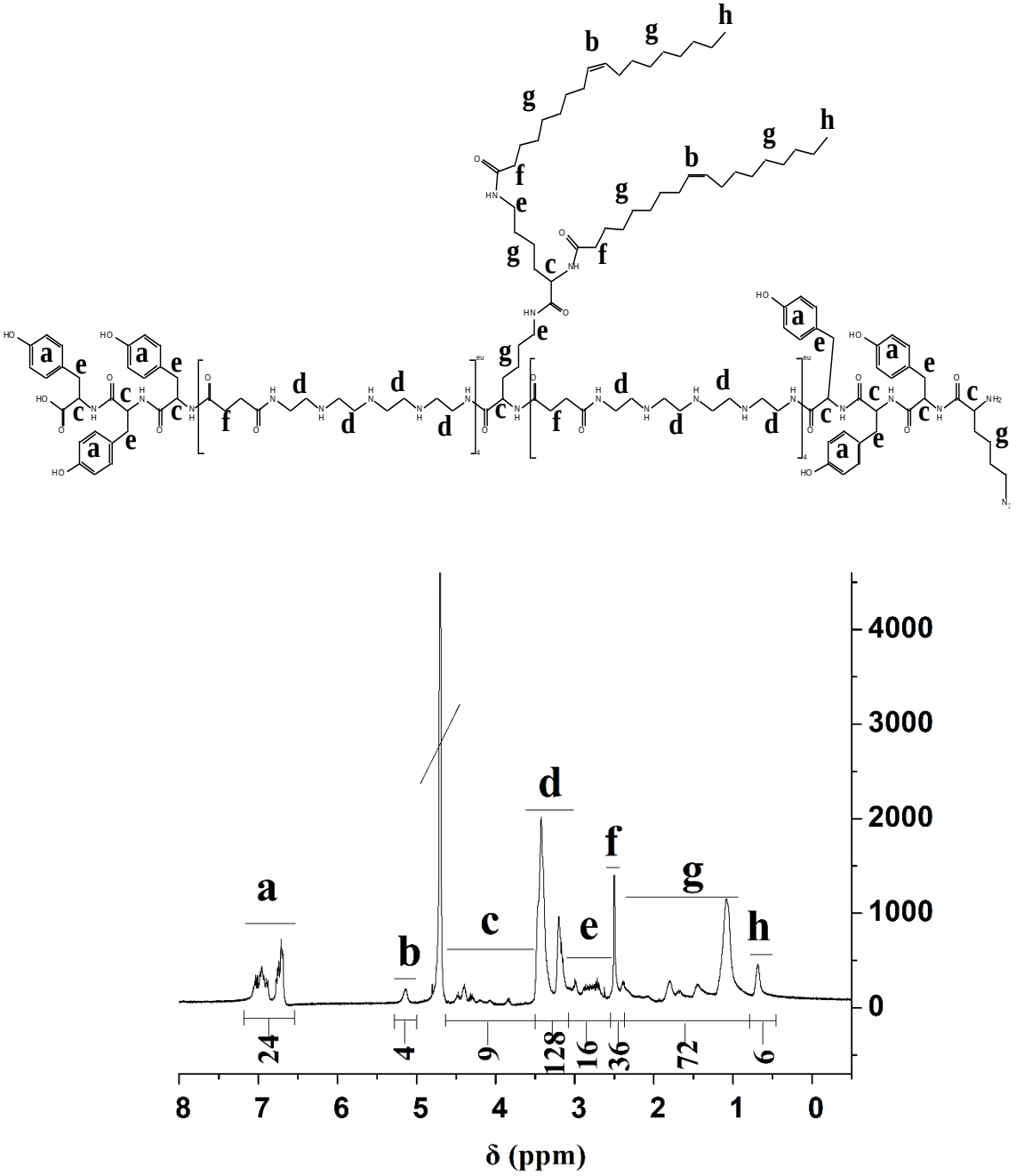

^{1}H NMR (500 MHz, Deuterium oxide) δ (ppm) = 0.60-0.85 (s, 6 H, -CH_3 oleic acid), 0.85-2.25 (m, 72 H, βγδH lysine, βγδεH azidolysine ,-CH_2- oleic acid), 2.25-2.60 (m, 36 H, -CO-CH_2-CH_2-CO- Stp, -CO-CH_2- oleic acid), 2.65-3.1 (m, 16 H, εH lysine and tyrosine), 3.1-3.65 (m, 128 H, -CH_2- Stp), 3.70-4.55 (m, 9 H, αH amino acids), 5.05 – 5.25 (s, 4 H, -CH=CH- oleic acid), 6.60 -7.15 (m, 24 H, -CH- tyrosine).

Fig. S2 (continued).

1211: Sequence (C→N) Y_3-(H-Stp)$_4$-H-[(OleA)$_2$-K]K-(H-Stp)$_4$-H-Y_3-K(N_3)

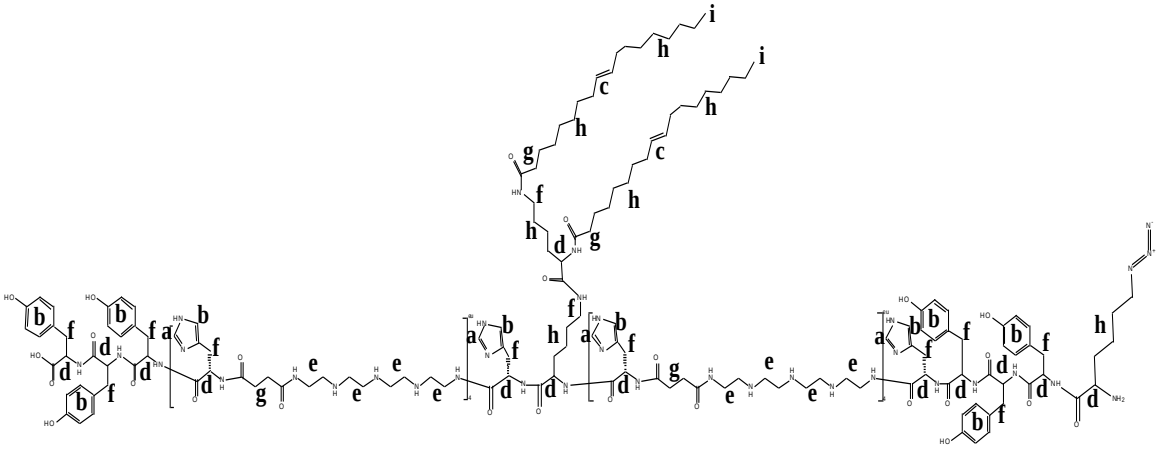

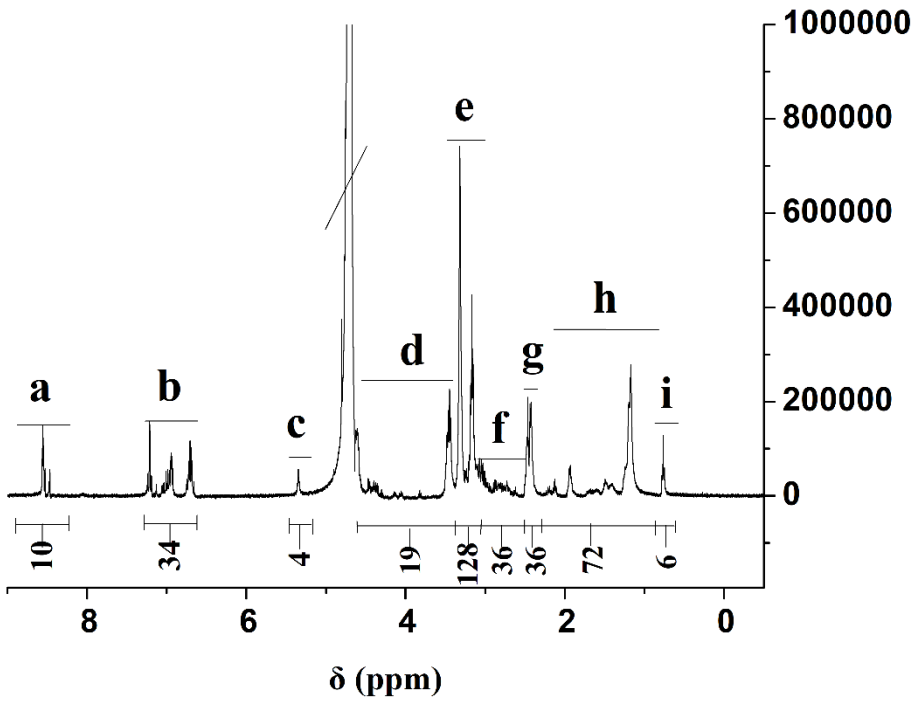

^{1}H NMR (500 MHz, Deuterium oxide) δ (ppm) = 0.60-0.85 (s, 6 H, -CH_3 oleic acid), 0.85-2.25 (m, 72 H, βγδH lysine, βγδεH azidolysine ,-CH_2- oleic acid), 2.25-2.60 (m, 36 H, -CO-CH_2-CH_2-CO- Stp, -CO-CH_2- oleic acid), 2.65-3.1 (m, 36 H, εH lysine, tyrosine and histidine), 3.1-3.65 (m, 128 H, -CH_2- Stp), 3.70-4.55 (m, 19 H, αH amino acids), 5.05 – 5.25 (s, 4 H, -CH=CH- oleic acid), 6.60 -7.15 (m, 34 H, -CH- tyrosine, aromatic H histidine), 8.45-8.60 (m, 10 H, aromatic H histidine).

Fig. S2 (continued).

1217: Sequence (C→N) Y_3-Stp_2-[$(OleA)_2$-K-ssbb-G]K-Stp_2-Y_3-K(N_3)

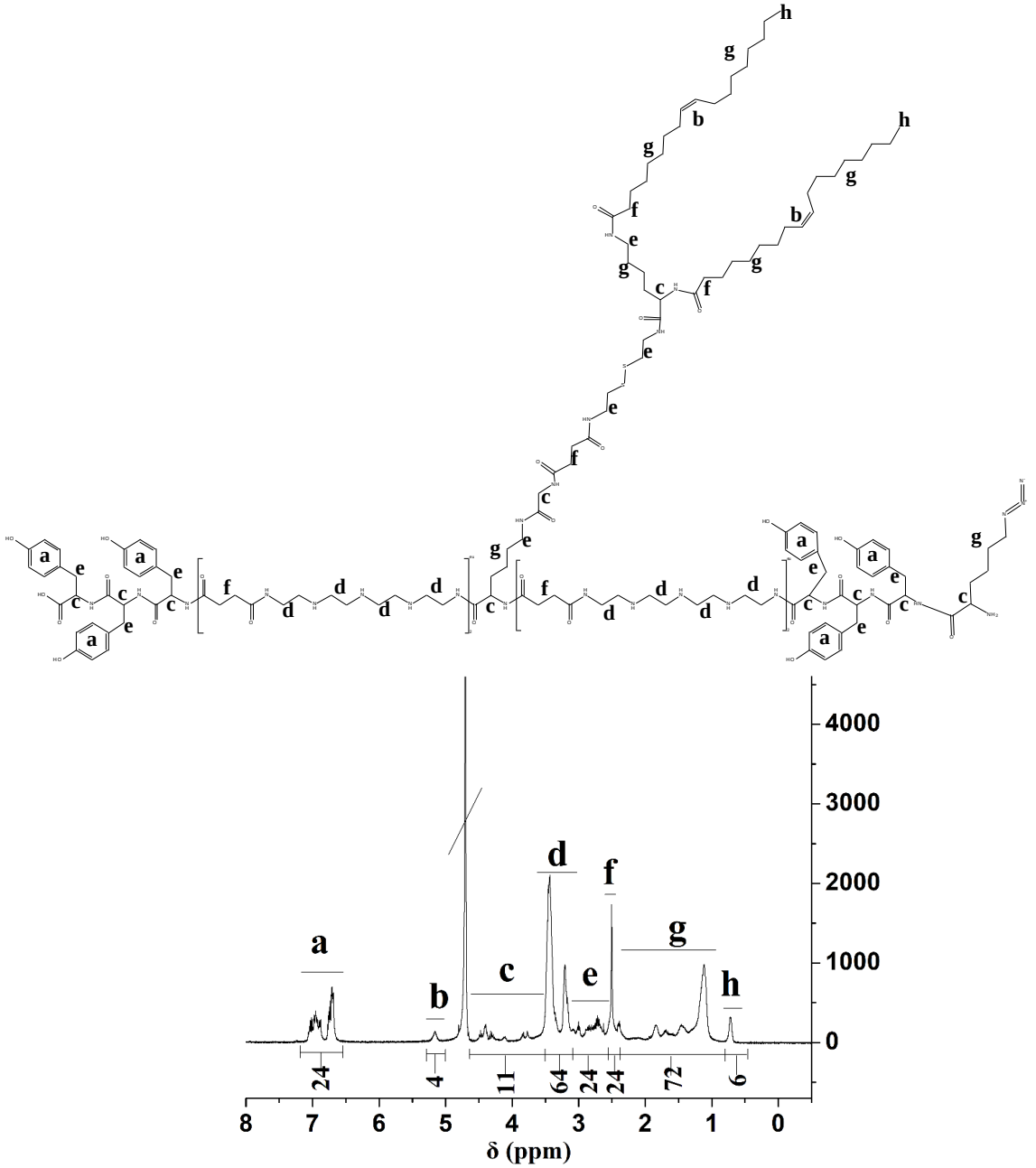

^{1}H NMR (500 MHz, Deuterium oxide) δ (ppm) = 0.60-0.85 (s, 6 H, -CH_3 oleic acid), 0.85-2.25 (m, 72 H, βγδH lysine, βγδεH azidolysine ,-CH_2- oleic acid), 2.25-2.60 (m, 24 H, -CO-CH_2-CH_2-CO- Stp and ssbb, -CO-CH_2- oleic acid), 2.65-3.1 (m, 24 H, εH lysine and tyrosine, -CH_2- ssbb), 3.1-3.65 (m, 64 H, -CH_2- Stp), 3.70-4.55 (m, 11 H, αH amino acids), 5.05 – 5.25 (s, 4 H, -CH=CH- oleic acid), 6.60 -7.15 (m, 24 H, -CH- tyrosine).

Fig. S2 (continued).

1218: Sequence (C→N) Y_3-(H-Stp)$_2$-H-[(OleA)$_2$-K-ssbb-G]K-H-(H-Stp)$_2$-Y_3-K(N_3)

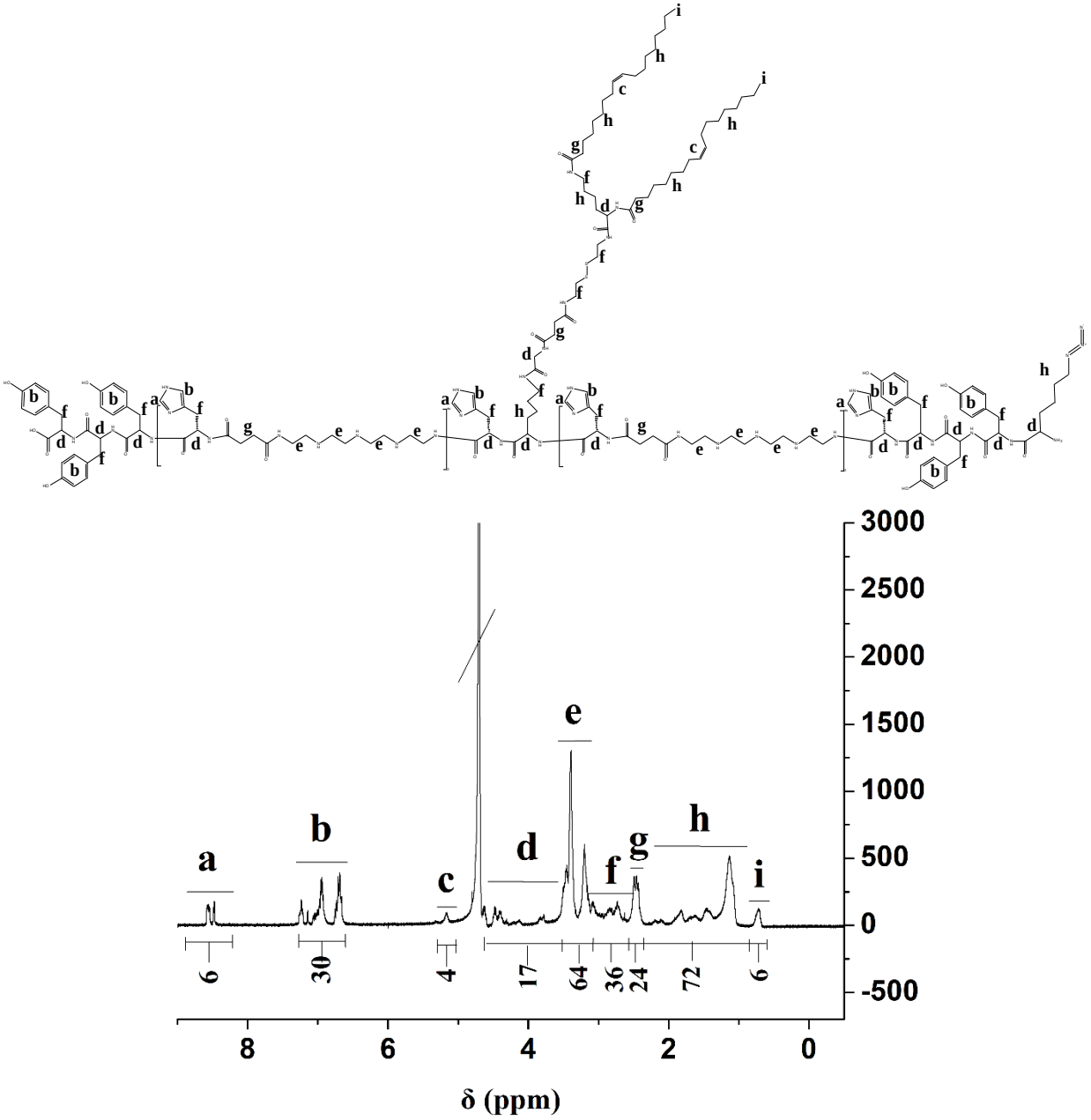

^{1}H NMR (500 MHz, Deuterium oxide) δ (ppm) = 0.60-0.85 (s, 6 H, -CH_3 oleic acid), 0.85-2.25 (m, 72 H, βγδH lysine, βγδεH azidolysine ,-CH_2- oleic acid), 2.25-2.60 (m, 24 H, -CO-CH_2-CH_2-CO- Stp and ssbb, -CO-CH_2- oleic acid), 2.65-3.1 (m, 36 H, εH lysine, tyrosine and histidine, -CH_2- ssbb), 3.1-3.65 (m, 64 H, -CH_2- Stp), 3.70-4.55 (m, 17 H, αH amino acids), 5.05 – 5.25 (s, 4 H, -CH=CH- oleic acid), 6.60 -7.15 (m, 30 H, -CH- tyrosine, aromatic H histidine), 8.45-8.60 (m, 6 H, aromatic H histidine).

Fig. S2 (continued).

1219: Sequence (C→N) Y_3-Stp_4-[$(OleA)_2$-K-ssbb-G]K-Stp_4-Y_3-K(N_3)

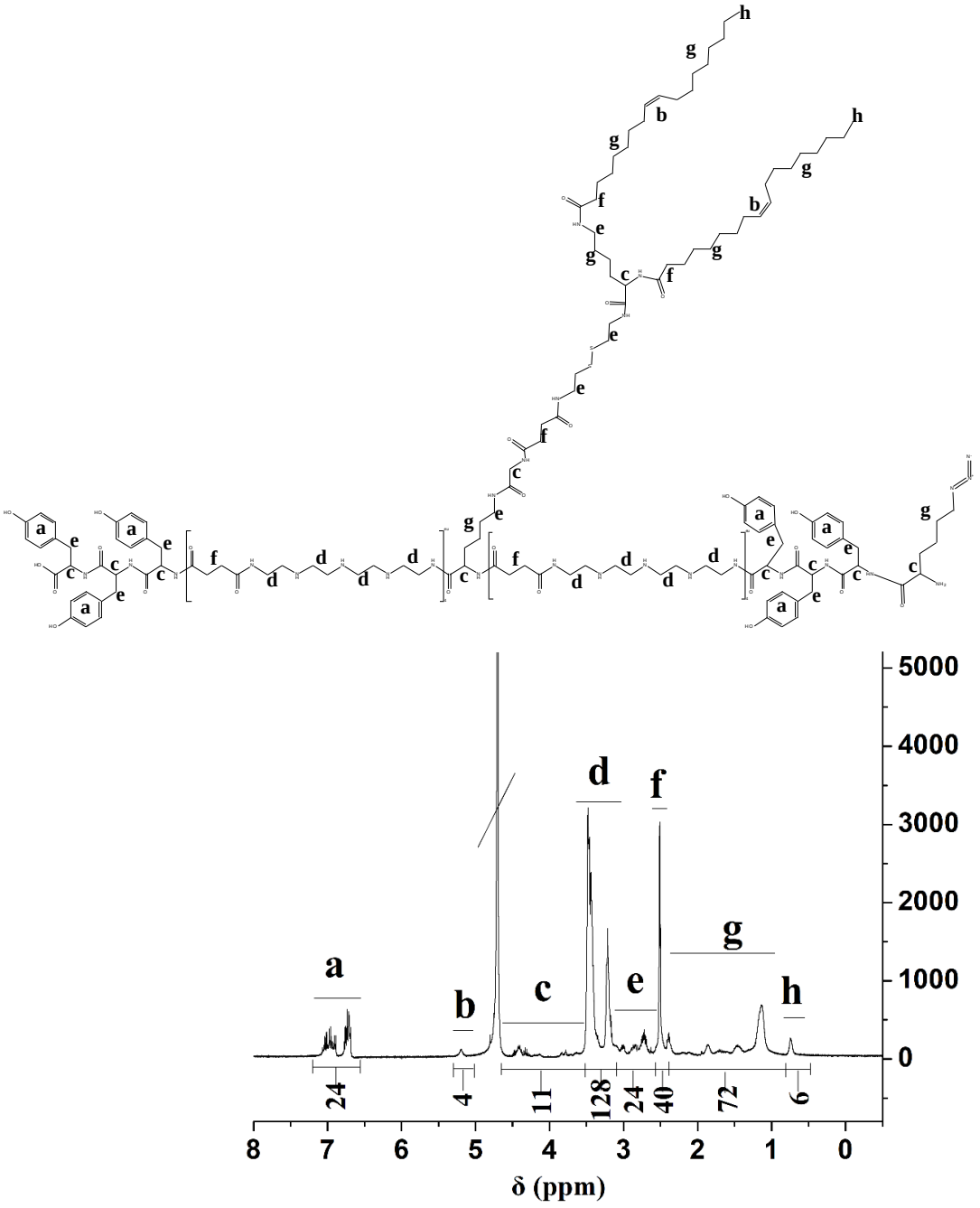

^{1}H NMR (500 MHz, Deuterium oxide) δ (ppm) = 0.60-0.85 (s, 6 H, -CH_3 oleic acid), 0.85-2.25 (m, 72 H, βγδH lysine, βγδεH azidolysine ,-CH_2- oleic acid), 2.25-2.60 (m, 40 H, -CO-CH_2-CH_2-CO- Stp and ssbb, -CO-CH_2- oleic acid), 2.65-3.1 (m, 24 H, εH lysine and tyrosine, -CH_2- ssbb), 3.1-3.65 (m, 128 H, -CH_2- Stp), 3.70-4.55 (m, 11 H, αH amino acids), 5.05 – 5.25 (s, 4 H, -CH=CH- oleic acid), 6.60 -7.15 (m, 24 H, -CH- tyrosine).

Fig. S2 (continued).

1220: Sequence (C→N) Y_3-(H-Stp)$_4$-H-[(OleA)$_2$-K-ssbb-G]K-H-(H-Stp)$_4$-Y_3-K(N_3)

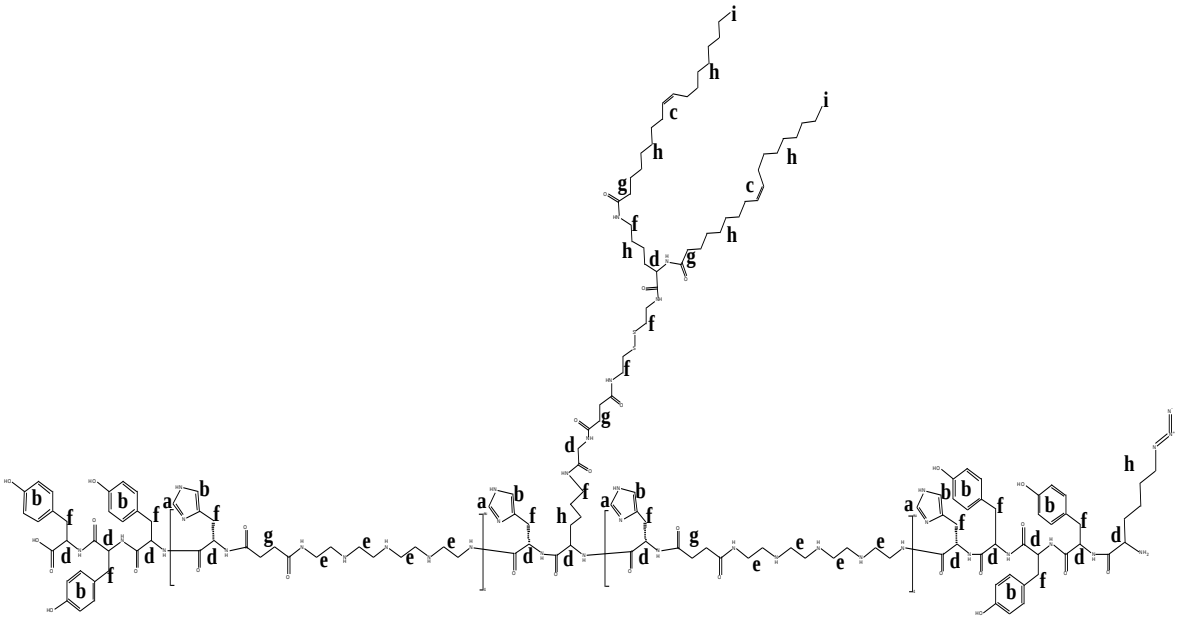

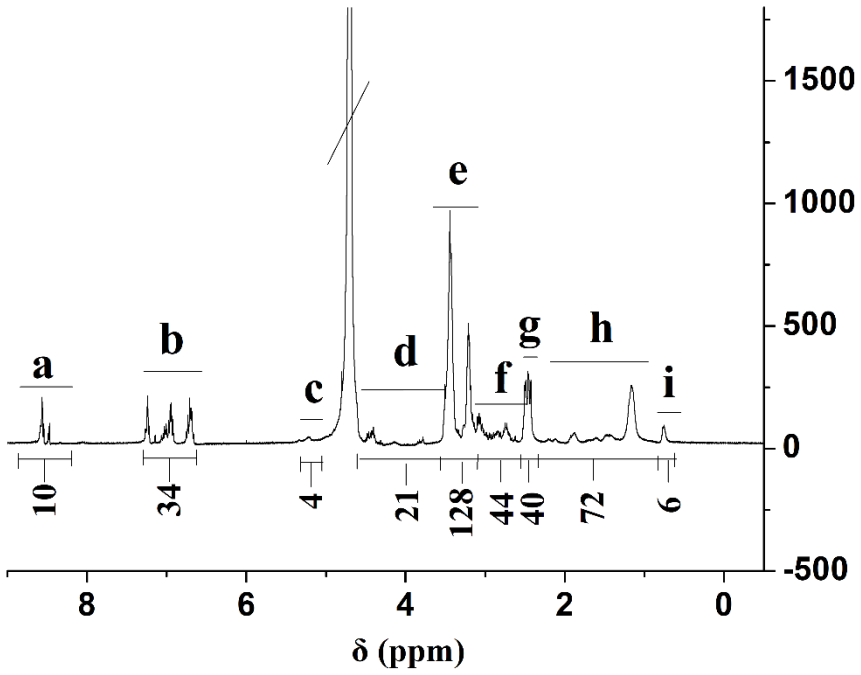

^{1}H NMR (500 MHz, Deuterium oxide) δ (ppm) = 0.60-0.85 (s, 6 H, -CH_3 oleic acid), 0.85-2.25 (m, 72 H, βγδH lysine, βγδεH azidolysine ,-CH_2- oleic acid), 2.25-2.60 (m, 40 H, -CO-CH_2-CH_2-CO- Stp and ssbb, -CO-CH_2- oleic acid), 2.65-3.1 (m, 44 H, εH lysine, tyrosine and histidine, -CH_2- ssbb), 3.1-3.65 (m, 128 H, -CH_2- Stp), 3.70-4.55 (m, 21 H, αH amino acids), 5.05 – 5.25 (s, 4 H, -CH=CH- oleic acid), 6.60 -7.15 (m, 34 H, -CH- tyrosine, aromatic H histidine), 8.45-8.60 (m, 10 H, aromatic H histidine).

Fig. S2 (continued).

Tab. S2 Synthesized sequence-defined oligomers. Definition of protonable amines in N/P calculations. For historic reasons and compatibility with our previous publications, only protonable nitrogens of the Stp backbone units were included in these calculations, but not the also protonable histidine nitrogens. Units of the oligomers: Y: tyrosine, K: lysine, H: histidine, Stp: succinoyl-tetraethylene-pentamine, G: glycine, C: cysteine, ssbb: succinoyl-cystamine, ss building block, PalA: palmitic acid, SteA: stearic acid, Ara: arachidic acid, BehA: behenic acid, LigA: lignoceric acid, OleA: oleic acid, LenA: linolenic acid. For siRNAs, the number of phosphates (P) of siRNA was always used as fixed value (i.e. 42).

Disulfide-stabilizing type of oligomers					
Oligomer (library ID number)	**MW free base**	**MW with HCl**	**amines in total**	**protonable amines(N)**	**sequence (from N- to C- terminus)**
1336	3176.11	3651	13	13	$K(N_3)$-C-Y_3-Stp_2-K(K($PalA)_2$)-Stp_2-Y_3-C
1337	3232.22	3707	13	13	$K(N_3)$-C-Y_3-Stp_2-K(K($SteA)_2$)-Stp_2-Y_3-C
1198	3228.18	3703	13	13	$K(N_3)$-C-Y_3-Stp_2-K(K($OleA)_2$)-Stp_2-Y_3-C
1383	3288.32	3763	13	13	$K(N_3)$-C-Y_3-Stp_2-K(K($AraA)_2$)-Stp_2-Y_3-C
1384	3344.43	3819	13	13	$K(N_3)$-C-Y_3-Stp_2-K(K($BehA)_2$)-Stp_2-Y_3-C
1385	3400.53	3875	13	13	$K(N_3)$-C-Y_3-Stp_2-K(K($LigA)_2$)-Stp_2-Y_3-C
1200	3220.12	3695	13	13	$K(N_3)$-C-Y_3-Stp_2-K(K($LenA)_2$)-Stp_2-Y_3-C
1277	3998.95	4692	19	13	$K(N_3)$-C-Y_3-$(H\text{-}Stp)_2$-H-K(K($PalA)_2$)-H-$(Stp\text{-}H)_2$-Y_3-C
1278	4055.05	4749	19	13	$K(N_3)$-C-Y_3-$(H\text{-}Stp)_2$-H-K(K($SteA)_2$)-H-$(Stp\text{-}H)_2$-Y_3-C
1214	4051.02	4745	19	13	$K(N_3)$-C-Y_3-$(H\text{-}Stp)_2$-H-K(K($OleA)_2$)-H-$(Stp\text{-}H)_2$-Y_3-C
1386	4111.16	4805	19	13	$K(N_3)$-C-Y_3-$(H\text{-}Stp)_2$-H-K(K($AraA)_2$)-H-$(Stp\text{-}H)_2$-Y_3-C
1387	4167.26	4861	19	13	$K(N_3)$-C-Y_3-$(H\text{-}Stp)_2$-H-K(K($BehA)_2$)-H-$(Stp\text{-}H)_2$-Y_3-C
1388	4223.37	4917	19	13	$K(N_3)$-C-Y_3-$(H\text{-}Stp)_2$-H-K(K($LigA)_2$)-H-$(Stp\text{-}H)_2$-Y_3-C
1390	4099.06	4793	19	13	$K(N_3)$-C-Y_3-$(H\text{-}Stp)_2$-H-K(K($LenA)_2$)-H-$(Stp\text{-}H)_2$-Y_3-C

Non-reducible type of oligomers					
Oligomer (library ID number)	**MW free base**	**MW with HCl**	**amines in total**	**protonable amines(N)**	**sequence (from N- to C- terminus)**
1360	2969.82	3444	13	13	$K(N_3)$-Y_3-Stp_2-$K(K(PalA)_2)$-Stp_2-Y_3
1361	3025.93	3500	13	13	$K(N_3)$-Y_3-Stp_2-$K(K(SteA)_2)$-Stp_2-Y_3
1208	3021.90	3496	13	13	$K(N_3)$-Y_3-Stp_2-$K(K(OleA)_2)$-Stp_2-Y_3
1371	3082.04	3557	13	13	$K(N_3)$-Y_3-Stp_2-$K(K(AraA)_2)$-Stp_2-Y_3
1372	3138.14	3613	13	13	$K(N_3)$-Y_3-Stp_2-$K(K(BehA)_2)$-Stp_2-Y_3
1373	3194.25	3669	13	13	$K(N_3)$-Y_3-Stp_2-$K(K(LigA)_2)$-Stp_2-Y_3
1320	3792.66	4486	19	13	$K(N_3)$-Y_3-$(H\text{-}Stp)_2$-H-$K(K(PalA)_2)$-H-$(H\text{-}Stp)_2$-Y_3
1321	3848.77	4542	19	13	$K(N_3)$-Y_3-$(H\text{-}Stp)_2$-H-$K(K(SteA)_2)$-H-$(H\text{-}Stp)_2$-Y_3
1209	3844.73	4538	19	13	$K(N_3)$-Y_3-$(H\text{-}Stp)_2$-H-$K(K(OleA)_2)$-H-$(H\text{-}Stp)_2$-Y_3
1374	3904.87	4598	19	13	$K(N_3)$-Y_3-$(H\text{-}Stp)_2$-H-$K(K(AraA)_2)$-H-$(H\text{-}Stp)_2$-Y_3
1375	3960.98	4654	19	13	$K(N_3)$-Y_3-$(H\text{-}Stp)_2$-H-$K(K(BehA)_2)$-H-$(H\text{-}Stp)_2$-Y_3
1376	4017.08	4711	19	13	$K(N_3)$-Y_3-$(H\text{-}Stp)_2$-H-$K(K(LigA)_2)$-H-$(H\text{-}Stp)_2$-Y_3

Bioreducible type of oligomers					
Oligomer (library ID number)	**MW free base**	**MW with HCl**	**amines in total**	**protonable amines(N)**	**sequence (from N- to C- terminus)**
1348	3261.21	3736	13	13	$K(N_3)$-Y_3-Stp_2-K(G-ssbb-K(PalA)$_2$)-Stp_2-Y_3
1349	3317.32	3792	13	13	$K(N_3)$-Y_3-Stp_2-K(G-ssbb-K(SteA)$_2$)-Stp_2-Y_3
1217	3313.29	3788	13	13	$K(N_3)$-Y_3-Stp_2-K(G-ssbb-K(OleA)$_2$)-Stp_2-Y_3
1377	3373.43	3848	13	13	$K(N_3)$-Y_3-Stp_2-K(G-ssbb-K(AraA)$_2$)-Stp_2-Y_3
1378	3429.53	3904	13	13	$K(N_3)$-Y_3-Stp_2-K(G-ssbb-K(BehA)$_2$)-Stp_2-Y_3
1379	3485.64	3960	13	13	$K(N_3)$-Y_3-Stp_2-K(G-ssbb-K(LigA)$_2$)-Stp_2-Y_3
1305	4084.05	4778	19	13	$K(N_3)$-Y_3-(H-Stp)$_2$-H-K(G-ssbb-K(PalA)$_2$)-H-(H-Stp)$_2$-Y_3
1306	4140.16	4834	19	13	$K(N_3)$-Y_3-(H-Stp)$_2$-H-K(G-ssbb-K(SteA)$_2$)-H-(H-Stp)$_2$-Y_3
1218	4136.12	4830	19	13	$K(N_3)$-Y_3-(H-Stp)$_2$-H-K(G-ssbb-K(OleA)$_2$)-H-(H-Stp)$_2$-Y_3
1380	4196.26	4890	19	13	$K(N_3)$-Y_3-(H-Stp)$_2$-H-K(G-ssbb-K(AraA)$_2$)-H-(H-Stp)$_2$-Y_3
1381	4252.37	4946	19	13	$K(N_3)$-Y_3-(H-Stp)$_2$-H-K(G-ssbb-K(BehA)$_2$)-H-(H-Stp)$_2$-Y_3
1382	4308.48	5002	19	13	$K(N_3)$-Y_3-(H-Stp)$_2$-H-K(G-ssbb-K(LigA)$_2$)-H-(H-Stp)$_2$-Y_3

Tab. S3 Mass spectral data of all oligomers recorded with a Bruker MALDI-TOF instrument in positive mode.

Disulfide stabilizing type of oligomers			
Oligomer ID	Molecular Formula	Calculated MASS	Found MASS
1336	$C_{158}H_{260}N_{36}O_{28}S_2$	3176.1	3175.2
1337	$C_{162}H_{268}N_{36}O_{28}S_2$	3232.2	3233.5
1198	$C_{162}H_{264}N_{36}O_{28}S_2$	3228.1	3227.2
1383	$C_{166}H_{276}N_{36}O_{28}S_2$	3288.3	3287.8
1384	$C_{170}H_{284}N_{36}O_{28}S_2$	3344.4	3343.2
1385	$C_{174}H_{292}N_{36}O_{28}S_2$	3400.5	3400.8
1200	$C_{162}H_{256}N_{36}O_{28}S_2$	3220.1	3220.6
1277	$C_{194}H_{302}N_{54}O_{34}S_2$	3998.9	3997.8
1278	$C_{198}H_{310}N_{54}O_{34}S_2$	4055.1	4054.2
1214	$C_{198}H_{306}N_{54}O_{34}S_2$	4051.0	4050.1
1386	$C_{202}H_{318}N_{54}O_{34}S_2$	4111.1	4111.1
1387	$C_{206}H_{326}N_{54}O_{34}S_2$	4167.2	4166.5
1388	$C_{210}H_{334}N_{54}O_{34}S_2$	4223.3	4222.2
1390	$C_{202}H_{306}N_{54}O_{34}S_2$	4099.1	4098.4

Non-reducible type of oligomers			
Oligomer ID	Molecular Formula	Calculated MASS	Found MASS
1360	$C_{152}H_{250}N_{34}O_{26}$	2969.8	2968.4
1361	$C_{156}H_{258}N_{34}O_{26}$	3025.9	3026.5
1208	$C_{156}H_{254}N_{34}O_{26}$	3021.8	3021.2
1371	$C_{160}H_{266}N_{34}O_{26}$	3082.0	3080.9
1372	$C_{164}H_{274}N_{34}O_{26}$	3138.1	3137.2
1373	$C_{168}H_{282}N_{34}O_{26}$	3194.2	3193.2
1320	$C_{188}H_{292}N_{52}O_{32}$	3792.6	3792.1
1321	$C_{192}H_{300}N_{52}O_{32}$	3848.7	3847.1
1209	$C_{192}H_{296}N_{52}O_{32}$	3844.7	3842.9
1374	$C_{196}H_{308}N_{52}O_{32}$	3904.8	3902.8
1375	$C_{200}H_{316}N_{52}O_{32}$	3960.9	3960.2
1376	$C_{204}H_{324}N_{52}O_{32}$	4017.1	4016.2

Bioreducible type of oligomers			
Oligomer ID	Molecular Formula	Calculated MASS	Found MASS
1348	$C_{162}H_{267}N_{37}O_{29}S_2$	3261.2	3260.2
1349	$C_{166}H_{275}N_{37}O_{29}S_2$	3317.3	3319.0
1217	$C_{166}H_{271}N_{37}O_{29}S_2$	3313.2	3312.0
1377	$C_{170}H_{283}N_{37}O_{29}S_2$	3373.4	3372.2
1378	$C_{174}H_{291}N_{37}O_{29}S_2$	3429.5	3428.4
1379	$C_{178}H_{299}N_{37}O_{29}S_2$	3485.6	3484.4
1305	$C_{198}H_{309}N_{55}O_{35}S_2$	4084.1	4083.2
1306	$C_{202}H_{317}N_{55}O_{35}S_2$	4140.1	4141.0
1218	$C_{202}H_{313}N_{55}O_{35}S_2$	4136.1	4135.0
1380	$C_{206}H_{325}N_{55}O_{35}S_2$	4196.2	4196.8
1381	$C_{210}H_{333}N_{55}O_{35}S_2$	4252.3	4253.2
1382	$C_{214}H_{341}N_{55}O_{35}S_2$	4308.4	4307.2

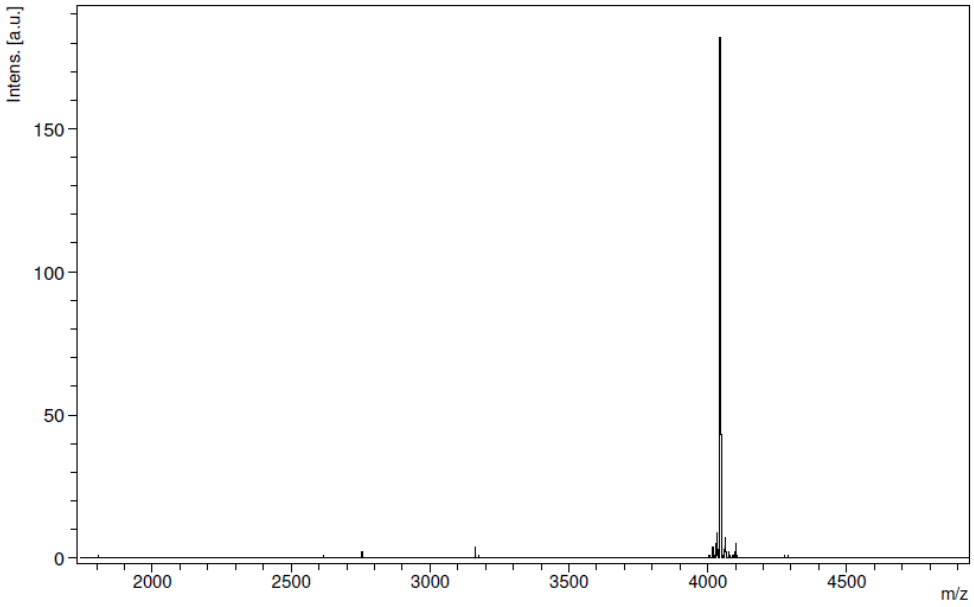

Fig. S3 MS data of the selected oligomer ***1214***.

***1214*:** Sequence (N→C) K(N_3)-C-Y_3-(H-Stp)$_2$-H-K(K(OleA)$_2$)-H-(H-Stp)$_2$-Y_3-C

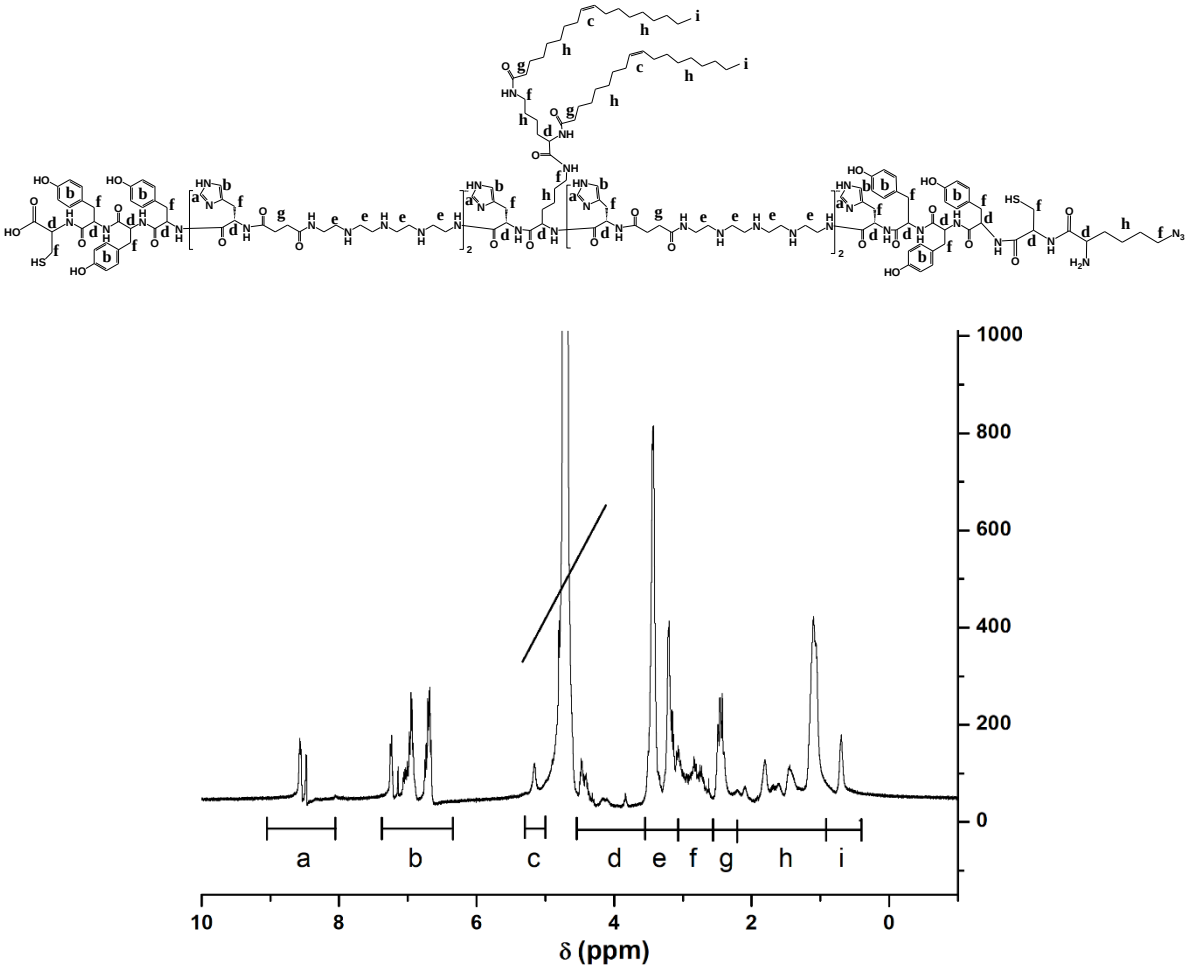

^{1}H NMR (500 MHz, Deuterium oxide) δ (ppm) = 0.60-0.85 (s, 6 H, -CH_3 oleic acid), 0.85-2.25 (m, 70 H, βγδH lysine, βγδH azidolysine ,-CH_2- oleic acid), 2.25-2.60 (m, 20 H, -CO-CH_2-CH_2-CO- Stp, -CO-CH_2- oleic acid), 2.65-3.1 (m, 34 H, εH lysine, tyrosine, histidine and azidolysine, βH cysteine), 3.1-3.65 (m, 64 H, -CH_2- Stp), 3.70-4.55 (m, 17 H, αH amino acids), 5.05 – 5.25 (s, 4 H, -CH=CH- oleic acid), 6.60 -7.15 (m, 30 H, -CH- tyrosine, aromatic H histidine), 8.45-8.60 (m, 6 H, aromatic H histidine).

Fig. S4 NMR data of the selected oligomer ***1214***.

NMR data of all listed oligomers

Disulfide-stabilizing type of oligomers

***1336*:** Sequence (N→C) K(N_3)-C-Y_3-Stp_2-K(K($PalA)_2$)-Stp_2-Y_3-C

^{1}H NMR (500 MHz, Deuterium oxide) δ (ppm) = 0.60-0.85 (s, 6 H, -CH_3 palmitic acid), 0.85-2.25 (m, 70 H, βγδH lysine, βγδH azidolysine ,-CH_2- palmitic acid), 2.25-2.60 (m, 20 H, -CO-CH_2-CH_2-CO- Stp, -CO-CH_2- palmitic acid), 2.65-3.1 (m, 22 H, εH lysine, tyrosine and azidolysine, βH cysteine), 3.1-3.65 (m, 64 H, -CH_2- Stp), 3.70-4.55 (m, 11 H, αH amino acids), 6.60 -7.15 (m, 24 H, -CH- tyrosine).

***1337*:** Sequence (N→C) K(N_3)-C-Y_3-Stp_2-K(K($SteA)_2$)-Stp_2-Y_3-C

^{1}H NMR (500 MHz, Deuterium oxide) δ (ppm) = 0.60-0.85 (s, 6 H, -CH_3 stearic acid), 0.85-2.25 (m, 78 H, βγδH lysine, βγδH azidolysine ,-CH_2- stearic acid), 2.25-2.60 (m, 20 H, -CO-CH_2-CH_2-CO- Stp, -CO-CH_2- stearic acid), 2.65-3.1 (m, 22 H, εH lysine, tyrosine and azidolysine, βH cysteine), 3.1-3.65 (m, 64 H, -CH_2- Stp), 3.70-4.55 (m, 11 H, αH amino acids), 6.60 -7.15 (m, 24 H, -CH- tyrosine).

***1199*:** Sequence (N→C) K(N_3)-C-Y_3-Stp_2-K(K($LinA)_2$)-Stp_2-Y_3-C

^{1}H NMR (500 MHz, Deuterium oxide) δ (ppm) = 0.60-0.85 (s, 6 H, -CH_3 linoleic acid), 0.85-2.25 (m, 58 H, βγδH lysine, βγδH azidolysine ,-CH_2- linoleic acid), 2.25-2.60 (m, 20 H, -CO-CH_2-CH_2-CO- Stp, -CO-CH_2- linoleic acid), 2.65-3.1 (m, 26 H, εH lysine, tyrosine and azidolysine, βH cysteine, -C=C-CH_2-C=C- linoleic acid), 3.1-3.65 (m, 64 H, -CH_2- Stp), 3.70-4.55 (m, 11 H, αH amino acids), 5.05 – 5.25 (s, 8 H, -CH=CH- linoleic acid), 6.60 -7.15 (m, 24 H, -CH- tyrosine).

***1383*:** Sequence (N→C) K(N_3)-C-Y_3-Stp_2-K(K($AraA)_2$)-Stp_2-Y_3-C

^{1}H NMR (500 MHz, Deuterium oxide) δ (ppm) = 0.60-0.85 (s, 6 H, -CH_3 arachidic acid), 0.85-2.25 (m, 86 H, βγδH lysine, βγδH azidolysine ,-CH_2- arachidic acid), 2.25-2.60 (m, 20 H, -CO-CH_2-CH_2-CO- Stp, -CO-CH_2- arachidic acid), 2.65-3.1 (m, 22 H, εH lysine, tyrosine and azidolysine, βH cysteine), 3.1-3.65 (m, 64 H, -CH_2- Stp), 3.70-4.55 (m, 11 H, αH amino acids), 6.60 -7.15 (m, 24 H, -CH- tyrosine).

***1384*:** Sequence (N→C) K(N_3)-C-Y_3-Stp_2-K(K($BehA)_2$)-Stp_2-Y_3-C

^{1}H NMR (500 MHz, Deuterium oxide) δ (ppm) = 0.60-0.85 (s, 6 H, -CH_3 behenic acid), 0.85-2.25 (m, 94 H, βγδH lysine, βγδH azidolysine ,-CH_2- behenic acid), 2.25-2.60 (m, 20 H, -CO-CH_2-CH_2-CO- Stp, -CO-CH_2- behenic acid), 2.65-3.1 (m, 22 H, εH lysine, tyrosine and azidolysine, βH cysteine), 3.1-3.65 (m, 64 H, -CH_2- Stp), 3.70-4.55 (m, 11 H, αH amino acids), 6.60 -7.15 (m, 24 H, -CH- tyrosine).

***1385*:** Sequence (N→C) K(N_3)-C-Y_3-Stp_2-K(K($LigA)_2$)-Stp_2-Y_3-C

^{1}H NMR (500 MHz, Deuterium oxide) δ (ppm) = 0.60-0.85 (s, 6 H, -CH_3 lignoceric acid), 0.85-2.25 (m, 102 H, βγδH lysine, βγδH azidolysine ,-CH_2- lignoceric acid), 2.25-2.60 (m, 20 H, -CO-CH_2-CH_2-CO- Stp, -CO-CH_2- lignoceric acid), 2.65-3.1 (m, 22 H, εH lysine, tyrosine and azidolysine, βH cysteine), 3.1-3.65 (m, 64 H, -CH_2- Stp), 3.70-4.55 (m, 11 H, αH amino acids), 6.60 -7.15 (m, 24 H, -CH- tyrosine).

***1200*:** Sequence (N→C) K(N_3)-C-Y_3-Stp_2-K(K($LenA)_2$)-Stp_2-Y_3-C

^{1}H NMR (500 MHz, Deuterium oxide) δ (ppm) = 0.60-0.85 (s, 6 H, -CH_3 linolenic acid), 0.85-2.25 (m, 46 H, βγδH lysine, βγδH azidolysine ,-CH_2- linolenic acid), 2.25-2.60 (m, 20 H, -CO-

CH_2-CH_2-CO- Stp, -CO-CH_2- linolenic acid), 2.65-3.1 (m, 30 H, εH lysine, tyrosine and azidolysine, βH cysteine, -C=C-CH_2-C=C- linolenic acid), 3.1-3.65 (m, 64 H, -CH_2- Stp), 3.70-4.55 (m, 11 H, αH amino acids), 5.05 – 5.25 (s, 12 H, -CH=CH- linolenic acid), 6.60 -7.15 (m, 24 H, -CH- tyrosine).

1277: Sequence (N→C) K(N_3)-C-Y_3-(H-Stp)$_2$-H-K(K(PalA)$_2$)-H-(H-Stp)$_2$-Y_3-C

^{1}H NMR (500 MHz, Deuterium oxide) δ (ppm) = 0.60-0.85 (s, 6 H, -CH_3 palmitic acid), 0.85-2.25 (m, 70 H, βγδH lysine, βγδH azidolysine ,-CH_2- palmitic acid), 2.25-2.60 (m, 20 H, -CO-CH_2-CH_2-CO- Stp, -CO-CH_2- palmitic acid), 2.65-3.1 (m, 34 H, εH lysine, tyrosine, histidine and azidolysine, βH cysteine), 3.1-3.65 (m, 64 H, -CH_2- Stp), 3.70-4.55 (m, 17 H, αH amino acids), 6.60 -7.15 (m, 30 H, -CH- tyrosine, aromatic H histidine), 8.45-8.60 (m, 6 H, aromatic H histidine).

1278: Sequence (N→C) K(N_3)-C-Y_3-(H-Stp)$_2$-H-K(K(SteA)$_2$)-H-(H-Stp)$_2$-Y_3-C

^{1}H NMR (500 MHz, Deuterium oxide) δ (ppm) = 0.60-0.85 (s, 6 H, -CH_3 stearic acid), 0.85-2.25 (m, 78 H, βγδH lysine, βγδH azidolysine ,-CH_2- stearic acid), 2.25-2.60 (m, 20 H, -CO-CH_2-CH_2-CO- Stp, -CO-CH_2- stearic acid), 2.65-3.1 (m, 34 H, εH lysine, tyrosine, histidine and azidolysine, βH cysteine), 3.1-3.65 (m, 64 H, -CH_2- Stp), 3.70-4.55 (m, 17 H, αH amino acids), 6.60 -7.15 (m, 30 H, -CH- tyrosine, aromatic H histidine), 8.45-8.60 (m, 6 H, aromatic H histidine).

1214**:** Sequence (N→C) K(N_3)-C-Y_3-(H-Stp)$_2$-H-K(K(OleA)$_2$)-H-(H-Stp)$_2$-Y_3-C

^{1}H NMR (500 MHz, Deuterium oxide) δ (ppm) = 0.60-0.85 (s, 6 H, -CH_3 oleic acid), 0.85-2.25 (m, 70 H, βγδH lysine, βγδH azidolysine ,-CH_2- oleic acid), 2.25-2.60 (m, 20 H, -CO-CH_2-CH_2-CO- Stp, -CO-CH_2- oleic acid), 2.65-3.1 (m, 34 H, εH lysine, tyrosine, histidine and azidolysine, βH cysteine), 3.1-3.65 (m, 64 H, -CH_2- Stp), 3.70-4.55 (m, 17 H, αH amino acids), 5.05 – 5.25 (s, 4 H, -CH=CH- oleic acid), 6.60 -7.15 (m, 30 H, -CH- tyrosine, aromatic H histidine), 8.45-8.60 (m, 6 H, aromatic H histidine).

1386: Sequence (N→C) K(N_3)-C-Y_3-(H-Stp)$_2$-H-K(K(AraA)$_2$)-H-(H-Stp)$_2$-Y_3-C

^{1}H NMR (500 MHz, Deuterium oxide) δ (ppm) = 0.60-0.85 (s, 6 H, -CH_3 arachidic acid), 0.85-2.25 (m, 86 H, βγδH lysine, βγδH azidolysine ,-CH_2- arachidic acid), 2.25-2.60 (m, 20 H, -CO-CH_2-CH_2-CO- Stp, -CO-CH_2- arachidic acid), 2.65-3.1 (m, 34 H, εH lysine, tyrosine, histidine and azidolysine, βH cysteine), 3.1-3.65 (m, 64 H, -CH_2- Stp), 3.70-4.55 (m, 17 H, αH amino acids), 6.60 -7.15 (m, 30 H, -CH- tyrosine, aromatic H histidine), 8.45-8.60 (m, 6 H, aromatic H histidine).

1387: Sequence (N→C) K(N_3)-C-Y_3-(H-Stp)$_2$-H-K(K(BehA)$_2$)-H-(H-Stp)$_2$-Y_3-C

^{1}H NMR (500 MHz, Deuterium oxide) δ (ppm) = 0.60-0.85 (s, 6 H, -CH_3 behenic acid), 0.85-2.25 (m, 94 H, βγδH lysine, βγδH azidolysine ,-CH_2- behenic acid), 2.25-2.60 (m, 20 H, -CO-CH_2-CH_2-CO- Stp, -CO-CH_2- behenic acid), 2.65-3.1 (m, 34 H, εH lysine, tyrosine, histidine and azidolysine, βH cysteine), 3.1-3.65 (m, 64 H, -CH_2- Stp), 3.70-4.55 (m, 17 H, αH amino acids), 6.60 -7.15 (m, 30 H, -CH- tyrosine, aromatic H histidine), 8.45-8.60 (m, 6 H, aromatic H histidine).

1388: Sequence (N→C) K(N_3)-C-Y_3-(H-Stp)$_2$-H-K(K(LigA)$_2$)-H-(H-Stp)$_2$-Y_3-C

^{1}H NMR (500 MHz, Deuterium oxide) δ (ppm) = 0.60-0.85 (s, 6 H, -CH_3 lignoceric acid), 0.85-2.25 (m, 102 H, βγδH lysine, βγδH azidolysine ,-CH_2- lignoceric acid), 2.25-2.60 (m, 20 H, -

CO-CH_2-CH_2-CO- Stp, -CO-CH_2- lignoceric acid), 2.65-3.1 (m, 34 H, εH lysine, tyrosine, histidine and azidolysine, βH cysteine), 3.1-3.65 (m, 64 H, -CH_2- Stp), 3.70-4.55 (m, 17 H, αH amino acids), 6.60 -7.15 (m, 30 H, -CH- tyrosine, aromatic H histidine), 8.45-8.60 (m, 6 H, aromatic H histidine).

***1390*:** Sequence (N→C) K(N_3)-C-Y_3-(H-Stp)$_2$-H-K(K(LenA)$_2$)-H-(H-Stp)$_2$-Y_3-C

^{1}H NMR (500 MHz, Deuterium oxide) δ (ppm) = 0.60-0.85 (s, 6 H, -CH_3 linolenic acid), 0.85-2.25 (m, 46 H, βγδH lysine, βγδH azidolysine ,-CH_2- linolenic acid), 2.25-2.60 (m, 20 H, -CO-CH_2-CH_2-CO- Stp, -CO-CH_2- linolenic acid), 2.65-3.1 (m, 42 H, εH lysine, tyrosine, histidine and azidolysine, βH cysteine, -C=C-CH_2-C=C- linolenic acid), 3.1-3.65 (m, 64 H, -CH_2- Stp), 3.70-4.55 (m, 17 H, αH amino acids), 5.05 – 5.25 (s, 12 H, -CH=CH- linolenic acid), 6.60 -7.15 (m, 30 H, -CH- tyrosine, aromatic H histidine), 8.45-8.60 (m, 6 H, aromatic H histidine).

Non-reducible type of oligomers

***1360*:** Sequence (N→C) K(N_3)-Y_3-Stp$_2$-K(K(PalA)$_2$)-Stp$_2$-Y_3

^{1}H NMR (500 MHz, Deuterium oxide) δ (ppm) = 0.60-0.85 (s, 6 H, -CH_3 palmitic acid), 0.85-2.25 (m, 70 H, βγδH lysine, βγδH azidolysine,-CH_2- palmitic acid), 2.25-2.60 (m, 20 H, -CO-CH_2-CH_2-CO- Stp, -CO-CH_2- palmitic acid), 2.65-3.1 (m, 18 H, εH lysine, tyrosine and azidolysine), 3.1-3.65 (m, 64 H, -CH_2- Stp), 3.70-4.55 (m, 9 H, αH amino acids), 6.60 -7.15 (m, 24 H, -CH- tyrosine).

***1361*:** Sequence (N→C) K(N_3)-Y_3-Stp$_2$-K(K(SteA)$_2$)-Stp$_2$-Y_3

^{1}H NMR (500 MHz, Deuterium oxide) δ (ppm) = 0.60-0.85 (s, 6 H, -CH_3 stearic acid), 0.85-2.25 (m, 78 H, βγδH lysine, βγδH azidolysine,-CH_2- stearic acid), 2.25-2.60 (m, 20 H, -CO-CH_2-CH_2-CO- Stp, -CO-CH_2- stearic acid), 2.65-3.1 (m, 18 H, εH lysine, tyrosine and azidolysine), 3.1-3.65 (m, 64 H, -CH_2- Stp), 3.70-4.55 (m, 9 H, αH amino acids), 6.60 -7.15 (m, 24 H, -CH- tyrosine).

***1208*:** Sequence (N→C) K(N_3)-Y_3-Stp$_2$-K(K(OleA)$_2$)-Stp$_2$-Y_3

^{1}H NMR (500 MHz, Deuterium oxide) δ (ppm) = 0.60-0.85 (s, 6 H, -CH_3 oleic acid), 0.85-2.25 (m, 70 H, βγδH lysine, βγδH azidolysine ,-CH_2- oleic acid), 2.25-2.60 (m, 20 H, -CO-CH_2-CH_2-CO- Stp, -CO-CH_2- oleic acid), 2.65-3.1 (m, 18 H, εH lysine, tyrosine and azidolysine), 3.1-3.65 (m, 64 H, -CH_2- Stp), 3.70-4.55 (m, 9 H, αH amino acids), 5.05 – 5.25 (s, 4 H, -CH=CH- oleic acid), 6.60 -7.15 (m, 24 H, -CH- tyrosine).

***1371*:** Sequence (N→C) K(N_3)-Y_3-Stp$_2$-K(K(AraA)$_2$)-Stp$_2$-Y_3

^{1}H NMR (500 MHz, Deuterium oxide) δ (ppm) = 0.60-0.85 (s, 6 H, -CH_3 arachidic acid), 0.85-2.25 (m, 86 H, βγδH lysine, βγδH azidolysine,-CH_2- arachidic acid), 2.25-2.60 (m, 20 H, -CO-CH_2-CH_2-CO- Stp, -CO-CH_2- arachidic acid), 2.65-3.1 (m, 18 H, εH lysine, tyrosine and azidolysine), 3.1-3.65 (m, 64 H, -CH_2- Stp), 3.70-4.55 (m, 9 H, αH amino acids), 6.60 -7.15 (m, 24 H, -CH- tyrosine).

***1372*:** Sequence (N→C) K(N_3)-Y_3-Stp$_2$-K(K(BehA)$_2$)-Stp$_2$-Y_3

^{1}H NMR (500 MHz, Deuterium oxide) δ (ppm) = 0.60-0.85 (s, 6 H, -CH_3 behenic acid), 0.85-2.25 (m, 94 H, βγδH lysine, βγδH azidolysine,-CH_2- behenic acid), 2.25-2.60 (m, 20 H, -CO-CH_2-CH_2-CO- Stp, -CO-CH_2- behenic acid), 2.65-3.1 (m, 18 H, εH lysine, tyrosine and azidolysine), 3.1-3.65 (m, 64 H, -CH_2- Stp), 3.70-4.55 (m, 9 H, αH amino acids), 6.60 -7.15 (m, 24 H, -CH- tyrosine).

1373**:** Sequence (N→C) K(N_3)-Y_3-Stp_2-K(K($LigA)_2$)-Stp_2-Y_3
^{1}H NMR (500 MHz, Deuterium oxide) δ (ppm) = 0.60-0.85 (s, 6 H, -CH_3 lignoceric acid), 0.85-2.25 (m, 102 H, βγδH lysine, βγδH azidolysine,-CH_2- lignoceric acid), 2.25-2.60 (m, 20 H, -CO-CH_2-CH_2-CO- Stp, -CO-CH_2- lignoceric acid), 2.65-3.1 (m, 18 H, εH lysine, tyrosine and azidolysine), 3.1-3.65 (m, 64 H, -CH_2- Stp), 3.70-4.55 (m, 9 H, αH amino acids), 6.60 -7.15 (m, 24 H, -CH- tyrosine).
1320**:** Sequence (N→C) K(N_3)-Y_3-(H-Stp)$_2$-H-K(K($PalA)_2$)-H-(H-Stp)$_2$-Y_3
^{1}H NMR (500 MHz, Deuterium oxide) δ (ppm) = 0.60-0.85 (s, 6 H, -CH_3 palmitic acid), 0.85-2.25 (m, 70 H, βγδH lysine, βγδH azidolysine ,-CH_2- palmitic acid), 2.25-2.60 (m, 20 H, -CO-CH_2-CH_2-CO- Stp, -CO-CH_2- palmitic acid), 2.65-3.1 (m, 30 H, εH lysine, tyrosine, histidine and azidolysine), 3.1-3.65 (m, 64 H, -CH_2- Stp), 3.70-4.55 (m, 15 H, αH amino acids), 6.60 -7.15 (m, 30 H, -CH- tyrosine, aromatic H histidine), 8.45-8.60 (m, 6 H, aromatic H histidine).
1321**:** Sequence (N→C) K(N_3)-Y_3-(H-Stp)$_2$-H-K(K($SteA)_2$)-H-(H-Stp)$_2$-Y_3
^{1}H NMR (500 MHz, Deuterium oxide) δ (ppm) = 0.60-0.85 (s, 6 H, -CH_3 stearic acid), 0.85-2.25 (m, 78 H, βγδH lysine, βγδH azidolysine ,-CH_2- stearic acid), 2.25-2.60 (m, 20 H, -CO-CH_2-CH_2-CO- Stp, -CO-CH_2- stearic acid), 2.65-3.1 (m, 30 H, εH lysine, tyrosine, histidine and azidolysine), 3.1-3.65 (m, 64 H, -CH_2- Stp), 3.70-4.55 (m, 15 H, αH amino acids), 6.60 -7.15 (m, 30 H, -CH- tyrosine, aromatic H histidine), 8.45-8.60 (m, 6 H, aromatic H histidine).
1209**:** Sequence (N→C) K(N_3)-Y_3-(H-Stp)$_2$-H-K(K($OleA)_2$)-H-(H-Stp)$_2$-Y_3
^{1}H NMR (500 MHz, Deuterium oxide) δ (ppm) = 0.60-0.85 (s, 6 H, -CH_3 oleic acid), 0.85-2.25 (m, 70 H, βγδH lysine, βγδH azidolysine ,-CH_2- oleic acid), 2.25-2.60 (m, 20 H, -CO-CH_2-CH_2-CO- Stp, -CO-CH_2- oleic acid), 2.65-3.1 (m, 30 H, εH lysine, tyrosine, histidine and azidolysine), 3.1-3.65 (m, 64 H, -CH_2- Stp), 3.70-4.55 (m, 15 H, αH amino acids), 5.05 – 5.25 (s, 4 H, -CH=CH- oleic acid), 6.60 -7.15 (m, 30 H, -CH- tyrosine, aromatic H histidine), 8.45-8.60 (m, 6 H, aromatic H histidine).
1374**:** Sequence (N→C) K(N_3)-Y_3-(H-Stp)$_2$-H-K(K($AraA)_2$)-H-(H-Stp)$_2$-Y_3
^{1}H NMR (500 MHz, Deuterium oxide) δ (ppm) = 0.60-0.85 (s, 6 H, -CH_3 arachidic acid), 0.85-2.25 (m, 86 H, βγδH lysine, βγδH azidolysine ,-CH_2- arachidic acid), 2.25-2.60 (m, 20 H, -CO-CH_2-CH_2-CO- Stp, -CO-CH_2- arachidic acid), 2.65-3.1 (m, 30 H, εH lysine, tyrosine, histidine and azidolysine), 3.1-3.65 (m, 64 H, -CH_2- Stp), 3.70-4.55 (m, 15 H, αH amino acids), 6.60 -7.15 (m, 30 H, -CH- tyrosine, aromatic H histidine), 8.45-8.60 (m, 6 H, aromatic H histidine).
1375**:** Sequence (N→C) K(N_3)-Y_3-(H-Stp)$_2$-H-K(K($BehA)_2$)-H-(H-Stp)$_2$-Y_3
^{1}H NMR (500 MHz, Deuterium oxide) δ (ppm) = 0.60-0.85 (s, 6 H, -CH_3 behenic acid), 0.85-2.25 (m, 94 H, βγδH lysine, βγδH azidolysine ,-CH_2- behenic acid), 2.25-2.60 (m, 20 H, -CO-CH_2-CH_2-CO- Stp, -CO-CH_2- behenic acid), 2.65-3.1 (m, 30 H, εH lysine, tyrosine, histidine and azidolysine), 3.1-3.65 (m, 64 H, -CH_2- Stp), 3.70-4.55 (m, 15 H, αH amino acids), 6.60 -7.15 (m, 30 H, -CH- tyrosine, aromatic H histidine), 8.45-8.60 (m, 6 H, aromatic H histidine).
1376**:** Sequence (N→C) K(N_3)-Y_3-(H-Stp)$_2$-H-K(K($LigA)_2$)-H-(H-Stp)$_2$-Y_3
^{1}H NMR (500 MHz, Deuterium oxide) δ (ppm) = 0.60-0.85 (s, 6 H, -CH_3 lignoceric acid), 0.85-2.25 (m, 102 H, βγδH lysine, βγδH azidolysine ,-CH_2- lignoceric acid), 2.25-2.60 (m, 20 H, -CO-CH_2-CH_2-CO- Stp, -CO-CH_2- lignoceric acid), 2.65-3.1 (m, 30 H, εH lysine, tyrosine,

histidine and azidolysine), 3.1-3.65 (m, 64 H, -CH_2- Stp), 3.70-4.55 (m, 15 H, αH amino acids), 6.60 -7.15 (m, 30 H, -CH- tyrosine, aromatic H histidine), 8.45-8.60 (m, 6 H, aromatic H histidine).

Bioreducible type of oligomers

1348: Sequence (N→C) K(N_3)-Y_3-Stp_2-K(G-ssbb-K($PalA)_2$)-Stp_2-Y_3

^{1}H NMR (500 MHz, Deuterium oxide) δ (ppm) = 0.60-0.85 (s, 6 H, -CH_3 palmitic acid), 0.85-2.25 (m, 70 H, βγδH lysine, βγδH azidolysine ,-CH_2- palmitic acid), 2.25-2.60 (m, 24 H, -CO-CH_2-CH_2-CO- Stp and ssbb, -CO-CH_2- palmitic acid), 2.65-3.1 (m, 26 H, εH lysine, tyrosine and azidolysine, -CH_2- ssbb), 3.1-3.65 (m, 64 H, -CH_2- Stp), 3.70-4.55 (m, 11 H, αH amino acids), 6.60 -7.15 (m, 24 H, -CH- tyrosine).

1349: Sequence (N→C) K(N_3)-Y_3-Stp_2-K(G-ssbb-K($SteA)_2$)-Stp_2-Y_3

^{1}H NMR (500 MHz, Deuterium oxide) δ (ppm) = 0.60-0.85 (s, 6 H, -CH_3 stearic acid), 0.85-2.25 (m, 78 H, βγδH lysine, βγδH azidolysine ,-CH_2- stearic acid), 2.25-2.60 (m, 24 H, -CO-CH_2-CH_2-CO- Stp and ssbb, -CO-CH_2- stearic acid), 2.65-3.1 (m, 26 H, εH lysine, tyrosine and azidolysine, -CH_2- ssbb), 3.1-3.65 (m, 64 H, -CH_2- Stp), 3.70-4.55 (m, 11 H, αH amino acids), 6.60 -7.15 (m, 24 H, -CH- tyrosine).

1217: Sequence (N→C) K(N_3)-Y_3-Stp_2-K(G-ssbb-K($OleA)_2$)-Stp_2-Y_3

^{1}H NMR (500 MHz, Deuterium oxide) δ (ppm) = 0.60-0.85 (s, 6 H, -CH_3 oleic acid), 0.85-2.25 (m, 70 H, βγδH lysine, βγδH azidolysine ,-CH_2- oleic acid), 2.25-2.60 (m, 24 H, -CO-CH_2-CH_2-CO- Stp and ssbb, -CO-CH_2- oleic acid), 2.65-3.1 (m, 26 H, εH lysine, tyrosine and azidolysine, -CH_2- ssbb), 3.1-3.65 (m, 64 H, -CH_2- Stp), 3.70-4.55 (m, 11 H, αH amino acids), 5.05 – 5.25 (s, 4 H, -CH=CH- oleic acid), 6.60 -7.15 (m, 24 H, -CH- tyrosine).

1377: Sequence (N→C) K(N_3)-Y_3-Stp_2-K(G-ssbb-K($AraA)_2$)-Stp_2-Y_3

^{1}H NMR (500 MHz, Deuterium oxide) δ (ppm) = 0.60-0.85 (s, 6 H, -CH_3 arachidic acid), 0.85-2.25 (m, 86 H, βγδH lysine, βγδH azidolysine ,-CH_2- arachidic acid), 2.25-2.60 (m, 24 H, -CO-CH_2-CH_2-CO- Stp and ssbb, -CO-CH_2- arachidic acid), 2.65-3.1 (m, 26 H, εH lysine, tyrosine and azidolysine, -CH_2- ssbb), 3.1-3.65 (m, 64 H, -CH_2- Stp), 3.70-4.55 (m, 11 H, αH amino acids), 6.60 -7.15 (m, 24 H, -CH- tyrosine).

1378: Sequence (N→C) K(N_3)-Y_3-Stp_2-K(G-ssbb-K($BehA)_2$)-Stp_2-Y_3

^{1}H NMR (500 MHz, Deuterium oxide) δ (ppm) = 0.60-0.85 (s, 6 H, -CH_3 behenic acid), 0.85-2.25 (m, 94 H, βγδH lysine, βγδH azidolysine ,-CH_2- behenic acid), 2.25-2.60 (m, 24 H, -CO-CH_2-CH_2-CO- Stp and ssbb, -CO-CH_2- behenic acid), 2.65-3.1 (m, 26 H, εH lysine, tyrosine and azidolysine, -CH_2- ssbb), 3.1-3.65 (m, 64 H, -CH_2- Stp), 3.70-4.55 (m, 11 H, αH amino acids), 6.60 -7.15 (m, 24 H, -CH- tyrosine).

1379: Sequence (N→C) K(N_3)-Y_3-Stp_2-K(G-ssbb-K($LigA)_2$)-Stp_2-Y_3

^{1}H NMR (500 MHz, Deuterium oxide) δ (ppm) = 0.60-0.85 (s, 6 H, -CH_3 lignoceric acid), 0.85-2.25 (m, 102 H, βγδH lysine, βγδH azidolysine ,-CH_2- lignoceric acid), 2.25-2.60 (m, 24 H, -CO-CH_2-CH_2-CO- Stp and ssbb, -CO-CH_2- lignoceric acid), 2.65-3.1 (m, 26 H, εH lysine, tyrosine and azidolysine, -CH_2- ssbb), 3.1-3.65 (m, 64 H, -CH_2- Stp), 3.70-4.55 (m, 11 H, αH amino acids), 6.60 -7.15 (m, 24 H, -CH- tyrosine).

1305: Sequence (N→C) K(N_3)-Y_3-(H-$Stp)_2$-H-K(G-ssbb-K($PalA)_2$)-H-(H-$Stp)_2$-Y_3

^{1}H NMR (500 MHz, Deuterium oxide) δ (ppm) = 0.60-0.85 (s, 6 H, -CH_3 palmitic acid), 0.85-2.25 (m, 70 H, βγδH lysine, βγδH azidolysine ,-CH_2- palmitic acid), 2.25-2.60 (m, 24 H, -CO-CH_2-CH_2-CO- Stp and ssbb, -CO-CH_2- palmitic acid), 2.65-3.1 (m, 38 H, εH lysine, tyrosine, histidine and azidolysine, -CH_2- ssbb), 3.1-3.65 (m, 64 H, -CH_2- Stp), 3.70-4.55 (m, 17 H, αH amino acids), 6.60 -7.15 (m, 30 H, -CH- tyrosine, aromatic H histidine), 8.45-8.60 (m, 6 H, aromatic H histidine).

1306: Sequence (N→C) K(N_3)-Y_3-(H-Stp)$_2$-H-K(G-ssbb-K(SteA)$_2$)-H-(H-Stp)$_2$-Y_3

^{1}H NMR (500 MHz, Deuterium oxide) δ (ppm) = 0.60-0.85 (s, 6 H, -CH_3 stearic acid), 0.85-2.25 (m, 78 H, βγδH lysine, βγδH azidolysine ,-CH_2- stearic acid), 2.25-2.60 (m, 24 H, -CO-CH_2-CH_2-CO- Stp and ssbb, -CO-CH_2- stearic acid), 2.65-3.1 (m, 38 H, εH lysine, tyrosine, histidine and azidolysine, -CH_2- ssbb), 3.1-3.65 (m, 64 H, -CH_2- Stp), 3.70-4.55 (m, 17 H, αH amino acids), 6.60 -7.15 (m, 30 H, -CH- tyrosine, aromatic H histidine), 8.45-8.60 (m, 6 H, aromatic H histidine).

1218: Sequence (N→C) K(N_3)-Y_3-(H-Stp)$_2$-H-K(G-ssbb-K(OleA)$_2$)-H-(H-Stp)$_2$-Y_3

^{1}H NMR (500 MHz, Deuterium oxide) δ (ppm) = 0.60-0.85 (s, 6 H, -CH_3 oleic acid), 0.85-2.25 (m, 70 H, βγδH lysine, βγδH azidolysine ,-CH_2- oleic acid), 2.25-2.60 (m, 24 H, -CO-CH_2-CH_2-CO- Stp and ssbb, -CO-CH_2- oleic acid), 2.65-3.1 (m, 38 H, εH lysine, tyrosine, histidine and azidolysine, -CH_2- ssbb), 3.1-3.65 (m, 64 H, -CH_2- Stp), 3.70-4.55 (m, 17 H, αH amino acids), 5.05 – 5.25 (s, 4 H, -CH=CH- oleic acid), 6.60 -7.15 (m, 30 H, -CH- tyrosine, aromatic H histidine), 8.45-8.60 (m, 6 H, aromatic H histidine).

1380: Sequence (N→C) K(N_3)-Y_3-(H-Stp)$_2$-H-K(G-ssbb-K(AraA)$_2$)-H-(H-Stp)$_2$-Y_3

^{1}H NMR (500 MHz, Deuterium oxide) δ (ppm) = 0.60-0.85 (s, 6 H, -CH_3 arachidic acid), 0.85-2.25 (m, 86 H, βγδH lysine, βγδH azidolysine ,-CH_2- arachidic acid), 2.25-2.60 (m, 24 H, -CO-CH_2-CH_2-CO- Stp and ssbb, -CO-CH_2- arachidic acid), 2.65-3.1 (m, 38 H, εH lysine, tyrosine, histidine and azidolysine, -CH_2- ssbb), 3.1-3.65 (m, 64 H, -CH_2- Stp), 3.70-4.55 (m, 17 H, αH amino acids), 6.60 -7.15 (m, 30 H, -CH- tyrosine, aromatic H histidine), 8.45-8.60 (m, 6 H, aromatic H histidine).

1381: Sequence (N→C) K(N_3)-Y_3-(H-Stp)$_2$-H-K(G-ssbb-K(BehA)$_2$)-H-(H-Stp)$_2$-Y_3

^{1}H NMR (500 MHz, Deuterium oxide) δ (ppm) = 0.60-0.85 (s, 6 H, -CH_3 behenic acid), 0.85-2.25 (m, 94 H, βγδH lysine, βγδH azidolysine ,-CH_2- behenic acid), 2.25-2.60 (m, 24 H, -CO-CH_2-CH_2-CO- Stp and ssbb, -CO-CH_2- behenic acid), 2.65-3.1 (m, 38 H, εH lysine, tyrosine, histidine and azidolysine, -CH_2- ssbb), 3.1-3.65 (m, 64 H, -CH_2- Stp), 3.70-4.55 (m, 17 H, αH amino acids), 6.60 -7.15 (m, 30 H, -CH- tyrosine, aromatic H histidine), 8.45-8.60 (m, 6 H, aromatic H histidine).

1382: Sequence (N→C) K(N_3)-Y_3-(H-Stp)$_2$-H-K(G-ssbb-K(LigA)$_2$)-H-(H-Stp)$_2$-Y_3

^{1}H NMR (500 MHz, Deuterium oxide) δ (ppm) = 0.60-0.85 (s, 6 H, -CH_3 lignoceric acid), 0.85-2.25 (m, 102 H, βγδH lysine, βγδH azidolysine ,-CH_2- lignoceric acid), 2.25-2.60 (m, 24 H, -CO-CH_2-CH_2-CO- Stp and ssbb, -CO-CH_2- lignoceric acid), 2.65-3.1 (m, 38 H, εH lysine, tyrosine, histidine and azidolysine, -CH_2- ssbb), 3.1-3.65 (m, 64 H, -CH_2- Stp), 3.70-4.55 (m, 17 H, αH amino acids), 6.60 -7.15 (m, 30 H, -CH- tyrosine, aromatic H histidine), 8.45-8.60 (m, 6 H, aromatic H histidine).

6. Abbreviations

ACN	Acetonitrile
Boc	*tert*-Butoxycarbonyl
BSA	Bovine serum albumin
D_2O	Deuterium oxide
DAPI	4',6-Diamidino-2-phenylindole
DBCO	Dibenzocyclooctyne group
DCM	Dichloromethane
Dde	1-(4,4-Dimethyl-2,6-dioxocyclohex-1-ylidene)-3-ethyl
DIPEA	*N,N*-Diisopropylethylamine
DLS	Dynamic laser-light scattering
DMEM	Dulbecco's modified Eagle's medium
DMF	*N,N*-Dimethylformamide
DMSO	Dimethylsulfoxide
dsRNA	Double-strand RNA
DTNB	5,5'-Dithio-bis(2-nitrobenzoic acid)
EDTA	Ethylendiaminetetraacetic acid
EGFP	Enhanced green fluorescent protein
FBS	Fetal bovine serum
FCS	Fluorescence correlation spectroscopy
FITC	Fluorescein isothiocyanate
Fmoc	Fluorenylmethoxycarbonyl
FolA	Folic acid
FR	Folate receptor

GSH	Glutathione
Gtt	Glutaroyl triethylene tetramine
HA	Hyaluronic acid
HBG	Hepes-buffered glucose
HBTU	2-(1H-benzotriazole-1-yl)-1,1,3,3-tetramethyluronium hexafluorophosphate
HCl	Hydrochloric acid
HEPES	*N*-(2-hydroxethyl) piperazine-*N*‘-(2-ethansulfonic acid)
HOBt	1-Hydroxybenzotriazole
INF7	An endosomolytic influenza virus derived peptide
ivDde	1-(4,4-dimethyl-2,6-dioxocyclohex-1-ylidene)-3-methylbutyl
LenA	Linolenic acid
LinA	Linoleic acid
MTBE	Methyl tert-butyl ether
MTT	3-(4,5-Dimethylthiazol-2-yl)-2,5-diphenyltetrazolium bromide
MWCO	Molecular Weight Cut Off
MyrA	Myristic acid
NaOH	Sodium hydroxide
NHS	*N*-Hydroxysuccinimide
NMR	Nuclear magnetic resonance
OleA	Oleic acid
PBS	Phosphate buffered saline
PDI	Polydispersity index
PEG	Polyethylene glycol

PyBOP	Benzotriazol-1-yloxy-tripyrrolidinophosphonium hexafluorophosphate
RNA	Ribonucleic acid
RNase A	Ribonuclease A
RP-HPLC	Reversed-phase high performance liquid chromatography
RPMI	Roswell Park Memorial Institute medium
RT	Room temperature
SEC	Size-exclusion chromatography
siRNA	Small interfering RNA
Sph	Succinoyl-pentaethylene hexamine
SPS	Solid-phase synthesis
SteA	Stearic acid
Stp	Succinoyl-tetraethylene pentamine
TEPA	Tetraethylene pentamine
TEM	Transmission electron microscopy
TFA	Trifluoroacetic acid
THF	Tetrahydrofuran
TIS	Triisopropylsilane

7. References

[1] D. Adams, A. Gonzalez-Duarte, W.D. O'Riordan, C.-C. Yang, M. Ueda, A.V. Kristen, I. Tournev, H.H. Schmidt, T. Coelho, J.L. Berk, K.-P. Lin, G. Vita, S. Attarian, V. Planté-Bordeneuve, M.M. Mezei, J.M. Campistol, J. Buades, T.H. Brannagan, B.J. Kim, J. Oh, Y. Parman, Y. Sekijima, P.N. Hawkins, S.D. Solomon, M. Polydefkis, P.J. Dyck, P.J. Gandhi, S. Goyal, J. Chen, A.L. Strahs, S.V. Nochur, M.T. Sweetser, P.P. Garg, A.K. Vaishnaw, J.A. Gollob, O.B. Suhr, Patisiran, an RNAi Therapeutic, for Hereditary Transthyretin Amyloidosis, New England Journal of Medicine 379(1) (2018) 11-21.

[2] L. Hartmann, E. Krause, M. Antonietti, H.G. Borner, Solid-phase supported polymer synthesis of sequence-defined, multifunctional poly(amidoamines), Biomacromolecules. 7(4) (2006) 1239-1244.

[3] L. Hartmann, S. Häfele, R. Peschka-Süss, M. Antonietti, H.G. Börner, Sequence Positioning of Disulfide Linkages to Program the Degradation of Monodisperse Poly(amidoamines), Macromolecules 40(22) (2007) 7771-7776.

[4] L. Hartmann, S. Hafele, R. Peschka-Suss, M. Antonietti, H.G. Borner, Tailor-Made Poly(amidoamine)s for Controlled Complexation and Condensation of DNA, Chemistry. 14(7) (2008) 2025-2033.

[5] S.A. Hill, C. Gerke, L. Hartmann, Recent Developments in Solid-Phase Strategies towards Synthetic, Sequence-Defined Macromolecules, Chemistry, an Asian journal 13(23) (2018) 3611-3622.

[6] W. Tai, X. Gao, Functional peptides for siRNA delivery, Advanced drug delivery reviews 110-111 (2017) 157-168.

[7] A.D. Tagalakis, D.H.D. Lee, A.S. Bienemann, H. Zhou, M.M. Munye, L. Saraiva, D. McCarthy, Z. Du, C.A. Vink, R. Maeshima, E.A. White, K. Gustafsson, S.L. Hart, Multifunctional, self-assembling anionic peptide-lipid nanocomplexes for targeted siRNA delivery, Biomaterials 35(29) (2014) 8406-8415.

[8] P. Majumder, S. Bhunia, J. Bhattacharyya, A. Chaudhuri, Inhibiting tumor growth by targeting liposomally encapsulated CDC20siRNA to tumor vasculature: Therapeutic RNA interference, Journal of Controlled Release 180 (2014) 100-108.

[9] Y. Huang, X. Wang, W. Huang, Q. Cheng, S. Zheng, S. Guo, H. Cao, X.-J. Liang, Q. Du, Z. Liang, Systemic Administration of siRNA via cRGD-containing Peptide, Scientific Reports 5(1) (2015) 12458.

[10] J. Jiang, S.-j. Yang, J.-c. Wang, L.-j. Yang, Z.-z. Xu, T. Yang, X.-y. Liu, Q. Zhang, Sequential treatment of drug-resistant tumors with RGD-modified liposomes containing siRNA or doxorubicin, European Journal of Pharmaceutics and Biopharmaceutics 76(2) (2010) 170-178.

[11] Q.R. Chen, L. Zhang, P.W. Luther, A.J. Mixson, Optimal transfection with the HK polymer depends on its degree of branching and the pH of endocytic vesicles, Nucleic Acids Res. 30(6) (2002) 1338-1345.

[12] Q. Leng, A.J. Mixson, Modified branched peptides with a histidine-rich tail enhance in vitro gene transfection, Nucleic Acids Res 33(4) (2005) e40.

[13] Q. Leng, P. Scaria, J. Zhu, N. Ambulos, P. Campbell, A.J. Mixson, Highly branched HK peptides are effective carriers of siRNA, J Gene Med 7(7) (2005) 977-986.
[14] Q. Leng, A.J. Mixson, Small interfering RNA targeting Raf-1 inhibits tumor growth in vitro and in vivo, Cancer Gene Ther. 12(8) (2005) 682-690.
[15] Q. Leng, S.T. Chou, P.V. Scaria, M.C. Woodle, A.J. Mixson, Increased tumor distribution and expression of histidine-rich plasmid polyplexes, J Gene Med 16(9-10) (2014) 317-28.
[16] Q. Leng, A.J. Mixson, The neuropilin-1 receptor mediates enhanced tumor delivery of H2K polyplexes, J Gene Med 18(7) (2016) 134-44.
[17] T. Lehto, R. Abes, N. Oskolkov, J. Suhorutsenko, D.M. Copolovici, I. Mager, J.R. Viola, O.E. Simonson, K. Ezzat, P. Guterstam, E. Eriste, C.I. Smith, B. Lebleu, A. Samir El, U. Langel, Delivery of nucleic acids with a stearylated (RxR)4 peptide using a non-covalent co-incubation strategy, J Control Release 141(1) (2010) 42-51.
[18] S.E. Andaloussi, T. Lehto, I. Mager, K. Rosenthal-Aizman, Oprea, II, O.E. Simonson, H. Sork, K. Ezzat, D.M. Copolovici, K. Kurrikoff, J.R. Viola, E.M. Zaghloul, R. Sillard, H.J. Johansson, F. Said Hassane, P. Guterstam, J. Suhorutsenko, P.M. Moreno, N. Oskolkov, J. Halldin, U. Tedebark, A. Metspalu, B. Lebleu, J. Lehtio, C.I. Smith, U. Langel, Design of a peptide-based vector, PepFect6, for efficient delivery of siRNA in cell culture and systemically in vivo, Nucleic Acids Res 39(9) (2011) 3972-87.
[19] K. Ezzat, S.E. Andaloussi, E.M. Zaghloul, T. Lehto, S. Lindberg, P.M. Moreno, J.R. Viola, T. Magdy, R. Abdo, P. Guterstam, R. Sillard, S.M. Hammond, M.J. Wood, A.A. Arzumanov, M.J. Gait, C.I. Smith, M. Hallbrink, U. Langel, PepFect 14, a novel cell-penetrating peptide for oligonucleotide delivery in solution and as solid formulation, Nucleic Acids Res 39(12) (2011) 5284-98.
[20] X.L. Wang, R. Xu, X. Wu, D. Gillespie, R. Jensen, Z.R. Lu, Targeted systemic delivery of a therapeutic siRNA with a multifunctional carrier controls tumor proliferation in mice, Mol Pharm. 6(3) (2009) 738-746.
[21] X.-L. Wang, R. Xu, Z.-R. Lu, A peptide-targeted delivery system with pH-sensitive amphiphilic cell membrane disruption for efficient receptor-mediated siRNA delivery, Journal of Controlled Release 134(3) (2009) 207-213.
[22] A.S. Malamas, M. Gujrati, C.M. Kummitha, R. Xu, Z.R. Lu, Design and evaluation of new pH-sensitive amphiphilic cationic lipids for siRNA delivery, J Control Release 171(3) (2013) 296-307.
[23] J.G. Parvani, M.D. Gujrati, M.A. Mack, W.P. Schiemann, Z.R. Lu, Silencing beta3 Integrin by Targeted ECO/siRNA Nanoparticles Inhibits EMT and Metastasis of Triple-Negative Breast Cancer, Cancer Res 75(11) (2015) 2316-2325.
[24] O. Boussif, F. Lezoualc'h, M.A. Zanta, M.D. Mergny, D. Scherman, B. Demeneix, J.P. Behr, A versatile vector for gene and oligonucleotide transfer into cells in culture and in vivo: polyethylenimine, Proc.Natl.Acad.Sci.U.S.A 92(16) (1995) 7297-7301.
[25] A. Kichler, C. Leborgne, E. Coeytaux, O. Danos, Polyethylenimine-mediated gene delivery: a mechanistic study, J Gene Med 3(2) (2001) 135-144.
[26] A. Hall, U. Lachelt, J. Bartek, E. Wagner, S.M. Moghimi, Polyplex Evolution: Understanding Biology, Optimizing Performance, Mol Ther 25(7) (2017) 1476-1490.

[27] D. Schaffert, N. Badgujar, E. Wagner, Novel Fmoc-polyamino acids for solid-phase synthesis of defined polyamidoamines, Organic letters 13(7) (2011) 1586-1589.
[28] D. Schaffert, C. Troiber, E.E. Salcher, T. Frohlich, I. Martin, N. Badgujar, C. Dohmen, D. Edinger, R. Klager, G. Maiwald, K. Farkasova, S. Seeber, K. Jahn-Hofmann, P. Hadwiger, E. Wagner, Solid-phase synthesis of sequence-defined T-, i-, and U-shape polymers for pDNA and siRNA delivery, Angew Chem Int Ed Engl 50(38) (2011) 8986-9.
[29] E. Wagner, Polymers for siRNA Delivery: Inspired by Viruses to be Targeted, Dynamic, and Precise, Acc Chem Res 45(7) (2012) 1005-13.
[30] C. Scholz, E. Wagner, Therapeutic plasmid DNA versus siRNA delivery: Common and different tasks for synthetic carriers, J Control Release 161(2) (2012) 554-65.
[31] E.E. Salcher, P. Kos, T. Fröhlich, N. Badgujar, M. Scheible, E. Wagner, Sequence-defined four-arm oligo (ethanamino) amides for pDNA and siRNA delivery: Impact of building blocks on efficacy, Journal of controlled release 164(3) (2012) 380-386.
[32] T. Frohlich, D. Edinger, R. Klager, C. Troiber, E. Salcher, N. Badgujar, I. Martin, D. Schaffert, A. Cengizeroglu, P. Hadwiger, H.P. Vornlocher, E. Wagner, Structure-activity relationships of siRNA carriers based on sequence-defined oligo (ethane amino) amides, J Control Release 160(3) (2012) 532-41.
[33] C. Dohmen, D. Edinger, T. Frohlich, L. Schreiner, U. Lachelt, C. Troiber, J. Radler, P. Hadwiger, H.P. Vornlocher, E. Wagner, Nanosized Multifunctional Polyplexes for Receptor-Mediated SiRNA Delivery, ACS Nano 6(6) (2012) 5198-208.
[34] C. Dohmen, T. Frohlich, U. Lachelt, I. Rohl, H.-P. Vornlocher, P. Hadwiger, E. Wagner, Defined Folate-PEG-siRNA Conjugates for Receptor-specific Gene Silencing, Mol Ther Nucleic Acids 1 (2012) e7.
[35] K. Mechtler, E. Wagner, Gene transfer mediated by influenza virus peptides: the role of peptide sequence, New J Chem 21 (1997) 105-11.
[36] C. Plank, B. Oberhauser, K. Mechtler, C. Koch, E. Wagner, The influence of endosome-disruptive peptides on gene transfer using synthetic virus-like gene transfer systems, J Biol.Chem. 269(17) (1994) 12918-12924.
[37] U. Lachelt, V. Wittmann, K. Muller, D. Edinger, P. Kos, M. Hohn, E. Wagner, Synthetic polyglutamylation of dual-functional MTX ligands for enhanced combined cytotoxicity of poly(I:C) nanoplexes, Mol Pharm 11(8) (2014) 2631-9.
[38] D.-J. Lee, E. Kessel, D. Edinger, D. He, P.M. Klein, L. Voith von Voithenberg, D.C. Lamb, U. Lächelt, T. Lehto, E. Wagner, Dual antitumoral potency of EG5 siRNA nanoplexes armed with cytotoxic bifunctional glutamyl-methotrexate targeting ligand, Biomaterials 77 (2016) 98-110.
[39] P.M. Klein, S. Reinhard, D.-J. Lee, K. Müller, D. Ponader, L. Hartmann, E. Wagner, Precise redox-sensitive cleavage sites for improved bioactivity of siRNA lipopolyplexes, Nanoscale 8(42) (2016) 18098-18104.
[40] J. Gilleron, W. Querbes, A. Zeigerer, A. Borodovsky, G. Marsico, U. Schubert, K. Manygoats, S. Seifert, C. Andree, M. Stöter, Image-based analysis of lipid nanoparticle–mediated siRNA delivery, intracellular trafficking and endosomal escape, Nature biotechnology 31(7) (2013) 638.

[41] A. Wittrup, A. Ai, X. Liu, P. Hamar, R. Trifonova, K. Charisse, M. Manoharan, T. Kirchhausen, J. Lieberman, Visualizing lipid-formulated siRNA release from endosomes and target gene knockdown, Nature biotechnology 33(8) (2015) 870.
[42] S. Reinhard, Y. Wang, S. Dengler, E. Wagner, Precise Enzymatic Cleavage Sites for Improved Bioactivity of siRNA Lipo-Polyplexes, Bioconjug Chem 29(11) (2018) 3649-3657.
[43] D.-J. Lee, D. He, E. Kessel, K. Padari, S. Kempter, U. Lächelt, J.O. Rädler, M. Pooga, E. Wagner, Tumoral gene silencing by receptor-targeted combinatorial siRNA polyplexes, Journal of controlled release 244 (2016) 280-291.
[44] D.-J. Lee, E. Wagner, Combinatorial siRNA Polyplexes for Receptor Targeting, in: L. Dinesh Kumar (Ed.), RNA Interference and Cancer Therapy: Methods and Protocols, Springer New York, New York, NY, 2019, pp. 83-98.
[45] P. Kos, U. Lächelt, A. Herrmann, F.M. Mickler, M. Döblinger, D. He, A.K. Levačić, S. Morys, C. Bräuchle, E. Wagner, Histidine-rich stabilized polyplexes for cMet-directed tumor-targeted gene transfer, Nanoscale 7(12) (2015) 5350-5362.
[46] D. He, K. Müller, A. Krhac Levacic, P. Kos, U. Lächelt, E. Wagner, Combinatorial optimization of sequence-defined oligo (ethanamino) amides for folate receptor-targeted pDNA and siRNA delivery, Bioconjugate chemistry 27(3) (2016) 647-659.
[47] D.-J. Lee, E. Kessel, T. Lehto, X. Liu, N. Yoshinaga, K. Padari, Y.-C. Chen, S. Kempter, S. Uchida, J.O. Rädler, Systemic delivery of folate-PEG siRNA lipopolyplexes with enhanced intracellular stability for in vivo gene silencing in leukemia, Bioconjugate chemistry 28(9) (2017) 2393-2409.
[48] K. Müller, E. Kessel, P.M. Klein, M. Höhn, E. Wagner, Post-PEGylation of siRNA lipo-oligoamino amide polyplexes using tetra-glutamylated folic acid as ligand for receptor-targeted delivery, Molecular pharmaceutics 13(7) (2016) 2332-2345.
[49] K. Müller, P.M. Klein, P. Heissig, A. Roidl, E. Wagner, EGF receptor targeted lipo-oligocation polyplexes for antitumoral siRNA and miRNA delivery, Nanotechnology 27(46) (2016) 464001.
[50] B. Steinborn, I. Truebenbach, S. Morys, U. Lächelt, E. Wagner, W. Zhang, Epidermal growth factor receptor targeted methotrexate and small interfering RNA co ‐ delivery, The journal of gene medicine 20(7-8) (2018) e3041.
[51] W. Zhang, K. Müller, E. Kessel, S. Reinhard, D. He, P.M. Klein, M. Höhn, W. Rödl, S. Kempter, E. Wagner, Targeted siRNA delivery using a lipo ‐ oligoaminoamide nanocore with an influenza peptide and transferrin shell, Advanced healthcare materials 5(12) (2016) 1493-1504.
[52] J. Luo, M. Höhn, S. Reinhard, D.M. Loy, P.M. Klein, E. Wagner, IL4-Receptor-Targeted Dual Antitumoral Apoptotic Peptide—siRNA Conjugate Lipoplexes, Advanced Functional Materials 29(25) (2019) 1900697.
[53] Y. Wang, J. Luo, I. Truebenbach, S.r. Reinhard, P.M. Klein, M. Höhn, S. Kern, S. Morys, D.M. Loy, E. Wagner, Double Click-Functionalized siRNA Polyplexes for Gene Silencing in Epidermal Growth Factor Receptor-Positive Tumor Cells, ACS Biomaterials Science & Engineering (2020).
[54] P. Klein, K. Klinker, W. Zhang, S. Kern, E. Kessel, E. Wagner, M. Barz, Efficient shielding of polyplexes using heterotelechelic polysarcosines, Polymers 10(6) (2018) 689.

[55] P.M. Klein, S. Kern, D.-J. Lee, J. Schmaus, M. Höhn, J. Gorges, U. Kazmaier, E. Wagner, Folate receptor-directed orthogonal click-functionalization of siRNA lipopolyplexes for tumor cell killing in vivo, Biomaterials 178 (2018) 630-642.
[56] I. Truebenbach, W. Zhang, Y. Wang, S. Kern, M. Höhn, S. Reinhard, J. Gorges, U. Kazmaier, E. Wagner, Co-delivery of pretubulysin and siEG5 to EGFR overexpressing carcinoma cells, International Journal of Pharmaceutics 569 (2019) 118570.
[57] P.M. Klein, E. Wagner, Click-Shielded and Targeted Lipopolyplexes, Oligonucleotide-Based Therapies, Springer2019, pp. 141-164.
[58] U. Lächelt, V. Wittmann, K. Müller, D. Edinger, P. Kos, M. Höhn, E. Wagner, Synthetic polyglutamylation of dual-functional MTX ligands for enhanced combined cytotoxicity of poly (I: C) nanoplexes, Molecular pharmaceutics 11(8) (2014) 2631-2639.
[59] J.M. Baskin, J.A. Prescher, S.T. Laughlin, N.J. Agard, P.V. Chang, I.A. Miller, A. Lo, J.A. Codelli, C.R. Bertozzi, Copper-free click chemistry for dynamic in vivo imaging, 104(43) (2007) 16793-16797.
[60] P.V. Chang, J.A. Prescher, E.M. Sletten, J.M. Baskin, I.A. Miller, N.J. Agard, A. Lo, C.R. Bertozzi, Copper-free click chemistry in living animals, 107(5) (2010) 1821-1826.
[61] V.V. Rostovtsev, L.G. Green, V.V. Fokin, K.B. Sharpless, A Stepwise Huisgen Cycloaddition Process: Copper(I)-Catalyzed Regioselective “Ligation” of Azides and Terminal Alkynes, 41(14) (2002) 2596-2599.
[62] D.M. Loy, P.M. Klein, R. Krzysztoń, U. Lächelt, J.O. Rädler, E. Wagner, A microfluidic approach for sequential assembly of siRNA polyplexes with defined structure–activity relationship, PeerJ Preprints, 2019.
[63] L.D. Mayer, T.O. Harasym, P.G. Tardi, N.L. Harasym, C.R. Shew, S.A. Johnstone, E.C. Ramsay, M.B. Bally, A.S. Janoff, Ratiometric dosing of anticancer drug combinations: Controlling drug ratios after systemic administration regulates therapeutic activity in tumor-bearing mice, Molecular Cancer Therapeutics 5(7) (2006) 1854-1863.
[64] I. Truebenbach, S. Kern, D.M. Loy, M. Höhn, J. Gorges, U. Kazmaier, E. Wagner, Combination Chemotherapy of L1210 Tumors in Mice with Pretubulysin and Methotrexate Lipo-Oligomer Nanoparticles, Molecular Pharmaceutics 16(6) (2019) 2405-2417.
[65] P.M. Klein, S. Kern, D.J. Lee, J. Schmaus, M. Hohn, J. Gorges, U. Kazmaier, E. Wagner, Folate receptor-directed orthogonal click-functionalization of siRNA lipopolyplexes for tumor cell killing in vivo, Biomaterials (2018).
[66] P.M. Klein, S. Reinhard, D.J. Lee, K. Muller, D. Ponader, L. Hartmann, E. Wagner, Precise redox-sensitive cleavage sites for improved bioactivity of siRNA lipopolyplexes, Nanoscale 8(42) (2016) 18098-18104.
[67] S. Reinhard, W. Zhang, E. Wagner, Optimized Solid-Phase-Assisted Synthesis of Oleic Acid Containing siRNA Nanocarriers, ChemMedChem 12(17) (2017) 1464-1470.
[68] S. Reinhard, Y. Wang, S. Dengler, E. Wagner, Precise Enzymatic Cleavage Sites for Improved Bioactivity of siRNA Lipo-Polyplexes, Bioconjugate Chemistry 29(11) (2018) 3649-3657.

[69] A. Fire, S. Xu, M.K. Montgomery, S.A. Kostas, S.E. Driver, C.C. Mello, Potent and specific genetic interference by double-stranded RNA in Caenorhabditis elegans, Nature 391(6669) (1998) 806-811.
[70] N. Adams, U.S. Schubert, Poly(2-oxazolines) in biological and biomedical application contexts, Advanced Drug Delivery Reviews 59(15) (2007) 1504-1520.
[71] D. Haussecker, Current issues of RNAi therapeutics delivery and development, J Control Release 195 (2014) 49-54.
[72] A. Wittrup, A. Ai, X. Liu, P. Hamar, R. Trifonova, K. Charisse, M. Manoharan, T. Kirchhausen, J. Lieberman, Visualizing lipid-formulated siRNA release from endosomes and target gene knockdown, Nat Biotechnol 33(8) (2015) 870-6.
[73] U. Lachelt, E. Wagner, Nucleic Acid Therapeutics Using Polyplexes: A Journey of 50 Years (and Beyond), Chem Rev 115(19) (2015) 11043-78.
[74] P.R. Cullis, M.J. Hope, Lipid Nanoparticle Systems for Enabling Gene Therapies, Mol Ther 25(7) (2017) 1467-1475.
[75] S. Reinhard, E. Wagner, How to Tackle the Challenge of siRNA Delivery with Sequence-Defined Oligoamino Amides, Macromol Biosci 17(1) (2017).
[76] G. Sahay, W. Querbes, C. Alabi, A. Eltoukhy, S. Sarkar, C. Zurenko, E. Karagiannis, K. Love, D. Chen, R. Zoncu, Y. Buganim, A. Schroeder, R. Langer, D.G. Anderson, Efficiency of siRNA delivery by lipid nanoparticles is limited by endocytic recycling, Nat Biotechnol 31(7) (2013) 653-8.
[77] L. Hartmann, H.G. Börner, Precision Polymers: Monodisperse, Monomer-Sequence-Defined Segments to Target Future Demands of Polymers in Medicine, Advanced Materials 21(32-33) (2009) 3425-3431.
[78] T. Lehto, O.E. Simonson, I. Mager, K. Ezzat, H. Sork, D.M. Copolovici, J.R. Viola, E.M. Zaghloul, P. Lundin, P.M. Moreno, M. Mae, N. Oskolkov, J. Suhorutsenko, C.I. Smith, S.E. Andaloussi, A peptide-based vector for efficient gene transfer in vitro and in vivo, Mol Ther 19(8) (2011) 1457-67.
[79] P. Kos, U. Lächelt, A. Herrmann, F.M. Mickler, M. Döblinger, D. He, A. Krhač Levačić, S. Morys, C. Bräuchle, E. Wagner, Histidine-rich stabilized polyplexes for cMet-directed tumor-targeted gene transfer, Nanoscale 7(12) (2015) 5350-5362.
[80] S. Wang, S. Reinhard, C. Li, M. Qian, H. Jiang, Y. Du, U. Lachelt, W. Lu, E. Wagner, R. Huang, Antitumoral Cascade-Targeting Ligand for IL-6 Receptor-Mediated Gene Delivery to Glioma, Mol Ther 25(7) (2017) 1556-1566.
[81] C. Scholz, P. Kos, L. Leclercq, X. Jin, H. Cottet, E. Wagner, Correlation of Length of Linear Oligo(ethanamino) Amides with Gene Transfer and Cytotoxicity, ChemMedChem (2014).
[82] K. Muller, P.M. Klein, P. Heissig, A. Roidl, E. Wagner, EGF receptor targeted lipo-oligocation polyplexes for antitumoral siRNA and miRNA delivery, Nanotechnology 27(46) (2016) 464001.
[83] Y. Lee, H. Koo, Y.B. Lim, H. Mo, J.S. Park, New cationic lipids for gene transfer with high efficiency and low toxicity: T-shape cholesterol ester derivatives, Bioorg.Med.Chem.Lett. 14(10) (2004) 2637-2641.

[84] K. Muller, E. Kessel, P.M. Klein, M. Hohn, E. Wagner, Post-PEGylation of siRNA Lipo-oligoamino Amide Polyplexes Using Tetra-glutamylated Folic Acid as Ligand for Receptor-Targeted Delivery, Mol Pharm 13(7) (2016) 2332-45.
[85] X. Wang, F. He, L. Li, H. Wang, R. Yan, L. Li, Conjugated oligomer-based fluorescent nanoparticles as functional nanocarriers for nucleic acids delivery, ACS applied materials & interfaces 5(12) (2013) 5700-8.
[86] F. Pittella, H. Cabral, Y. Maeda, P. Mi, S. Watanabe, H. Takemoto, H.J. Kim, N. Nishiyama, K. Miyata, K. Kataoka, Systemic siRNA delivery to a spontaneous pancreatic tumor model in transgenic mice by PEGylated calcium phosphate hybrid micelles, J Control Release 178 (2014) 18-24.
[87] S. Khargharia, K. Kizzire, M.D. Ericson, N.J. Baumhover, K.G. Rice, PEG length and chemical linkage controls polyacridine peptide DNA polyplex pharmacokinetics, biodistribution, metabolic stability and in vivo gene expression, J Control Release 170(3) (2013) 325-33.
[88] Y. Sakurai, H. Hatakeyama, Y. Sato, M. Hyodo, H. Akita, H. Harashima, Gene silencing via RNAi and siRNA quantification in tumor tissue using MEND, a liposomal siRNA delivery system, Mol Ther 21(6) (2013) 1195-203.
[89] S. Morys, S. Urnauer, C. Spitzweg, E. Wagner, EGFR Targeting and Shielding of pDNA Lipopolyplexes via Bivalent Attachment of a Sequence-Defined PEG Agent, Macromol Biosci 18(1) (2018).
[90] T.M. Kapoor, T.U. Mayer, M.L. Coughlin, T.J. Mitchison, Probing spindle assembly mechanisms with monastrol, a small molecule inhibitor of the mitotic kinesin, Eg5, J Cell Biol 150(5) (2000) 975-88.
[91] A.D. Judge, M. Robbins, I. Tavakoli, J. Levi, L. Hu, A. Fronda, E. Ambegia, K. McClintock, I. MacLachlan, Confirming the RNAi-mediated mechanism of action of siRNA-based cancer therapeutics in mice, J Clin Invest 119(3) (2009) 661-73.
[92] D. Edinger, R. Kläger, C. Troiber, C. Dohmen, E. Wagner, Gene Silencing and Antitumoral Effects of Eg5 or Ran siRNA Oligoaminoamide Polyplexes, Drug deliv. and Transl. Res. (2013) in press.
[93] H.M. Ellerby, W. Arap, L.M. Ellerby, R. Kain, R. Andrusiak, G.D. Rio, S. Krajewski, C.R. Lombardo, R. Rao, E. Ruoslahti, D.E. Bredesen, R. Pasqualini, Anti-cancer activity of targeted pro-apoptotic peptides, Nat.Med. 5(9) (1999) 1032-1038.
[94] M.A. Rogy, B.G. Beinhauer, W. Reinisch, L. Huang, P. Pokieser, Transfer of interleukin-4 and interleukin-10 in patients with severe inflammatory bowel disease of the rectum 97, Hum.Gene Ther. 11(12) (2000) 1731-1741.
[95] S.S. Diebold, M. Cotten, E. Wagner, M. Zenke, Gene-modified dendritic cells by receptor-mediated transfection, Adv.Exp.Med Biol. 451 (1998) 449-455.
[96] A. Avraméas, D. McIlroy, A. Hosmalin, B. Autran, P. Debré, M. Monsigny, R.C. Roche, P. Midoux, Expression of a mannose/fucose membrane lectin on human dendritic cells 33, Eur J Immunol 25 (1996).
[97] D. Schaffert, N. Badgujar, E. Wagner, Novel Fmoc-polyamino acids for solid-phase synthesis of defined polyamidoamines, Org Lett 13(7) (2011) 1586-9.

[98] B. Steinborn, I. Truebenbach, S. Morys, U. Lächelt, E. Wagner, W. Zhang, Epidermal growth factor receptor targeted methotrexate and small interfering RNA co-delivery, The Journal of Gene Medicine 20(7-8) (2018) e3041.
[99] P. Zhang, D. He, P.M. Klein, X. Liu, R. Röder, M. Döblinger, E. Wagner, Enhanced Intracellular Protein Transduction by Sequence Defined Tetra-Oleoyl Oligoaminoamides Targeted for Cancer Therapy, Advanced Functional Materials 25(42) (2015) 6627-6636.
[100] A.K. Levacic, S. Morys, S. Kempter, U. Lächelt, E. Wagner, Minicircle Versus Plasmid DNA Delivery by Receptor-Targeted Polyplexes, Human Gene Therapy 28(10) (2017) 862-874.
[101] D.J. Lee, E. Kessel, T. Lehto, X. Liu, N. Yoshinaga, K. Padari, Y.C. Chen, S. Kempter, S. Uchida, J.O. Radler, M. Pooga, M.T. Sheu, K. Kataoka, E. Wagner, Systemic Delivery of Folate-PEG siRNA Lipopolyplexes with Enhanced Intracellular Stability for In Vivo Gene Silencing in Leukemia, Bioconjug Chem 28(9) (2017) 2393-2409.
[102] A. Kwok, S.L. Hart, Comparative structural and functional studies of nanoparticle formulations for DNA and siRNA delivery, Nanomedicine 7(2) (2011) 210-9.
[103] C. Troiber, D. Edinger, P. Kos, L. Schreiner, R. Klager, A. Herrmann, E. Wagner, Stabilizing effect of tyrosine trimers on pDNA and siRNA polyplexes, Biomaterials 34(5) (2013) 1624-33.
[104] W. Zhang, K. Muller, E. Kessel, S. Reinhard, D. He, P.M. Klein, M. Hohn, W. Rodl, S. Kempter, E. Wagner, Targeted siRNA Delivery Using a Lipo-Oligoaminoamide Nanocore with an Influenza Peptide and Transferrin Shell, Adv Healthc Mater 5(12) (2016) 1493-504.
[105] P.V. Chang, J.A. Prescher, E.M. Sletten, J.M. Baskin, I.A. Miller, N.J. Agard, A. Lo, C.R. Bertozzi, Copper-free click chemistry in living animals, Proceedings of the National Academy of Sciences 107(5) (2010) 1821-1826.
[106] L. Brulisauer, N. Kathriner, M. Prenrecaj, M.A. Gauthier, J.C. Leroux, Tracking the bioreduction of disulfide-containing cationic dendrimers, Angew Chem Int Ed Engl 51(50) (2012) 12454-8.
[107] M.E. Davis, J.E. Zuckerman, C.H.J. Choi, D. Seligson, A. Tolcher, C.A. Alabi, Y. Yen, J.D. Heidel, A. Ribas, Evidence of RNAi in humans from systemically administered siRNA via targeted nanoparticles, Nature 464(7291) (2010) 1067-1070.
[108] J. Tabernero, G.I. Shapiro, P.M. LoRusso, A. Cervantes, G.K. Schwartz, G.J. Weiss, L. Paz-Ares, D.C. Cho, J.R. Infante, M. Alsina, M.M. Gounder, R. Falzone, J. Harrop, A.C. White, I. Toudjarska, D. Bumcrot, R.E. Meyers, G. Hinkle, N. Svrzikapa, R.M. Hutabarat, V.A. Clausen, J. Cehelsky, S.V. Nochur, C. Gamba-Vitalo, A.K. Vaishnaw, D.W. Sah, J.A. Gollob, H.A. Burris, 3rd, First-in-humans trial of an RNA interference therapeutic targeting VEGF and KSP in cancer patients with liver involvement, Cancer discovery 3(4) (2013) 406-17.
[109] A. Wittrup, J. Lieberman, Knocking down disease: a progress report on siRNA therapeutics, Nat Rev Genet 16(9) (2015) 543-52.
[110] A. Rawshani, A. Rawshani, S. Franzén, N. Sattar, B. Eliasson, A.-M. Svensson, B. Zethelius, M. Miftaraj, D.K. McGuire, A. Rosengren, S. Gudbjörnsdottir, Risk Factors, Mortality, and Cardiovascular Outcomes in Patients with Type 2 Diabetes, New England Journal of Medicine 379(7) (2018) 633-644.
[111] M. Ratner, Patients with porphyria bask in sunlight of FDA approval, Nature Biotechnology 37(12) (2019) 1390-1391.

[112] D.P. Judge, A.V. Kristen, M. Grogan, M.S. Maurer, R.H. Falk, M. Hanna, J. Gillmore, P. Garg, A.K. Vaishnaw, J. Harrop, C. Powell, V. Karsten, X. Zhang, M.T. Sweetser, J. Vest, P.N. Hawkins, Phase 3 Multicenter Study of Revusiran in Patients with Hereditary Transthyretin-Mediated (hATTR) Amyloidosis with Cardiomyopathy (ENDEAVOUR), Cardiovasc Drugs Ther 34(3) (2020) 357-370.
[113] I.A. Khalil, Y. Yamada, H. Harashima, Optimization of siRNA delivery to target sites: issues and future directions, Expert Opin Drug Deliv 15(11) (2018) 1053-1065.
[114] Y. Dong, K.T. Love, J.R. Dorkin, S. Sirirungruang, Y. Zhang, D. Chen, R.L. Bogorad, H. Yin, Y. Chen, A.J. Vegas, C.A. Alabi, G. Sahay, K.T. Olejnik, W. Wang, A. Schroeder, A.K.R. Lytton-Jean, D.J. Siegwart, A. Akinc, C. Barnes, S.A. Barros, M. Carioto, K. Fitzgerald, J. Hettinger, V. Kumar, T.I. Novobrantseva, J. Qin, W. Querbes, V. Koteliansky, R. Langer, D.G. Anderson, Lipopeptide nanoparticles for potent and selective siRNA delivery in rodents and nonhuman primates, Proceedings of the National Academy of Sciences 111(11) (2014) 3955-3960.
[115] Y. Sakurai, T. Hada, A. Kato, Y. Hagino, W. Mizumura, H. Harashima, Effective Therapy Using a Liposomal siRNA that Targets the Tumor Vasculature in a Model Murine Breast Cancer with Lung Metastasis, Molecular therapy oncolytics 11 (2018) 102-108.
[116] A.F. Ibrahim, U. Weirauch, M. Thomas, A. Grünweller, R.K. Hartmann, A. Aigner, MicroRNA Replacement Therapy for miR-145 and miR-33a Is Efficacious in a Model of Colon Carcinoma, Cancer Research 71(15) (2011) 5214-5224.
[117] C. Plank, K. Mechtler, F.C. Szoka, E. Wagner, Activation of the Complement System by Synthetic DNA Complexes: A Potential Barrier for Intravenous Gene Delivery, Human Gene Therapy 7(12) (1996) 1437-1446.
[118] M. Ogris, S. Brunner, S. Schuller, R. Kircheis, E. Wagner, PEGylated DNA/transferrin-PEI complexes: reduced interaction with blood components, extended circulation in blood and potential for systemic gene delivery, Gene Ther 6(4) (1999) 595-605.
[119] O.M. Merkel, R. Urbanics, P. Bedocs, Z. Rozsnyay, L. Rosivall, M. Toth, T. Kissel, J. Szebeni, In vitro and in vivo complement activation and related anaphylactic effects associated with polyethylenimine and polyethylenimine-graft-poly(ethylene glycol) block copolymers, Biomaterials 32(21) (2011) 4936-42.
[120] D. Rosenblum, N. Joshi, W. Tao, J.M. Karp, D. Peer, Progress and challenges towards targeted delivery of cancer therapeutics, Nat Commun 9(1) (2018) 1410.
[121] Q. Sun, Z. Kang, L. Xue, Y. Shang, Z. Su, H. Sun, Q. Ping, R. Mo, C. Zhang, A Collaborative Assembly Strategy for Tumor-Targeted siRNA Delivery, Journal of the American Chemical Society 137(18) (2015) 6000-6010.
[122] E.C. Dreaden, S.W. Morton, K.E. Shopsowitz, J.-H. Choi, Z.J. Deng, N.-J. Cho, P.T. Hammond, Bimodal Tumor-Targeting from Microenvironment Responsive Hyaluronan Layer-by-Layer (LbL) Nanoparticles, ACS Nano 8(8) (2014) 8374-8382.
[123] T. Sato, M. Nakata, Z. Yang, Y. Torizuka, S. Kishimoto, M. Ishihara, In vitro and in vivo gene delivery using chitosan/hyaluronic acid nanoparticles: Influences of molecular mass of hyaluronic acid and lyophilization on transfection efficiency, The Journal of Gene Medicine 19(8) (2017) e2968.

[124] A.E. Dillinger, M. Guter, F. Froemel, G.R. Weber, K. Perkumas, W.D. Stamer, A. Ohlmann, R. Fuchshofer, M. Breunig, Intracameral Delivery of Layer-by-Layer Coated siRNA Nanoparticles for Glaucoma Therapy, Small 14(50) (2018) 1803239.
[125] L. Chen, C. Fu, Q. Zhang, C. He, F. Zhang, Q. Wei, The role of CD44 in pathological angiogenesis, FASEB journal : official publication of the Federation of American Societies for Experimental Biology (2020).
[126] A.W. Griffioen, M.J.H. Coenen, C.A. Damen, S.M.M. Hellwig, D. H.J. van Weering, W. Vooys, G.H. Blijham, G. Groenewegen, CD44 Is Involved in Tumor Angiogenesis; an Activation Antigen on Human Endothelial Cells, Blood 90(3) (1997) 1150-1159.
[127] L. Beckert, L. Kostka, E. Kessel, A. Krhac Levacic, H. Kostkova, T. Etrych, U. Lachelt, E. Wagner, Acid-labile pHPMA modification of four-arm oligoaminoamide pDNA polyplexes balances shielding and gene transfer activity in vitro and in vivo, Eur J Pharm Biopharm 105 (2016) 85-96.
[128] S. Urnauer, S. Morys, A. Krhac Levacic, A.M. Muller, C. Schug, K.A. Schmohl, N. Schwenk, C. Zach, J. Carlsen, P. Bartenstein, E. Wagner, C. Spitzweg, Sequence-defined cMET/HGFR-targeted Polymers as Gene Delivery Vehicles for the Theranostic Sodium Iodide Symporter (NIS) Gene, Mol Ther 24(8) (2016) 1395-404.
[129] P.M. Klein, K. Klinker, W. Zhang, S. Kern, E. Kessel, E. Wagner, M. Barz, Efficient Shielding of Polyplexes Using Heterotelechelic Polysarcosines, Polymers 10(6) (2018).
[130] P.M. Klein, S. Kern, D.J. Lee, J. Schmaus, M. Hohn, J. Gorges, U. Kazmaier, E. Wagner, Folate receptor-directed orthogonal click-functionalization of siRNA lipopolyplexes for tumor cell killing in vivo, Biomaterials 178 (2018) 630-642.
[131] P.M. Klein, K. Muller, C. Gutmann, P. Kos, A. Krhac Levacic, D. Edinger, M. Hohn, J.C. Leroux, M.A. Gauthier, E. Wagner, Twin disulfides as opportunity for improving stability and transfection efficiency of oligoaminoethane polyplexes, J Control Release 205 (2015) 109-19.
[132] S.T. Chou, Q. Leng, P. Scaria, J.D. Kahn, L.J. Tricoli, M. Woodle, A.J. Mixson, Surface-modified HK:siRNA nanoplexes with enhanced pharmacokinetics and tumor growth inhibition, Biomacromolecules 14(3) (2013) 752-60.
[133] U. Lachelt, P. Kos, F.M. Mickler, A. Herrmann, E.E. Salcher, W. Rodl, N. Badgujar, C. Brauchle, E. Wagner, Fine-tuning of proton sponges by precise diaminoethanes and histidines in pDNA polyplexes, Nanomedicine 10(1) (2014) 35-44.
[134] F. Fazlollahi, S. Angelow, N.R. Yacobi, R. Marchelletta, A.S.L. Yu, S.F. Hamm-Alvarez, Z. Borok, K.-J. Kim, E.D. Crandall, Polystyrene nanoparticle trafficking across MDCK-II, Nanomedicine : nanotechnology, biology, and medicine 7(5) (2011) 588-594.
[135] Z.-h. Sui, H. Xu, H. Wang, S. Jiang, H. Chi, L. Sun, Intracellular Trafficking Pathways of Edwardsiella tarda: From Clathrin- and Caveolin-Mediated Endocytosis to Endosome and Lysosome, Frontiers in Cellular and Infection Microbiology 7(400) (2017).
[136] D. Dutta, J.G. Donaldson, Search for inhibitors of endocytosis: Intended specificity and unintended consequences, Cell Logist 2(4) (2012) 203-208.
[137] M. Koivusalo, C. Welch, H. Hayashi, C.C. Scott, M. Kim, T. Alexander, N. Touret, K.M. Hahn, S. Grinstein, Amiloride inhibits macropinocytosis by lowering submembranous pH and preventing Rac1 and Cdc42 signaling, The Journal of Cell Biology 188(4) (2010) 547-563.

[138] J.-S. Kim, T.-J. Yoon, K.-N. Yu, M.-S. Noh, M. Woo, B.-G. Kim, K.-H. Lee, B.-H. Sohn, S.-B. Park, J.-K. Lee, M.-H. Cho, Cellular uptake of magnetic nanoparticle is mediated through energy-dependent endocytosis in A549 cells, J Vet Sci 7(4) (2006) 321-326.
[139] H.J. Greyner, T. Wiraszka, L.S. Zhang, W.M. Petroll, M.E. Mummert, Inducible macropinocytosis of hyaluronan in B16-F10 melanoma cells, Matrix Biol 29(6) (2010) 503-10.
[140] K. von Gersdorff, N.N. Sanders, R. Vandenbroucke, S.C. De Smedt, E. Wagner, M. Ogris, The Internalization Route Resulting in Successful Gene Expression Depends on both Cell Line and Polyethylenimine Polyplex Type, Molecular Therapy 14(5) (2006) 745-753.
[141] Z. Zheng, R.D. Cummings, P.E. Pummill, P.W. Kincade, Growth as a solid tumor or reduced glucose concentrations in culture reversibly induce CD44-mediated hyaluronan recognition by Chinese hamster ovary cells, The Journal of clinical investigation 100(5) (1997) 1217-1229.
[142] Y. Matsumura, H. Maeda, A new concept for macromolecular therapeutics in cancer chemotherapy: mechanism of tumoritropic accumulation of proteins and the antitumor agent smancs, Cancer Res. 46(12 Pt 1) (1986) 6387-6392.
[143] F. Yuan, M. Dellian, D. Fukumura, M. Leunig, D.A. Berk, V.P. Torchilin, R.K. Jain, Vascular permeability in a human tumor xenograft: molecular size dependence and cutoff size, Cancer Res 55(17) (1995) 3752-3756.
[144] Y. Shi, R. van der Meel, X. Chen, T. Lammers, The EPR effect and beyond: Strategies to improve tumor targeting and cancer nanomedicine treatment efficacy, Theranostics 10(17) (2020) 7921-7924.
[145] S. Wilhelm, A.J. Tavares, Q. Dai, S. Ohta, J. Audet, H.F. Dvorak, W.C.W. Chan, Analysis of nanoparticle delivery to tumours, Nature Reviews Materials 1(5) (2016) 16014.
[146] A.E. Hansen, A.L. Petersen, J.R. Henriksen, B. Boerresen, P. Rasmussen, D.R. Elema, P.M.a. Rosenschöld, A.T. Kristensen, A. Kjær, T.L. Andresen, Positron Emission Tomography Based Elucidation of the Enhanced Permeability and Retention Effect in Dogs with Cancer Using Copper-64 Liposomes, ACS Nano 9(7) (2015) 6985-6995.
[147] G. Thurston, J.W. McLean, M. Rizen, P. Baluk, A. Haskell, T.J. Murphy, D. Hanahan, D.M. McDonald, Cationic liposomes target angiogenic endothelial cells in tumors and chronic inflammation in mice, The Journal of clinical investigation 101(7) (1998) 1401-1413.
[148] M. Dellian, F. Yuan, V.S. Trubetskoy, V.P. Torchilin, R.K. Jain, Vascular permeability in a human tumour xenograft: molecular charge dependence, British Journal of Cancer 82(9) (2000) 1513-1518.
[149] H.-X. Wang, Z.-Q. Zuo, J.-Z. Du, Y.-C. Wang, R. Sun, Z.-T. Cao, X.-D. Ye, J.-L. Wang, K.W. Leong, J. Wang, Surface charge critically affects tumor penetration and therapeutic efficacy of cancer nanomedicines, Nano Today 11(2) (2016) 133-144.
[150] J.E. Schnitzer, gp60 is an albumin-binding glycoprotein expressed by continuous endothelium involved in albumin transcytosis, American Journal of Physiology-Heart and Circulatory Physiology 262(1) (1992) H246-H254.
[151] P. Oh, J.E. Testa, P. Borgstrom, H. Witkiewicz, Y. Li, J.E. Schnitzer, In vivo proteomic imaging analysis of caveolae reveals pumping system to penetrate solid tumors, Nature Medicine 20(9) (2014) 1062-1068.

[152] S. Sindhwani, A.M. Syed, J. Ngai, B.R. Kingston, L. Maiorino, J. Rothschild, P. MacMillan, Y. Zhang, N.U. Rajesh, T. Hoang, J.L.Y. Wu, S. Wilhelm, A. Zilman, S. Gadde, A. Sulaiman, B. Ouyang, Z. Lin, L. Wang, M. Egeblad, W.C.W. Chan, The entry of nanoparticles into solid tumours, Nature Materials 19(5) (2020) 566-575.
[153] Y. Liu, Y. Huo, L. Yao, Y. Xu, F. Meng, H. Li, K. Sun, G. Zhou, D.S. Kohane, K. Tao, Transcytosis of Nanomedicine for Tumor Penetration, Nano Letters 19(11) (2019) 8010-8020.
[154] I. de Lázaro, D.J. Mooney, A nanoparticle's pathway into tumours, Nature Materials 19(5) (2020) 486-487.
[155] S. Pandit, D. Dutta, S. Nie, Active transcytosis and new opportunities for cancer nanomedicine, Nature Materials 19(5) (2020) 478-480.
[156] Challenging paradigms in tumour drug delivery, Nature Materials 19(5) (2020) 477-477.
[157] K. Xiao, Y. Li, J. Luo, J.S. Lee, W. Xiao, A.M. Gonik, R.G. Agarwal, K.S. Lam, The effect of surface charge on in vivo biodistribution of PEG-oligocholic acid based micellar nanoparticles, Biomaterials 32(13) (2011) 3435-3446.
[158] E. Blanco, H. Shen, M. Ferrari, Principles of nanoparticle design for overcoming biological barriers to drug delivery, Nature Biotechnology 33(9) (2015) 941-951.

8. Publications

Original articles

Luo J, Höhn M, Reinhard S, Loy DM, Klein PM, Wagner E (2019) IL4-Receptor-Targeted Dual Antitumoral Apoptotic Peptide—siRNA Conjugate Lipoplexes. *Advanced Functional Materials,* **29**, 1900697.

Luo J, Schmaus J, Cui M, Hörterer E, Wilk U, Höhn M, Däther M, Berger S, Benli-Hoppe T, Peng L, Wagner E (2020) Hyaluronate siRNA nanoparticles with positive charge display rapid attachment to tumor endothelium and penetration into tumors. *Journal of Controlled Release,* DOI:

Wang Y., **Luo J**, Truebenbach I, Reinhard S, Klein PM, Höhn M, Kern S, Morys S, Loy DM, Wagner E, Zhang W. (2020) Double Click-Functionalized siRNA Polyplexes for Gene Silencing in Epidermal Growth Factor Receptor-Positive Tumor Cells. *ACS Biomaterials Science and Engineering,* **6**, 1074-1089.

Review

Luo J, Wagner E, Wang YF (2020) Artificial Peptides for Antitumoral siRNA Delivery. *Journal of Materials Chemistry B,* 2020, **8**, 2020-2031.

Poster presentation

Luo J, Schmaus J, Cui M, Hörterer E, Wagner E. Surface charge of lipopolyplexes influences on the tumor penetration. The Controlled Release Society German Local Chapter, Munich, Germany, February 20-21, 2020. (Best Poster Presentation)

9. Acknowledgements

Time flies! At the end of my PhD study, I would like to express my gratitude to all people supporting me during the past four years.

First of all, I would like to thank my supervisor Prof. Dr. Ernst Wagner for giving me the opportunity to do my PhD in his research group. I greatly appreciate his scientific support and professional guidance. I have learned a lot from not only the informative discussions with him but also the email communications with him even after midnight.

I would like to thank Johannes Schmaus, Mochen Cui, and Elisa Hörterer for their generous help on the animal experiment. I also thanks Dr. Philipp Klein, Dr. Sören Reinhard, and Dr. Ines Trrübenbach for teaching me synthesis, as well as Dr. Ulrich Lächelt, Dr. Wei Zhang, Dr. Dianjang Lee, and Dr. Peng Zhang for discussion about my project. I would also like to thank Dominik M. Loy for his help with TEM and Nader Danaf for the FCS measurements. I want to thank Miriam for her instructions on cell culture at the beginning of my PhD, Andi for the safety instructions, as well as Yanfang for keeping the cell culture room tidy and clean. I am very grateful to Wolfgang for solving the computer and equipment problems, as well as Anna, Ursula, Melinda, Marus and Olga for keeping the lab running. I also thanks Teoman for MASS, Simone for co-synthesis of oligomers and discussions with projects, Bianca, Ann-Katrin for teaching qPCR.

Many thanks to Uli for preparing the traditional Weißwurst, St. Nicholas chocolate and Glühwein, as well as Ines, Jasmin and Dominik for the organization of lab activities, especially the impressive and great music played by our Christmas band, Dominik, Philipp H. and Ines. I would also like to thank our lunch groups, in my first two years of PhD, (Dianjang Lee, Peng Zhang, Wei Zhang, Yanfang Wang) and in my later two years of PhD,(Peng Lun, Yi Lin, Meng Lv, Yanfang Wang) for the interesting and extensive discussions. Many thanks to all the AK Wagner members for the nice

atmosphere and unforgettable time we spent together. Special thanks to China Scholarship Council for supporting my study and life in Munich. Many thanks to all my friends for helping and caring me all the time.

Finally, I want to express my gratitude to my parents for their constant support and trust in my life. Whenever I’m in trouble, they always make me calm and optimistic.